Novel Approaches for the Elemental and Morphological Characterisation of Particulate Material

Michelle Barker

A thesis submitted in fulfilment of the requirements of the

University of Sheffield for the degree of Doctor of Philosophy

Department of Chemistry   **January 2014**

University of Sheffield

For Nana Sybil

"All human endeavours, even industrial ones, are perfectible"

From a plaque to commemorate the victims of the Meuse Valley fog

Declaration

I declare that this thesis, submitted in fulfilment of the degree of Doctor of Philosophy at the University of Sheffield, is my own work. It has not previously been submitted for a degree at this or any other university.

Michelle Barker

University of Sheffield

January 2014

Acknowledgements

First and foremost I would like to express my sincere thanks to my supervisor Professor Cameron McLeod. He has supported, directed and guided me throughout my doctorate and for that I am extremely grateful. I would also like to thank John Pugh and Neil Bramall, from the University of Sheffield, for sharing their invaluable knowledge and expertise within analytical chemistry with me. Secondly thanks go to Tata Steel for their support and financial assistance. I would like to specifically thank Diane Ciaparra, Kevin Jackson and David Anderson for their continued supervision and assistance in both starting and completing the work within this thesis. Thanks also go to all members of Group Environment, especially Oliver Woods, Joe Darwin and Steve Woolass who were there to talk things through with when they did not go to plan.

I would like to extend my appreciation to Andy Whitehouse and all members of Applied Photonics, who assisted me greatly in using the LIBS system and also commissioned the internal sample chamber which made a large proportion of this work possible. I would also like to acknowledge Delphine Bard and the Health and Safety Laboratory in Buxton, who allowed me to complete primary studies within one of their laboratories.

Last but by no means least I would like to express my heartfelt thanks to my family and friends, without you this doctorate would have been a lot harder to complete. To my parents and siblings, thank you for your support and helping to make me smile on a bad day. To Abbs, thank you for being the best friend a girl could wish for, for listening to my rants and for always being there no matter what. Finally to Andy, I would never have finished this without you. Words cannot describe the gratitude and love I wish to convey to you. Thank you for putting up with me through the ups and downs of the last four years. Now we can move on with our lives together.

Abbreviations

A_f	Asymmetry factor
AES	Atomic emission spectroscopy
APS	Aerodynamic particle sizer
ASAS	Aerosol shape analysis system
BAT	Best available technique
BS	British standard
CCD	Charge coupled device
CRM	Certified reference material
DEFRA	Department for environment, food and rural affairs
DMA	Differential mobility analyser
D_p	Aerodynamic diameter
ELPI	Electrical low pressure impactor
EN	European norm
FMPS	Fast mobility particle scanner
HSE	Health and safety executive
ICP	Inductively coupled plasma
ISO	International organisation for standardisation
LA	Laser ablation
LAS	Laser aerosol spectrometry
LIBS	Laser induced breakdown spectroscopy
LOD	Limit of detection
MOUDI	Micro orifice uniform deposit impactor
MS	Mass spectrometry
Nd:YAG	Neodymium-doped yttrium aluminium garnet
NIST	National institute of standards and technology
OPC	Optical particle counter
PAH	Polyaromatic hydrocarbon
PCDD	Polychlorinated dibenzo-p-dioxin
PM	Particulate matter
PM_{10}	Mass of particles that pass a sampler entry with 50% efficiency at 10 µm
PMT	Photomultiplier tube
QC	Quality control
RDS	Rotating drum sampler
REACH	Registration, evaluation, authorisation and restriction of chemicals
RFCS	Research fund for coal and steel
RSD	Relative standard deviation
SEM	Scanning electron microscopy
SMPS	Scanning mobility particle sizer
SRM	Standard reference material
TEM	Transmission electron microscope
UKAS	The United Kingdom accreditation service
XRF	X-Ray fluorescence

Abstract

In view of the environmental and health implications that particulate matter can cause the characterisation of the chemical and physical properties of particulates is of significant importance. This characterisation enables our understanding of particulate generation to be furthered and thus efficient abatement procedures can be devised. Novel methods to physically and chemically characterise particulates have been developed using a morphology analyser, an electrical low pressure impactor, a rotating drum sampler and a laser ablation unit. Further analysis was also completed using inductively coupled plasma emission spectroscopy, inductively coupled plasma mass spectrometry and scanning electron microscopy. These novel methods were utilised to complete two studies. The first study characterised four materials obtained from an integrated steelworks, two Brazilian iron ores, a blast furnace flue dust and a sinter dust. The second study examined laser generated aerosols produced from the ablation of six solid materials, a carbon rod, high purity zinc, polyethylene, a carbon steel, boron nitride and glass. Two different laser wavelengths and ablation atmospheres were also scrutinised. For both studies, morphological profiles were obtained alongside number and mass distributions. Chemical analysis of all particulates, which had been collected onto substrates, was completed to allow the quantitative determination of the multielement composition of each material, as well as the elemental distributions. The compiling of the obtained chemical and physical information permitted the generation of characteristic 'fingerprints' for each individual material. For the first study these fingerprints allowed an insight into the sources of emissions from an integrated steelworks. This insight could be used during on site testing to help determine further emission sources and allow the relevant abatement procedures to be put into place. For the second study these fingerprints have allowed an understanding of the complicated interactions between a laser and a solid material.

Table of Contents

Chapter One

Introduction

1.1 Background

1.1.1 Aerosols

Aerosols are widely recognised throughout the world for their local, regional and global impacts. Their effects on both human health and the environment are a major concern and large amounts of research are carried out into these two fields.[1] Aerosols are also greatly used in commercial applications, such as beauty products, household cleaners, pesticides and medicine.

An aerosol is a suspension of solid and/or liquid particulates in a gaseous medium, such as the atmosphere.[2] The particulates are described as PM[3] and most commonly discussed as PM_{10} which is expressed as "the mass of particles that pass through a sampler entry with 50% efficiency at ten micrometres"[4] or particulates with a diameter of ten micrometers or less. Particulate matter is a natural component of the atmosphere,[5] however, it is also considered as a pollutant,[6] especially when formed from anthropogenic sources such as industry and transport.[7] The concentration of particulates present within the atmosphere is more important than their presence and some aerosols have no safe concentrations.[8] In some cases increased concentrations could damage buildings and habitats, whilst also causing health problems.[2] Aerosol particulates range from 1 nm to approximately 10 µm in size, with atmospheric aerosols having a typical D_p of 1 µm.[9] Aerodynamic diameter is defined as the diameter of a spherical particle with a density of 1 g/cm^3.[10] Aerosols may be grouped into three different size ranges known as modes: nuclei, accumulation and coarse.[11] The nuclei

mode consists of ultrafine particulates which have a diameter of 3 nm to 50 nm.[11, 12] These particulates have a short lifetime, a low total mass, due to their size, and originate from a range of different combustion sources.[11] Fine particulates, present in the accumulate mode, range from 50 nm to 1 µm. A large number of particulates are contained in this mode and have a relatively large total mass due to their larger size. Examples include metal fumes and sea salt nuclei. They have a lifetime of a few days to a few weeks and may be formed directly, via anthropogenic or natural sources, or indirectly by the growth of smaller particulates.[11] Particulates present in both the nuclei and the accumulate modes are inhalable,[11] with ultrafine particulates in particular widely believed to be responsible for adverse effects upon human health.[12] Particulates present in the coarse mode have a size range of 1 µm to 50 µm. Due to their large size coarse particulates readily settle out, due to gravitational forces, or through impact with surfaces which will reduce their lifetime in the atmosphere to a few hours or days. Examples of coarse particulates include cement dusts, coal dusts and windblown dusts.[11] Figure 1-1 shows some of the characteristic size ranges of typical aerosols.

Figure 1-1: Characteristic size ranges of typical aerosols (adapted from reference[10])
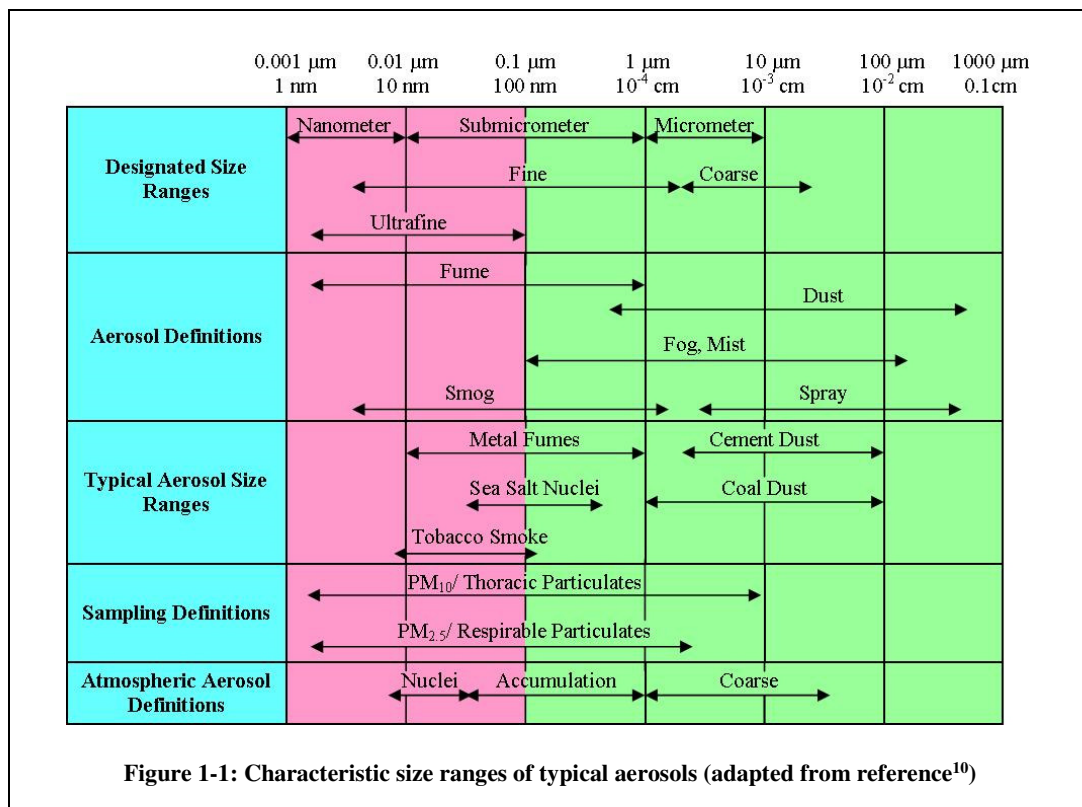
As well as being grouped into size ranges aerosols may also be classified as primary or secondary. Primary aerosols are emitted directly into the atmosphere, from both natural and anthropogenic sources.

Natural aerosols include those which cause climate change, epidemics and pollution, such as windblown dust, sea salt and volcanic dust. A recent example of a natural aerosol affecting a large number of travellers, approximately 10 million, was the eruption of a volcano in Iceland in April, 2010.[13] Melt waters from the Eyjafjallajökull glacier mixed with hot magmas, causing a volcanic eruption which sent an exceptional amount of fine ash almost ten kilometres, through the troposphere and into the stratosphere. This fine ash was blown both east and south causing most of the airspace over Europe to be closed for a week. Concerns in both Iceland and across Europe were also had regarding ash inhalation [13]

Anthropogenic aerosols are used in many different applications. They are not necessarily harmful to human health and in some cases can be used in drug delivery, for example asthma inhalers. They can be generated from combustion processes, hot processes and transport. Anthropogenic aerosols are also needed in ICP spectroscopy, a trace elemental analysis technique. A liquid sample is passed through a nebuliser to form an aerosol which may then be sprayed into the plasma. Nebulisation was discussed by Browner and Boorn in 1984.[14] The different types of nebulisers available for use with ICP were discussed, mainly concentrating on the pneumatic nebuliser, but also discussing others such as, the ultrasonic, the cross flow and the Babington high solids nebuliser.[14] Another type of aerosol, used within ICP, is that which is generated when using laser ablation as a sample introduction system. By firing a laser at a solid sample, fine particulates are generated which are carried by an argon gas flow, as an aerosol, to the ICP for analysis.

Secondary aerosols consist of particulates formed through chemical reactions in the atmosphere, for example oxidation or conversion from vapour to aerosol. Concentrations of

these secondary aerosols may vary according to season, distance from precursor source and the availability of particulates.[15] The processes of aerosol growth can vary depending on the starting material. Growth tends to occur via nucleation, condensation and coagulation. The three main routes for growth are detailed in Figure 1-2.

Figure 1-2: Aerosol growth processes (adapted from reference[16])
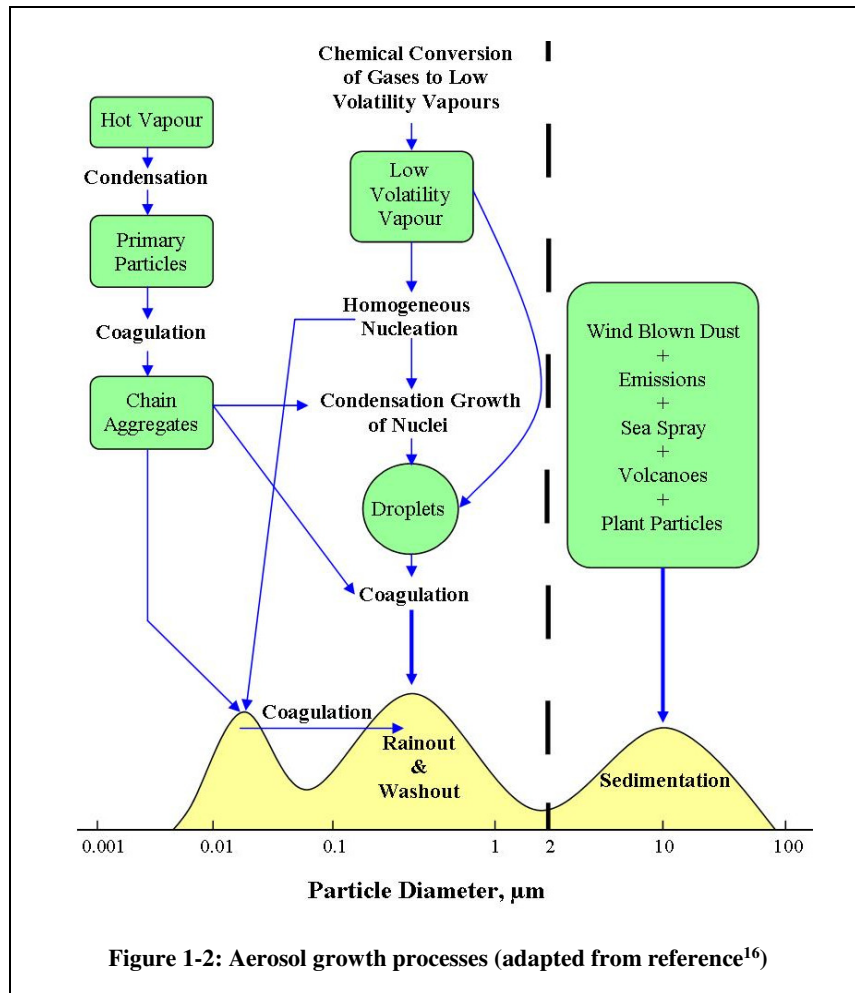
Nucleation occurs in the atmosphere and is the formation of molecular clusters. These clusters have a high number concentration of sub micrometer particulates with a narrow size distribution.[10] The formation of particulate clusters from a supersaturated, low volatility vapour without the assistance of condensation nuclei is known as homogenous nucleation. As well as in the atmosphere, nucleation also occurs when undergoing laser ablation. Fine particulates are generated, due to the laser being fired onto the sample, which then cluster together before forming an aerosol as mentioned previously. Once formed clusters may grow via condensation, as detailed in Figure 1-3. Condensation occurs when other substances such

as low volatility organics and water take part in the growth process.[17] The rate of growth via condensation is controlled by saturation ratio and particulate size.[10] If particulates are formed indirectly through smaller particulates colliding with one another and adhering, it is known as coagulation.[10]

Figure 1-3: Nucleation and condensation of H_2SO_4 and H_2O[17]
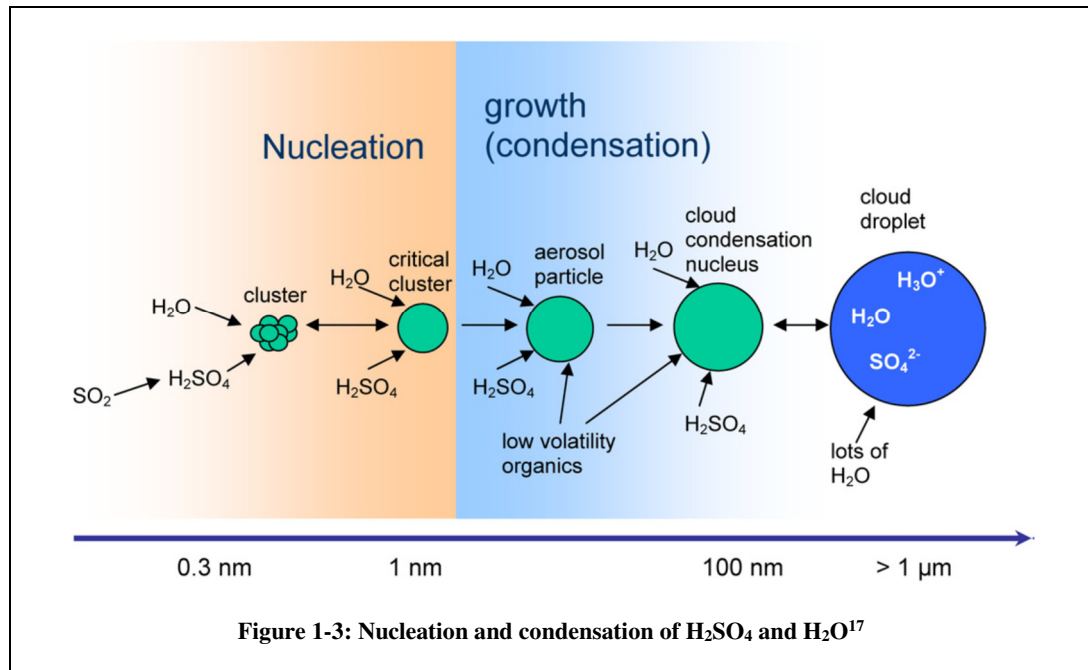
1.1.2 Air Quality

Overview

Air quality is "the measure of concentrations of gaseous pollutants and size or number of particulates."[18] A pollutant is classed as a substance which is present in the environment and can cause negative effects.[19] There are a number of pollutants which are classed as the main foundation of poor air quality in the UK. These pollutants are summarised in Table 1-1 alongside their sources.[20] As the concentration of these and other pollutants, within the atmosphere, and their exposure rates increase so do their effects. There a number of key effects which poor air quality can cause, listed here and further described in Section 1.1.3.

- Damage to human health

- Damage to ecosystems through processes such as acidification, eutrophication and bioaccumulation

- Damage to buildings and materials

- Atmospheric visibility reduction

Pollutant	Primary source/s
Particulate matter	Sea spray, Saharan dust, road transport, quarrying, construction, combustion
Nitrogen oxides	All combustion processes, road transport, industrial processes
Ozone	Chemical reactions between air pollutants
Sulphur dioxide	Combustion of coal and heavy oil
PAHs	Domestic coal and wood burning, fires, industrial processes, road transport
Benzene	All combustion processes, road transport
1,3-butadiene	Petrol combustion
Carbon monoxide	Incomplete combustion of carbon containing fuels, road transport,
Lead	Combustion of coal, iron and steel
Ammonia	Agriculture, such as manure and fertilisers

Table 1-1: Typical UK pollutants and their sources[20]

Currently the most problematic pollutants in Europe are airborne particulates and ozone. The main source of these pollutants is domestic emissions, such as the burning of fuel (coal and wood), however, the transport of pollutants across countries and continents is also a key issue.[21]

Concentrating on particulate matter specifically the total UK emission of PM_{10} in 2001 was 180 kilo tonnes. Road transport and industry, combined accounted for 54 percent of these emissions, with domestic emissions accounting for 17 percent.[22] Although the technology to

reduce emissions from road transport is becoming more advanced this is offset by the increasing number of vehicles which are appearing on the roads within the UK. 23 percent of the emissions from road transport are from tyre and brake wear, with resuspended road dust close behind. Emissions from road transport decreased by 37 percent between 1990 and 2000 indicating a step in the right direction. These road transport particulate emissions mainly consist of elemental carbon and heavy hydrocarbons, however, they also contain metals such as zinc and iron.[22]

In 2010 the annual mean particulate matter concentrations were reported for different air quality stations across Europe. The UK generally reported concentrations which did not exceed the European limits. However countries such as Bulgaria, Poland and Turkey all reported concentrations which exceeded the annual European limit.[21] This indicates that although there are a lot of emissions into the atmosphere from the UK other countries across Europe emit a larger number of particulates on an annual basis. Therefore any abatement procedures put into place in the UK should be utilised across Europe as well.

As seen in Table 1-1, a large number of emissions are generated through industry. As a result of worldwide industrialisation anthropogenic air pollution has seen a dramatic development.[23] This research will focus on the iron and steel making industry, with specific reference to sites in the UK.

Emissions within the iron and steel making industry

Steel is a vital material[24] and is used in the manufacture of many products including vehicles and domestic appliances as well as in the construction and rail industries. It is also recyclable and can be remelted and reshaped into new products when required. Iron and steel, together with coal and cotton were among the principal materials of the industrial revolution and their production has been increasing ever since, especially outside of Europe. There are two routes

to manufacture steel, the integrated steel making route and the electric arc furnace. The integrated steel making route consists of various interdependent processes which allow iron ore to be reduced to iron in the blast furnace and then converted to liquid steel by using the basic oxygen steelmaking process. Electric arc furnaces recycle scrap metal by passing a high voltage electric current through the steel causing it to melt and allowing recasting.[24] The total world crude steel production in 2010 was 1,412 million tonnes, with 627 million tonnes of this produced by China alone.[25] The UK currently has two integrated steelworks, located in Port Talbot and Scunthorpe, and an electric arc furnace, located in Rotherham. These plants are operated by Tata Steel Europe which is currently Europe's second largest producer of steel.[26] UK production in 2012 equated to 9.7 million tonnes with Tata Steel Europe producing 7.3 million tonnes through the integrated process.[27] The integrated steel making process, along with the inputs and outputs of each production unit is shown in Figure 1-4.

Each of the independent processes within the integrated process suffers from its own individual air quality and environmental issues, however, most processes emit particulate matter, sulphur and nitrogen oxides, carbon monoxide and organic micro pollutants. Emissions from the sinter plant account for 50 percent of the emissions from an integrated steelworks[28] and the particulates generated by this process are very fine compared to other dusts emitted from the works.[29] Typical concentrations of these emissions, from a main sinter stack and a blast furnace are listed in Table 1-2.

Emission	Main sinter stack (g/ton sinter)	Blast furnace (g/ton hot metal)
PM_{10}	66.3-177	0.23-25.9
NO_2	302-1031	7.34-194
SO_2	220-973	2.08-2.08
CO	8783-37000	21.5-35.6

Table 1-2: Typical concentrations of emissions from a main sinter stack and a blast furnace[28]

All of these emissions need to be analysed and tested, especially those which are not emitted through stacks, as these are tested on a regular basis. A large proportion of the onsite testing which is completed involves the collection of emissions onto substrates for further analysis, mainly gravimetric, within a laboratory environment. This can delay the rate at which the results are obtained since gravimetric analysis is a very slow process. Some instruments do provide real time analysis, although these can be expensive to purchase so are only generally used for large sampling campaigns. One of the main reasons to analyse and test emissions, produced within the steel industry is to allow compliance with legislation set by the European Union.

Process inputs

Coal

Fluxes, ore fines, coke fines, flue dust, waste material

Pellets, iron ore, sinter, coke, limestone, slag

Mg, CaC, Ca$_2$O, carrier gas, hot metal

Oxygen, hot metal, scrap, lime, fluorspar, coke

Liquid steel, alloys

Liquid steel, alloys and powders

Steel and oils

Coke ovens

Coke   Fluxes   Iron ore

Return fines, sinter plant

Injectants

Blast furnaces

Transfer ladle   Torpedo ladle

Mixer

Basic oxygen furnace

CAS-OB   Ladle furnace   Vacuum degasser   Ladle stirring, alloy injection

Continuous casting

Ingot or casting   Scarfing

Rolling mills

Process waste materials

Dust, CO, H$_2$S, tar, phenol, ammonia, SO$_X$, NO$_X$, cyanide, BOD, SS, PAH, BTX

Flue gases, CO, dust, HCl, SO$_X$, NO$_X$, sulphides, fluorides, heavy metals, PAH, PCDD/F, PCB

Flue gases, sludge, phenol dust, sulphides, cyanides, NO$_X$, H$_2$S, slag

Flue dust, fume, slag

Fume, slag

Sludge, basic slag, flue dust, (high iron content) CO, Zn, fume

Fume, H$_2$, CO$_2$, CO, Mn, Zn, fluorides, slag

Scale, slag, scrap, oil

SO$_X$, NO$_X$, scale, oil, fume, emulsion

Figure 1-4: Integrated steel making process, with inputs and outputs[28]

10

Air Quality Legislation

Air quality legislation was firstly introduced in the twentieth century. Any legislation available before this time was difficult to implement and only regarded smoke abatement from industry, whilst also ignoring any reference to effects on health.[30] The main reasoning for the introduction of legislation and the scientific proof of the potential for atmospheric pollution to cause deaths was the Meuse Valley fog of 1930.[31] The Meuse Valley was an industrialised area in 1930 and for five days in December of that year a thick fog covered a large proportion of Belgium, including this valley. From the third day onwards hundreds of people suffered from respiratory problems and more than sixty people died. Investigations indicated that the symptoms that were experienced by both adults and children were directly due to the excess particulates present within the atmosphere. This fog provided the evidence needed to prove that atmospheric pollution could cause health problems and lead to increased deaths. It also led to the Belgium government appointing a commissioner to asses air quality legislation, however, at that time poor air quality was considered as an "unavoidable consequence of prosperity."[31]

In December 1952, a four day smog covered London and in excess of four thousand people died.[32] The main source of the smog was the burning of bituminous coal which lead to increased levels of black smoke and sulphur dioxide[32] and at that time it was thought that this smog along with increased temperature levels were to blame for the increase in deaths, mostly due to respiratory and cardiovascular complications.[33] Due to this fog, and the influenza epidemic that followed it,[33] clean air acts were introduced to the UK in 1956 and 1968.[34] These acts gave local authorities the power to control the emission of dark smoke, grit, dust and fumes from industrial buildings whilst also declaring "smoke control areas" where the emission of smoke from domestic properties was banned. This meant that coal could no longer be used domestically for the heating of homes and cooking.[34] These acts, along with other clean air legislation were consolidated by the clean air act of 1993 which provided legislative controls.

A large number of countries have now introduced air quality standards which include maximum acceptable concentrations for particulate release and assist in the development and implementation of air quality policies.[35] In the UK, the Environment Act (1995) requires the government to produce a national air quality strategy containing standards, objectives and measures for improving ambient air quality. The first air quality strategy was published in 1997 and since then air quality has generally improved. The most recent air quality strategy was published in 2007 by DEFRA, the UK Department for Environment Food and Rural Affairs. It provides details on air quality, pollutants, current policies and new measures which were expected to be proposed in the coming years.[20]

Since 1970 and the introduction of air quality limits UK PM_{10} values have declined substantially, mainly due to an overall reduction in coal use. A 67 percent overall reduction in emissions was seen between 1970 and 2001.[22] This was helped by standard setting bodies around the world broadly agreeing on a complete set of particulate size selective criteria and using it as the basis for aerosol exposure standards.[36] European air quality limit values for PM_{10} are currently 50 µg/m^3 as a 24hr mean, not to be exceeded more than 35 times per year with an annual average limit of 40 µg/m^3. All these limits are to be reached by 1st January 2015.[21] Consequently the release of PM_{10} is currently under investigation allowing sources to be identified and measures taken to avoid further release of particulates into the atmosphere.[37]

1.1.3 Impacts on Human Health and the Environment

As described in Section 1.1.2 poor air quality can have negative effects on both human health and the environment. If atmospheric particulates, either natural or anthropogenic, enter the respiratory system they can cause severe health problems.[22, 38] Some of these health effects relating to an increase in PM_{10} include increased asthma attacks, attacks of chronic obstructive pulmonary disease, increases in hospital admissions for cardiovascular causes,

deaths from heart attacks, strokes and respiratory causes.[39] In terms of environmental effects, it is almost impossible to perform an industrial activity without emitting dust into the atmosphere,[23] hence, as the amount of industrial activity is increasing so are the effects on the atmosphere.

Health Effects

To enter the respiratory system atmospheric particulates must be of a certain size. The three size fractions known as inhalable, thoracic and respirable are described by the British Standard Institution and the European Committee of Standardisation in BS EN 481[40]. The inhalable fraction can enter the nose and mouth during breathing and deposits within the respiratory tract. The thoracic fraction penetrates beyond the larynx and due to its small size, the respirable fraction is able to enter the gas exchange region of the lungs.[41] The gas exchange region consists of alveoli which have a surface area of approximately 75 m^2 and are covered with more than 2000 km of capillaries. Therefore any particulates which reach the alveoli are able to be absorbed into the bloodstream through this network of capillaries.[10] Figure 1-5 shows the deposition of the three different size fractions within the human respiratory system.

Figure 1-5: Human respiratory system[42]
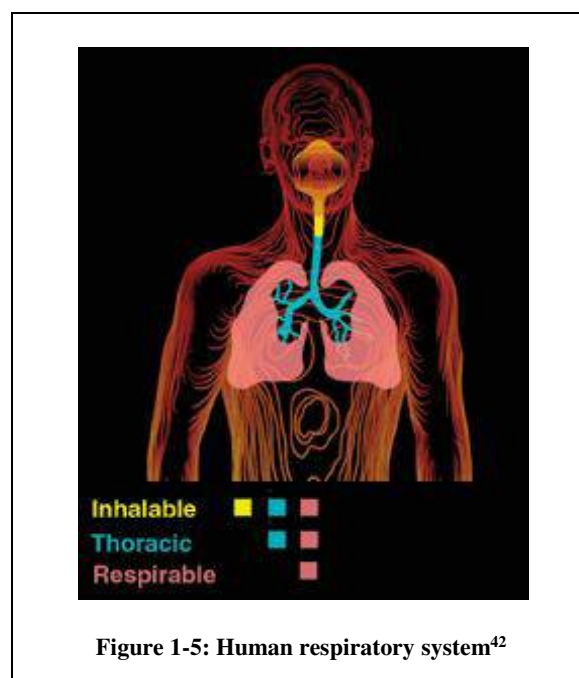
Over recent decades asthma occurrence in children has increased. This may be due to better diagnosis but may also be affected by environmental factors such as pollution.[35] Schwartz[43] carried out research into particulates in the atmosphere and found that exposure to particulates was linked with respiratory disease, specifically chronic bronchitis.[43] Silverman and Ito[44] concluded that warm weather patterns of particulates can affect children with asthma and these have been found responsible for severe asthma attacks.[44]

Although it is expected that particulates would affect the respiratory system, the majority of the effects of increased particulate levels are upon the cardiovascular system. The effects upon the cardiovascular system start with the inhalation of particulates, which can then either cause an inflammatory response or become soluble in the blood and be carried to the cardiovascular system leading to vasoconstriction and thrombosis.[45] Franck et al.[46] studied emergency service calls, in Germany, relating to cardiovascular diseases, for twelve months, whilst also studying particulate exposure levels. They found that increased particulate exposure had a positive association with cardiovascular disease and concluded that in general ultrafine particulates, smaller than 100 nm in diameter, caused the most adverse affects.

Environmental Effects

On a global scale atmospheric pollution is currently increasing[6] and the impacts it has extend from industrialised, highly populated areas to remote regions of the earth.[35] There are three routes which may be used for the entrance of pollutants into the atmosphere. These include planned emission (intended and within regulated limits), fugitive emission (unplanned and due to a leak of fumes) and finally accidental emissions (from accidental valve opening or chemical plant incidents).[8] The most obvious effect these airborne particulates have once emitted is a reduction and distortion of visibility.[35] Pollution has no natural or political boundaries and its harmful effects are likely to continue even if emissions decrease.[35] It can

directly impact the public by affecting health, food supply, building degradation, forests, rivers, coastlines and ecosystems.[8] For example animals feed on plants where particulate matter has fallen. Once present in this first animal, the elements present within the particulate matter can be passed to other animals further up the food chain, resulting in an increase in elemental concentration in other species. Therefore birds of prey have higher elemental concentrations within their system than the organisms which are in close contact with the original particulates. This is known as biomagnification.[5] Pollutants that are of current concern include nitrogen oxide, carbon monoxide, volatile organics and particulate matter.[30]

Particulate sampling techniques, both passive and real time, will now be discussed, followed by an introduction into the generation of particulates in a laboratory environment. The morphological and chemical analysis of particulates, using direct and indirect methods, will then be examined and the overall aims of this work detailed.

1.2 Particulate Sampling

1.2.1 Overview

Sampling is the collection of material from an environment that needs to be characterised. Collected material should represent the overall concentration of the substance being measured and the distribution of the interested substance within the characterised environment.[19] Ambient air measurement of particulate matter is not easy. There are a range of techniques available, however a chosen technique can influence the results gained. The techniques available include both passive samplers, which generally collect particulates onto substrates or filters for further analysis and direct samplers which allow measurements to be taken continuously and in real time.[22] These two sampling techniques, passive and direct are further discussed within Sections 1.2.2 and 1.2.3, respectively.

1.2.2 Passive Sampling

Passive sampling is generally a method used to collect particulates onto substrates or filters, however it may be used to monitor the concentrations of pollutants within the local environment, through biomonitors.[47] One example of a biomonitor, is the accumulation of airborne particulate matter on tree bark, lichens, moss, soil and leaves.[48] The subsequent collection and analysis of these environmental samples may be used to allow a retrospective assessment of air pollution in a particular region.[3]

Tree bark is a useful collector of airborne particulate matter because it is permanently in contact with the atmosphere.[49] A number of studies, which have collected and analysed tree bark, have been completed.[48, 50-52] The first paper regarding tree bark analysis was published in 1974. Ward, Brooks and Reed,[53] based in New Zealand, collected bark, leaf and trunk core samples from a range of trees lining a busy thoroughfare. Background bark samples were obtained from trees that were at least eighty meters from the nearest road. These bark

samples were digested and the respective solutions analysed using an atomic absorption spectrometer to determine the concentration of lead in each sample. Findings showed that concentrations of lead were higher in trees closer to the traffic as well as on the side of the tree facing the traffic.[53]

In 2006, Suzuki[48] collected tree bark from four different locations. Direct analysis of the collected bark was completed using SEM and laser ablation inductively coupled plasma mass spectroscopy (LA-ICP-MS) both of which are described further in Sections 1.2.4 and 1.5.3, respectively. Following direct analysis of the bark samples, Suzuki was able to distinguish between heavy metals which had originated from the atmosphere and other sources.[48]

1.2.3 Direct Sampling

There are many instruments that are able to directly sample particulate matter in real time, including the APS, the SMPS and the ELPI.

An APS measures a particulates aerodynamic diameter in real time as well as using light scattering to provide further information about an aerosols composition. It is able to size particulates between 0.5 µm and 20 µm.[54] 0.5 µm is the base line since the wavelength of light in the visible range is about 0.5 µm. For particulates smaller than this the light scattering is uniform and therefore does not provide reliable data. Particulates greater than 20 µm cannot be characterised since they absorb the light rather than reflecting it, reducing the efficiency of the light scattering measurement.[55] An SMPS charges particulates, separates them, according to their electrical mobility and then counts them. It is able to size particulates between 10 nm and 487 nm.[56] Both of these instruments are manufactured by TSI, High Wycombe, UK.[57]

The ELPI, manufactured by Dekati, Kangasala, Finland,[58] is mainly a direct particulate sampler, however it also works as a passive sampler by collecting particulates onto substrates for further gravimetric and chemical analysis. As a direct sampler it can provide information on number and mass size distributions of particulates within an ambient atmosphere.[12, 59]

First developed in 1992,[59] an ELPI, Figure 1-6, contains thirteen electrically isolated stages which are able to characterise and collect particulate matter between 30 nm and 10 µm.[60] The size range is controlled by the stages and the cut points of those stages are decided by the manufacturer. However this size range allows the characterisation of ultrafine, fine and coarse particulate matter, which is all classed as PM_{10}. Other impactors are available to characterise different size ranges.

Figure 1-6: ELPI schematic[60]
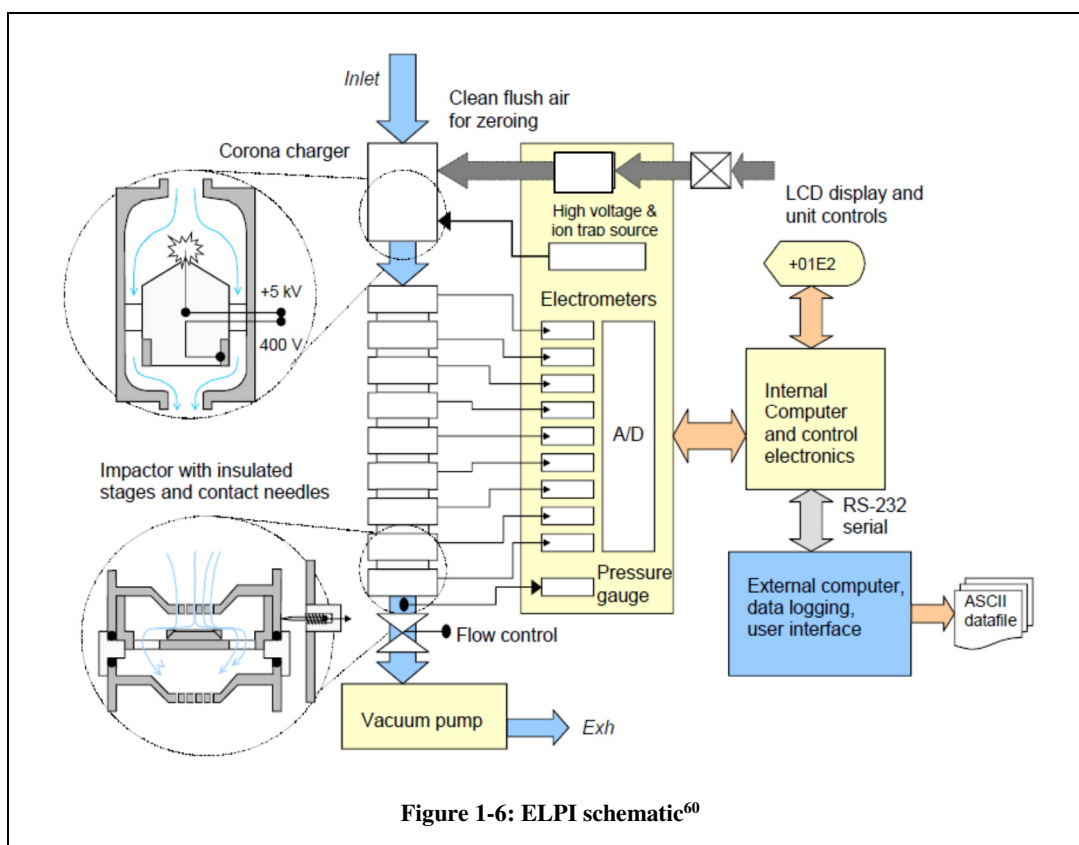
To allow real time characterisation, particulates are charged using a corona charger. The corona charger generates a discharge around a tungsten wire which results in ion production.

Positive ions migrate from the wire and charge the particulates with a known charge. Once charged, particulates enter an electrical ion trap which is used to remove positive ions as well as particulates which are too small to be measured.[61] When charged particulates impact with one of the thirteen electrically isolated stages they are detected and the current is measured using a multi channel electrometer.[59] The process behind impaction is shown in Figure 1-7. Larger particulates impact upon higher stages, whilst smaller particulates impact on lower stages. This is due to the air pressure within the impactor decreasing between each stage, causing particulates to lose momentum and impact upon one of the thirteen stages.[60]
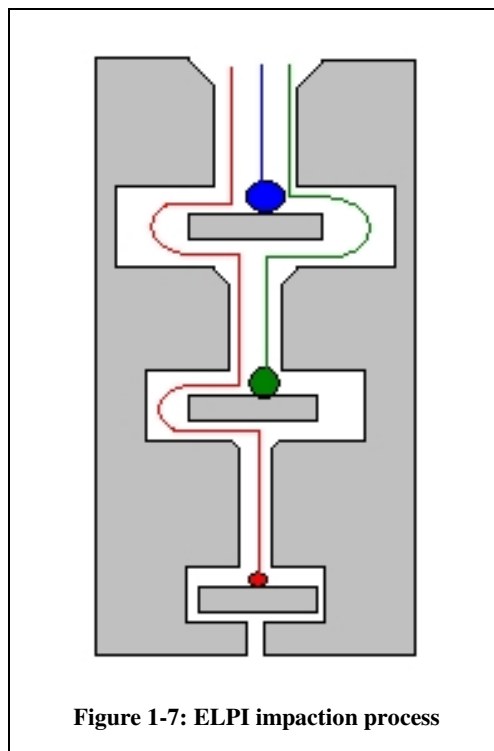
Figure 1-7: ELPI impaction process

Although gravimetric analysis of the particulate holding substrates may be performed, the direct counting of particulates is preferred especially for particulates between 30 nm and 1 µm in diameter. The small size of these particulates means that their weight is miniscule and the accurate weighing of the substrates is a difficult task.

A large amount of research has been carried out into the use of an ELPI for the direct and passive sampling of particulate matter.[62-66] One paper, published in 2009, characterised airborne particulate matter in Sheffield, UK.[66] Using an ELPI, placed on the roof of the

Department of Chemistry at the University of Sheffield, direct sampling of ambient air was undertaken for approximately two weeks. 25 mm polycarbonate substrates were used and these were changed on a daily basis. The substrates were weighed before and after use to allow gravimetric analysis to be undertaken. A bimodal mass size particulate distribution was found with large peaks in particulate mass at 0.32 µm to 0.49 µm and 1.97 µm to 3.12 µm. These results, combined with air mass trajectories, provided information on the sources of particulates within the urban atmosphere of Sheffield.[66]

1.2.4 Scanning Electron Microscopy

If using a passive technique to collect either biomonitors or material onto substrates, one possible way of viewing the specimens at high resolutions is SEM. The first electron microscope was manufactured commercially in 1965 by Cambridge Instruments,[67] however, research into the SEM had been ongoing since 1935,[68] with the main underlying principles first published in 1938.[68] The scanning electron microscope uses a beam of electrons, focused on a small spot to produce an image of the sample of interest.[69] Electrons are generated, typically using a heated tungsten wire, and then accelerated down a column to the sample. The electron beam is rastered over the sample surface and the electrons, either secondary or backscattered, are detected to render the image. To allow the acceleration of electrons onto the sample samples must be conducting, therefore, most samples are coated in gold or carbon before being placed under a vacuum for examination.[67] Quantitative analysis of a sample may also be completed through energy dispersive x-ray spectroscopy. The inner shell electrons in the target materials are displaced by the accelerated electrons to produce characteristic x-rays. The energy of each individual x-ray is then determined and used to generate a spectrum.[70]

Ault et al.[71] completed the single particulate analysis of iron containing particulates collected in an urban environment. Sampling was completed in 2008, 2009 and 2010 in Ohio, USA. Sampling was completed over 25 sites, using polycarbonate substrates in a passive sampler

housing. A large number of particulates, between 29,000 and 53,000 for the three years, were collected and analysed using SEM. The study tended to concentrate on coarse particulates between 1 µm and 10 µm. Images of the particulates were obtained and maps of a number of elements, such as iron, oxygen, aluminium and calcium were generated. It was found that a large number of the particulates were iron containing. This correlated to the industrial sources present within the urban environment, especially since the particulate concentration decreased as the distance from the sources increased.[71]

1.3 Particulate Generation

1.3.1 Overview

Although the sampling of particulates is generally completed outside in an ambient atmosphere, sometimes it is necessary to complete direct sampling in a laboratory environment, allowing the simulation of a particulate containing aerosol. One method to allow this to be completed is the use of a dustiness tester which is normally used to quantify the dustiness of a solid sample. There are currently four methods available to quantify dustiness, the single drop, fluidisation, the continuous drop and the rotating drum sampler.[72] The single drop method drops a given quantity of material, from a defined height, to liberate particulate matter, which is collected onto substrates.[72] The fluidisation method works by spreading a material across a bed of beads and blowing air through it for agitation. This allows particulates to become airborne and be collected onto substrates.[73] The other two methods are standard methods as described in BS EN 15051.[74]

1.3.2 Standard Methods

The continuous drop method involves continuously dropping a material from a sample container down a vertical pipe, with a slow air current. The material is carried by the airflow to the sampling section where different size fractions are collected. Material is dropped at approximately eight grams per minute for ten minutes.[75]

The RDS was developed by Warren Springs Laboratories, funded by the HSE, in the 1990's to simulate the general handling of powdery material. The method was chosen because of its ability to sample moist, dry, coarse and fine samples as well as its continuous rolling action, which simulated the material handling process well.[76] The method generally uses three porous foams which allow the separation of the sample into three size fractions, respirable, thoracic and inhalable, as described in Section 1.1.3 and defined by BS EN 481.[40] 1994 saw

the first use of a rotating drum to establish dustiness indices of twenty three different materials including carbon black, talc and granular fertilizer.[77] Since then the RDS has been used in many different areas of research,[3, 77-81] some examples are briefly described here.

Hjemsted and Schneider, 1996,[82] characterised twenty three materials, including animal feed, talc, insulation and dolomite, using an RDS under standard conditions. They calculated dustiness indices and concluded that the drum was a good method for characterising a range of different materials.[82]

Breum, 1999,[78] studied the variability of the dustiness of six materials using a rotating drum. The six materials were tested in triplicate at four different masses: 25 g, 50 g, 100 g and 200 g. The results indicated that the sample and the mass present had a significant effect on the dustiness indices calculated and in general the dustiness was positively correlated to the mass of material.[78]

Hammelmann and Schmidt, 2005[79] compared the dustiness indices obtained using two different methods, a rotating drum and a single drop tester, to analyse industrial powders such as fumed silica. Differences were found in the results which were obtained from each method and it was concluded that to obtain reliable results the kind of stressing applied to a dust needed to be taken into consideration.[79]

Boundy, Leith and Polton, 2006,[83] developed a miniature RDS, requiring only 10 mg of sample, for occupational health testing of pharmaceutical powders. They concluded that by knowing and understanding the dustiness information of a sample a researcher may be able to select powder formulations with low airborne concentrations for industrial use.[83]

Schneider and Jensen, 2008[81] completed dustiness tests using a combined single drop/rotating drum sampler. 6g of material was used per replicate and materials included

titanium dioxide, zirconia granules, silica, and talc. A fast mobility particle sizer and an aerodynamic particle sizer were used to count and size the generated particles. Reproducible size distributions were obtained for each sample. By combining the two standard methods a new easy method was developed for the characterisation of materials in relation to various handling scenarios.[81]

Tsai et al., 2009,[84] used a rotating drum to determine the dustiness of two nanopowders, titanium dioxide and zinc oxide. A modified sampling train was used to allow number and mass distributions to be obtained from an SMPS and an APS. It was found that very few particles below 100 nm were released from these samples. The study concluded that although the SMPS and the APS were convenient, the measurements may not be accurate due to the morphologies of the released particles.[84]

Pensis et al., 2010,[75] tested a range of industrial minerals using both the RDS and the continuous drop method, as described in BS EN 15051. Materials included feldspar, talc, chalk and marble. The two methods showed that the handling of a material could have an influence on particulate generation. However, by having two standard methods the risks in the workplace could be properly assessed depending upon the handling of a specific material. It was also suggested that the standard (BS EN 15051) be revised as it is currently inadequate for classification and labelling of industrial materials.[75]

Evans et al., 2013[85] developed a novel dustiness testing device for the testing of small quantities of pharmaceutical powders and evaluated it using twenty seven fine and nano scale powders. It was concluded that the novel method provided a more energetic dispersion that other dustiness methods and may be best used to simulate a worst case scenario in a workplace.[85]

1.4 Morphological Analysis

1.4.1 Overview

The shape of particulates can be of critical importance in relation to the respiratory system.[86] One example of this is asbestos, where exposure to asbestos dust can cause a range of fatal diseases such as asbestosis, lung cancer and mesothelioma.[87, 88] Asbestos is a term for materials which occur naturally as fibres and in the mid twentieth century was an indispensible material used in a large range of applications, such as cars, buildings, domestic products and electrical distribution systems. In 1924, Cooke found that inhalation of asbestos dust could cause fibrosis of the lung.[89] This led to a large amount of research into asbestos related respiratory illnesses and a full ban of the use of the material in 1999. Unfortunately due to past exposures death and disease related to asbestos will continue into the foreseeable future.[87] This example indicates the need to characterise particulates and determine their shape. This is especially critical for small particulates since they may have a greater surface area, due to their shape, than larger particulates and they also have an increased chance of penetrating into the alveolar region of the lungs, where more damage can be caused.[86]

1.4.2 Light Scattering Instrumentation

An instrument which used the scattering of laser light to determine the morphology of particulates was first developed in 1992 by Reid, Martin and Clark[90] and was known as the ASAS. By using the light scattered by an individual particulate, shape and size parameters could be derived. The instrument was found to be able to classify spheres, cubes, cylinders and flakes between 1 µm and 10 µm in diameter. A paper published by Kaye et al.[91] expanded upon the paper published by Reid, Martin and Clark[90] and also compared light scattering profiles to SEM images of the same particulates, such as 12 µm silicon dioxide fibres as shown in Figure 1-8. The light scattering profile shown corresponded well with the SEM image, since both the profile and the image indicated the presence of fibres.[91]
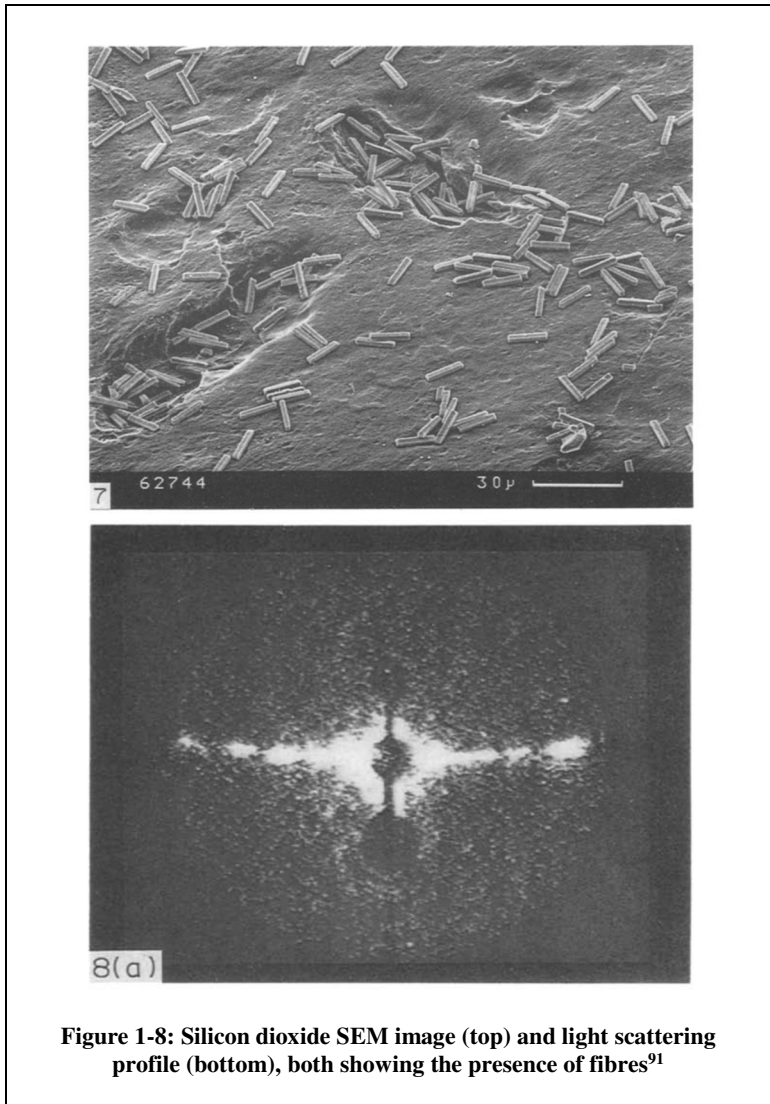
Figure 1-8: Silicon dioxide SEM image (top) and light scattering profile (bottom), both showing the presence of fibres[91]

From 1992, when the use of ASAS technology was first reported, many other papers, as shown in Table 1-3 have gone on to discuss the characterisation of particulates, particularly airborne ones.[92-97] ASAS technology has also been employed by the military since 1995, mainly for biological characterisation of warfare agents.[95] Biological warfare agents are pathogenic organisms which cause disease in humans but are chemically and physically similar to biological particulates naturally present within the atmosphere. By using ASAS technology the direct analysis of particulates could be completed easily in the field.[95] Today ASAS technology is used within an instrument known as the Aspect. The Aspect, which is manufactured by Biral, Bristol, UK, is the only commercially available direct sampling instrument able to determine a particulates shape and size using light scattering.[98]

Author/s	Date	Material/s	Comments
Kaye, Hirst and Micheli[99]	1992	Polystyrene spheres, silica fibres and copper flakes	One of the first papers to use the instrument. They were able to obtain different scattering profiles for each material
Hirst and Kaye[93]	1996	Polystyrene spheres, silica fibres, sodium chloride crystals, copper flakes and asbestos fibres	Compared light scattering profiles to theoretical scattering profiles to allow the first step to be taken in allowing pattern recognition to be completed
Kaye[92]	1998	Asbestos fibres	Used neural networks for classification of fibres
Kaye, Barton, Hirst and Clark[94]	2000	Water droplets, hematite grains, gypsum dust and Bacillus globigii spores	Use of fluorescence, alongside light scattering, to aid in classifying particulates within an ambient aerosol
Secker, Kaye, Greenaway, Hirst, Bartleyand Videen[97]	2000	Deformed liquid droplets and droplets with inclusions	First paper to examine deformed liquid droplets and obtain scattering profiles

Table 1-3: Summary of papers using ASAS technology

1.4.3 Aspect Morphology Analyser

The measurement chamber of the Aspect is illustrated in Figure 1-9. Single particulates are delivered to this chamber with their major axis aligned in a direction parallel to the direction of the air flow. The particulates intersect a laser beam, of wavelength 639 nm and with a beam power of approximately 5 mW,[100] at the primary focus of a lens system causing light to scatter at both high and low angles. If the laser light is scattered at a low angle it informs the instrument of the presence of a particulate and is used to contribute to the size measurement. Light scattered at high angles is collected by the lenses and imaged onto three PMTs, which allow the particulates A_f to be calculated and also help determine the intensity of the scattered light so the particulates size may be established.[100] Particulates between 0.5 µm and

20 µm can be characterised by the Aspect. This range is the same as the APS instrument and the size range is set as this for the same reasoning.[55]

Figure 1-9: Aspect morphology analyser measurement chamber[100]
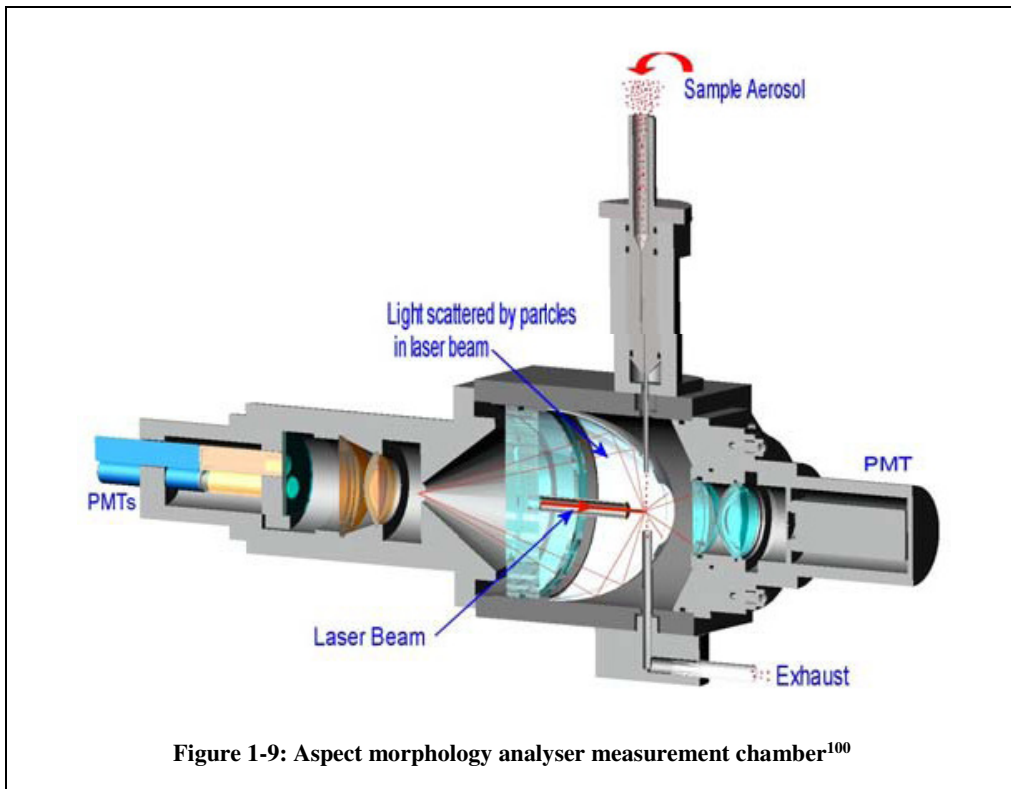
A spherical particle which is symmetrical about all axes passing through its centre would scatter the light with equal intensity to all three detectors, whereas a particulate with an irregular shape, such as an infinitely long fibre, would scatter light in unequal amounts to the three detectors. The ratio of light detected is used to define the asymmetry factor for these irregular particulates. An asymmetry factor of zero indicates spherical particulates, such as polystyrene spheres, whilst an asymmetry factor of one hundred indicates fibrous particulates, such as asbestos fibres.

1.5 Chemical Analysis

1.5.1 Overview

The chemical analysis of particulates is important since it allows both major and trace elemental concentrations to be determined. This is important since elements can cause damage to the environment, buildings and food sources as well as affecting the health of the general public. For particulates which are contained within an aerosol this is particularly important as, once airborne, particulates may travel over thousands of kilometres, affecting the air quality of another town or even country.[8] The detailed analysis of aerosols containing metallic particulates is vital to allow a better understanding of these particulates in the atmosphere.[101]

There are two general categories which chemical analysis techniques can fall into. The first is indirect chemical analysis, usually completed in solution, and direct analysis, usually of solid materials. If both types of analysis can be completed upon a sample the data provided can be indispensable.[101] Indirect and direct chemical analysis will be discussed separately and techniques which fall into each of the categories summarised.

Firstly a number of key concepts used within analytical chemistry will be described.

Precision -   the ability of a measurement to be consistently reproduced

Accuracy -   the ability of a measurement to match the actual value of the quantity being measured

Sensitivity -   the ability of an analytical instrument to respond to a change in elemental concentration

Limit of detection -   smallest amount of detectable material within a matrix, calculated using three times the standard deviation (3σ)

1.5.2 Indirect Chemical Analysis

Indirect analysis generally requires a sample to be in a liquid form rather than a solid. Therefore one of the key steps to allow indirect chemical analysis to be completed is to first digest the solid samples to break them down into their basic constituents,[102] generally using high temperatures and possibly high pressures. For effective digestion a solid sample must be completely dissolved and all of the elements of interest released into solution.[103] Once this has been completed analysis of the digestion solution may be carried out. There are a large range of techniques available for indirect chemical analysis including atomic absorption spectroscopy, ion chromatography and mass spectrometry. This chapter as well as following chapters will concentrate on ICP techniques, such as ICP-atomic emission spectroscopy (ICP-AES) and ICP-mass spectrometry (ICP-MS).

The indirect chemical analysis of particulate matter generally involves sample collection followed by subsequent analysis. It can be a rather slow process which is labour intensive. The sampling and transportation of samples can also lead to chemical transformations of constituents, or loss of volatile compounds.[11] However, a range of off line analytical techniques, such as ICP and also SEM, can be invaluable in determining chemical compositions and particulate sizes and morphologies, respectively, as well as obtaining reproducible information.[104]

Acid Dissolution techniques

A range of acids may be used for sample digestion, and acid selection should be based upon the characteristics of the sample which is to be digested.[105] Commonly used acids include hydrochloric acid, nitric acid, hydrofluoric acid, sulphuric acid and perchloric acid.[106] These acids, along with hydrogen peroxide, can be used in a range of mixtures, some examples are shown in Table 1-4. Aqua regia, sometimes used for sample digestion, is a 1:3 ratio of concentrated nitric acid to hydrochloric acid. Nitric acid acts as an oxidant to decompose any

organic matter whilst hydrochloric acid is generally used for samples with inorganic matrices and is able to improve the quality of the digestion.[107] When these two acids are mixed to form aqua regia they react to form chlorine and nitrosyl chloride, which are very strong reducing agents.[108]

$$3HCl + HNO_3 \rightarrow 2H_2O + NOCl + Cl_2$$

For a large number of samples it is ideal to use hydrofluoric acid[106] to allow the full digestion of silicates and elements which may remain trapped within the silica matrix.[105] Due to the safety precautions needed when using hydrofluoric acid it is not used for all digestions.

Author/s	Year	Material	Technique	Acids
Knechtel and Fraser[109]	1979	Environmental Samples	Hot blocks	HNO_3 and H_2SO_4
Rodushkin, Ruth and Huhtasaari[110]	1999	Plant material	Hot blocks	HNO_3
			Microwave	HNO_3 and H_2O_2
Sastre, Sahuquillo, Vidal and Rauret[111]	2002	Environmental samples	Hot blocks	Aqua Regia
			Hot blocks	HNO_3
			Microwave	HNO_3, HF and $HClO_4$
			Microwave	HNO_3, H_2O_2, H_2O_2 and $HClO_4$
Lo and Sakamoto[112]	2005	Marine sediments	Microwave	HNO_3 and HF
			Microwave	Aqua regia and HF
Recommended by CEM[113]	2009	Iron ore	Microwave	HCl, H_2O, HNO_3 and HF

Table 1-4: An example of acid mixtures used for digestion

The three most typically used digestion techniques are hot blocks, a hot plate and a microwave. Hot block and hot plate digestion allows good control of temperature[102] and high sample throughput,[111] whereas microwaves are claimed to give increased precision[102] and

allow volatile elements to be digested.[111] Microwaves are also closed systems, compared with hot block and hot plate which are open, so can therefore withstand higher pressure. This permits higher temperatures to be achieved with greater digestion efficiency. Rodushkin, Ruth and Huhtasaari[110] compared the use of a microwave and hot blocks for the digestion of plant material, such as seeds, bark and pine needles. Different procedures were applied to the two techniques, however the digestion solutions were analysed using the same ICP-AES and ICP-MS instruments. Similar elemental concentrations were achieved between the two procedures, both with good precision. Rodushkin, Ruth and Huhtasaari concluded that both techniques were able to successfully digest material that is to be analysed using ICP and that only the experiments individual needs should be taken into account when choosing between them.[110] Once fully digested, samples may be analysed using techniques such as ICP-AES and ICP-MS.

Inductively Coupled Plasma Spectrometry

The ICP is a versatile high temperature discharge which may be used as an excitation and/or ionisation source for elemental emission and elemental mass spectrometry.[114] The ICP uses a highly ionised electrically neutral gas, normally argon, which is capable of heating aerosols to temperatures of approximately 7500 K to produce a plasma which excites and ionises the liquid sample's elements.[114] Both ICP-AES and ICP-MS produce an argon plasma in the same way but differ in the way they utilise the plasma and collect and analyse resultant sample ions.

The ICP was first developed in the 1960's, sixty years after the first studies into time resolved optical emission spectroscopy were reported.[115] Reed[116] first completed pioneering work into radiofrequency plasma generation in 1961. The generation of stable plasmas using inductive coupling was investigated and an electrodeless torch which could be used with a range of gasses at high temperature was described.[116] Following this research the use of a

plasma as an excitation source, for trace element analysis, was investigated independently by both Greenfield, Jones and Berry[117] and Wendt and Fassel.[118] They both went on to separately complete preliminary work into the use of high pressure plasmas and each group described different designs of plasma torches, which are both still in use today. Greenfield, Jones and Berry's torch differed from the one described by Wendt and Fassel as they used a stream of argon gas to cool the torch. Finally in 1974, Scott, Fassel, Kniseley and Nixon developed an ICP-AES system for the determination of trace metallic elements in solution.[119] Following this, in 1978, Houk[120] considered the possibility of interfacing a mass spectrometer to a plasma torch to demonstrate the feasibility of ICP-MS for trace elemental analysis of solutions.[120] This was successful and the instrument was produced commercially by Sciex in 1983. In order to analyse a liquid sample it must firstly be transformed into an aerosol. The flow of the sample to the plasma, generated by the plasma torch, must be consistent and this is achieved by using a specialised sample introduction system,[121] as illustrated in Figure 1-10. The sample introduction system consists of three stages, the peristaltic pump, the nebuliser and the spray chamber.

- Firstly a peristaltic pump draws the sample from a sample container using the peristaltic action to feed a sample to a nebuliser at approximately 1 mL/min.[122]
- The nebuliser forms the aerosol which consists of liquid sample droplets, suspended in argon, from approximately ten to hundreds of micrometers in diameter.[122] This generated aerosol passes to a spray chamber which connects the nebuliser to the plasma torch.
- The spray chamber is required to remove any excessively large droplets from the argon gas stream,[114] since the argon plasma is unable to excite droplets which are larger than approximately twenty micrometers in diameter. The spray chamber has a double pass configuration which directs fine aerosol to the plasma[117] and large droplets to a waste container.[114]

The argon plasma is formed inside a quartz torch. The torch consists of three concentric tubes for three separate argon flows. The first tube, tube one in Figure 1-10, is used to carry argon, at a flow rate of 12 L/min to form the plasma. The second tube, tube two in Figure 1-10, carries the auxiliary gas which supports the plasma and allows the height of the plasma to be changed. The third tube, tube three in Figure 1-10, carries the sample aerosol up to the plasma. Once the aerosol reaches the top of the tube it punches a hole or channel through the plasma where the sample constituents in aerosol form become ionised through collisions with excited free electrons.[121, 123] At the top of the torch, to form and sustain the plasma, there is an induction coil which is connected to a radio frequency generator.[124] When radio frequency power is applied to the coil an alternating current oscillates within it, producing heat. When argon gas is passed through the torch and a high voltage spark applied to it, argon ions and free electrons are formed resulting in a high temperature plasma.[123]

Figure 1-10: Nebuliser, spray chamber and torch set up for both ICP-AES and ICP-MS[125]
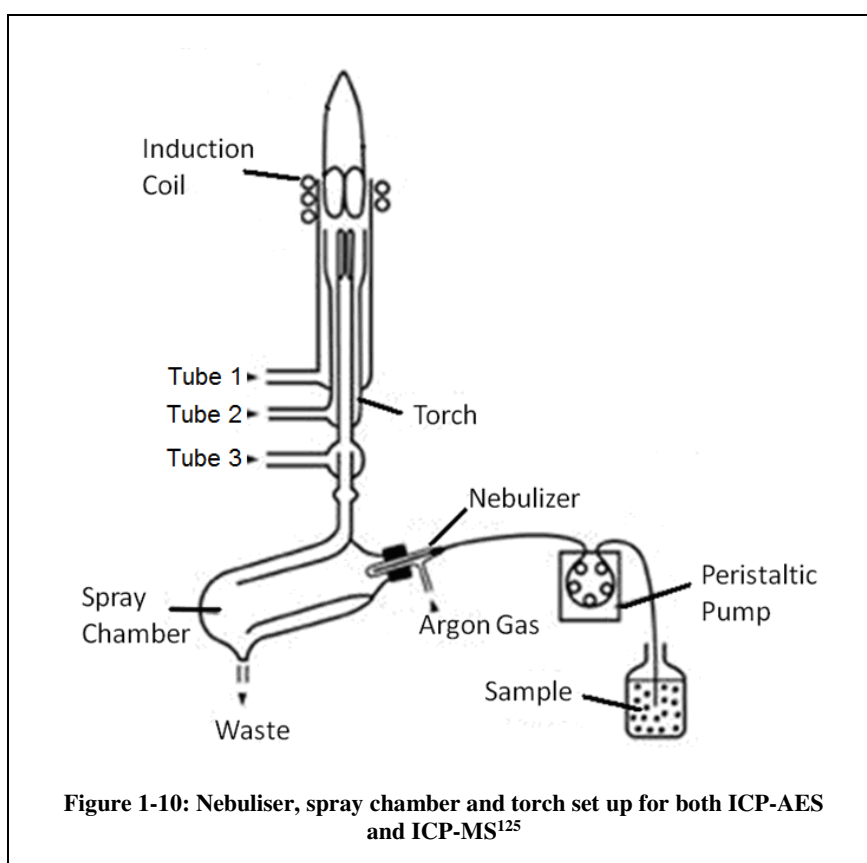
Atomic Emission Spectroscopy

Spectroscopy is defined as "the interaction of light and matter". By using emitted, absorbed or scattered light the elemental concentration of a species in a particular system can be determined.[126] Atomic emission spectroscopy uses the emission of light radiation and generally involves three main steps, atom formation, excitation and finally emission. In terms of ICP-AES atomization and excitation occur within the plasma. The aerosol, generated by the nebuliser and spray chamber, punches a channel through the plasma and is converted into a gas. Any gas phase bonds are broken so that only the ground state atoms remain. These atoms collide with free electrons within the plasma causing the atoms to be excited from their ground states. Once excited the atoms relax back down to their ground state and emit electromagnetic radiation, generally with a wavelength of between 120 nm and 900 nm. This emission is then separated by a diffraction grating into a spectrum and detected using CCDs.[126] Charge coupled devices measure the intensity of the emitted light according to its wavelength.[127] Each atom emits radiation with a specific wavelength. The intensity of the radiation which is emitted at an element's precise wavelength is proportional to the concentration of that element within the sample.[114] Figure 1-11 details the processes that take place in the ICP, as well as the excitation and relaxation of the atoms.

Figure 1-11: ICP processes and excitation and relaxation of atoms[128]
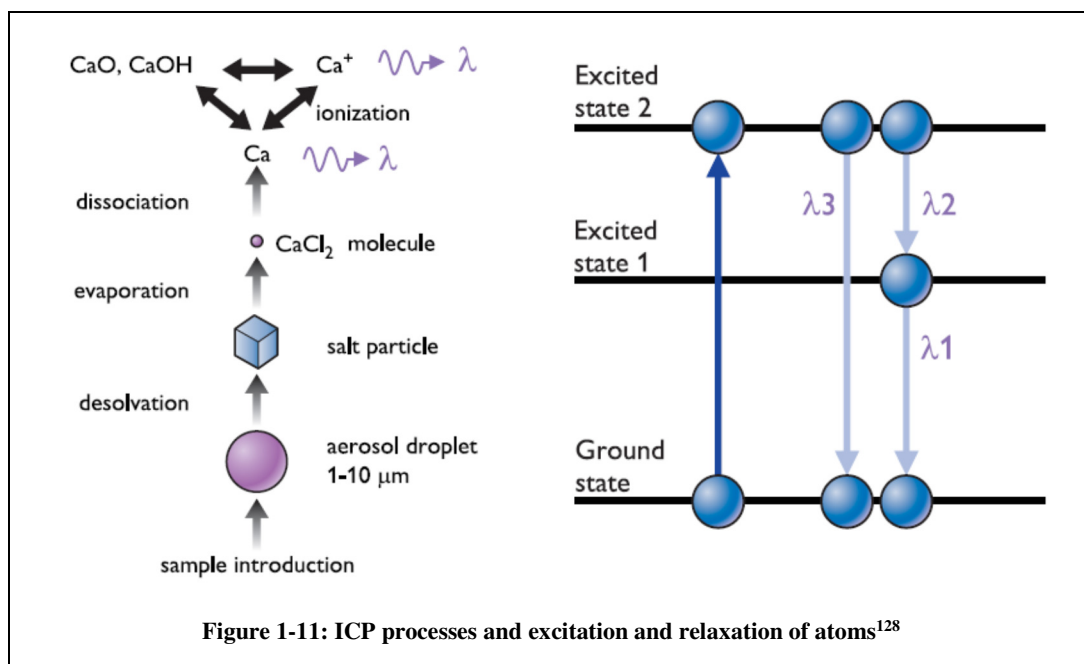
ICP-AES is capable of detecting elements with concentrations as low as µg/L.[126] However the results can be subject to interferences. Interferences are chemical or physical processes which can affect the measurement of a samples elemental concentration. One of the main types of interferences associated with ICP-AES is spectral interferences. This is when two or more elements within a sample emit radiation at the same wavelength. One example is copper and argon which emit radiation at 515.323 nm and 515.139 nm, respectively. To allow the detection of elements which encounter spectral interferences other wavelengths should be used since most elements emit radiation over a number of wavelengths. Another type of interference associated with ICP-AES is the formation of ions for elements such as iron, Fe and Fe^{2+}. Each ion has its own emission spectra and therefore the wavelengths for the ion of interest must be known.[126]

Mass Spectrometry

ICP-MS is a technique with a detection power better than that of ICP-AES. It can detect elemental concentrations as low as ng/L.[129] A schematic of an ICP-MS, manufactured by Agilent, is shown in Figure 1-12.
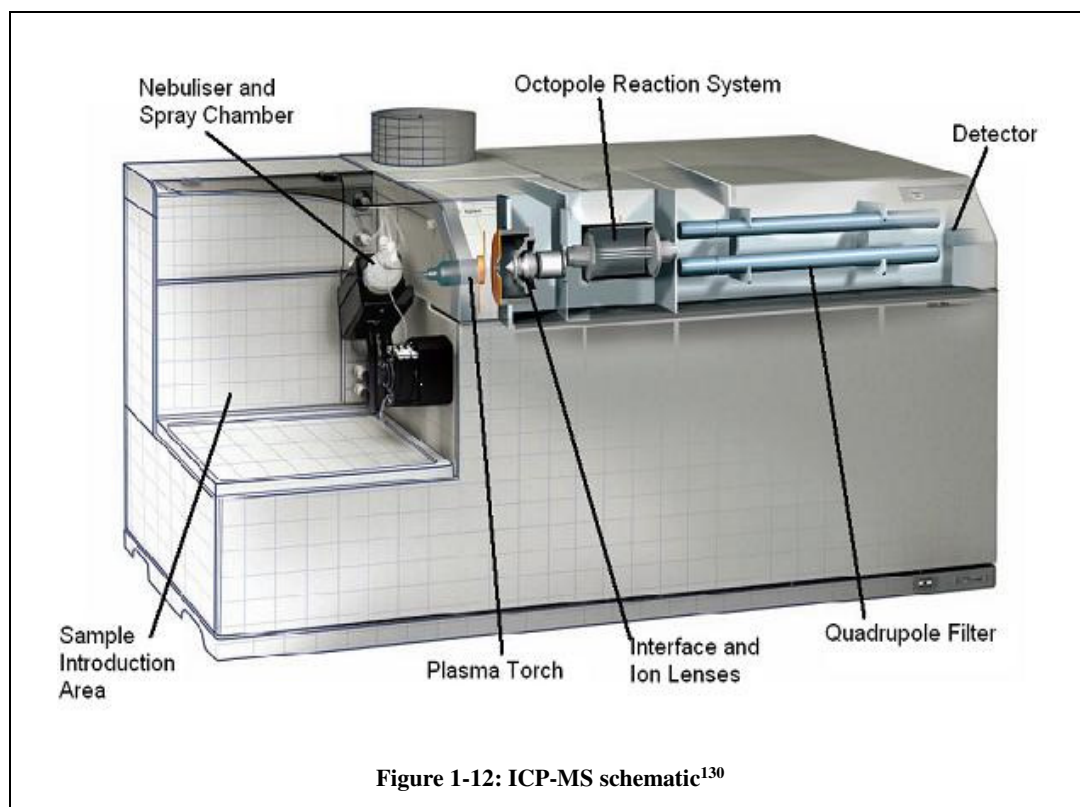
Figure 1-12: ICP-MS schematic[130]

As mentioned previously, the sample introduction is the same as for the ICP-AES, but it is not unusual to use a horizontal torch rather than a vertical one. This allows the instrument to be more streamline for bench top use and tends to offer lower limits of detection.[126] In a similar way to ICP-AES the plasma within the ICP-MS atomises and ionises elements, to generally produce positively charged elements, however it is how the ions are sampled that differs. Rather than returning to their ground state the ions are directed into the mass spectrometer, where they are analysed. There are number of steps to this analysis, each described here.

Firstly the ion bearing plasma is sampled and extracted into the interface region. The interface region consists of two cones, the sampler and skimmer, which can be made from platinum or nickel, depending on the elements of interest, and cooled by water.[114] They are under a vacuum of around 266 Pa. The sampler cone is the closest to the plasma and has an orifice of 0.8 mm to 1.2 mm. The second cone, the skimmer, is located behind the sampler cone and has an orifice of 0.4 mm to 0.8 mm. Once through the cones the ions are focused by the ion lenses. The main role of these lenses is to ensure than only ions pass through them to the next stage of detection and any matrix components and non analyte species are rejected. The lenses are placed in series and have a voltage applied to them, allowing only positively charged ions through to the mass separation device or quadrupole.[131] A quadrupole separates ions based on their mass/charge (m/z) ratio.[127] It consists of four concentric rods which operate at a frequency of two to three megahertz. They are approximately 1 cm in diameter and 15 cm in length. A direct current voltage is applied to one pair of the rods whilst a radio frequency voltage is applied to opposite pair. By varying this voltage, ions of a selected mass can pass through the quadrupole into the detector. Ions of other masses will pass in between the rods and not reach the detector.[132] The detector within an ICP-MS is an electron multiplier. Once a positive ion hits the detector electrons form. These electrons

strike onto other areas of the detector generating more and more electrons which are detected by a multichannel analyzer to produce a spectrum.[133]

As with ICP-AES, ICP-MS can also encounter interferences. There are two common types of interferences with ICP-MS, non-spectral and spectral. Non-spectral interferences include matrix interferences, high mass elements affecting the signals of low mass elements and easily ionised elements, e.g. Na and K, being preferentially ionised and thus reducing the plasma temperature.[134] Spectral interferences tend to be more serious than non-spectral.[135] They originate from mass overlaps of elements with oxides or polyatomic ions. One of the most common spectral interferences is overlaps of argon or argon containing species with other ions with a similar spectrum. For example $^{40}Ar_2^+$ interferes with ^{80}Se and $^{40}Ar^{16}O^+$ interferes with ^{56}Fe.[114] A full table of interferences was published by Atomic Spectroscopy.[136]

To allow spectral interferences to be eliminated octopole collision/reaction cells are commonly used in ICP-MS. They use ion-molecule collisions and reactions to clear the ions of polyatomic and molecular interferences. As shown in Figure 1-11 an octopole cell is placed between the ion lenses and the quadrupole and can be used with two gasses, helium and hydrogen.[135] Helium is used in the collision mode and removes polyatomic interferences by converting them into non-interfering species. Hydrogen is used in the reaction mode and removes intense peaks formed by the plasma such as Ar^+ and ArO^+. The reactions are both exothermic and have high reaction efficiency with polyatomic interferences, allowing them to be removed with ease.[137] The two reactions used are

$$\text{Hydrogen atom transfer: } M^+ + H_2 \rightarrow MH^+ + H$$

$$\text{Charge transfer: } M^+ + H_2 \rightarrow M + H_2^+$$

High resolution ICP-MS can further reduce and possibly eliminate interferences using a magnetic sector to separate and focus the ions. It is the most powerful ICP-MS technique

available. However these instruments are very expensive and are a lot more complex to operate than quadrupole ICP-MS instruments. Therefore this study will not use high resolution ICP-MS.

A large amount of research has been completed individually using ICP-AES[6, 37, 138, 139] and ICP-MS[111, 140-142] alongside research which has compared both techniques.[143] Rommers and Boumans,[143] completed an assessment of the two methods and reviewed the positives and negatives for each technique. They found that ICP-AES was a more rugged and adaptable technique which is greatly used in analytical chemistry, whilst ICP-MS tends to be more suited to ultra-trace and survey analysis. It was also mentioned that on their own neither method could fulfil all of an analytical chemists requirements and that they supplemented and complemented each other well.

Although ICP instruments are generally simple to operate[16] due to the techniques ability to analyse samples at very low concentrations, contamination can be an issue. Therefore for solid samples direct analysis may be a preferred technique to indirect analysis.[12]

1.5.3 Direct Chemical Analysis

Direct analysis often requires minimal sample preparation, if any, and allows specific areas of interest on a sample to be analysed. When compared with indirect analysis, direct analysis reduces the risk of contamination as well as the sample volume required for analysis. It can also be used to characterise inclusions which may have been introduced through manufacturing processes.[144]

The direct chemical analysis of particulates allows them to be collected and then characterised almost instantly.[104] It also allows in situ sample information to be obtained in real time and continuous emission monitoring to be completed[145] without involving any sample handling.[146] Nore, Gomes, Bacri and Cabe[38] developed apparatus for the on line, real

time monitoring of metallic concentrations in aerosols to determine air quality. The apparatus involved the use of a plasma to atomise, excite and ionize metallic elements and a high throughput pump for sample introduction. This research allowed the direct detection of metallic atmospheric pollutants to be completed.[38] Timmermans, de Groote, Jonkers, Gamero, Sola and van der Mullen[145] developed an on line diagnostic measurement system for the analysis of elements in combustion gases. Elements analysed included calcium, chromium, copper, iron, manganese, lead, titanium and zinc. The use of ICP was originally investigated but due to its inability to detect low concentrations, a microwave induced plasma torch was used instead.[145]

There are a number of direct analysis techniques available including XRF, LA-ICP and LIBS. The second two, LA-ICP and LIBS, involve the use of lasers and will be described here. However lasers and their interaction with material will be first be introduced and discussed.

Lasers

Laser is an acronym of 'light amplification of stimulated emission of radiation'. Lasers were first developed in the 1960s and quickly came to the attention of analytical chemists who saw the potential for their use in direct analysis. They are capable of generating coherent, collimated and monochromatic pulses of energy which have a very short duration and a specific wavelength.[147] Table 1-5 lists a number of typical lasers, alongside their wavelengths.

Laser	Wavelength	Comments
Nd:YAG	1064 nm	Most common laser, used in a very wide range of applications
Ruby	694 nm	First laser used for ablation, used in tattoo removal
ArF	193 nm	Used in medical applications and semiconductor manufacturing
Ti: Sapphire	700 nm-1000 nm	Used in spectroscopy

Table 1-5: Examples of different lasers and their applications[147-150]

Stimulated emission is the emission of a photon from an excited state. All photons which are emitted have the same frequency and if more photons are present more will be stimulated to be formed. To allow stimulated emission the excited state must be metastable and a population inversion is also required.[148] This means that more molecules, over 50 percent, must be present in the upper state than the lower state to allow stimulated emission to occur.[147] A large number of ablation systems use Nd:YAG lasers, since they are generally cheap and easy to maintain, and this chapter will focus on these lasers. Nd:YAG lasers are neodymium doped yttrium aluminium garnet rods a few millimetres in diameter. They operate at 1064 nm, however their frequency may be doubled (532 nm) or quadrupled (266 nm) depending on the wavelength required.[147] Nd:YAG lasers are four level lasers, with two levels between which the radiation is emitted.[147] Using an intense flash of light molecules are pumped from the ground state to the intermediate state which gives up some of its energy to change into a metastable state and causing a population inversion. As the molecules then drop to the lower state photons are emitted, resulting in laser action. The molecules then return to the ground state quite quickly, keeping the population inversion between the metastable state and the lower state.[148] Photons emitted can have wavelengths ranging from ultraviolet to infrared depending of the laser used.[147] This is illustrated in Figure 1-13.

Figure 1-13: Transitions in a four level laser (Adapted from [148])
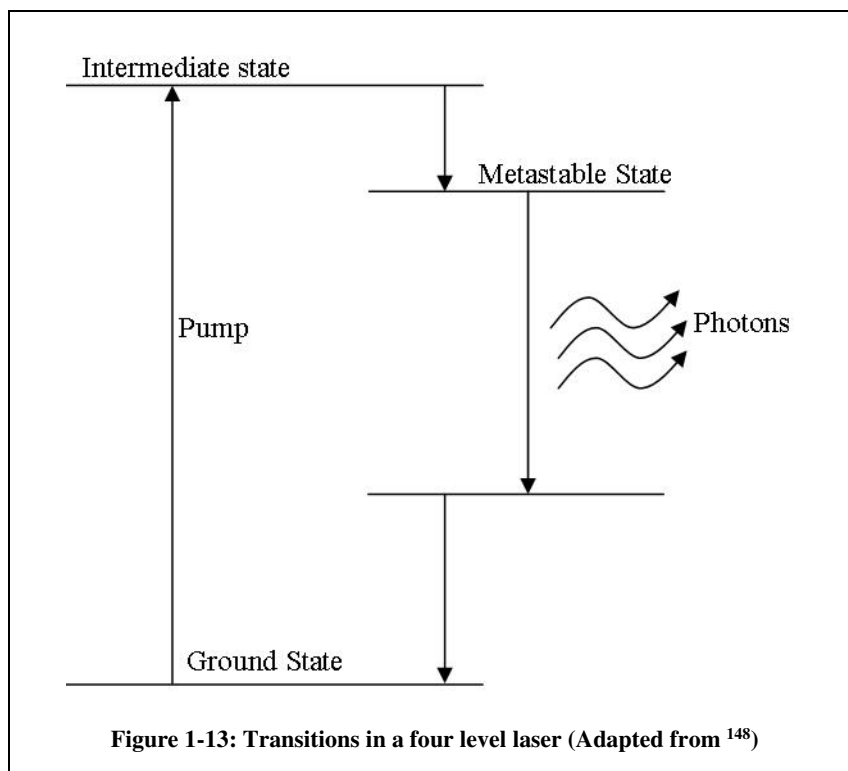
Laser Material Interaction

Before discussing the two laser based, direct analysis, techniques in detail the mechanism behind the interaction of a laser with a material will be discussed. Understanding the mechanism behind the laser material interaction is vital to applying lasers for chemical and physical analyses.[151] The main process which occurs is the excitation of electrons to their excited states by the absorption of the photons generated through stimulated emission.[152] These electrons as well as positive ions and neutral monomers, form negative ions, through charging, and neutral dimers by coagulation. These go on to form clusters and particulates through further charging and coagulation.[153] This is shown in Figure 1-14. The solid sample can also melt causing it to eject molten material from the crater generated on the solid's surface.[154] This molten material as well as the clusters and particulates should be representative of the ablated material and analysing them should provide an insight into the chemical and physical properties of the material.

Figure 1-14: Particulate formation in a laser ablation plasma (adapted from reference[153])
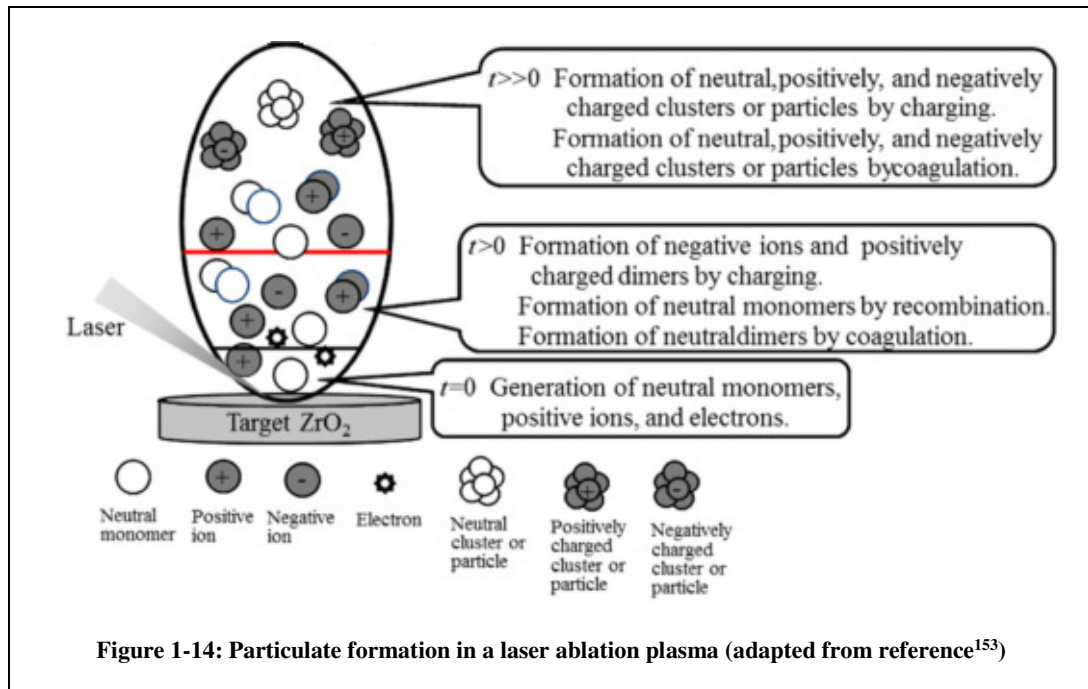
The number of particulates that are generated as well as their physical characteristics can depend upon the way that the laser has interacted with the ablated material. This can be down to a number of factors such as the fluence of the laser, the wavelength of the laser, the atmosphere the ablation is completed in as well as the properties of the material itself, such as melting point, brittleness and thermal conductivity.[149, 155]

Laser fluence is a measure of the energy (in Joules) delivered per unit area (in cm^2). The equation for calculating laser fluence[156] is

$$\text{Fluence (Jcm}^{-2}) = \frac{\text{Laser pulse energy (J)}}{\text{Focal spot area (cm}^2)}$$

Brygo et al.[157] investigated the effect of laser fluence on laser ablation in 2006. A Nd:YAG laser, with a wavelength of 532 nm was used with a laser fluence of 0.1 Jcm^{-2} to 5 Jcm^{-2}. Epoxy grey paint on concrete, with a thickness of greater than five hundred micrometers was ablated and the effect the ablation had on the crater examined. Brygo et al. found that the removal of paint like material from a solid sample could be achieved at a low fluence. If a deep crater is required then a higher fluence should be used.[157]

Chan and Russo[151] discussed the characteristics of laser material interactions monitored by ICP-AES. A KrF laser with a wavelength of 248 nm was used to ablate copper and brass samples. They found that the laser sampling of metals generated a large number of particulates ranging from 1 µm to 10 µm in diameter, with particulates below 2 µm accounting for 90 percent of the number but only a small percent of the total particulate mass. Chan and Russo also discussed the effect of a samples composition on the particulate size distribution, stating that for a brittle material with a low thermal conductivity the changes in distribution are expected to be more significant than when ablating ductile, high thermal conductivity materials. They concluded that laser material interaction involved complex processes where the number of particulates generated and their size distribution could change with laser fluence.[151]

Laser Ablation ICP Spectrometry

Laser ablation, when used as a sample introduction system for ICP, is considered as a "well accepted analytical technique for in situ trace element analysis".[158] It allows the generation of a particulate containing aerosol from a solid sample. Generally this aerosol is carried to an ICP-AES or ICP-MS, using argon as a carrier gas and, skipping the nebuliser and spray chamber, punches a channel straight through the plasma. LA-ICP allows minimal sample preparation[159, 160] as well as retention of a sample since only its surface is ablated. Gray[161] first discussed the use of laser ablation as a sample introduction method for ICP-MS in 1985,[161] however work had been carried out into the use of laser ablation with ICP-AES previously to this by Thompson, Goulter and Sieper in 1981.[162] A laser ablation system consists of a laser and an ablation chamber, which is connected via tubing to an ICP. A schematic of LA-ICP-MS is shown in Figure 1-15.

Figure 1-15: LA-ICP-MS schematic[163]
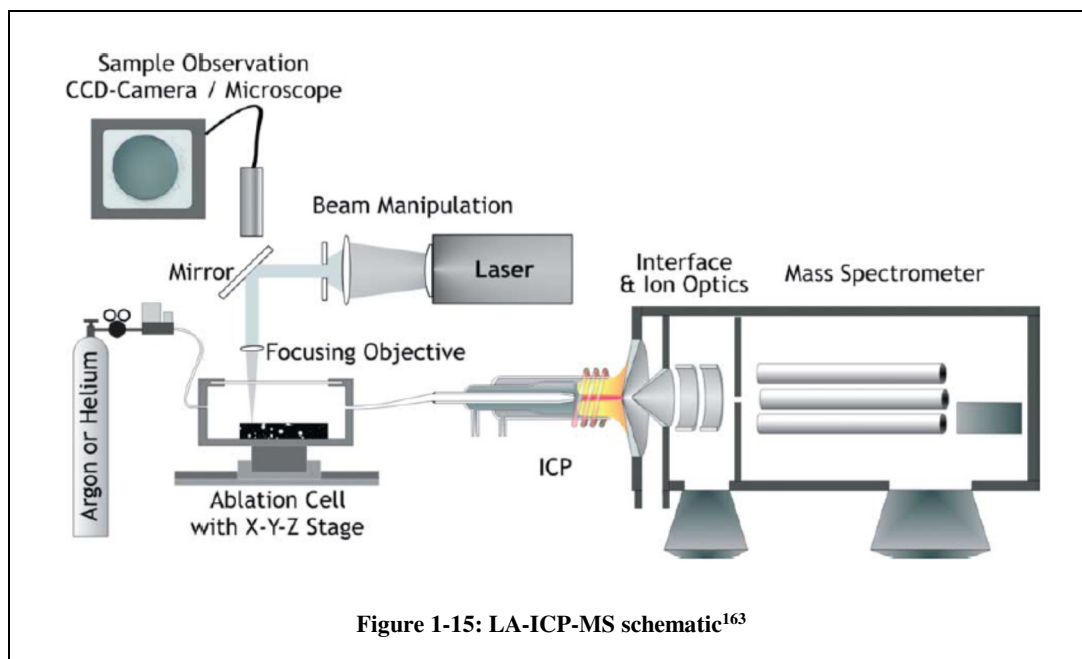
For ablation, a sample is placed into the air tight ablation chamber. Ablation chambers tend to make use of an adjustable stage to allow the focusing of the laser onto the sample. They also have a camera to allow the easy positioning of the sample within the chamber. The chamber is flushed with argon gas to allow an inert atmosphere and also to carry the generated particulates to the ICP.[144] Once the sample has been positioned and the laser beam focussed onto the sample the laser is fired. The laser converts a proportion of the solid into a particulate containing aerosol, allowing transportation to the ICP in the argon gas stream.[144]

Ishibashi[164] completed the ablation of eighteen steel reference materials, using LA-ICP-AES with a Nd:YAG laser. It was found that LA-ICP-AES gave more accurate results than spark emission methods and Ishibashi concluded that the technique was effective for rapid analysis.[164]

LA-ICP-MS lends itself to a wide range of applications ranging from the analysis of inclusions in steel[165] to the imaging of biological tissue.[166-170] An application of particular interest to this research is the analysis of atmospheric particular matter.[23, 171, 172] This requires the collection of samples onto substrates, which are then rapidly ablated and chemically

analysed for a variety of elements. Tanaka et al.[159] investigated the simultaneous multi-element analysis of atmospheric particulate matter using LA-ICP-MS. A method was developed for the analysis of trace metals in particulate matter which has since been successfully applied in Japan.[159] Research has also been carried out in Sheffield, the UK's fourth largest city, by Chung et al..[173] The overall objective of this research was to characterise airborne particulate matter in a city environment. Substrates were collected over a seven month period. The elemental composition of the particulates was determined by LA-ICP-MS and a number of samples were traced back to the metallic elements used in the iron and steel industry. SEM analysis was also completed to determine the characteristics and morphology of individual particulates, therefore providing an insight into the sources of the particulates.[173] Hsieh et al. completed investigations into the elemental composition of airborne particulates.[63] An ELPI was used for the collection of particulates onto PTFE substrates followed by the use of LA-ICP-MS for substrate analysis. Alongside the ELPI another air sampler was used to collect coarse and fine PM onto two substrates which were digested in acid and their elemental concentration analysed by solution ICP-MS. Calibration of the LA-ICP-MS was undertaken using substrates with known amounts of a standard solution dried onto them. Similar trends in the data were viewed for each method and the elemental concentrations obtained compared well with each other. Hsieh et al. concluded that the developed method allowed better limits of detection and quicker sampling and analysis stages than other established methods. Furthermore the developed method allowed improved time resolution for air quality investigations.[63]

Comparisons of LA-ICP-MS and traditional solution ICP-MS were carried out by Wang, Jeng and Shieh in 1997[116] and Wang, Chin, Luo and Men in 1999[117] by concentrating on specific elements, such as arsenic and chromium. In both cases airborne particulate matter was collected onto substrates prior to indirect chemical and direct analysis. Results from both methods correlated well with each other but LA-ICP-MS had the advantage of being a rapid and direct technique.

Laser Induced Breakdown Spectroscopy

Another example of direct laser analysis is LIBS. It is an atomic emission technique, similar to LA-ICP-AES. Over the past thirty years it has greatly developed as an analytical technique and is now used in a range of applications, such as analysis of geomaterials,[174-178] analysis of aerosols and gases,[179-183] particulate sizing,[184] analysis of steel[185, 186] and most recently in the Mars rover, Curiosity.[187] There are a range of factors which can affect quantitative LIBS measurements. These include, airborne particulate matter intercepting the laser beam, an irregular sample surface and a difference between chemical composition of the calibration materials and the sample of interest.[188] Therefore a number of LIBS studies concentrate on qualitative analysis.

LIBS uses a pulsed laser, to ablate a sample and excite the constituent atoms and ions as shown in Figure 1-16. When the laser is fired onto a small spot on a material a high electron density plasma is formed and the material is broken down, vaporised, atomised and partially ionised. Most LIBS systems use a Nd:YAG laser with a wavelength of 1064 nm to generate the plasma.[189] The plasma generated is described as a local assembly of atoms, ions and free electrons and is overall electronically neutral. A LIBS plasma should be optically thin, in thermodynamic equilibrium and have the same elemental composition as the sample.[188]

Figure 1-16: LIBS processes[177]
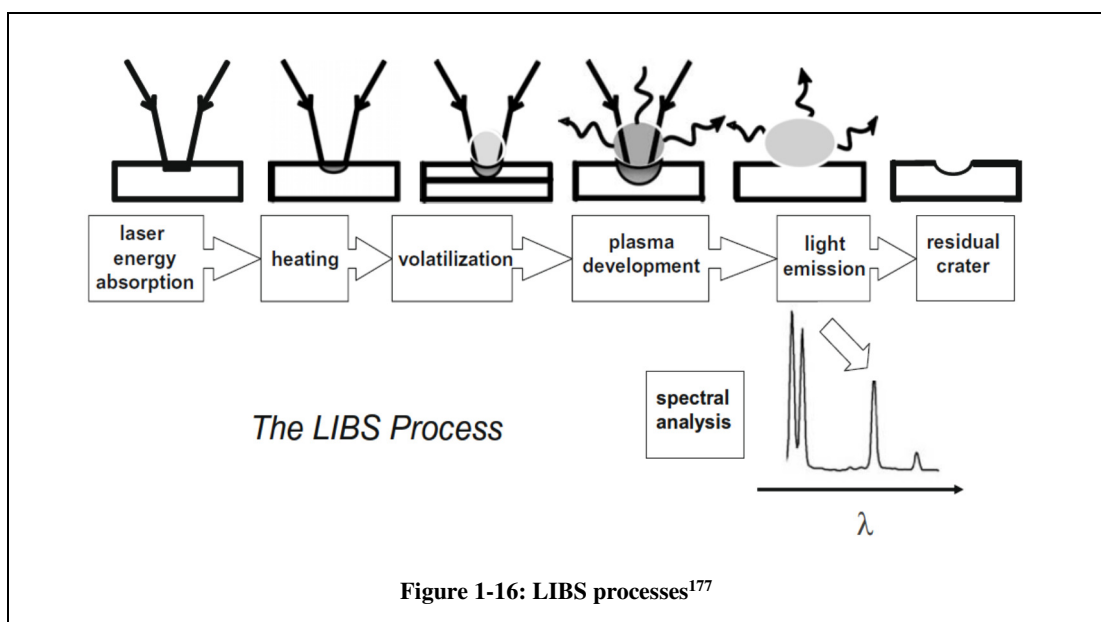
Once the elements within the sample have been atomised the excited species drop down to their ground state and emit radiation at a wavelength specific to that element, generally within the UV and visible light range. As with ICP-AES the intensity of the radiation emitted is proportional to the concentration of that element within the sample. The radiation emitted is transmitted down fibre optics to the spectrometers.[189] Light is collected in a very short time window, typically 20 µs. This collected light generates an emission spectrum which is then used to determine the samples elemental constitution.[188] The main components of a LIBS system are a pulsed Nd:YAG laser, a focusing system, a sample holder, a light collection system, a detection system and a computer[188] as detailed in Figure 1-17.

Figure 1-17: Schematic of a LIBS system[177]
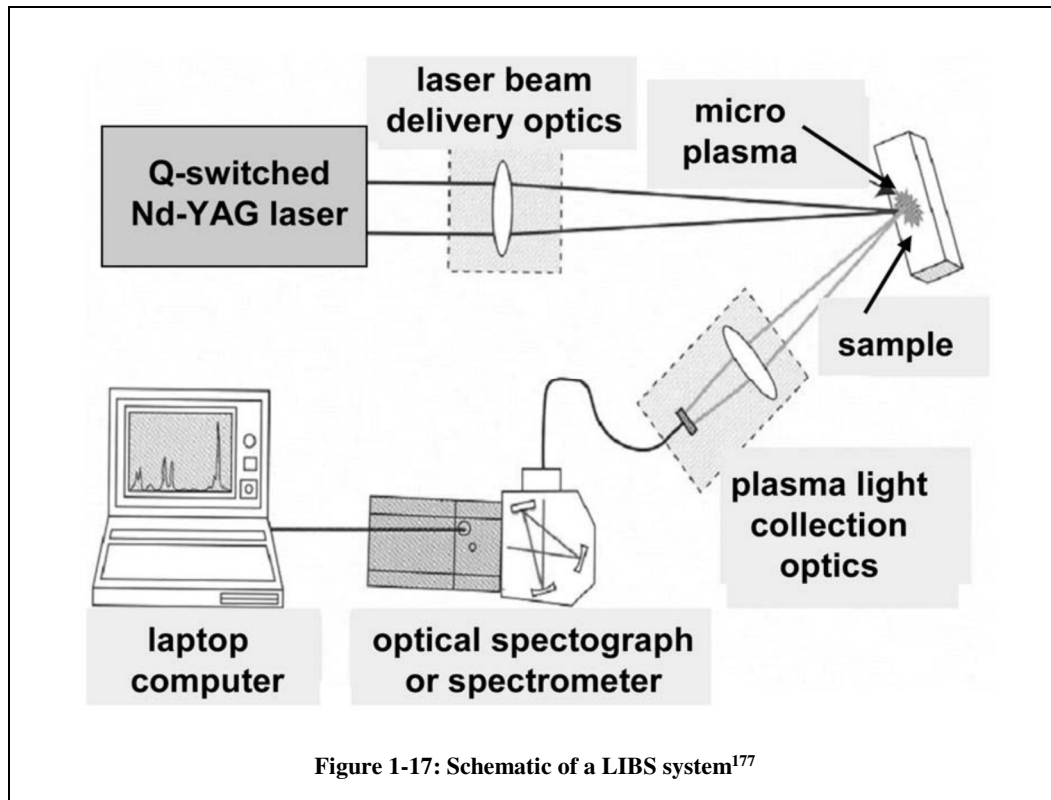
In 2000 Hahn and Lunden[181] published a paper focusing on the characterisation of LIBS aerosol particles in a laboratory environment. Calcium and magnesium aerosols in a nitrogen stream were generated using both an ICP-AES nebuliser and a pneumatic medical nebuliser. A particle flow rate of 0.5 L/min was applied. This was the first paper which introduced the use of a stainless steel cross shaped sample chamber. A flow of nitrogen was used, allowing the particle velocity to reach 0.15 m/s through the cross. Two sets of experiments were

completed. The first set used a differential mobility analyser to produce a monodisperse flow of particles, at 150 nm in diameter, from the polydisperse source. This experiment allowed a sampling rate of approximately one percent, which corresponded to the analysis of approximately 44 calcium particles. The second set of experiments bypassed the differential mobility analyser allowing the polydisperse source to pass directly to the LIBS analyser. This allowed a sampling rate of 59 percent to be obtained, which is much higher than the one percent for monodisperse particles but also suggests that the particulates may not have been analysed singularly. Alongside both experiments size analysis by LAS was also completed. The LAS was placed in parallel with the LIBS sample chamber and used scattering of laser light to size particulates in terms of its refractive index.[181]

The coupling of a laser ablation unit to a LIBS system was discussed in 2009.[190] The coupling was proposed as a novel technique to improve analyte response and allow the use of non matrix matched standards whilst using direct analysis, avoiding the need for sample preparation. The LA unit was used to ablate a solid sample and the ablated aerosol carried in a gas stream to the LIBS for elemental analysis. This gave two distinct phases, the ablation stage and the analysis stage, which were linked via a stainless steel tube, with an internal diameter of 3.5 cm. Some of the experiments undertaken also coupled an aerosol particle counter after the LIBS sample chamber. Nitrogen gas, at a flow rate of 3 L/min was used as the carrier gas because it allowed the best emission signals to be obtained. Seven standard reference materials were analysed for five different elements, which were aluminium, copper, iron, magnesium and manganese. Comparisons were made between the novel LA-LIBS technique and the LIBS instrument. The precision for the LA-LIBS technique was always superior to the LIBS when run as a standalone unit. Very promising results were obtained from this novel technique with further work on improving it expected in the near future.[190] Finally it has been proposed that during the last decade a lot of the key processes behind the LIBS instrument have been discussed and by further studying the plasma particle interface LIBS could progress as a technique for direct chemical analysis.[191]

1.6 Aims of Research

The principle aim of this research is to develop novel methods to chemically and physically characterise particulate matter. New instrumental configurations and associated method development will be required to allow an insight into the characteristics of particulate matter in real time.

As mentioned in Section 1.2.2 to characterise atmospheric emissions they tend to be collected onto substrates for analysis once back in a laboratory environment, this can be a slow and time consuming procedure. Therefore there is a need to allow the characterisation of particulates quickly and in real time. To be able to complete this real time analysis there is a need to complete a range of proof of concept studies which will allow primary data to be obtained in a laboratory environment. Laboratory scale studies will be completed using a rotating drum sampler coupled successively to both an Aspect morphology analyser and an ELPI. The real time data will consist of morphological profiles and number distributions. Other data, obtained through gravimetric and chemical analysis will include mass and elemental distributions. Materials which will be investigated, that have been obtained from an integrated steelworks, will include two different Brazilian ores, a sinter dust and a blast furnace flue dust.

Once this primary data has been obtained and the studies have been developed they can be used to allow a wider range of materials to be characterised. This data can then be used to allow a database to be developed. The database would contain characteristic fingerprints of each of the materials and possible emission sources which are found upon or near an integrated steelworks. Thus, when completing on site analysis in future the database could be referred to when on site to confirm the sources of the emissions which are being characterised.

Following these studies, using the rotating drum system, the physical and chemical characterisation of laser generated aerosols will be undertaken. This will allow a fuller understanding of the aerosols generated by ablating a solid material with a laser as well as the interactions which occur between a laser and a solid material. The direct physical characterisation of the particulates which are generated when ablating a solid material has not been greatly researched, especially when using real time techniques. Therefore, by coupling a laser ablation system to an Aspect morphology analyser and an ELPI, morphological profiles and number distributions of the generated particulates may be obtained. Further data can also be obtained through gravimetric and chemical analysis. Whilst completing the couplings different parameters such as laser wavelength and ablation atmosphere will be investigated. Six materials will be characterised, a carbon rod, high purity zinc, polyethylene, a carbon steel, boron nitride and glass. Again these studies will allow primary data to be obtained and the methods to be developed.

By completing the characterisation of particulates, using morphological analysis, indirect chemical analysis and direct analysis, an insight into the unique compositions of a range of aerosols may be gained.

1.7 References

1.   D. T. Suess and K. A. Prather, *Chemical Reviews*, 1999, **99**, 3007-3036.
2.   G. W. vanLoon and S. J. Duffy, *Environmental Chemistry: A global perspective*, 2nd edn., Oxford University Press, New York, 2005.
3.   K. Jackson, PhD Thesis, University of Sheffield, 2009.
4.   A. Charron and R. M. Harrison, *Environmental Science & Technology*, 2005, **39**, 7768-7776.
5.   R. N. Reeve, *Environmental Analysis*, John Wiley & Sons, Chichester, 1994.
6.   M. L. Sammut, Y. Noack, J. Rose, J. L. Hazemann, O. Proux, M. Depoux, A. Ziebel and E. Fiani, *Chemosphere*, 2010, **78**, 445-450.
7.   H. Puxbaum, in *Metals and their compounds in the environment*, ed. E. Merian, VCH, New York, 1991.
8.   B. J. Alloway and D. C. Ayres, *Chemical Principles of Environmental Pollution*, Blackie Academic and Professional, Glasgow, 1993.
9.   I. Ford, Introduction to Aerosol Science, UCL, 2009.
10.   W. C. Hinds, *Aerosol Technology*, 2nd edn., Wiley and Sons, New York, 1999.
11.   F. Aubriet and V. Carré, *Analytica Chimica Acta*, 2010, **659**, 34-54.
12.   J. P. Shi, A. A. Khan and R. M. Harrison, *Science of the Total Environment*, 1999, **235**, 51-64.
13.   S. R. Gislason, T. Hassenkam, S. Nedel, N. Bovet, E. S. Eiriksdottir, H. A. Alfredsson, C. P. Hem, Z. I. Balogh, K. Dideriksen, N. Oskarsson, B. Sigfusson, G. Larsen and S. L. S. Stipp, *Proceedings of the National Academy of Sciences*, 2011, **108**, 7307-7312.
14.   R. F. Browner and A. W. Boorn, *Analytical Chemistry*, 1984, **56**, 875A-888A.
15.   R. Kinnersley, Introduction to Aerosol science, UCL, 2009.
16.   K. T. Whitby, *Atmospheric Environment*, 1978, **12**, 135-159.
17.   J. Curtius, *Comptes Rendus Physique*, 2006, **7**, 1027-1045.
18.   P. S. Monks, C. Granier, S. Fuzzi, A. Stohl, M. L. Williams, H. Akimoto, M. Amann, A. Baklanov, U. Baltensperger, I. Bey, N. Blake, R. S. Blake, K. Carslaw, O. R. Cooper, F. Dentener, D. Fowler, E. Fragkou, G. J. Frost, S. Generoso, P. Ginoux, V. Grewe, A. Guenther, H. C. Hansson, S. Henne, J. Hjorth, A. Hofzumahaus, H. Huntrieser, I. S. A. Isaksen, M. E. Jenkin, J. Kaiser, M. Kanakidou, Z. Klimont, M. Kulmala, P. Laj, M. G. Lawrence, J. D. Lee, C. Liousse, M. Maione, G. McFiggans, A. Metzger, A. Mieville, N. Moussiopoulos, J. J. Orlando, C. D. O'Dowd, P. I. Palmer, D. D. Parrish, A. Petzold, U. Platt, U. Pöschl, A. S. H. Prévôt, C. E. Reeves, S. Reimann, Y. Rudich, K. Sellegri, R. Steinbrecher, D. Simpson, H. ten Brink, J. Theloke, G. R. van der Werf, R. Vautard, V. Vestreng, C. Vlachokostas and R. von Glasow, *Atmospheric Environment*, 2009, **43**, 5268-5350.
19.   B. B. Kebbekus and S. Mitra, *Environmental Chemical Analysis*, Blackie Academic and Professional, London, 1998.
20.   *Volume 1, Air Quality Strategy for England, Scotland, Wales and Northern Ireland*, DEFRA, London, 2007.
21.   *Air Quality in Europe - 2012 Report*, European Environment Agency,Copenhagen, 2012.
22.   *Particulate Matter in the United Kingdom*, Air Quality Expert Group (AQEG), DEFRA, London, 2005.
23.   C. Lüdke, E. Hoffmann and J. Skole, *Fresenius' Journal of Analytical Chemistry*, 1994, **350**, 272-276.
24.   *Making Steel*, Corus Education Service, London, 2008.
25.   *Key Statistics 2011*, UK Steel, London, 2011.
26.   www.tatasteeleurope.com/en/company, Accessed 4th July 2013
27.   *Tata Steel*, e-Learning System, 2012.

28. *Best Available Techniques Reference Document for Iron and Steel Production*, European Comission, Seville, 2013.
29. N. Menad, H. Tayibi, F. G. Carcedo and A. Hernández, *Journal of Cleaner Production*, 2006, **14**, 740-747.
30. *Air Quality in the UK,* Postnote188, Parlimentary Office of Science and Technology, London, 2002.
31. B. Nemery, P. H. M. Hoet and A. Nemmar, *The Lancet*, 2001, **357**, 704-708.
32. R. M. Harrison and J. Yin, *Science of the Total Environment*, 2000, **249**, 85-101.
33. A. Whittaker, K. BéruBé, T. Jones, R. Maynard and R. Richards, *Science of the Total Environment*, 2004, **334-335**, 435-445.
34. http://smokecontrol.defra.gov.uk, Accessed 4th July 2013
35. R. Bargagli, *Trace Elements in Terrestrial Plants*, Springer, Berlin, 1998.
36. J. H. Vincent, *Journal of Environmental Monitoring*, 2012, **14**, 340-347.
37. A. Limbeck, M. Handler, C. Puls, J. Zbiral, H. Bauer and H. Puxbaum, *Atmospheric Environment*, 2009, **43**, 530-538.
38. D. Nore, A. M. Gomes, J. Bacri and J. Cabe, *Spectrochimica Acta Part B: Atomic Spectroscopy*, 1993, **48**, 1411-1419.
39. K. Donaldson, V. Stone, A. Clouter, L. Renwick and W. MacNee, *Occupational and Environmental Medicine*, 2001, **58**, 211-216.
40. *Workplace atmospheres - Size fraction definitions for measurement of airborne particles,* BS EN 481, BSI, London, 1993.
41. E. Petavratzi, S. Kingman and I. Lowndes, *Minerals Engineering*, 2005, **18**, 1183-1199.
42. www.skcinc.com/product_images/ACGIH_particle_size.jpg, Accessed 4th July 2013
43. J. Schwartz, *Environmental Research*, 1993, **62**, 7-13.
44. R. A. Silverman and K. Ito, *Journal of Allergy and Clinical Immunology*, 2010, **125**, 367-373.
45. R. D. Brook, *Clinical Science*, 2008, **115**, 175-187.
46. U. Franck, S. Odeh, A. Wiedensohler, B. Wehner and O. Herbarth, *Science of the Total Environment*, 2011, **409**, 4217-4221.
47. J. Namieśnik, B. Zabiegała, A. Kot-Wasik, M. Partyka and A. Wasik, *Analytical and Bioanalytical Chemistry*, 2005, **381**, 279-301.
48. K. Suzuki, *Atmospheric Environment*, 2006, **40**, 2626-2634.
49. J. Hertz, in *Metals and their compounds in the environment*, ed. E. Merian, VCH, New York, 1991.
50. E. Schelle, B. G. Rawlins, R. M. Lark, R. Webster, I. Staton and C. W. McLeod, *Environmental Pollution*, 2008, **155**, 164-173.
51. D. Bellis, R. Ma, N. Bramall, C. W. McLeod, N. Chapman and K. Satake, *Environmental Pollution*, 2001, **114**, 383-387.
52. R. Ma, D. Bellis and C. W. McLeod, *Analytical Chemistry*, 2000, **72**, 4878-4881.
53. N. I. Ward, R. R. Brooks and R. D. Reeves, *Environmental Pollution*, 1974, **6**, 149-158.
54. *Aerodynamic Particle Sizer, Model 3321, Specification Sheet*, TSI, 2012.
55. http://www.che.utah.edu/~ring/ChE-6960/Chapter_5_Ring.pdf, Accessed 4th July 2013
56. *Scanning Mobility Particle Sizer Spectrometer, Model 3936, Specification Sheet*, TSI, 2012.
57. www.tsi.com, Accessed 4th July 2013
58. www.dekati.com, Accessed 4th July 2013
59. J. Keskinen, K. Pietarinen and M. Lehtimäki, *Journal of Aerosol Science*, 1992, **23**, 353-360.
60. *ELPI User Manual*, Dekati Ltd, 2008.
61. M. Marjamäki, J. Keskinen, D.-R. Chen and D. Y. H. Pui, *Journal of Aerosol Science*, 2000, **31**, 249-261.

62. H. Price, R. Arthur, K. Sexton, C. Gregory, B. Hoogendoorn, I. Matthews, T. Jones and K. BéruBé, *Journal of Toxicology and Environmental Health, Part A*, 2010, **73**, 355 - 367.

63. Y.-K. Hsieh, L.-K. Chen, H.-F. Hsieh, C.-H. Huang and C.-F. Wang, *Journal of Analytical Atomic Spectrometry*, 2011, **26**, 1502-1508.

64. R. Yoshiie, Y. Yamamoto, S. Uemiya, S. Kambara and H. Moritomi, *Powder Technology*, 2008, **180**, 135-139.

65. T. Kuhlen, C. Fricke-Begemann, N. Strauss and R. Noll, *Spectrochimica Acta Part B: Atomic Spectroscopy*, 2008, **63**, 1171-1176.

66. R. Xie, K. A. Jackson, H. M. Seip, C. W. McLeod, G. Wibetoe, M. J. Schofield, D. Anderson and J. E. Hanssen, *Journal of Environmental Monitoring*, 2009, **11**, 336-343.

67. A. R. Clarke and C. N. Eberhardt, *Microscopy techniques for materials science*, Woodhead Publishing Ltd, Cambridge, 2002.

68. C. W. Oatley, *Journal of Applied Physics*, 1982, **53**, R1-R13.

69. K. C. A. Smith and C. W. Oatley, *British Journal of Applied Physics*, 1955, **6**, 391-399.

70. A. Argast and C. F. Tennis, *Journal of Geoscience Education*, 2004, **52**, 213-217.

71. A. P. Ault, T. M. Peters, E. J. Sawvel, G. S. Casuccio, R. D. Willis, G. A. Norris and V. H. Grassian, *Environmental Science & Technology*, 2012, **46**, 4331-4339.

72. T. Schneider and K. Jensen, *Journal of Nanoparticle Research*, 2009, **11**, 1637-1650.

73. S. A. Sethi and T. Schneider, *Journal of Aerosol Science*, 1996, **27**, S305-S306.

74. *Workplace atmospheres - Measurement of the dustiness of bulk materials - Requirements and reference test methods,* BS EN 15051, BSI, London, 2006.

75. I. Pensis, J. Mareels, D. Dahmann and D. Mark, *The Annals of Occupational Hygiene*, 2010, **54**, 204-216.

76. C. P. Lyons, D. Mark, K. Y. K. Chung and G. Burdett, *Journal of Aerosol Science*, 1992, **23**, S607-S610.

77. K. Y. K. Chung and G. J. Burdett, *The Annals of Occupational Hygiene*, 1994, **38**, 945-949.

78. N. O. Breum, *The Annals of Occupational Hygiene*, 1999, **43**, 557-566.

79. F. Hamelmann and E. Schmidt, *China Particuology*, 2005, **3**, 90-93.

80. F. Hamelmann and E. Schmidt, *Chemical Engineering & Technology*, 2004, **27**, 844-847.

81. T. Schneider and K. A. Jensen, *The Annals of Occupational Hygiene*, 2008, **52**, 23-34.

82. K. Hjemsted and T. Schneider, *The Annals of Occupational Hygiene*, 1996, **40**, 627-643.

83. M. Boundy, D. Leith and T. Polton, *The Annals of Occupational Hygiene*, 2006, **50**, 453-458.

84. C.-J. Tsai, C.-H. Wu, M.-L. Leu, S.-C. Chen, C.-Y. Huang, P.-J. Tsai and F.-H. Ko, *Journal of Nanoparticle Research*, 2009, **11**, 121-131.

85. D. E. Evans, L. A. Turkevich, C. T. Roettgers, G. J. Deye and P. A. Baron, *The Annals of Occupational Hygiene*, 2013, **57**, 261-277.

86. K. Ravindra, A. K. Mittal and R. Van Grieken, *Review on Environmental Health*, 2001, **16**, 169-189.

87. P. W. J. Bartrip, *Postgraduate Medical Journal*, 2004, **80**, 72-76.

88. www.livingwithmesothelioma.co.uk/, Accessed 4th July 2013

89. W. E. Cooke, *BMJ*, 1924, **2**, 147-148.

90. K. Reid, A. T. Martin and J. M. Clark, *Journal of Aerosol Science*, 1992, **23**, S325-S328.

91. P. H. Kaye, E. Hirst, J. M. Clark and F. Micheli, *Journal of Aerosol Science*, 1992, **23**, 597-611.

92. P. H. Kaye, *Measurement Science and Technology*, 1998, **9**, 141-149.

93. E. Hirst and P. H. Kaye, *Journal of Geophysical Research*, 1996, **101**, 19231-19235.
94. P. H. Kaye, J. E. Barton, E. Hirst and J. M. Clark, *Applied Optics*, 2000, **39**, 3738-3745.
95. J. M. Clark, M. J. Shelton, S. P. Evans, P. D. Smith, I. A. Simpson and P. H. Kaye, Optically Based Biological and Chemical Sensing and Optically Based Materials for Defence, Bruges, Belgium, 2005.
96. E. Hirst, P. H. Kaye and J. R. Guppy, *Applied Optics*, 1994, **33**, 7180-7186.
97. D. R. Secker, P. H. Kaye, R. S. Greenaway, E. Hirst, D. L. Bartley and G. Videen, *Applied Optics*, 2000, **39**, 5023-5030.
98. www.biral.com, Accessed 4th July 2013
99. P. H. Kaye, E. Hirst and F. Micheli, *Journal of Aerosol Science*, 1992, **23**, S321-S324.
100. *Aspect User Manual*, Biral, Bristol, 2010.
101. A. Grekula, E. Ristolainen, V. P. Tanninen, H. K. Hyvärinen and P. L. Kalliomäki, *Journal of Aerosol Science*, 1986, **17**, 1-9.
102. F. Hoke, *The Scientist*, 1992, **6**, 19.
103. K. J. Lamble and S. J. Hill, *Analyst*, 1998, **123**, 103R-133R.
104. K.-P. Hinz and B. Spengler, *Journal of Mass Spectrometry*, 2007, **42**, 843-860.
105. B. D. Zehr, *American Lab*, 1992, **December**, 24-29.
106. M. Balcerzak, *Analytical Sciences*, 2002, **18**, 737-750.
107. H. Matusiewiez, in *Sample Preparation for Trace Element Analysis* eds. Z. Mester and R. E. Sturgeon, Elsevier, Amsterdam, 2003, vol. 41.
108. M. Chen and L. Q. Ma, *Soil Science Society of America Journal*, 2001, **65**, 491-499.
109. J. R. Knechtel and J. L. Fraser, *Analytical Chemistry*, 1979, **51**, 315-317.
110. I. Rodushkin, T. Ruth and Å. Huhtasaari, *Analytica Chimica Acta*, 1999, **378**, 191-200.
111. J. Sastre, A. Sahuquillo, M. Vidal and G. Rauret, *Analytica Chimica Acta*, 2002, **462**, 59-72.
112. J. M. Lo and H. Sakamoto, *Analytical Sciences*, 2005, **21**, 1181-1184.
113. www.cem.com, Accessed 4th July 2013
114. M. Thompson and J. N. Walsh, *Handbook of Inductively Coupled Plasma Spectrometry*, 2nd edn., Blackie, Glasgow, 1989.
115. V. Thomsen, *Spectroscopy*, 2006, **21**, 32-42.
116. T. B. Reed, *Journal of Applied Physics*, 1691, **32**, 821-824.
117. S. Greenfield, I. L. Jones and C. T. Berry, *Analyst*, 1964, **89**, 713-720.
118. R. H. Wendt and V. A. Fassel, *Analytical Chemistry*, 1965, **37**, 920-922.
119. R. H. Scott, V. A. Fassel, R. N. Kniseley and D. E. Nixon, *Analytical Chemistry*, 1974, **46**, 75-80.
120. R. S. Houk, V. A. Fassel, G. D. Flesch, H. J. Svec, A. L. Gray and C. E. Taylor, *Analytical Chemistry*, 1980, **52**, 2283-2289.
121. C. A. Coutinho and V. Thomsen, *Spectroscopy*, 2011.
122. R. Thomas, *Spectroscopy*, 2001, **16**, 56-60.
123. R. Thomas, *Spectroscopy*, 2001, **16**, 26-30.
124. A. Montaser, J. A. McLean, H. Liu and J. M. Mermet, *Inductively Coupled Mass Spectrometry*, Wiley-VCH, New York, 1998.
125. www.cleanwatertesting.com/ICP-OES_diagram.jpg, Accessed 4th July 2013
126. T. J. Manning and W. R. Grow, *The Chemical Educator*, 1997, **2**, 1-19.
127. A. Seubert, *TrAC Trends in Analytical Chemistry*, 2001, **20**, 274-287.
128. *Inductively Coupled Plasma-Atomic Emissions Spectrometry (ICP-AES)*, Philips, 2008.
129. R. Thomas, *Spectroscopy*, 2002, **17**, 28-35.
130. *Inductively Coupled Plasma: A Primer*, Agilent Technologies, 2005.
131. R. Thomas, *Spectroscopy*, 2001, **16**, 38-44.
132. R. Thomas, *Spectroscopy*, 2001, **16**, 44-48.
133. R. Thomas, *Spectroscopy*, 2002, **17**, 34-39.

134.	*Student Manual for Agilent 7500*, Agilent Technologies, Revision 1.
135.	R. Thomas, *Spectroscopy*, 2002, **17**, 24-31.
136.	T. W. May and R. H. Wiedmeyer, *Atomic Spectroscopy*, 1998, **19**, 150-155.
137.	T. Yamada and N. Yamada, *Agilent ICP-MS Journal*, 2002, **13**, 2.
138.	C. Hung-Lung and H. Yao-Sheng, *Atmospheric Environment*, 2009, **43**, 4014-4022.
139.	S. D. Machemer, *Environmental Science & Technology*, 2003, **38**, 381-389.
140.	A. R. Date, Y. Y. Cheung, M. E. Stuart and J. Xiu-Hua, *Journal of Analytical Atomic Spectrometry*, 1988, **3**, 653-658.
141.	K. Swami, C. D. Judd, J. Orsini, K. X. Yang and L. Husain, *Fresenius' Journal of Analytical Chemistry*, 2001, **369**, 63-70.
142.	U. M. Joshi, K. Vijayaraghavan and R. Balasubramanian, *Chemosphere*, 2009, **77**, 526-533.
143.	P. Rommers and P. Boumans, *Fresenius' Journal of Analytical Chemistry*, 1996, **355**, 763-770.
144.	R. E. Russo, X. Mao, H. Liu, J. Gonzalez and S. S. Mao, *Talanta*, 2002, **57**, 425-451.
145.	E. A. H. Timmermans, F. P. J. de Groote, J. Jonkers, A. Gamero, A. Sola and J. J. A. M. van der Mullen, *Spectrochimica Acta Part B: Atomic Spectroscopy*, 2003, **58**, 823-836.
146.	A.-M. Gomes, J.-P. Sarrette, L. Madon and A. Almi, *Spectrochimica Acta Part B: Atomic Spectroscopy*, 1996, **51**, 1695-1705.
147.	D. Günther, S. E. Jackson and H. P. Longerich, *Spectrochimica Acta Part B: Atomic Spectroscopy*, 1999, **54**, 381-409.
148.	P. Atkins and J. d. Paula, *Atkins' Physical Chemistry*, 7th edn., Oxford University Press, New York, 2002.
149.	S. F. Durrant, *Journal of Analytical Atomic Spectrometry*, 1999, **14**, 1385-1403.
150.	M. J. Webber, *Handbook of Laser Wavelengths*, CRC Press, Boca Raton, Florida, 1999.
151.	W. T. Chan and R. E. Russo, Laser Ablation Mechanisms and Application, Oak Ridge, Tennessee, USA, 1991.
152.	P. Schaff, ed., *Laser Processing of Materials*, Springer-Verlag, Berlin, 2010.
153.	S. Kuroda, S. Kaihara, Y. Fujii, T. Kinoshita and M. Adachi, *Journal of Aerosol Science*, 2012, **50**, 38-56.
154.	H. Ki, P. S. Mohanty and J. Mazumder, *Journal of Physics D, Applied Physics*, 2001, **34**, 364-372.
155.	M. Thompson, S. Chenery and L. Brett, *Journal of Analytical Atomic Spectrometry*, 1990, **5**, 49-55.
156.	http://lidaris.com/glossary-2/fluence/, Accessed 4th July 2013
157.	F. Brygo, C. Dutouquet, F. Le Guern, R. Oltra, A. Semerok and J. M. Weulersse, *Applied Surface Science*, 2006, **252**, 2131-2138.
158.	M. Guillong and D. Günther, *Journal of Analytical Atomic Spectrometry*, 2002, **17**, 831-837.
159.	S. Tanaka, N. Yasushi, N. Sato, T. Fukasawa, S. J. Santosa, K. Yamanaka and T. Ootoshi, *Journal of Analytical Atomic Spectrometry*, 1998, **13**, 135-140.
160.	S. A. Darke and J. F. Tyson, *Journal of Analytical Atomic Spectrometry*, 1993, **8**, 145-209.
161.	A. L. Gray, *Analyst*, 1985, **110**, 551-556.
162.	M. Thompson, J. E. Goulter and F. Sieper, *Analyst*, 1981, **106**, 32-39.
163.	D. Günther and B. Hattendorf, *TrAC Trends in Analytical Chemistry*, 2005, **24**, 255-265.
164.	Y. Ishibashi, *Analytical Sciences*, 2001, **17, Supplement**, i53-i55.
165.	C. Dubuisson, A. G. Cox, C. W. McLeod, I. Whiteside, R. Jowitt and H. Falk, *ISIJ International*, 2007, **44**, 1859-1866.
166.	J. S. Becker, M. Zoriy, J. S. Becker, J. Dobrowolska and A. Matusch, *Journal of Analytical Atomic Spectrometry*, 2007, **22**, 736-744.

167. S. Gligorovski, J. T. van Elteren and I. Grgic, *Science of the Total Environment*, 2008, **407**, 594-602.
168. J. Seuma, J. Bunch, A. Cox, C. McLeod, J. Bell and C. Murray, *Proteomics*, 2008, **8**, 3775-3784.
169. D. Hare, F. Burger, C. Austin, F. Fryer, R. Grimm, B. Reedy, R. A. Scolyer, J. F. Thompson and P. Doble, *The Analyst*, 2009, **134**, 450-453.
170. J. A. T. Pugh, A. G. Cox, C. W. McLeod, J. Bunch, B. Whitby, B. Gordon, T. Kalber and E. White, *Journal of Analytical Atomic Spectrometry*, 2011, **26**, 1667-1673.
171. C.-J. Chin, C.-F. Wang and S.-L. Jeng, *Journal of Analytical Atomic Spectrometry*, 1999, **14**, 663-668.
172. T. Okuda, J. Kato, J. Mori, M. Tenmoku, Y. Suda, S. Tanaka, K. He, Y. Ma, F. Yang, X. Yu, F. Duan and Y. Lei, *Science of the Total Environment*, 2004, **330**, 145-158.
173. W. Chung, V. N. Sharifi, J. Swithenbank, O. Osammor and A. Nolan, *Modern Applied Science*, 2008, **2**, 17-32.
174. M. Dong, J. Lu, S. Yao, J. Li, J. Li, Z. Zhong and W. Lu, *Journal of Analytical Atomic Spectrometry*, 2011, **26**, 2183-2188.
175. K. J. Grant, G. L. Paul and J. A. O'Neill, *Applied Spectroscopy*, 1991, **45**, 701-705.
176. S. Yao, J. Lu, J. Zheng and M. Dong, *Journal of Analytical Atomic Spectrometry*, 2012, **27**, 473-478.
177. R. S. Harmon, J. Remus, N. J. McMillan, C. McManus, L. Collins, J. L. Gottfried Jr, F. C. DeLucia and A. W. Miziolek, *Applied Geochemistry*, 2009, **24**, 1125-1141.
178. D. L. Death, A. P. Cunningham and L. J. Pollard, *Spectrochimica Acta Part B: Atomic Spectroscopy*, 2009, **64**, 1048-1058.
179. G. Gallou, J. B. Sirven, C. Dutouquet, O. L. Bihan and E. Frejafon, *Aerosol Science and Technology*, 2011, **45**, 918-926.
180. E. D. McNaghten, A. M. Parkes, B. C. Griffiths, A. I. Whitehouse and S. Palanco, *Spectrochimica Acta Part B: Atomic Spectroscopy*, 2009, **64**, 1111-1118.
181. D. W. Hahn and M. M. Lunden, *Aerosol Science and Technology*, 2000, **33**, 30-48.
182. E. M. Cahoon and J. R. Almirall, *Analytical Chemistry*, 2012, **84**, 2239-2244.
183. L. J. Radziemski, T. R. Loree, D. A. Cremers and N. M. Hoffman, *Analytical Chemistry*, 1983, **55**, 1246-1252.
184. D. W. Hahn, *Applied Physics Letters*, 1998, **72**, 2960-2962.
185. F. Boué-Bigne, in *Cetas 2011: Progress in Analytical Chemistry & Materials Characterisation in the Steels and Metals Industries*, Luxembourg, 2011.
186. M. A. Khater, *Spectrochimica Acta Part B: Atomic Spectroscopy*, 2013, **81**, 1-10.
187. F. J. Fortes, J. Moros, P. Lucena, L. M. Cabalín and J. J. Laserna, *Analytical Chemistry*, 2012, **85**, 640-669.
188. D. A. Cremers and L. J. Radziemski, *Handbook of Laser-Induced Breakdown Spectroscopy*, 1st edn., Wiley, Chichester, 2006.
189. R. S. Harmon, F. C. DeLucia, C. E. McManus, N. J. McMillan, T. F. Jenkins, M. E. Walsh and A. Miziolek, *Applied Geochemistry*, 2006, **21**, 730-747.
190. B. C. Windom and D. W. Hahn, *Journal of Analytical Atomic Spectrometry*, 2009, **24**, 1665-1675.
191. D. W. Hahn, *Spectroscopy*, 2009, **24**, 26-33.

Chapter Two

Multielement analysis of two iron ores, a flue dust and a sinter dust, from an integrated steelworks

2.1: Introduction

The production of metals, such as steel, results in the formation of a number of unwanted emissions consisting of solids, liquids and gasses. Emissions are emitted directly, from processes, or indirectly, from utilities such as electricity, and may be toxic. Examples include cadmium and lead and at high levels copper. These emissions and the impacts they have on the environment must be reduced.[1] Therefore all pollutants from industry must be controlled. All of the European Union's main policies currently have environmental protection integrated within them, an example being REACH. This is a European Community Regulation on chemicals and their safe use which deals with the Registration, Evaluation, Authorisation and Restriction of Chemical Substances. Information gaps are being assessed to identify and allow the implementation of risk management measures to protect humans and the environment.[2] Laboratories that perform studies in the context of REACH have to implement a documented quality system. This could be Good Laboratory Practice or ISO Standards. This allows the laboratories to attach credibility, validity and comparability to their results.

For the steelmaking industry one main challenge that they face is to achieve satisfactory environmental performance in a cost effective manner and allow competitiveness to be maintained. Hence, BAT for individual industries have been implemented by the European Commission to aid the control of these pollutants.[3, 4] Environmental studies must also be undertaken to fully understand the sources of these emissions.

The elemental analysis of raw materials and by-products from the iron and steel making industry is of great importance to environmental studies. One reason for determining the elemental concentration of raw materials is the possibility of *de novo* synthesis occurring during the sintering process. Any trace metals present within high temperature processes between 250 and 400 °C, for example sintering, can cause the production of organic micro pollutants, such as PCDDs,[4, 5] which are simply known as dioxins. Other emissions released from the sinter stack include particulate matter, sulphur and nitrogen oxides, hydrogen chloride, hydrogen fluoride, carbon monoxide and carbon dioxide. The particulates generated by the sinter process are very fine compared to other dusts emitted from the integrated works[6] and are released from four different procedures. These procedures include the crushing of coke to form coke breeze, the blending and mixing of ore and coke breeze and the formation and cooling of the sinter.[3] A further reason for conducting elemental analysis is that any raw materials and by-products that become airborne or are released from an integrated steelmaking works contain metallic elements. The handing of raw materials, through transport, to or around a plant, as well as material storage, in large stockpiles,[3] are possible ways that particulates and therefore metallic elements can enter the atmosphere, causing negative effects to the environment,[7] health, food supply and building degradation.[8] Therefore by collecting and chemically characterising dusts before they are released, the concentration of metallic elements entering the atmosphere can be determined. If any of the determined elemental concentrations are higher than anticipated, or above the values stated in legislation, measures can be put in place to control their release or decrease them to acceptable levels. Current legislation has set defined target values for a selection of metals.[9] The current European air quality limit values for PM_{10}, which were implemented in 2005, are 50 µg/m^3 as a 24 hr mean, not to be exceeded more than 35 times per year and an annual average limit of 40 µg/m^3.[10] Air quality measurements are taken at council run monitoring stations across the country. North Lincolnshire currently operates one of these sites, known as Santon, in Scunthorpe, next to Tata Steel's integrated steelworks.[11] The monitoring station is housed north east of the steelworks and it collects and analyses particulate matter on an

hourly basis. For 2012 the maximum daily mean was 90 µg/m^3 and the maximum hourly mean was 277 µg/m^3. The monthly results for 2012 are tabulated in Table 2-1.

	January	February	March	April	May	June	July	August	September	October	November	December
Hourly mean (µg/m^3)	33	33	44	25	27	24	33	39	48	30	30	24

Table 2-1: Monthly PM$_{10}$ air quality data from Santon monitoring station in 2012 (µg/m^3)[11]

During 2012 there were a large number of exceedences in daily PM$_{10}$ means for this site. There were 285 low exceedences, 36 moderate exceedences and seven high exceedences. In January and February of 2013 there were 51 days of low exceedences and three days of moderate exceedences[11]. The wind direction on the days of these exceedences is unknown and therefore the origin of the particulates cannot be discussed. However other monitoring sites in the North Lincolnshire area do not show as many exceedences as the Santon monitoring station. Some elements, mostly heavy metals, are of higher environmental concern than other metals. Twenty two heavy metals are currently monitored by the centre for ecology and hydrology, including cadmium, chromium, copper, iron, lead, manganese, titanium, and zinc. These heavy metals are naturally present within the Earth's crust and therefore low concentrations are expected within the environment. In recent years the concentrations of these elements, within the environment, has increased due to the larger amount of industrial activities undertaken.[9] The monitored metals tend to accumulate in both soils and the atmosphere and once airborne they can be transported and deposited in a different location to the original source. For example cadmium, lead and mercury can accumulate within organs in the human body through long term exposure.[12] Both lead and cadmium can contribute to cardiomyopathy,[12] disease of the heart muscle, which can lead to heart failure. Mercury can affect the heart and the kidneys as well as the nervous and immune systems by causing memory loss and multiple sclerosis.[13] There are currently

atmospheric limits for the concentration of lead and cadmium within the atmosphere. These are 0.5 µg/m^3 for lead and 5 ng/m^3 for cadmium, both expressed as annual means.[14]

Previous work into the digestion and multielement analysis of both iron ores and other environmental materials has been completed. One of the first publications to discuss the analysis of iron ores by ICP-MS was published in 1988 by Date et al.[15] They used a two stage dissolution process, to digest two UK iron ores, using hot blocks and compared the use of nitric acid and hydrochloric acid when used alongside hydrofluoric acid and perchloric acid. The ICP-MS used was the second UK prototype system. They found that the use of nitric acid instead of hydrochloric acid was feasible and allowed increased trace elemental coverage. Since 1988 the use of closed systems, such as microwaves, has become more common[16] along with the use of aqua regia for the digestion of solids. Sun, Chi and Shiue[17] compared the digestion of environmental samples, such as sediment and soil, by means of both a microwave and hot blocks. The volume of each of the acids used for digestion, nitric acid, hydrochloric acid and hydrofluoric acid was also compared. Sun, Chi and Shiue found that to achieve the total digestion of sample matrices a microwave assisted digestion should be used with a combination of nitric, hydrochloric and hydrofluoric acid. This would also allow for the dissolution of all elements of interest in an effective and efficient way.[17] Sastre et al.[18] determined concentrations of cadmium, copper, lead and zinc within environmental samples. Both a microwave and hot block were used for digestion followed by ICP-MS analysis. Hot block digestion was completed using aqua regia, whereas two procedures were undertaken for microwave digestion using varying amounts of nitric acid, hydrofluoric acid, perchloric acid and hydrogen peroxide. It was concluded that the digestion of a sample is the most time consuming step for heavy metal analysis. Therefore the use of both a microwave and hydrofluoric acid ensures a total digestion in the shortest time. However it was also found that the use of hot blocks allowed more samples to be digested simultaneously with similar results.[18]

One aim of this chapter is to indirectly determine the chemical composition of four materials using recognised methods. Another is to establish the preferred ICP technique for characterising materials from a steelworks. Tata Steel, the second largest steel producer in Europe,[19] currently use microwave digestion followed by ICP-MS analysis to determine the multielemental concentrations of materials from steelworks, such as iron ores, coke breeze and electrostatic precipitator dusts, which may become airborne. The method used by Tata Steel has been validated in house and is accredited by UKAS on its ability to conform to ISO 17025, an international standard which specifies the general requirements for the competence of testing and calibration laboratories. This same method will be used for in this chapter, although analysis of the digestion solutions will also be completed using ICP-AES.

Four different materials will be investigated, two iron ores, a flue dust and a sinter dust all obtained from an integrated steelworks. The materials were chosen because they give an overview of the different processes that occur at an integrated steelworks, from raw material storage and handling to the sinter plant and finally the blast furnace. They were also chosen because a background study indicated that each of the four materials had different physical compositions and therefore it was assumed that they may have different chemical compositions also. Two Brazilian iron ores were chosen to allow comparisons to be undertaken between their chemical compositions. These materials were all digested and analysed alongside an iron ore certified CRM.

2.2 Experimental

2.2.1 Materials

The four materials, including two iron ores, ore D and ore F, a flue dust and a sinter dust were obtained from an integrated steelworks. Both iron ores had been imported from overseas and the materials were obtained from stock piles at a local integrated steelworks. The two dusts were obtained from the same site, the flue dust from the blast furnace and the sinter dust from the sinter plant. The materials were ground, using a mill, and stored in glass bottles prior to digestion. BCS-CRM 517 was digested and analysed alongside the four materials as well as being digested and analysed separately. Ore E was digested and analysed, using ICP-MS and the results from interbatch and intrabatch analysis were compared.

2.2.2 Digestion Procedure

Digestion was achieved using a CEM Corporation MARS unit. Approximately 0.4 g of each material was accurately weighed into the digestion vessels followed by the addition of 9 mL of hydrochloric acid (Aristar, VWR) and 3 mL of nitric acid (Aristar, VWR), also known as aqua regia. One acid blank and one CRM were included in each digestion. Three digestions were completed in total. Table 2-2 details the microwave method used.

Stage	Power (W)	% Power	Ramp time (min)	Digest time (min)	Temp (ºC)	Pressure (psi)
1	1200	100	5	5	100	500
2	1200	100	5	5	130	500
3	1200	100	5	10	180	500
4	1200	100	5	45	220	500

Table 2-2: Microwave method used for digestion

After the digestion process and once the vessels had cooled they were rinsed with high purity de-ionised water (18.2 MΩ.cm, Millipore). The digested materials were transferred to 50 mL sample tubes and made up to 50 mL with high purity water (18.2 MΩ.cm, Millipore). The digestion method was accredited by UKAS, the UK accreditation service, and fulfilled the requirements of ISO 17025 which specifies the general requirements for the competence of testing and calibration laboratories.

2.2.3 ICP-AES Procedure

Using 10 mg/L stock elemental solutions, (PlasmaCal elemental standards, 100 mL, 5 % HNO_3) two multielement calibration standards of 0.5 mg/L and 1 mg/L were prepared. 1000 mg/L stock elemental solutions (PlasmaCal elemental standards, 100 mL, 5 % HNO_3) were then used to prepare a multielemental calibration standard of 10 mg/L. The elements present within these standards were barium, cadmium, cobalt, chromium, copper, iron, manganese, nickel, potassium, vanadium and zinc. Finally a calibration standard containing 200 mg/L of aluminium and zinc and 1000 mg/L of iron, potassium and manganese was prepared from individual elemental 10000 mg/L stock solutions. A QC solution of 500 µg/L, containing the same elements as the calibration standards, was also prepared. All solutions were made up using one percent nitric acid (Aristar, VWR). Calibration standards, QC solutions and digested materials were directly nebulised into the ICP torch. A Spectro Ciros Vision ICP-AES instrument was used for analysis, with the operating conditions as listed in Table 2-3.

Plasma power	1.4 kW
Coolant flow	12 L/min
Auxiliary flow	1 L/min
Nebuliser flow	0.85 L/min
Acquisition time	24 seconds
Measurements per replicate	3

Table 2-3: ICP-AES operating conditions

2.2.4 ICP-MS Procedure

A calibration set containing five multielement standards was prepared from a 10 mg/L stock solution (PlasmaCal elemental standards, 100 mL, 5 % HNO_3). The five calibration standards had concentrations of 20 µg/L, 50 µg/L, 100 µg/L, 200 µg/L, 500 µg/L and 700 µg/L and contained barium, cadmium, cobalt, chromium, copper, lead, manganese, nickel, potassium, vanadium and zinc. A multielemental QC solution, of 50 µg/L and containing the same elements as the calibration standards, was also prepared. All solutions were made up using one percent nitric acid (Aristar, VWR). Calibration, QC and limit of detection solutions were analysed directly, whereas digestion solutions were diluted, using high purity water (18.2 MΩ.cm, Millipore), by a factor of twenty before analysis. Analysis was performed using an Agilent 7500ce ORS ICP-MS, with operating conditions as listed in Table 2-4. The ICP-MS was fitted with a collision cell to reduce isotopic interferences. This ICP-MS method has been accredited by UKAS.

Plasma power	1.55 kW
Carrier gas flow	0.85 L/min
Make up gas flow	0.2 L/min
Integration time	0.5 seconds
Sampling depth	8 mm

Table 2-4: ICP-MS operating conditions

2.3: Results and Discussion

2.3.1 Reference Material Analysis

The results obtained from six digestions and analyses of BCS-CRM 517 are tabulated in Table 2-5. Digestion and analysis of the six replicates was completed over four days rather than in the same batch. In general good percentage recoveries were obtained, with most reporting a recovery of over 90 percent, which indicted good accuracy. The only element with a low percentage recovery was lead, 59 percent, which would have remained trapped within the silica matrix during the digestion process. This behaviour was discussed by Dean[20] who noted that for a silica containing matrix, the only acid that will digest silica and therefore liberate the metals of interest is hydrofluoric acid.[20] Excluding lead, all elemental concentrations were within the limits specified by the CRM certificate. The RSDs were all calculated to be below 15 percent which indicated good precision over the six replicates.

Element	Certified concentration (μg/g)	ICP-MS (μg/g)	% Recovery	RSD (%)
Cu 63	88 ± 6	82.3 ± 9	94	11.4
K 39	105 ± 11	97.8 ± 13	93	13.2
Mn 55	6790 ± 70	6727 ± 534	99	7.93
Pb 208	28 ± 4	16.4 ± 3	59	15.0
V 51	40 ± 7	41.8 ± 4	105	9.42
Zn 66	47 ± 4	42.9 ± 6	91	14.1

Table 2-5: ICP-MS CRM percentage recoveries (n=6)

16 separate digestions and analyses of Tata Steel's internal reference material, ore E, were completed over a duration of six months. These results were compared to Tata Steel's reference values, which were taken from an average of 50 replicate digestions and analyses, performed by two analysts based at Tata Steel. Results are tabulated in Table 2-6. The percentage recoveries were all close to 100 percent as well as the elemental concentrations being within the limits, which confirmed that both the digestions and analyses were

successful and of a good quality. The RSDs were all below 20 percent demonstrating good precision between the sixteen replicates.

Element	Tata Steel reference, n=50 (μg/g)	Interbatch average, n=16 (μg/g)	% Recovery	RSD (%)
Ba 137	165 ± 9	160 ± 9	97	5.87
Cd 111	<LOD	<LOD	-	-
Co 59	13.6 ± 2	13.9 ± 2	104	10.9
Cr 53	88.4 ± 5	88.9 ± 6	101	6.77
Cu 63	79.3 ± 4	75.4 ± 7	95	8.78
K 39	263 ± 17	265 ± 19	101	7.08
Mn 55	12110 ± 536	12019 ± 654	99	5.44
Ni 60	14.2 ± 3	14.4 ± 2	101	15.8
Pb 208	19.1 ± 3	19.1 ± 2	100	9.61
V 51	38.6 ± 3	38.9 ± 3	101	7.35
Zn 66	43.5 ± 10	41.9 ± 8	96	19.6

Table 2-6: Ore E interbatch analysis

The intrabatch analysis of ore E was also completed. It involved one digestion solution being diluted eight times and then analysed, results are tabulated in Table 2-7. Percentage recoveries tended to be above 100 percent apart from nickel (90 percent). The majority of the concentrations were also within the limits, set by Tata Steel, apart from chromium and manganese which were both above the top limit. This indicated that the analyses were generally precise, however, impurities may have been present in the digestion vessels or ICP vials, causing contamination. Excellent RSD values were also obtained, generally below eight percent, indicating that the dilutions and the subsequent analyses were acceptable.

Element	Tata Steel reference, n=50 (µg/g)	Intrabatch average, n=8 (µg/g)	% Recovery	RSD (%)
Ba 137	165 ± 9	175 ± 7	106	3.75
Cd 111	<LOD	<LOD	-	-
Co 59	13.6 ± 2	16.6 ± 1	124	4.99
Cr 53	88.4 ± 5	102 ± 5	115	5.15
Cu 63	79.3 ± 4	84.7 ± 5	107	6.26
K 39	263 ± 17	283 ± 20	108	7.26
Mn 55	12110 ± 536	13339 ± 625	110	4.68
Ni 60	14.2 ± 3	12.8 ± 2	90	12.4
Pb 208	19.1 ± 3	22.2 ± 1	116	4.06
V 51	38.6 ± 3	43.7 ± 2	113	5.14
Zn 66	43.5 ± 10	47.5 ± 6	109	12.3

Table 2-7: Ore E intrabatch analysis

2.3.2 ICP-AES Analytical Performance

The LOD is defined as: the concentration, derived from the smallest measure, which can be detected with reasonable certainty for a given analytical procedure.[21] In this study one percent nitric acid was analysed 10 times, and the results used to determine the detection limits through 3 times the standard deviation (σ), 3σ. Limits of detection, for this method, along with the measured concentrations are reported for in Tables 2-8. The measured concentrations were generally negative values. The negative values were reported by the instrument and generally indicated that those elements were not present within the solution, as expected. The values were only used to calculate the limits of detection.

In general the limits of detection were below 6 µg/L, with two exceptions, iron, 54.2 µg/L and potassium, 64 µg/L. These two increased limits did not affect the measured elemental concentrations of the four materials or the CRM. However a few other elements did return concentrations below the limits of detection, they were cadmium results for all four materials, chromium results for ore D, nickel results for ore F and vanadium results for both ores and the sinter dust. The limits of detection obtained here corresponded well with those

from literature. Apart from barium and iron all elements reported detection limits with the same order of magnitude as those theoretically calculated. Barium and iron reported detection limits one order of magnitude greater than those theoretically determined. Detection limits were also compared to those obtained in a similar study by Jackson.[22] Again apart from barium, which was one order of magnitude greater than reported, all of the limits of detection were very similar to the reported values. Iron was not analysed by Jackson and therefore the detection limits could not be compared.

Element	1	2	3	4	5	6	7	8	9	10	Average	Standard deviation	LOD
Ba 455.404	-3.00	-2.90	-2.50	-3.60	-3.80	-3.70	-3.60	-3.60	-4.20	-4.00	-3.49	0.528	**1.58**
Cd 228.802	-9.90	-10.7	-10.2	-9.8	-10.7	-10.9	-10.4	-10.7	-10.8	-10.0	-10.4	0.407	**1.22**
Co 228.616	-10.2	-10.5	-11.0	-10.6	-10.7	-10.7	-11.0	-12.0	-13.0	-11.0	-11.1	0.829	**2.47**
Cr 206.149	3.80	3.60	3.20	4.10	3.30	4.00	3.90	3.60	3.60	3.20	3.63	0.323	**0.970**
Cu 327.396	-4.50	-5.70	-5.20	-4.60	-5.80	-4.20	-4.70	-5.70	-5.80	-5.20	-5.14	0.604	**1.81**
Fe 239.562	65.8	34.6	55.1	52.9	53.3	31.3	5.2	51.9	53.9	62.2	46.6	18.1	**54.2**
K 766.491	35.2	70.1	67.3	10.1	21.8	12.1	48.3	30.3	38.2	56.2	39.0	21.3	**64.0**
Mn 260.569	3.40	4.50	4.90	5.30	4.50	5.00	3.40	4.30	5.60	5.90	4.68	0.840	**2.52**
Ni 231.604	3.20	4.70	3.20	2.90	5.10	4.40	5.30	3.70	5.40	3.20	4.11	0.978	**2.93**
V 292.464	5.80	5.50	7.40	7.70	2.50	6.20	2.30	5.20	4.00	5.00	5.16	1.82	**5.45**
Zn 213.856	3.10	3.10	1.80	1.00	0.300	1.00	0.600	1.00	1.70	2.40	1.60	0.998	**2.99**

Table 2-8: ICP-AES limits of detection (µg/L), calculated using 3σ

The QC solution was analysed after each calibration, which was completed following the analysis of every six solutions. This allowed the reliability of both the calibration and the elemental concentration of the materials to be determined. A QC of 500 µg/L was used with the ICP-AES and the recoveries obtained are listed in Tables 2-9.

The recovery values obtained for the QC analysis were good which indicated that the calibration solutions were accurate and reliable elemental concentrations had been obtained for the four materials and the CRM. Measurement precision was excellent, with RSDs for the QC below three percent for all but potassium. Although the potassium RSD value was slightly raised it was still acceptable.

Element	Reference value (µg/L)	ICP-AES, (µg/L)	RSD (%)
Ba 455.404	500	551 ± 9	1.72
Cd 228.802	500	529 ± 14	2.60
Co 228.616	500	524 ± 14	2.75
Cr 206.149	500	549 ± 12	2.19
Cu 327.396	500	535 ± 9	1.74
Fe 239.562	500	532 ± 24	4.46
K 766.491	500	561 ± 47	8.37
Mn 260.569	500	532 ± 10	1.96
Ni 231.604	500	544 ± 13	2.46
V 292.464	500	531 ± 11	2.16
Zn 213.856	500	525 ± 14	2.62

Table 2-9: ICP-AES QC (500 µg/L) average results (n=10)

BCS-CRM 517 was digested and analysed three times, alongside the four materials, to establish the reliability of the digestions. Results are shown in Table 2-10. Not all of the elements examined within this study were present within the CRM and therefore the results were only used as a guide to the digestion reliability. Generally the percentage recoveries were greater than 90 percent for most elements, indicating good digestions and accurate analyses. Vanadium could not be detected in any of the three digestion solutions which was due to the low level of vanadium present within the CRM. As well as iron and potassium

reporting recoveries of 120 percent, the majority of the elements, apart from zinc, reported concentrations which were above the certified limits. This was most likely due to contamination during the digestion but may have also been due poor analysis by the ICP-AES. The digestions were completed at Tata Steel where the digestion vessels are used on a regular basis for the digestion of both iron ores and iron containing materials. Excellent precision for the determination of copper and manganese in the CRM was obtained for ICP-AES analysis and RSDs of 0.84 percent and 0.41 percent respectively were calculated. The other three elements reported RSDs higher than this, yet they were all still below 12 percent indicating good precision. When compared with the previous CRM analysis, detailed in Section 2.3.1, the results obtained here do not vary greatly, however the precision of the elemental analysis increases, as shown by a decrease in the RSD values.

Element	Certified concentration (µg/g)	ICP-AES, (µg/g)	% Recovery	RSD (%)
Cu 327.396	88 ± 6	79.7 ± 1	91	0.837
Fe 239.562	663000 ± 600	843540 ± 102006	127	12.0
K 766.491	105 ± 11	131 ± 3	124	2.66
Mn 260.569	6790 ± 70	6088 ± 25	90	0.413
V 292.464	40 ± 7	<LOD	<LOD	-
Zn 213.856	47 ± 4	50.3 ± 2	107	4.04

Table 2-10: ICP-AES CRM percentage recoveries (n=3)

2.3.3 ICP-MS Analytical Performance

Limits of detection, for ICP-MS analysis, along with the concentrations of the ten blanks are reported in Table 2-11. A large proportion of the elements reported limits of detection below 0.8 µg/L except for potassium, manganese, nickel and zinc, which reported detection limits of 5.97 µg/L, 7.59 µg/L, 2.23 µg/L and 1.34 µg/L respectively. Although slightly increased these limits did not affect the elemental results of the four materials. The only materials to report elemental concentrations below the limits of detection were ore D and ore F, which

both reported undetectable limits of cadmium. This indicated very low levels of cadmium were present within these two materials.

Limits of detection obtained with the ICP-MS were generally three orders of magnitude greater than theoretically calculated values, provided by the manufacturer. The two exceptions to this were potassium and manganese which were respectively two and four levels of magnitude greater. This was to be expected due to spectral interferences and possible contamination which would not have been accounted for when calculating the theoretical limits. Detection limits obtained here are very similar to those obtained by Jackson.[22] Three elements, barium, potassium and vanadium, reported limits with the same order of magnitude as Jackson with chromium reporting a detection limit which was one magnitude smaller. Cadmium, cobalt and nickel reported detection limits two order of magnitude greater than Jackson and all other elements, copper, manganese, lead and zinc were just one order of magnitude greater. Similar variations in detection limits were also seen when comparing limits of detection obtained here to those obtained by Date, Cheung, Stuart and Xiu-Hua[15] who completed the digestion and analysis of iron containing materials using an ICP-MS. Six of the elements, barium, cadmium, chromium, copper and lead, produced detection limits which were the same order of magnitude, with the other four elements, cobalt, manganese, nickel and vanadium reporting detection limits one or two orders of magnitudes greater than Date, Cheung, Stuart and Xiu-Hua.[15]

Element	1	2	3	4	5	6	7	8	9	10	Average	Standard deviation	LOD
Ba 137	0.030	0.013	0.003	0.018	0.140	0.015	0.015	0.006	0.801	0.011	0.106	0.248	**0.743**
Cd 111	0.025	0.006	0.0005	0.015	0.005	0.004	0.011	0.004	0.798	0.0006	0.087	0.250	**0.750**
Co 59	0.296	0.120	0.030	0.296	0.227	0.137	0.195	0.176	0.844	0.042	0.236	0.232	**0.696**
Cr 53	0.105	0.064	0.0002	0.062	0.029	0.061	0.043	0.068	0.859	0.003	0.130	0.258	**0.774**
Cu 63	1.13	1.03	1.08	0.904	1.14	0.851	1.20	0.929	0.878	0.836	0.998	0.135	**0.404**
K 39	6.14	7.40	6.12	3.00	3.74	3.73	6.87	2.49	5.07	8.34	5.29	1.99	**5.97**
Mn 55	0.952	0.212	0.039	0.843	0.310	0.630	0.511	0.602	8.39	0.026	1.25	2.53	**7.59**
Ni 60	1.85	1.14	0.424	1.73	1.49	0.444	0.521	2.30	2.47	1.28	1.36	0.743	**2.23**
Pb 208	0.081	0.075	0.124	0.137	0.155	0.013	0.006	0.070	0.818	0.085	0.157	0.237	**0.712**
V 51	0.027	0.007	0.004	0.015	0.010	0.006	0.013	0.005	0.812	0.003	0.090	0.254	**0.761**
Zn 66	0.070	0.308	0.00	0.044	0.253	0.063	0.089	0.012	1.47	0.028	0.234	0.447	**1.34**

Table 2-11: ICP-MS limits of detection (μg/L), calculated using 3σ (n=10)

Good recoveries, listed in Table 2-12, were obtained from the analysis of the 50 µg/L QC which was used with the ICP-MS. This indicated that the analysis was reliable and that the calibration solutions were accurate. The majority of the elements reported RSDs below four percent, except for potassium and nickel which had RSDs of 11.0 percent and 7.5 percent respectively. These RSDs, although raised, still indicated good precision.

Element	Reference value (µg/L)	ICP-MS, (µg/L)	RSD (%)
Ba 137	50	52.2 ± 2	3.60
Cd 111	50	51.1 ± 1	2.18
Co 59	50	52.8 ± 1	1.93
Cr 53	50	55.3 ± 1	2.52
Cu 63	50	52.9 ± 1	2.50
K 39	50	56.8 ± 6	11.0
Mn 55	50	57.5 ± 1	2.05
Ni 60	50	53.6 ± 4	7.50
Pb 208	50	51.3 ± 1	1.81
V 51	50	53.3 ± 1	1.68
Zn 66	50	56.3 ± 2	3.96

Table 2-12: ICP-MS QC (50 µg/L) average results (n=10)

Results from the analysis of the three CRM replicate analyses using ICP-MS are listed in Table 2-13. In general excellent recoveries of above 99 percent were reported and elemental concentrations were within the certified limits which both showed that an accurate digestion was completed. The two exceptions to this were manganese whose elemental concentration was above the certified limit, most likely due to contamination from the digestion vessel and lead which reported a recovery of 63 percent a similar percentage to what was seen in Section 2.3.1. This confirmed that lead could not be fully digested using aqua regia and remained trapped in the undigested silica matrix.[20] All other elements produced greater percentage recoveries than those obtained in Section 2.3.1 indicating a better and more accurate digestion. The precision of the analysis, determined by the RSD values, was also better than in Section 2.3.1, all values were below eight percent, indicating better precision.

Element	Certified concentration (µg/g)	ICP-MS, (µg/g)	% Recovery	RSD (%)
Cu 63	88 ± 6	90.5 ± 5	103	5.93
K 39	105 ± 11	117 ± 8	112	7.05
Mn 55	6790 ± 70	7327 ± 179	108	2.44
Pb 208	28 ± 4	17.5 ± 1	63	6.77
V 51	40 ± 7	44.6 ± 1	112	3.27
Zn 66	47 ± 4	46.5 ± 3	99	5.57

Table 2-13: ICP-MS CRM percentage recoveries (n=3)

2.3.4 Comparison of the Analytical Performance for ICP-AES and ICP-MS

Comparisons can be made of the analytical performance between the ICP- AES and ICP-MS analyses of the digestion solutions.

As expected the detection limits obtained using the ICP-AES were higher than that obtained when using the ICP-MS. The ICP-AES produced detection limits generally below 6 µg/L and the ICP-MS produced detection limits generally below 0.8 µg/L. Both instruments gave increased limits for iron and potassium, however, this did not affect any of the material or CRM results. A number of the materials gave elemental concentrations which were below the limits of detection, especially when analysed by ICP-AES. This indicated that on occasion it is necessary to use both ICP instruments to get a full elemental profile of a material. For example in this work by completing analysis using both ICP instruments it was possible to determine elemental concentrations for cadmium, chromium, nickel and vanadium, which would not have been possible if only ICP-AES had been used. At the same time by using ICP-AES it was possible to determine iron concentrations which were too high for analysis by ICP-MS. Both sets of detection limits corresponded well with values obtained from literature, although only the emission detection limits were comparable with the manufacturer's theoretical limits of detection.

QC's of differing concentration were used with each of the ICP instruments due to their dissimilar detection powers. However, the recoveries obtained were very similar. Both instruments also gave excellent RSD values, indicating excellent precision over the ten replicates completed with each instrument. The three increased RSDs, for potassium with ICP-AES and potassium and nickel with ICP-MS, were due to the variation in the QC results over the ten replicates. There may have been a small amount of contamination within the ICP vials which caused this variation.

The CRM results were superior when completing analysis using ICP-MS. The ICP-AES results did not tend to correspond well with the certified limits and also produced varied percentage recoveries indicating poor precision. The ICP-MS results were much improved, with better percentage recoveries and only one element reporting a concentration above the certified limit. RSDs values were slightly higher when using the ICP-MS, but both instruments provided accurate results. The results from the multielement analysis will now be tabulated and discussed and a final comparison between the two ICP instruments will be completed.

2.3.5 Multielement Analysis of Four Steelworks Materials

Results from the multielement analysis of the four materials, using ICP-AES and ICP-MS, are reported by material, in Tables 2-14 to 2-17, alongside the RSD values. The results tabulated within this chapter have been calculated from the raw data obtained from the instruments. The averaged results from the digestion blanks were taken away from the ICP results to account for any contamination with the digestion vessels. The mass of the solid sample used for the digestion was then taken into consideration to allow the results to be reported in µg/g.

In general RSD values for all four materials were below ten percent with some exceptions which are noted here as well as in Table 2-18. Slightly better precision was obtained for ICP-AES compared to ICP-MS, on the other hand more elemental concentrations were below the limit of detection with this technique. The results from the two instruments do differ from each other and are not within the stated error limits. This is due to the differing detection powers of the two instruments and it is commonplace in analytical work to get slight variation in the results from each instrument.

Iron concentrations were only determined using ICP-AES due to the high concentrations present within the material. The determination of lead concentrations was only undertaken with ICP-MS due to the spectral iron interference which was present when using ICP-AES, as shown in Figure 2-1 and discussed in Chapter One. The presence of high iron concentrations within all four materials caused a spectral interference by emitting light at a similar wavelength to lead and producing an additional peak in the spectrum. This additional peak affected the peak height, and therefore the perceived concentration, of lead and hence the determined elemental results were discarded.

Figure 2-1: Wavelength scan of lead, shown in red, with iron interference shown in green
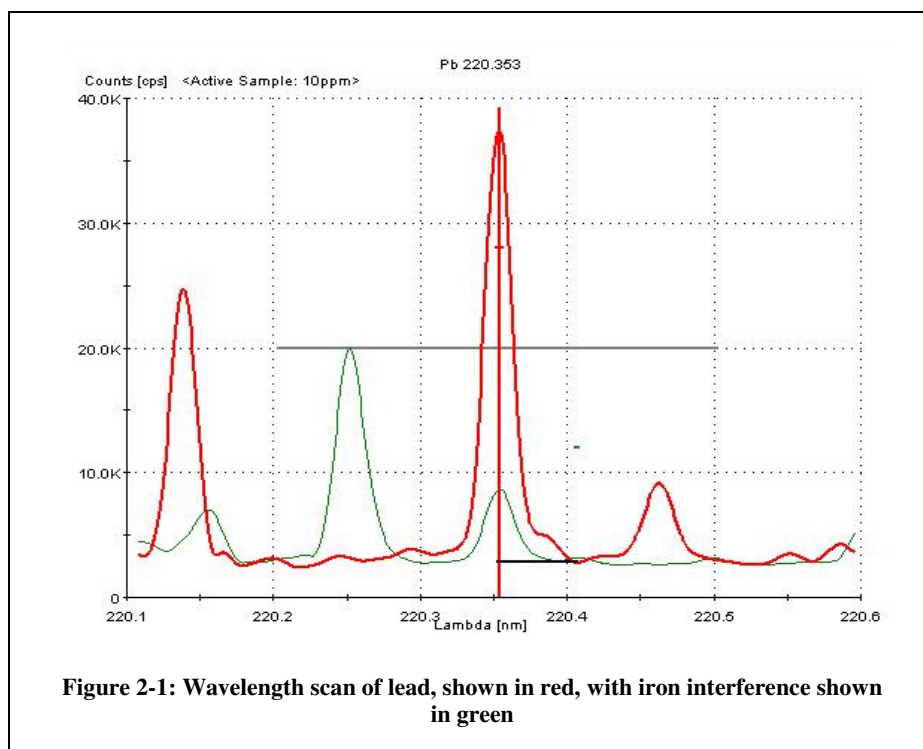
Ore D results are tabulated in Table 2-14. RSD values calculated for the three replicates were generally below six percent which indicated excellent precision. Potassium showed an increased RSD value of 11 percent for ICP-MS. Although raised this was still acceptable. The elemental results obtained using the two methods were very similar, with high concentrations of iron and manganese, which were expected due to the Brazilian origin of the ore. Cadmium levels were very low and undetectable using either ICP instrument. The other elements all showed similar concentrations, below 100 µg/L.

Element	ICP-AES (µg/g)	ICP-AES RSD (%)	ICP-MS (µg/g)	ICP-MS RSD (%)
Ba	78.3 ± 0.4	0.448	91.4 ± 3	2.82
Cd	<LOD	<LOD	<LOD	<LOD
Co	18.5 ± 0.3	1.76	19.9 ± 1	5.19
Cr	20.1 ± 0.04	0.216	18.7 ± 0.2	1.23
Cu	8.6 ± 0.2	1.85	10.1 ± 0.3	3.35
Fe	932171 ± 14253	1.53	-	-
K	99.0 ± 6	6.38	52.3 ± 6	11.0
Mn	2136 ± 14	0.676	2836 ± 158	5.56
Ni	12.2 ± 0.3	2.07	21.5 ± 0.7	3.12
Pb	-	-	5.99 ± 0.3	4.29
V	<LOD	<LOD	27.7 ± 1	4.25
Zn	26.7 ± 1	4.26	20.8 ± 0.7	3.27

Table 2-14: Multielement analysis of Ore D (n=3)

Elemental results for ore F are tabulated in Table 2-15. Except for the ICP-MS analysis of zinc, all RSDs were below ten percent, showing excellent method precision. The reason for the high zinc RSD was that one of the three zinc concentrations was below the limit of detection and the other two results were not very comparable, 13.3 µg/L and 8.88 µg/L. This indicated that there was some zinc contamination possibly from the digestion vessel causing the three values to vary greatly from each other. The same digestion vessel was used for all of the ore F replicates explaining why this anomaly was only seen for the one material. As with ore D high concentrations of both iron and magnesium were calculated and cadmium was undetectable. The other elements produced similar concentrations from both ICP analyses, however the use of the ICP-MS allowed nickel and vanadium concentrations,

which were below the ICP-AES detection limits, to be determined. Elemental concentrations were comparable for each instrument, indicating good accuracy.

Element	ICP-AES (µg/g)	ICP-AES RSD (%)	ICP-MS (µg/g)	ICP-MS RSD (%)
Ba	56.5 ± 4	6.32	66.2 ± 4	6.59
Cd	<LOD	<LOD	<LOD	<LOD
Co	14.8 ± 0.3	2.07	15.5 ± 0.5	3.12
Cr	32.0 ± 0.5	1.67	35.2 ± 1	2.87
Cu	5.59 ± 0.1	1.24	8.27 ± 0.7	8.03
Fe	885057 ± 63852	7.21	-	-
K	90.4 ± 9	9.96	81.9 ± 7	8.35
Mn	1056 ± 18	1.73	1461 ± 50	3.42
Ni	<LOD	<LOD	8.66 ± 0.5	5.48
Pb	-	-	7.53 ± 0.5	6.91
V	<LOD	<LOD	52.0 ± 3	4.99
Zn	22.1 ± 1	8.73	11.1 ± 3	28.1

Table 2-15: Multielement analysis of Ore F (n=3)

The flue dust material (Table 2-16) indicated much higher concentrations of most elements, except iron, than either of the ores. By using both ICP instruments elemental concentrations for all elements were able to be determined, with no elements returning concentrations below the limits of detection. The highest elemental concentrations were seen for iron, potassium, manganese, lead and zinc which all reported concentrations above 2500 µg/L. The high elemental concentrations of these specific elements in a flue dust are confirmed by Zeydabadi, Mowla, Shariat and Kalajahi.[23] By completing XRF on a flue dust they determined four separate categories of elements, majority elements (iron), first order minority elements (zinc), second order minority elements (potassium, manganese and lead) and trace elements (cadmium and cobalt). These four categories correspond excellently with the elemental results obtained by this study.[23] The other elements analysed here were not studied and therefore cannot be compared. In terms of RSD values all elements reported values below nine percent which demonstrated good precision. Some variation was seen in the elemental concentrations between the two methods, most concentrations were of the same order of magnitude though, illustrating good precision.

Element	ICP-AES (µg/g)	ICP-AES RSD (%)	ICP-MS (µg/g)	ICP-MS RSD (%)
Ba	89.9 ± 0.3	0.361	102 ± 2	1.74
Cd	<LOD	<LOD	7.65 ± 0.2	2.99
Co	95.4 ± 0.6	0.582	131 ± 2	1.47
Cr	217 ± 3	1.50	238 ± 9	3.78
Cu	264 ± 4	1.61	316 ± 26	8.37
Fe	534122 ± 33183	6.21	-	-
K	2864 ± 188	6.57	3382 ± 256	7.56
Mn	5985 ± 59	0.980	8227 ± 320	3.89
Ni	213 ± 2	1.01	305 ± 6	1.95
Pb	-	-	3112 ± 66	2.11
V	199 ± 4	2.08	377 ± 12	3.26
Zn	7166 ± 125	1.74	9885 ± 171	1.73

Table 2-16: Multielement analysis of flue dust (n=3)

The elemental concentrations and RSD values for the sinter dust material are tabulated in Table 2-17. The precision of the measurements was excellent with all RSDs reported to be below seven percent. The use of both instruments allowed concentrations to be determined for all elements. The most concentrated elements were iron, potassium, manganese and lead, which all reported concentrations of above 2000 µg/L. Sinter dust is mainly made up of small iron ore particulates which could not be put straight into the blast furnace without being agglomerated, which explains the high concentrations of iron and manganese. Sinter dust is also made up of fluxes which illustrates why other elements are also in abundance. Each instrument reported elemental concentrations which were of the same order of magnitude, indicating good accuracy. In general lower RSD values were obtained for analyses completed using ICP-AES.

Element	ICP-AES (µg/g)	ICP-AES RSD (%)	ICP-MS (µg/g)	ICP-MS RSD (%)
Ba	176 ± 4	2.39	167 ± 6	3.52
Cd	<LOD	<LOD	45.2 ± 2	5.13
Co	16.5 ± 0.2	1.08	11.2 ± 0.5	4.55
Cr	121 ± 3	2.07	136 ± 4	3.00
Cu	40.5 ± 0.3	0.684	200 ± 12	6.23
Fe	690894 ± 19345	2.80	-	-
K	928 ± 50	5.34	15822 ± 942	5.96
Mn	4177 ± 24	0.565	3527 ± 175	4.97
Ni	42.1 ± 0.2	0.460	89.4 ± 5	5.87
Pb	-	-	2275 ± 84	3.71
V	<LOD	<LOD	64.2 ± 3	5.05
Zn	166 ± 1	0.729	159 ± 6	3.63

Table 2-17: Multielement analysis of sinter dust (n=3)

2.3.6 Comparison of the Multielement Analysis of Four Steelworks Materials for ICP-AES and ICP-MS

In general the RSD values were lower when completing analysis using ICP-AES, which indicated better method precision. A larger number of elements were below the limits of detection with this technique and due to spectral interferences the analysis of lead was not possible. Potassium and zinc also have spectral iron interferences, when using ICP-AES, as shown in Figures 2-2 and 2-3.

Figure 2-2: Wavelength scan of potassium, in red, with iron interference shown in green

Figure 2-3: Wavelength scan of zinc, in red, with iron interference shown in green
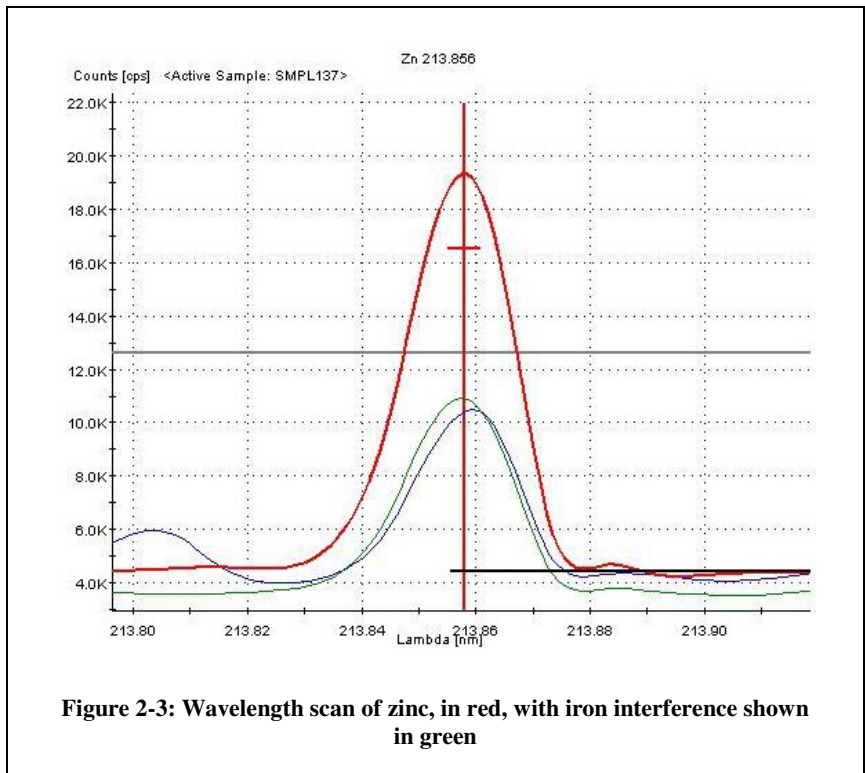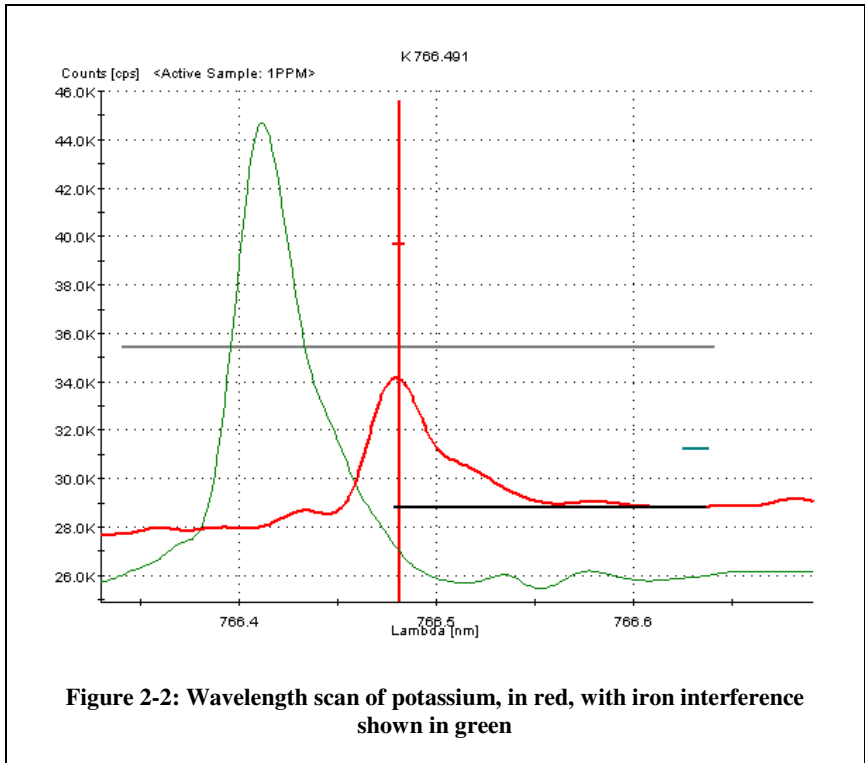
For both iron ores, ore D and ore F, the elemental results obtained using each ICP instrument were comparable which indicates excellent method accuracy. When completing analysis of the two dusts, flue dust and sinter dust, the elemental concentrations were not as comparable,

but the results from each instrument did tend to have the same order of magnitude. This indicated that the accuracy of the measurements was still of a good standard but could be improved. The reason for this difference is most likely due to the composition of the dusts and the increased concentrations that were determined for a number of the elements. The accuracy of the results could not be fully determined since the elemental concentrations of the four samples have only been determined within this work and nowhere else. Overall the reproducibility of the elemental concentrations, between instruments, for each material was good with ICP-MS returning higher elemental concentrations, in most cases. Taking into account the analytical performance of both instruments and the determined elemental concentrations, Table 2-18 indicates the preferred method for analysis in future work.

Element	ICP-AES precision	ICP-MS precision	Preferred technique
Ba	Good	Good	Either
Cd	All concentrations below LOD	Good for both dusts, below LOD for both ores	ICP-MS
Co	Good	Good	Either
Cr	Good	Good	Either
Cu	Good	Good	Either
Fe	Good	-	ICP-AES
K	Good	Generally good, high for ore D (11.0 %)	ICP-MS due to interference
Mn	Good	Good	Either
Ni	Generally good, below LOD for ore F	Good	ICP-MS
Pb	-	Good	ICP-MS
V	Good for flue dust, sinter dust and both ores below LOD	Good	ICP-MS
Zn	Good	Good for both dusts and ore D, poor for ore F (28.1 %)	ICP-MS due to interference

Table 2-18: Precision of analyses and preferred method for future work

2.4: Main Findings

Two reference materials, one CRM and one internal, have been digested and inter and intra batch ICP-MS analysis has been undertaken. Subsequently four materials from an integrated steelworks, alongside an iron ore CRM, were digested and analysed using both ICP-AES and ICP-MS. The elemental results have been tabulated and the accuracy and precision of the analyses determined. Results from each of the ICP instruments have also been compared.

Analysis of the reference materials generally showed good precision and accuracy over a number of replicates. Low levels of lead were determined within the CRM. This was most likely due to the trapping of the element within the undigested silica matrix, as discussed by Dean.[20] Similar percentage recoveries were obtained for both the inter and intra batch analysis of Tata Steel's internal reference material, ore E, indicating that a good digestion was completed and the dilution and analysis of the digestion solutions was accurate.

Following the analysis of the reference materials the analytical performance of both the ICP-AES and the ICP-MS was examined. Low limits of detection were obtained with each instrument, below 6 µg/L for ICP-AES and below 0.8 µg/L for ICP-MS, which corresponded well with literature values. Quality control solutions were analysed alongside the calibration standards to determine the reliability of the calibration solutions. Good recoveries were obtained, especially for ICP-MS, as well as low RSD values, generally below nine percent, illustrating that the calibration standards were both precise and accurate. The accuracy of the elemental results was established by examining the percentage recoveries obtained for the CRM. Generally a good degree of accuracy was achieved as determined by the percentage recoveries which in general were above 90 percent. Precision of the CRM analysis was also good, for both instruments, with all RSDs below 12 percent. For lead analysis, with the ICP-MS, a poor recovery of 63 percent was calculated, indicating the trapping of elements within the undigested silica matrix. To allow full digestion, of solid materials, in future experiments

a higher strength acid such as hydrofluoric acid should be used.[20] In using hydrofluoric acid, there would also be a need to use a specialised sample introduction system which would avoid corrosion of any glass components.

The elemental results, as well as RSD values used to determine method precision, have been calculated and compared for all four steelworks materials, ore D, ore F, flue dust and sinter dust. Iron and lead, were only analysed using one ICP, AES and MS respectively, whereas concentrations for all other elements were determined using both ICP instruments. Both ores reported high elemental concentrations of iron and manganese, which was to be expected, cadmium was undetectable by either instrument. The analysis of each ore was precise, with all RSDs values generally below 11 percent for both instruments. Elemental concentrations were comparable between each instrument for both iron ores, indicating that a good level of accuracy was achieved for both methods. The flue dust material reported high concentrations, over 2500 µg/L, of iron, potassium, manganese, lead and zinc agreeing with literature published by Zeydabadi, Mowla, Shariat and Kalajahi.[23] Analysis of all elements was possible by using both ICP instruments and good method accuracy and precision was achievable, with RSD values below nine percent. Concentrations could be determined for all elements within the sinter dust material with four elements, iron, potassium, manganese and lead, returning concentrations over 2000 µg/L. In general better method precision was attained when using ICP-AES, however all RSD values, for both instruments, were below seven percent. Comparisons between the elemental concentrations determined by each instrument could be made, indicating the analyses were completed with good accuracy.

Overall the RSD values for all analyses were smaller when using ICP-AES, indicating a more precise method. Due to the increased limits of detection and spectral interferences it has been decided that ICP-MS should be the preferred technique for analysis of steelworks materials, although solutions containing elements in high concentrations, such as iron, should be analysed by ICP-AES or highly diluted for analysis with an ICP-MS. To allow the

full digestion of lead in any future work varying combinations of acid should be investigated as well as the use of hydrofluoric acid, as recommended by both Agilent[24] and CEM[25] for the microwave digestion of iron ores.

This research has provided the concentrations of cadmium and lead in each material, two of the heavy metals currently being monitored within the atmosphere and which also cause the most health risks. If the concentration of these heavy metals in materials is known it allows abatement procedures to be concentrated on the plants which either generate or use those specific materials. In this study it was found that both iron ores had undetectable levels of cadmium, followed by flue dust, 7.65 µg/g, and finally sinter dust had the highest cadmium concentration at 45.2 µg/g. In terms of lead, both ores, D and F, reported low concentrations, 5.99 µg/g and 7.53 µg/g respectively, followed by sinter dust at 2275 µg/g and flue dust at 3112 µg/g. Fisher[26] stated that under low wind speeds, the number of particulates that become airborne from stockpiles is low. This statement, along with the results obtained within this research both indicate that abatement procedures should be concentrated on the sinter plant and the blast furnace rather than material handling and storage.

This chapter has allowed an insight into the current indirect methods used to analyse particulate containing materials. To allow the full characterisation of the four steelworks materials to be undertaken novel direct experiments must be developed and undertaken.

The following two chapters will discuss the coupling of a rotating drum system with an Aspect morphology analyser and an ELPI. The coupling of these instruments will allow morphological profiles as well as number and mass-size distributions to be obtained. Substrates from the ELPI will also be digested, using a similar method to that used in this chapter, to determine whether particulates can successfully be collected onto substrates, before their elemental composition is determined through ICP analysis. The determined compositions will be compared with those discussed in this chapter. Subsequently the

coupling of a LIBS unit to an Aspect morphology analyser and an ELPI will be completed. This will allow the physical characterisation of a laser generated aerosol and an insight into the laser material interaction. The ELPI substrates, and the particulates collected upon them, obtained from the LIBS-ELPI coupling, will then be digested and analysed using an ICP-MS to allow the chemical composition of the laser generated aerosol to be established.

2.5: References

1. T. E. Norgate, S. Jahanshahi and W. J. Rankin, *Journal of Cleaner Production*, 2007, **15**, 838-848.
2. http://ec.europa.eu/environment/chemicals/reach/reach_intro.htm, Accessed 4th July 2013
3. *Best Available Techniques Reference Document for Iron and Steel Production*, European Comission, 2010.
4. N. Schofield, R. Fisher and D. R. Anderson, *Ironmaking & Steelmaking*, 2004, **31**, 428-431.
5. E. Aries, D. R. Anderson, R. Fisher, T. A. T. Fray and D. Hemfrey, *Chemosphere*, 2006, **65**, 1470-1480.
6. N. Menad, H. Tayibi, F. G. Carcedo and A. Hernández, *Journal of Cleaner Production*, 2006, **14**, 740-747.
7. *Best Available Techniques for the Production of Iron and Steel*, European Comission, Integrated Pollution Prevention and Control (IPPC), July 2009.
8. B. B. Kebbekus and S. Mitra, *Environmental Chemical Analysis*, Blackie Academic and Professional, London, 1998.
9. B. J. Alloway and D. C. Ayres, *Chemical Principles of Environmental Pollution*, Blackie Academic and Professional, Glasgow, 1993.
10. http://www.uk-pollutantdeposition.ceh.ac.uk/heavy_metals, 26th January 2011
11. *Air Quality in Europe - 2012 Report*, European Environment Agency,Copenhagen, 2012.
12. http://www.nlincsair.info/index.php, Accessed 4th July 2013
13. J. O. Nriagu, *Environmental Pollution*, 1988, **50**, 139-161.
14. F. Zahir, S. J. Rizwi, S. K. Haq and R. H. Khan, *Environmental Toxicology and Pharmacology*, 2005, **20**, 351-360.
15. www.uk-pollutantdeposition.ceh.ac.uk/heavy_metals, Accessed 4th July 2013
16. A. R. Date, Y. Y. Cheung, M. E. Stuart and J. Xiu-Hua, *Journal of Analytical Atomic Spectrometry*, 1988, **3**, 653-658.
17. F. E. Smith and E. A. Arsenault, *Talanta*, 1996, **43**, 1207-1268.
18. Y.-C. Sun, P.-H. Chi and M.-Y. Shiue, *Analytical Sciences*, 2001, **17**, 1395-1399.
19. J. Sastre, A. Sahuquillo, M. Vidal and G. Rauret, *Analytica Chimica Acta*, 2002, **462**, 59-72.
20. www.tatasteeleurope.com/en/company, Accessed 4th July 2013
21. J. R. Dean, *Practical Inductively Coupled Plasma Spectroscopy*, John Wiley and Sons, New York, 2005.
22. http://goldbook.iupac.org/, Accessed 4th July 2013
23. K. Jackson, PhD Thesis, University of Sheffield, 2009.
24. B. Asadi Zeydabadi, D. Mowla, M. H. Shariat and J. Fathi Kalajahi, *Hydrometallurgy*, 1997, **47**, 113-125.
25. S. Richter, A. Meckelburg, S. Recknagel, R. Matschat and U. Panne, *Agilent ICP-MS Journal*, 2009, **38**, 4-5.
26. www.cem.com, Accessed 4th July 2013
27. R. Fisher, *The Coke Oven Manager's Year-Book*, 2001, 87-105.

Chapter Three

Morphological studies of particulates using an RDS-Aspect method

3.1 Introduction

The handling, storage and mixing of materials in industrial processes all lead to the liberation of dust particulates[1] which once airborne can become a significant occupational hazard as well as causing damage to equipment and products.[2] The composition of dust particulates is not always the same as its source and, therefore, the analysis and characterisation of the particulates themselves is of paramount importance.[2] Dust particulates can cause a range of problems to the cardiopulmonary system,[3] such as the aggravation of respiratory and cardiovascular disease, cancer and premature death.[4] The three health related particulate size fractions, which are defined by the standard BS EN 481[5] were described in detail in Section 1.1.3.

In relation to the respiratory system especially, the shape and size of dust particulates are a critical factor in terms of penetration, deposition and rate of particulate removal. There are, therefore, increasing studies into the shape and size of particulates.[4, 7-10]

There are a range of techniques used to study the shape and size of particulates, including sieving techniques, microscopy techniques and light scattering techniques,[11] as detailed in Table 3-1. The oldest of these techniques is sieving, which separates particulates depending on their size, however it is unable to determine particulate morphology. It is also generally only used to test particulates between 125 mm and 20 µm.[11]

The technique most frequently used to study both the shape and size of particulates is microscopy. This technique provides the means to characterise a particulate's size, size distribution and its morphology. Microscopy techniques, such as SEM, also allow a wide range of materials to be studied. SEM is designed primarily for imaging of particulates. As a material is scanned by an electron beam, the signal from the electron detector is displayed on a computer screen as an image. This image shows the shape of a particulate and by knowing what magnification was used, a particulate's size can be determined.[12] Studies into the use of SEM for particulate characterisation have been completed.[13-17] For example, in 1984 Kaufherr and Lichtman[14] used a cascade impactor to collect particulates onto stainless steel substrates at a coal burning power station. The collected particulates were then studied using a SEM to determine their shape. Particulates were typically spherical although particulates with irregular shapes were also found.[14] More recently, in 2004, Moreno, Jones and Richards[16] collected airborne particulates from both industrial and urban sites in Wales. Particulates were collected onto polyurethane foams using a high volume cascade impactor. To allow the shape and size of particulates to be determined SEM photographs were taken. Moreno, Jones and Richards found a selection of particulates of different shape and sizes from a range of sources, such as the sea, the motorway and a nearby integrated steelworks.[16] This study involved the collection of particulates before analysis which can be time consuming and does not allow in-situ analysis to be completed.

Technique	Size range	Operating mode	Strengths	Limitations
Sieving	20 µm to 125 mm	Off line	Broad size range, Simple principles	Long analysis time, Size measurements only
SEM	1 nm to 1 mm	Off line	Simple sample preparation, Shape and size measurements	Samples may not be representative, Lots of training required
Morphologi G3, Malvern	0.5 µm to 1 mm	Off line	Automated technique, Shape and size measurements	Particulates must be on substrates, Greyscale imaging only
Light Scattering	0.04 µm to 8 mm	Generally off line	Rapid analysis, Simple sample preparation	Can get errors if particulates are not spherical, Cannot distinguish between particulates and agglomerates
APS, TSI	0.5 µm to 20 µm	On or off line	Measures light scattering intensity, as well as particulate size	Dry sample characterisation only, Size measurements only
SMPS, TSI	10 nm to 487 nm	On or off line	Unattended operation, Characterises large concentrations	Small size range, Size measurements only
Aspect, Biral	0.5 µm to 20 µm	On or off line	Unattended operation, Shape and size measurements	Cannot distinguish between particulates and agglomerates, Dry sample characterisation only

Table 3-1: Techniques for characterising particulates[11, 12, 18, 20-22]

There are a selection of other instruments commercially available which use microscopy techniques to determine the shape and size of particulates. One such instrument is the Morphologi G3, manufactured by Malvern Instruments, UK. The Morphologi G3 captures static images of particulates by scanning a material, allowing the size and morphological properties of the material to be determined.[18] This technique does not currently allow the in situ or real time analysis of particulates.

Two real time particulate size characterisation techniques, currently manufactured by TSI are the scanning mobility particle sizer and the aerodynamic particle sizer,[19] as described in Section 1.2.3.

A large range of light scattering techniques are commercially available for particulate sizing, fewer are available which allow the determination of both a particulate's shape and size. The only commercially available real time technique, capable of determining the shape and size of particulates, using light scattering, is the Aspect morphology analyser, which is manufactured by Biral[22] and was fully described in Section 1.4.

One of the first papers regarding the use of the ASAS was published in 1992. Reid, Martin and Clark[23] completed characterisation of commercial spherical calibration standards. The ASAS technology proved to be good at classifying particles of a well defined morphology and was able to discriminate between particles of similar shapes.[23] Since its development the ASAS has been used in the characterisation of a number of aerosols. Hirst and Kaye[24] helped to develop the ASAS through studying aerosol particulates of known shape and size. Spheres, cubes and fibres were all characterised and scattering patterns obtained for each. These were compared with theoretical data and good agreement between the two was obtained.[24] Kaye[25] used an ASAS to complete real time characterisation of asbestos fibres. Scattering profiles were obtained indicating horizontal scattering, which would be expected for fibres.[25] 2005 saw the use of the ASAS as a biological detection agent by the UK

Ministry of Defence.[26] The use of the system, alongside an aerosol fluorescence monitor, was a major advancement in the field of airborne biological agent detection and reduced the number of false alarm rates.[26]

An RDS[27] is commonly used to measure the dustiness of a material, defined as "the propensity of materials to produce airborne dust during handling",[6] as well as collecting size fractionated particulate matter into the three health related size fractions. It was developed from a rolling drum test previously used by Warren Springs Laboratory and was chosen because it was the best method to simulate materials handling processes of a wide range of materials. To simulate handling processes a series of eight blades were fixed to the inside of the drum to allow the test material to be lifted before falling, as the drum rotated. These blades and the rotating motion of the drum are what allow the testing of fine, lumpy, dry or damp materials.[28] Porous polyurethane foams are used at one end of the drum for the collection of particulates into the three health related size fractions. Since its development the RDS has now been recognised, by BS EN 15051, as one of the reference test methods to classify the dustiness of bulk solid materials.[6]

This work aims to use an Aspect morphology analyser to characterise the four materials which were chemically characterised in Chapter Two, ore D, ore F, flue dust and sinter dust. An Aspect will be coupled to an RDS to allow the generation of dust particulates followed by the characterisation of their shape and size, in real time. The four materials will be characterised both individually as well as within binary mixtures to determine if the unique fingerprints of each material can be extracted from a mixed fingerprint. Both the data obtained and the comparisons that will be undertaken can help to further the understanding about particulate composition.

Due to its recent commercial manufacture, the Aspect morphology analyser and the morphology of airborne particulates have not been greatly researched, especially on site, in

an industrial environment. This work has been completed alongside a European Commission project sponsored by the RFCS. Therefore, although the majority of the work completed here will be laboratory based the Aspect instrument has been used by other groups in source apportionment studies. The use of the Aspect for source apportionment has to the best of our knowledge not been reported before and therefore the preliminary studies discussed in this chapter will allow proof of concept.

3.2 Experimental

3.2.1 Materials

Four materials, ore D, ore F, flue dust and sinter dust, have been characterised using the RDS-Aspect method. These materials were chemically characterised in Chapter Two and their chemical compositions are listed in Table 3-2.

| Element	Ore D (µg/g)	Ore F (µg/g)	Flue Dust (µg/g)	Sinter Dust (µg/g)
Ba	91.4 ± 3	66.2 ± 4	102 ± 2	167 ± 6
Cd	<LOD	<LOD	7.65 ± 0.2	45.2 ± 2
Co	19.9 ± 1	15.5 ± 0.5	131 ± 2	11.2 ± 0.5
Cr	18.7 ± 0.2	35.2 ± 1	238 ± 9	136 ± 4
Cu	10.1 ± 0.3	8.27 ± 0.7	316 ± 26	200 ± 12
Fe	932171 ± 14253	885057 ± 63852	534122 ± 33183	690894 ± 19345
K	52.3 ± 6	81.9 ± 7	3382 ± 256	15822 ± 942
Mn	2836 ± 158	1461 ± 50	8227 ± 320	3527 ± 175
Ni	21.5 ± 0.7	8.66 ± 0.5	305 ± 6	89.4 ± 5
Pb	5.99 ± 0.3	7.53 ± 0.5	3112 ± 66	2275 ± 84
V	27.7 ± 1	52.0 ± 3	377 ± 12	64.2 ± 3
Zn	20.8 ± 0.7	11.1 ± 3	9885 ± 171	159 ± 6

Table 3-2: Chemical composition of materials, determined using ICP-MS

Prior to characterisation each material was sieved, using a 45 µm sieve, to stop any larger particles disrupting or agglomerating with the smaller particles. Following sieving, the four materials were separately stored in glass bottles and analysed directly, without being milled, to retain their morphological characteristics. Eight grams of material was used for charging the RDS. Two binary material mixes, specifically chosen due to their dissimilar morphological fingerprints, were also characterised. The two binary mixes were flue dust with ore D and flue dust with sinter dust. Four grams of each of the materials were mixed together before completing characterisation. Titanium dioxide (Huntsman Pigments, Stockton-on-Tees, UK) was used as a control material to confirm that the equipment was set up and functioning correctly. An eight gram sample was analysed directly without sieving.

3.2.2 Instrumentation

The RDS used in this work was manufactured by JS Holdings and conformed to BS 15051, the standard for the measurement of the dustiness of bulk material.[6] This research did not use foams to establish dustiness indices of solid materials, as stated in BS 15051, but was used instead to simulate material handling processes, through the drum's rotation. A schematic diagram of the RDS, along with a cross section, is shown in Figure 3-1.

Figure 3-1: Rotating drum sampler schematic
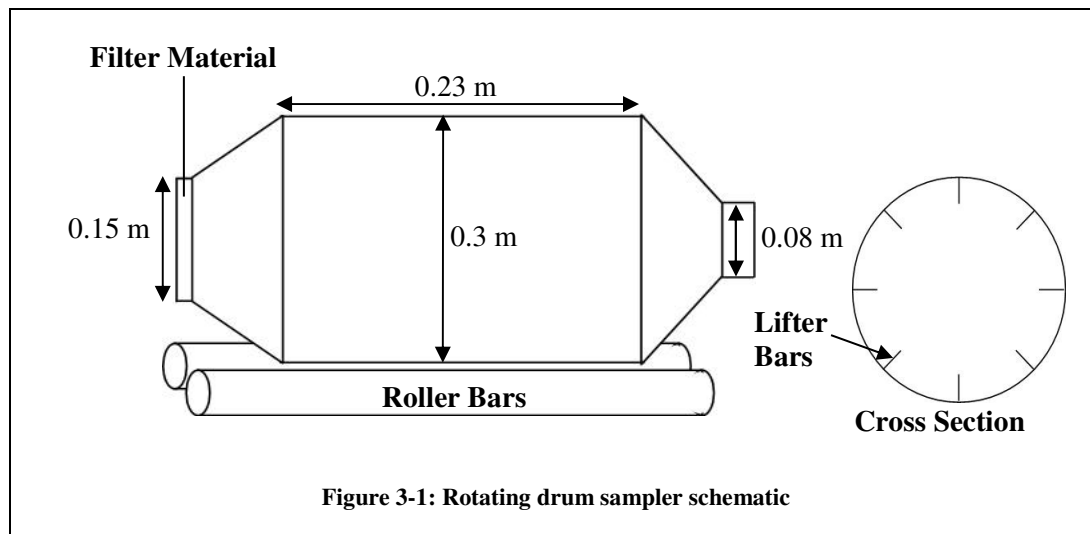
Coupled to the RDS was an Aspect morphology analyser, manufactured by Biral and shown in Figure 3-2. The Aspect uses ASAS to determine the shape and size of particulates, between 0.5 µm and 20 µm, through the scattering and detection of laser light. The flow rate of the Aspect is 7 L/min. Approximately 1 L/min of this is sample flow with the other 6 L/min used to ensure that the sample flow remains stable and no particulates are deposited inside the measurement chamber.

Figure 3-2: Aspect morphology analyser
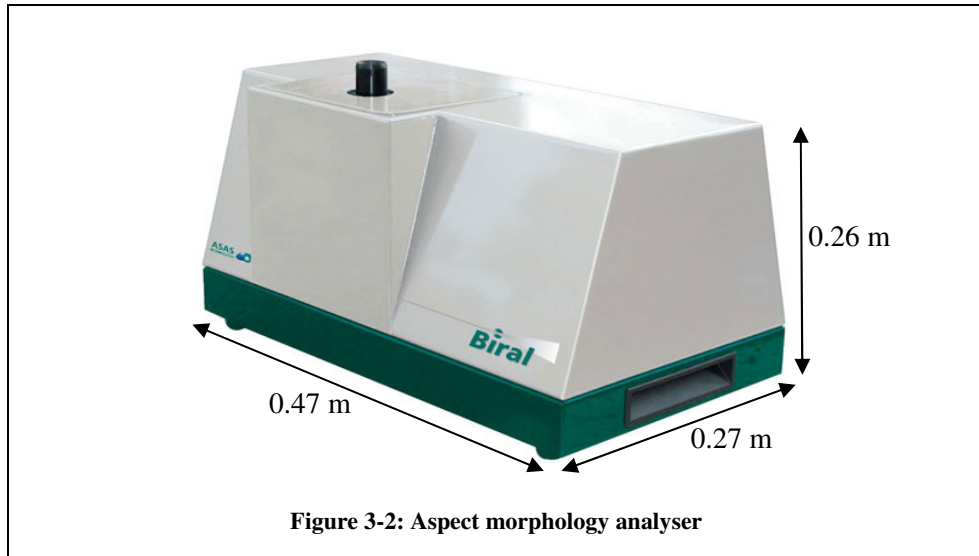
The Aspect is designed to characterise up to 20,000 particulates per second. With a flow of 1 L/min, this equates to a concentration of 1,200 particulates per cubic centimetre of air.[22] Particulates flow into the measurement chamber with their major axis aligned in a direction parallel to the direction of the air flow allowing light to scatter. The intensity of the light scattered indicates the size of the particles and the regularity (or irregularity) of the scattered light indicates the particles shape through the A_f. Particulates with an A_f of 0 are spherical. Above this particulates have edges on them, and particulates with an A_f of 100 are fiberous. Examples of this are shown in Figure 3-3

Figure 3-3: Light scattering for a sphere (top) and a fibre (bottom)[22]
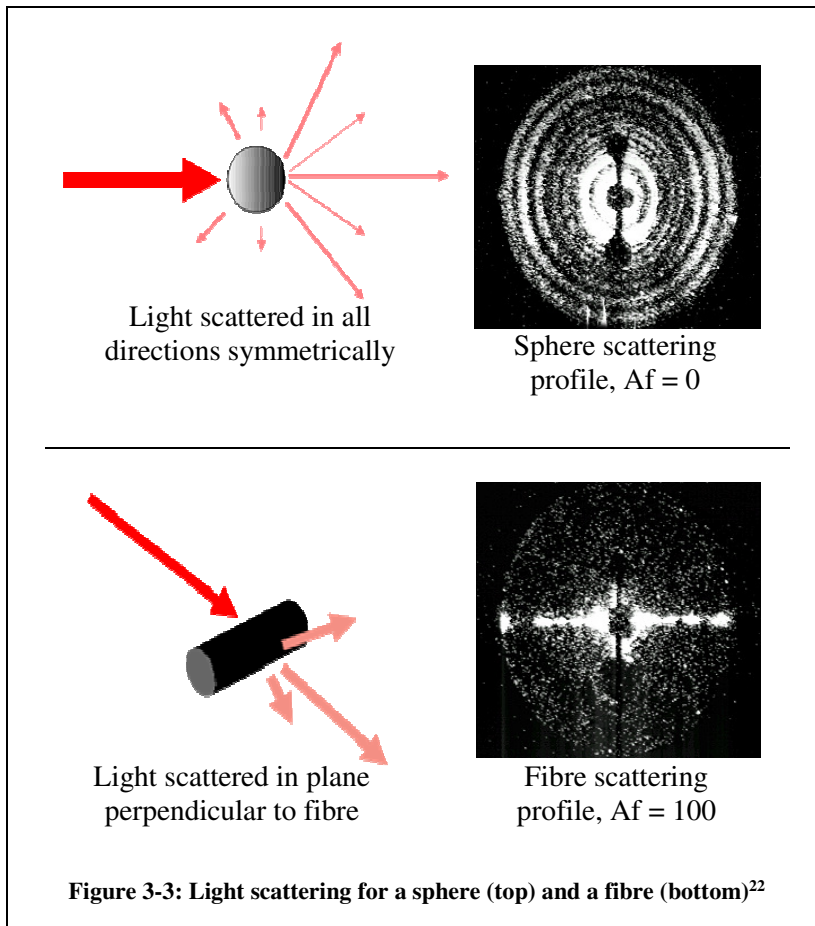
The Aspect produces two plots, the centroid plot and the contour plot, as well as a temporal plot which indicates the number of particulates detected over a period of time. The triangular centroid plot indicates the shape of the particulates, the numbers one to three corresponding to the three photomultipler tubes, whilst the contour plot shows the correlation between particulate diameter in micrometers and asymmetry factor. Examples of the three plots, illustrating the characterisation of spherical particulates, are shown in Figure 3-4. It is known that the particulates are spherical because the centroid plot shows a dark blue circle at it's centre, which corresponds to light being scattered regularly by the particulates. The contour plot indicates the presence of spherical particulates, through the red squares at an A_f of 0, as well as specifying the particulates size. In the example particulates range from 1 µm to 16 µm. The light blue squares indicate background particulates at low concentrations. The particulate count for the material is illustrated by a scale of colours, shown in the key next to each plot.

Figure 3-4: Aspect profile for titanium dioxide
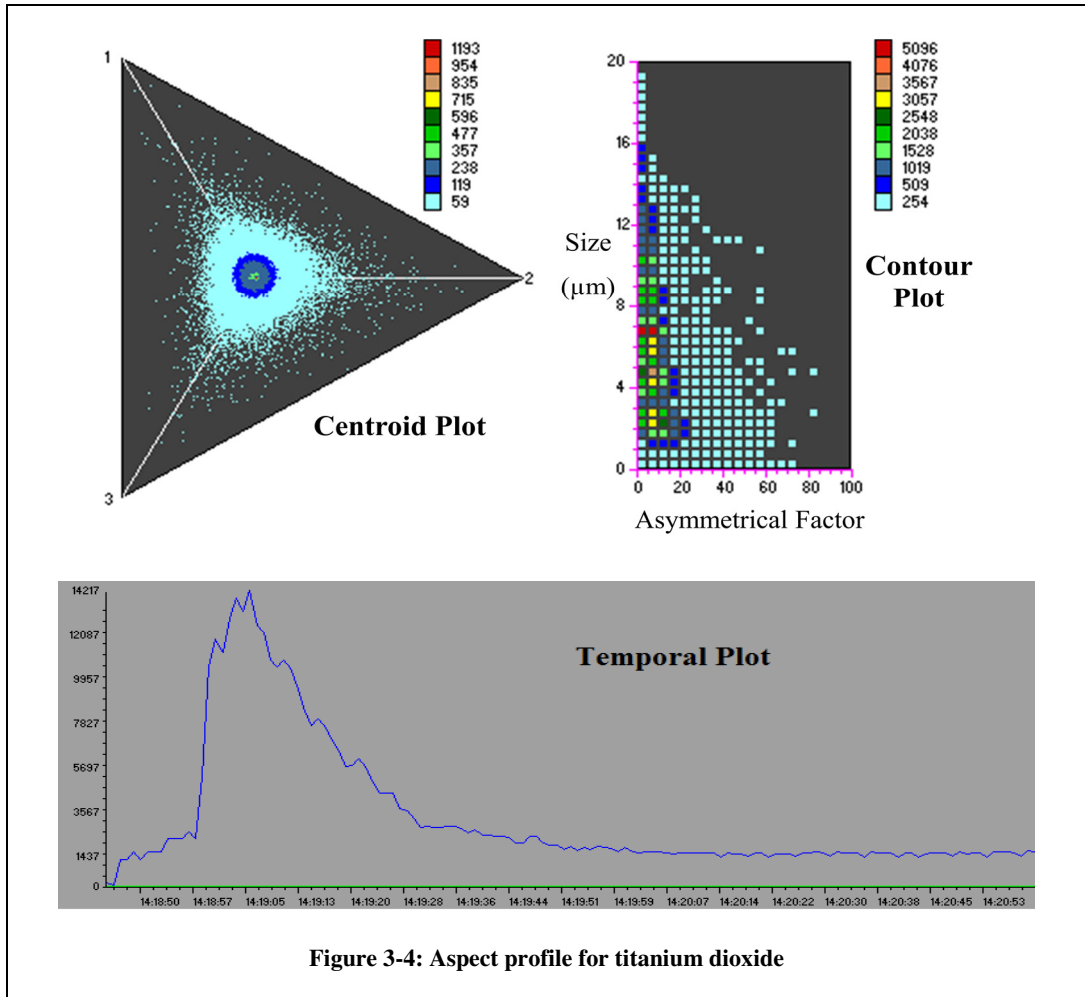
To connect the RDS to the Aspect and allow the morphological characterisation of the generated dusts a freely rotating connector and conductive silicone tubing was used. To prevent particle deposition or settling in the tubing, a minimal length, of one metre, was used and sharp bends were avoided. This setup is detailed in Figure 3-5.

Figure 3-5: Instrumentation setup schematic
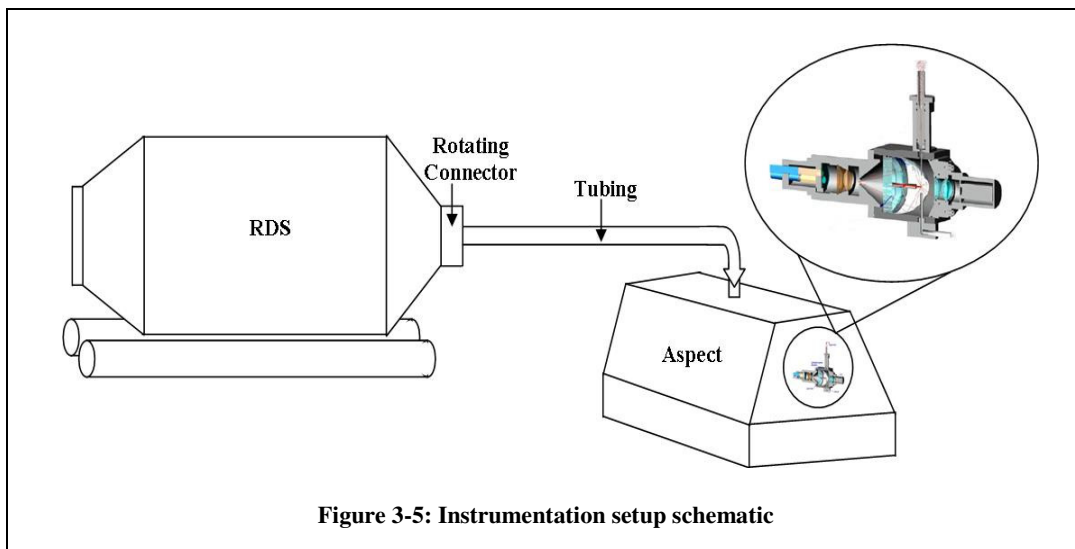
3.2.3 Procedure

Following the coupling of the RDS and Aspect the drum was charged with the material of interest and then sealed with technostat filter material. Technostat is approximately 5 mm thick and consists of blended synthetic fibre attached to polypropylene gauze. It was used to stop any particulates entrained within the atmospheric air entering the drum and at the same time stop any generated particulates from exiting the drum, and entering the atmosphere. No pre-characterisation steps were required for the Aspect.

Simultaneously the Aspect's software and pump, operating at an overall flow rate of approximately 7 L/min, and the rotation of the RDS were started. Each experiment involved rotating the RDS for four minutes, at a rate of four revolutions per minute. At the end of the four minutes the RDS's rotation as well as the Aspect's pump and software were stopped. The Aspect was disconnected from the RDS and any dust remaining was allowed to settle. The remaining dust was disposed of and the RDS was placed in a fume cupboard for cleaning. The RDS was rinsed once with water and twice with isopropanol before being left to air dry. No post-characterisation steps were needed for the Aspect. Each experiment, for both individual and mixed materials, was completed in duplicate with the replicates being

completed on two different days but at similar temperatures and relative humidities, approximately 20 ℃ and 45 %.

As a separate study, completed on one day with a temperature of 19 ℃ and a relative humidity of 70 %, three replicates were completed in quick succession with a gap of eighteen minutes between each replicate. The three replicates were completed using ten grams of sinter dust and the RDS was not cleaned in between each replicate, nor was any extra of sinter dust added. The Aspect software and pump were started and then stopped between each replicate before being started again for the next replicate.

3.2.4 SEM Analysis

The four materials were also characterised by SEM to allow comparisons with the morphological data. A Philips XL30 SEM was used and the materials were mounted, using double sided carbon type, onto a SEM stub, before being carbon coated for conductive purposes. For each material, photographs were taken of two random areas at a magnification of x400, using the Back-Scattered Electron signal.

3.3 Results and Discussion

3.3.1 Initial Study

Titanium dioxide was characterised twice using the RDS-Aspect method to confirm that the equipment was set up and functioning correctly. It was known that the titanium dioxide particulates were spherical and therefore high concetrations of particulates with small A_f values were expected. The morphological profiles, from the replicate analyses of titanium dioxide, are shown in Figure 3-6. Both profiles indicated the presence of a range of particulates with a spread of A_f values, 0 to 50, and diameters from 0.5 µm to 16 µm. High concentration of spherical particulates, with an A_f of 0, were present at 7 µm with increased concentrations also notable at 0.5 µm, 2 µm and 10 µm. Both centroid plots indicated a presence of spherical particulates through the small circle at their centre, which showed that the laser light was scattered symmetrically in all directions.

The sizes of the particulates were not provided from the manufacturers and therefore comparisons could not be made. Comparisons could be made in relation to previous literature. Tsai[29] measured the dustiness of TiO_2 using a RDS followed by size distribution measurements which were undertaken with a SMPS and an APS. The median diameter obtained when using the APS was 0.86 µm and when using the SMPS was 0.37 µm.[29] The results obtained using the SMPS and the APS are comparable with the high concentration of particulates seen at 0.5 µm in this initial study. Results are summarised in Table 3-3.
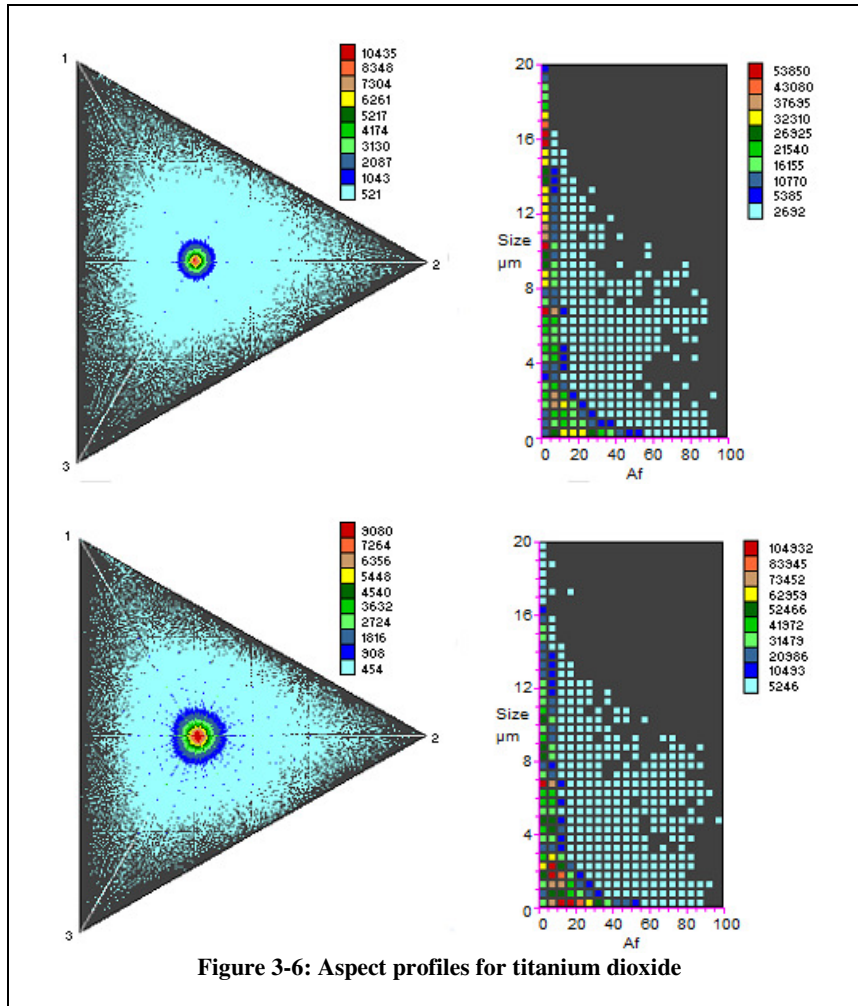
Figure 3-6: Aspect profiles for titanium dioxide

Material	Size of largest concentration	Shape of largest concentration
Titanium Dioxide	7 µm	Spherical particulates

Table 3-3: Summary of the morphological characterisation of the control material

This initial study indicated that the equipment had been set up and was functioning correctly. The results obtained corresponded well with the literature which indicated that further experiments using the RDS-Aspect method should provide credible results.

3.3.2 Morphological Characterisation of Materials

Morphological profiles and SEM photographs for each of the four materials, ore D, ore F, flue dust and sinter dust, are presented in Figures 3-7 to 3-14. Each material's morphological profile is discussed in turn, whilst also being compared with the SEM photographs of that particular material as well as the morphological profiles of the other materials.

Ore D

Ore D had particulates between 0.5 µm and 7 µm in size with A_f values of 0 to 50. A high concentration of particulates was present at approximately 2 µm with an A_f of 10, indicating that the majority of the particulates were scattering the light and were therefore irregular in shape. This was confirmed by the dark blue and green triangles within the centroid plots. Both the centroid and contour plots obtained for ore D, shown in Figure 3-7, were almost identical and the number of particulates characterised was alike, signifying good reproducibility overall. The SEM photographs of ore D, Figure 3-8, indicated that the particulates present within the material were asymmetric, concurring with the morphological profiles.

Figure 3-7: Aspect profiles for ore D
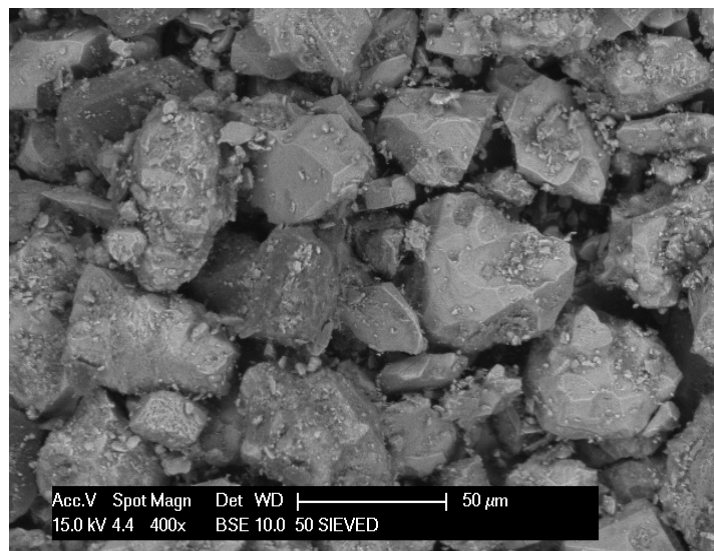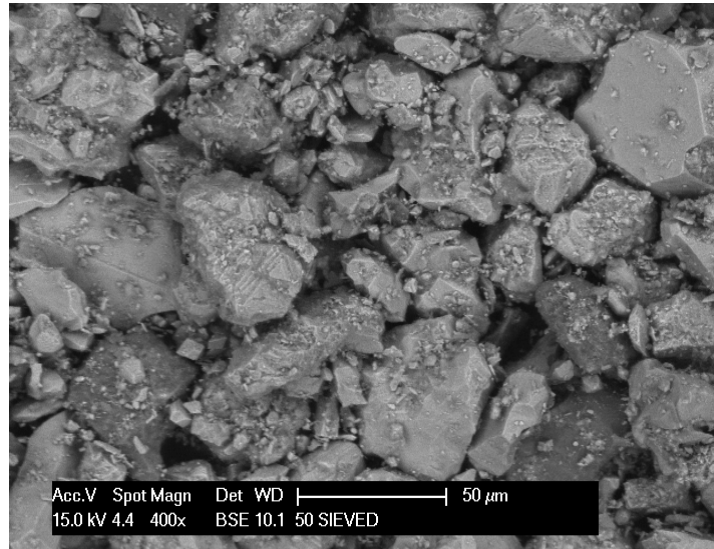
Figure 3-8: SEM photographs for ore D

Ore F

The ore F profiles, shown in Figure 3-9, indicated particulates with a range of sizes, 0.5 µm to 16 µm and shapes, A_f values between 0 and 50. High concentrations of particulates were visible at 2 µm, 7 µm and 11 µm. In terms of particulate shape there were two distinct populations. Firstly a very spherical population with a spread of sizes but all with a low A_f, secondly a population with edges which were scattering the light more irregularly, had a wider spread of A_f values, from 0 to 50, and a diameter of between 0.5 µm and 4 µm. This was shown by the contour plot as well as the centroid plot. The red circle showed the first

population and the blue triangle the second. The replicates indicated good reproducibility with similar numbers of particles detected for each. The profiles obtained here presented a number of different characteristics when compared with ore D. This indicated that although the particulate chemical compositions were similar the shapes and sizes of the particulates differed and therefore this technique could be used to differentiate between the two ores. Figure 3-10 shows the SEM photographs of ore F. These photographs also indicated the presence of larger particulates, which was seen in the Aspect morphological profiles. The first very spherical population was not fully visible within the SEM photographs due to the small size of particulates within this population as well as the high proportion of larger, asymmetric particulates present, which was the second population.
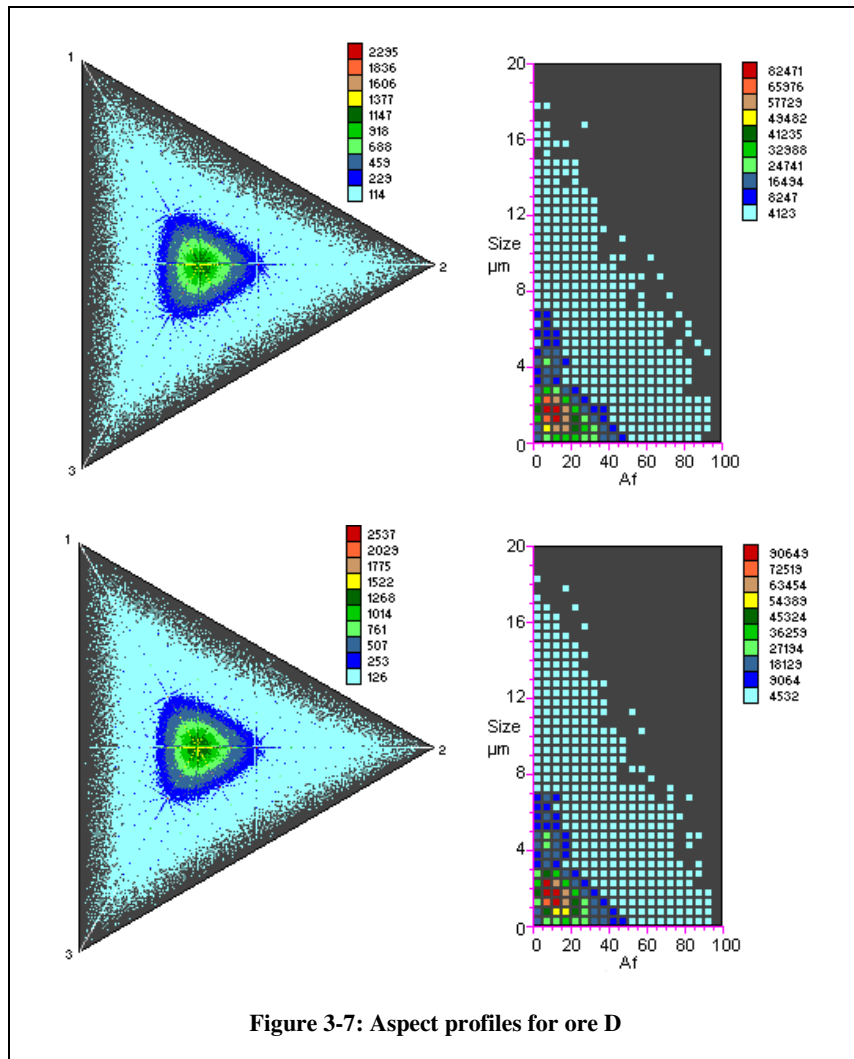

Figure 3-9: Aspect profiles for ore F

Figure 3-10: SEM photographs for ore F
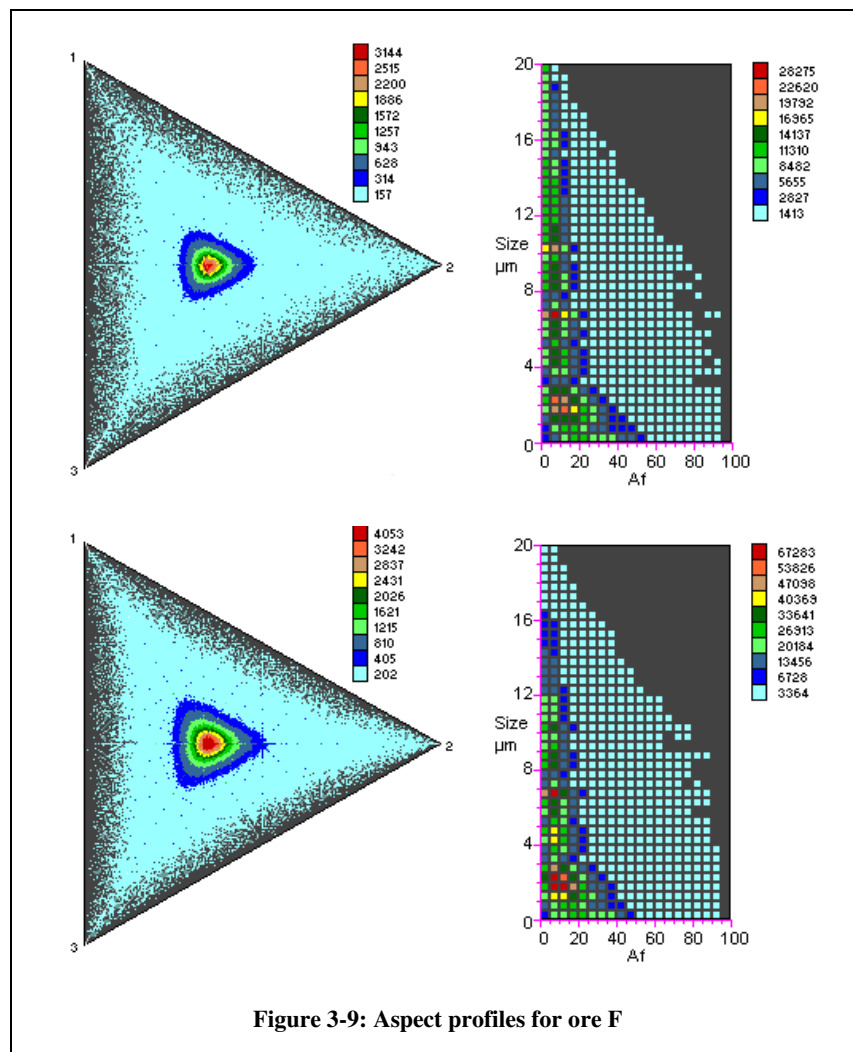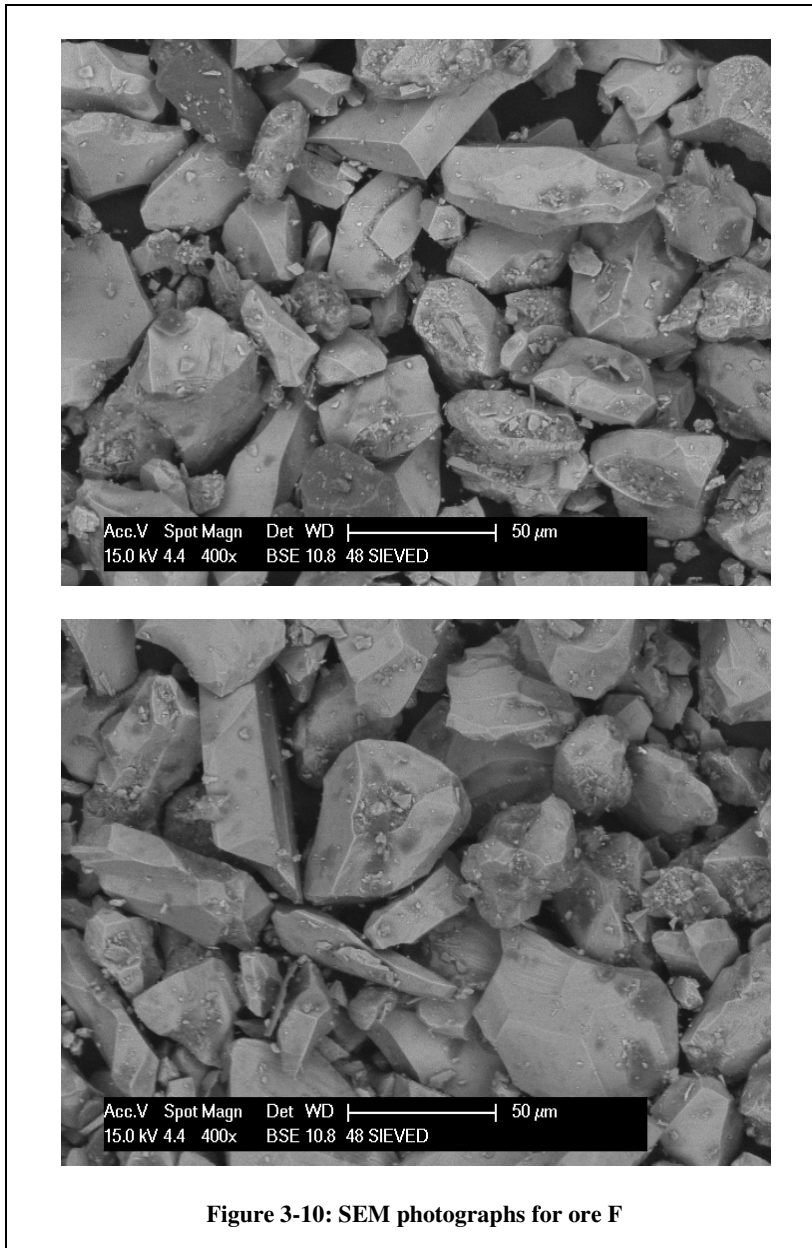
Flue Dust

The centroid plots for the flue dust, shown in Figure 3-11, indicated that the majority of the particulates within the material were spherical, due to the presence of the small red circles at the centre of the two plots. The dark blue triangles indicated that there were also some particulates present which had edges and were scattering the light irregularly. This was confirmed by the contour plots which showed the presence of particulates between 1 µm and 19 µm in size with A_f values of between 0 and 30. The contour plots also indicated a high concentration of particulates at approximately 7 µm, with an A_f of 0 to 10, which signified

the small spherical particulates. The number of particulates characterised during each of the flue dust replicates was similar as were the profiles which were produced. The morphological profiles for the flue dust material were similar to those obtained for ore F, however the spread of particulates with small diameters was not as large. The SEM photographs of the flue dust are shown in Figure 3-12. These photographs showed both spherical and irregular particulates, as well as particulates with a range of sizes, which agreed with the obtained morphological profiles.

Figure 3-11: Aspect profiles for flue dust
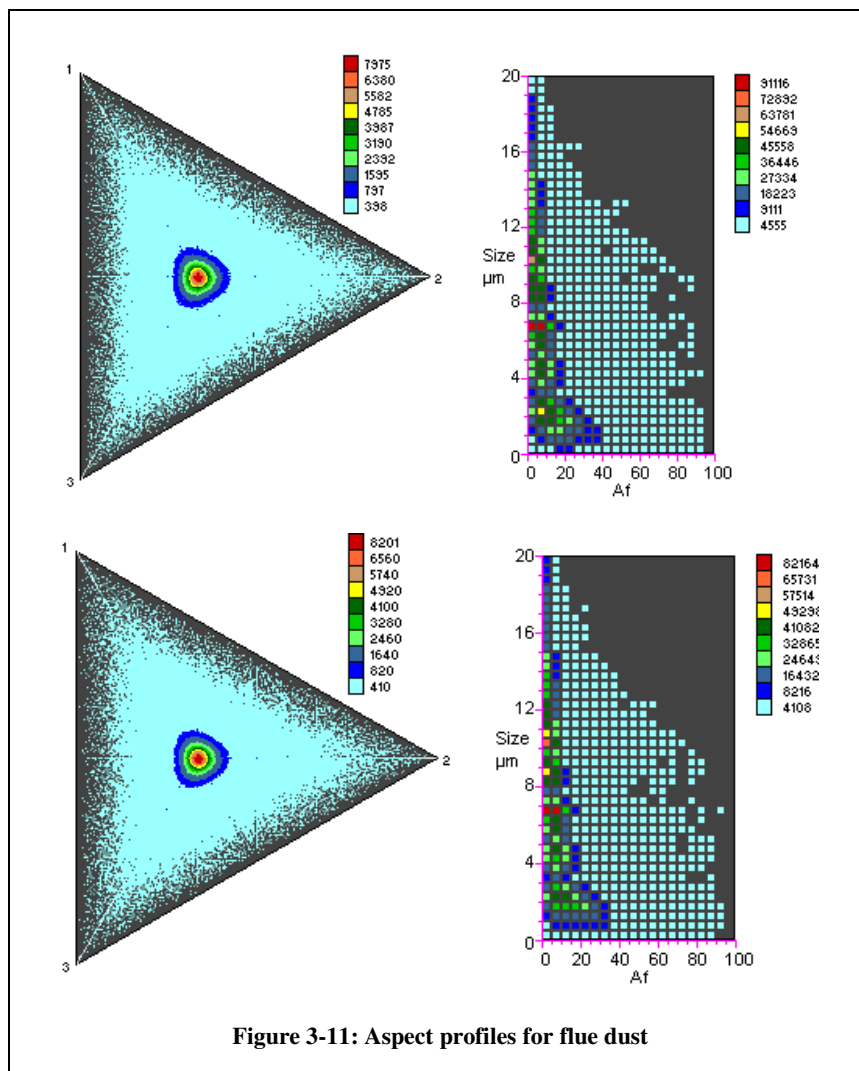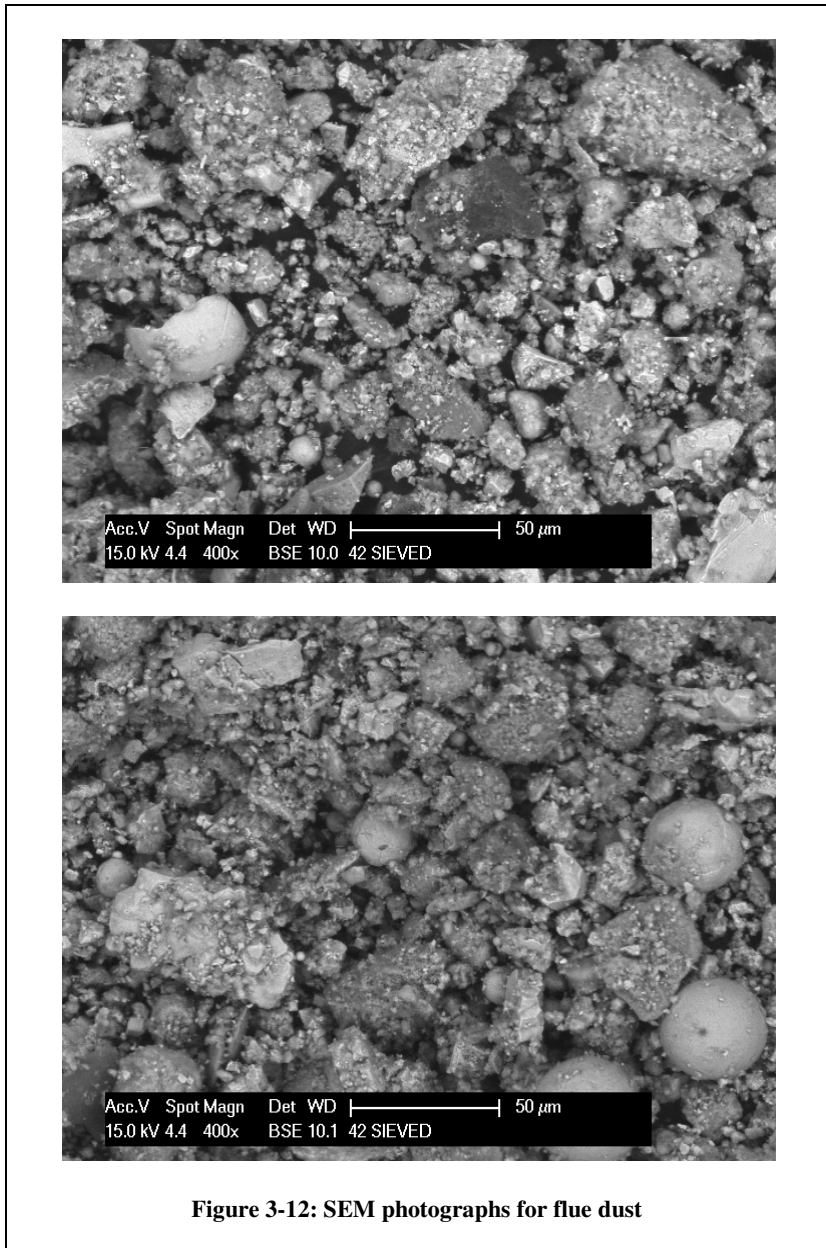
Figure 3-12: SEM photographs for flue dust

Sinter Dust

The sinter dust replicates both produced very similar morphological profiles with similar numbers of particulates characterised for each replicate (Figure 3-13). The sinter dust particulates were between 0.5 µm and 7 µm in size with A_f values of between 0 and 40 indicating that they scattered the light and were therefore asymmetric, also shown by the blue and green triangles on the centroid plot. A high concentration of particulates was present at approximately 1 µm to 3 µm in diameter with an A_f of 5 to 10. There was also a spread of non-background particulates up to 7 µm. The sinter dust morphological profile was

similar to the ore D morphological profile. Since their chemical compositions were not the same, the two materials could be differentiated from one another, when completing full characterisation. The SEM photographs of sinter dust, Figure 3-14, indicated a large number of small particulates, which were not fully symmetrical and had edges present on them as seen in the morphological profiles.
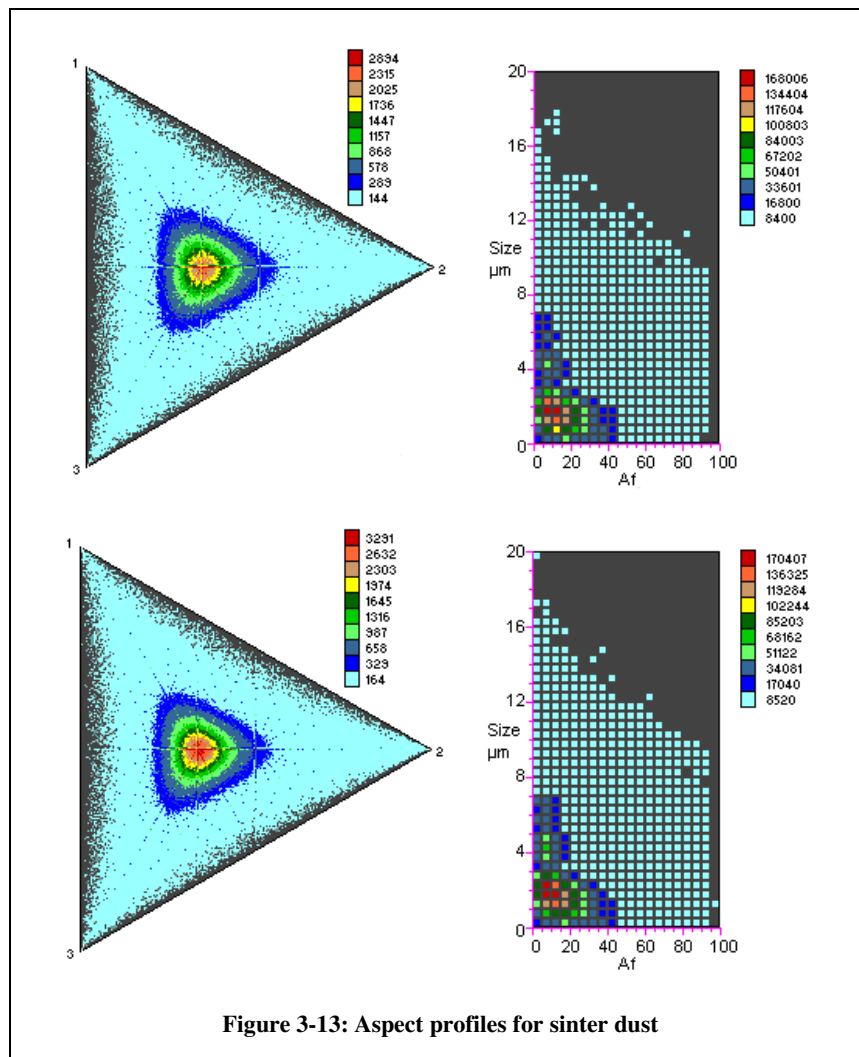
Figure 3-13: Aspect profiles for sinter dust

Figure 3-14: SEM photographs for sinter dust
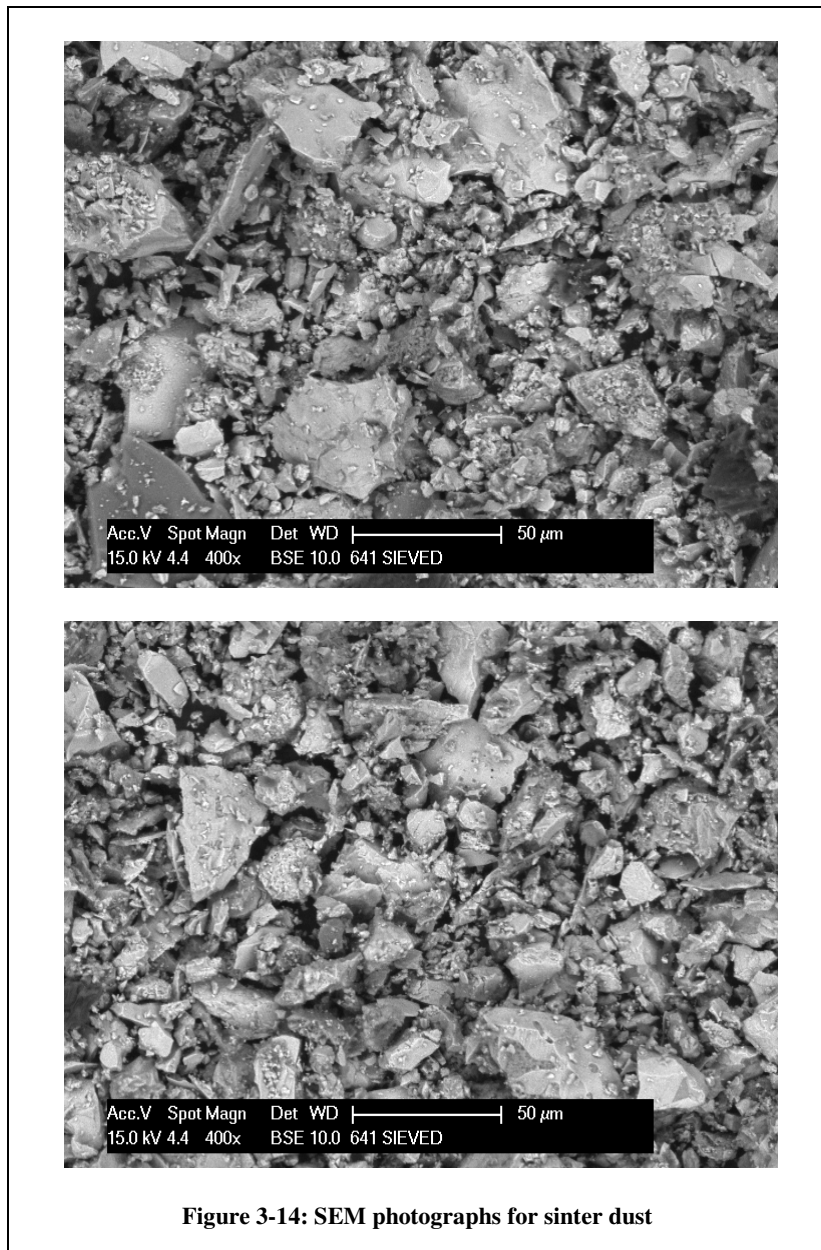
Completing both morphological characterisation and SEM analysis of these four materials has allowed the determination of the shape and size of the particulates present within each material to be completed, alongside comparison of each material's morphological profile. These results are tabulated in Table 3-4.

Material	Size of largest concentration	Shape of largest concentration
Ore D	2 µm	Asymmetric particulates
Ore F	2, 7 and 11 µm	Two populations, one of spherical particulates and one of asymmetric particulates
Flue Dust	7 µm	Spherical particulates
Sinter Dust	1 to 3 µm	Asymmetric particulates

Table 3-4: Summary of the morphological characterisation of the four materials

Although some materials showed similarities in the shapes and sizes of their particulates it was possible to obtain characteristic fingerprints for each material. For example ore F and flue dust both produced similar contour plots, with a wide range of particulate sizes. However, when combining these results with the chemical compositions, obtained in Chapter Two and noted in Table 3-1, the materials may be differentiated from each other. The same may be said of the ore D and sinter dust materials.

Whilst both ores indicated the presence of small particulates, within the materials, ore F showed a much larger spread of particulates with different shapes and sizes than ore D, which showed mainly small asymmetric particulates. Therefore even though their chemical compositions were similar their morphological profiles allow them to be distinguished from one another.

All of the replicates completed corresponded well with each other, indicating good reproducibility when using the RDS-Aspect method. The four materials also showed good agreement between the SEM photographs and the morphological profiles, which demonstrated that the Aspect was producing and providing characteristic profiles which were true to the material undergoing characterisation. Due to the small amount of research published using the Aspect instrument, no comparisons could be made between the

morphological profiles. Comparisons can be made with SEM images obtained by other groups.

A number of the particulates which were characterised, using SEM, by Moreno, Jones and Richards[16] came from the integrated steelworks, in Port Talbot. They found most of the iron particulates that they characterised were small, below 2 µm, and spherical (Figure 3-15), although some irregular particulates were also analysed. The iron particulates they characterised were most likely to be from the local steelworks.[16] Their results were similar to those obtained in this study, especially for the characterisation of ore F, where high concentrations of spherical particulates approximately 2 µm in size were found. Although the materials used in this study were from the integrated steelworks in Scunthorpe, the iron ores, characterised here and which would have also been used in Port Talbot, would have undergone similar mining and transport procedures. Therefore although not fully comparable these results give an indication that iron ores in general do have some spherical particulates.

Figure 3-15: SEM photograph of iron particulates analysed by Moreno, Jones and Richards[16]
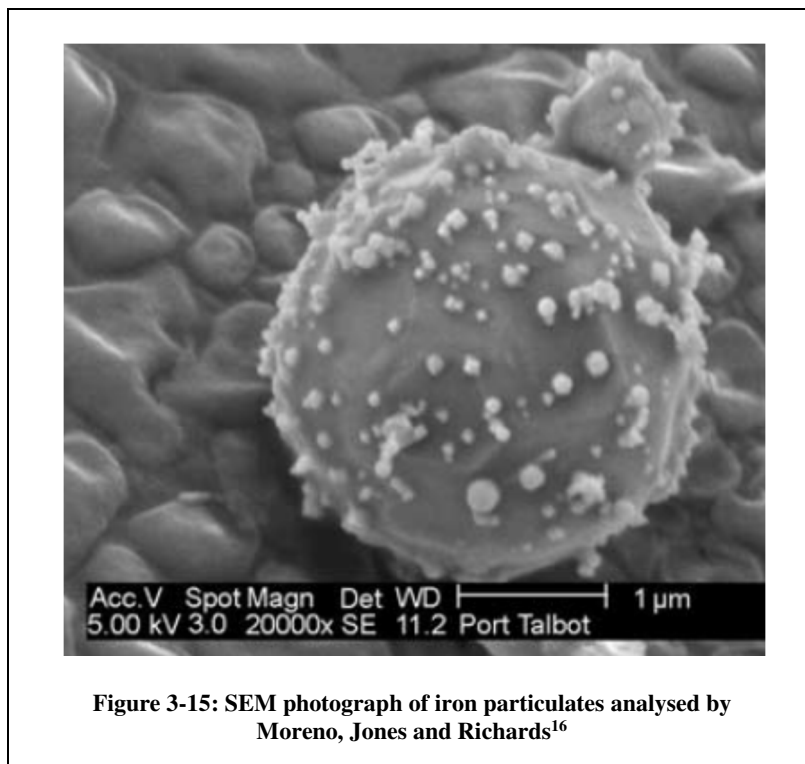
3.3.3 Morphological Characterisation of Binary Mixes

When handling materials on an industrial site, particulates are released. At the same time different particulates are also being released from other sources on the plant and the two types of particulates can mix together. Therefore, to simulate these mixed emissions, binary mixes have been characterised using the RDS-Aspect method. The characterisation of these binary mixes has also been used to confirm whether it would be possible to extract unique and characteristic morphological fingerprints from a mixed material. The results from the two binary mixtures are detailed below and the morphological profiles shown in Figures 3-16 to 3-20.

Flue Dust and Ore D Mixture

The characterisation of the flue dust and ore D mixture indicated a large size range, 0.5 µm to 20 µm, of mainly spherical particles, with A_f values of between 0 and 40 (Figure 3-16). This was shown both on the centroid plot, illustrated by the circle in the middle of the three axes, and the contour plot where the high particulate concentrations, at 7 µm, 8µm and 10 µm, had A_f values of 10, indicating the light was scattered regularly. The replicate profiles both exhibited similar characteristics, with high and low concentrations present at the same parameters. The number of particulates characterised was higher for the first analysis, although this did not affect the profiles overall reproducibility.
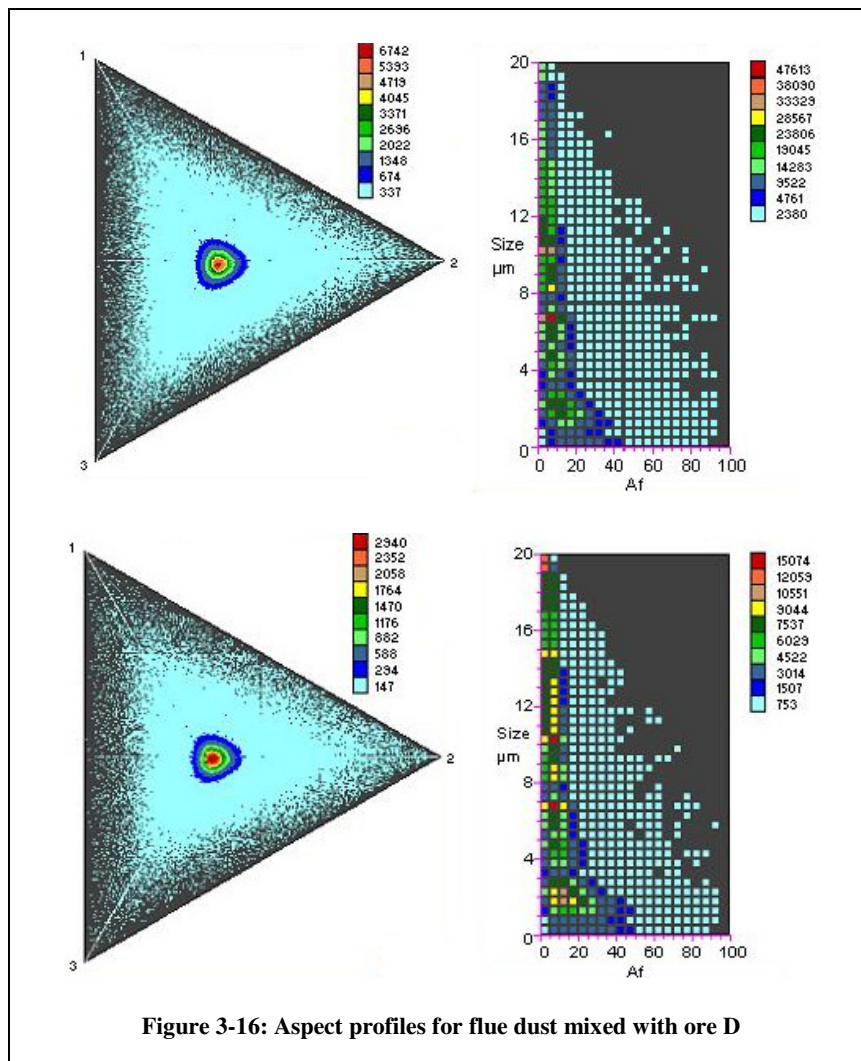
Figure 3-16: Aspect profiles for flue dust mixed with ore D

The mixed morphological profile was very similar to the individual flue dust profile. However, by completing data filtering, a new profile could be extracted from the mixed profile. Data filtering was completed by altering the A_f and the particulate diameter values to only show particulates with an A_f of between 0 and 30 and a diameter of between 0.5 µm and 4 µm. This new profile, shown in Figure 3-17, corresponded well with the ore D profile which was obtained previously. By filtering the data again and increasing the maximum A_f to 40 and the maximum diameter to 8 µm another new fingerprint could be obtained, shown in Figure 3-18. When examining the centroid plot of this fingerprint it appeared to be a mixture of the two individual flue dust and ore D fingerprints.

Figure 3-17: First filtered morphological profile, showing similarity with ore D profile

Figure 3-18: Second filtered morphological profile, showing mix of ore D and flue dust within the centroid plot
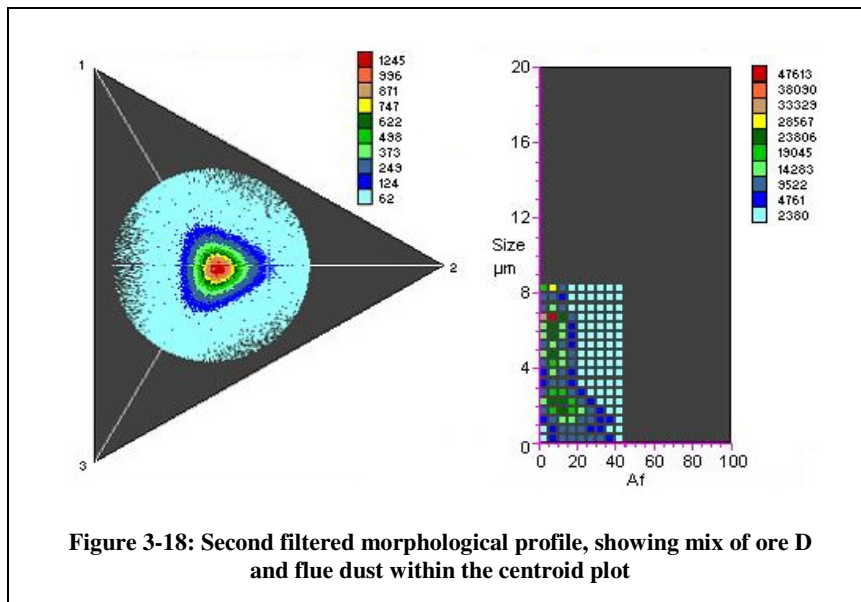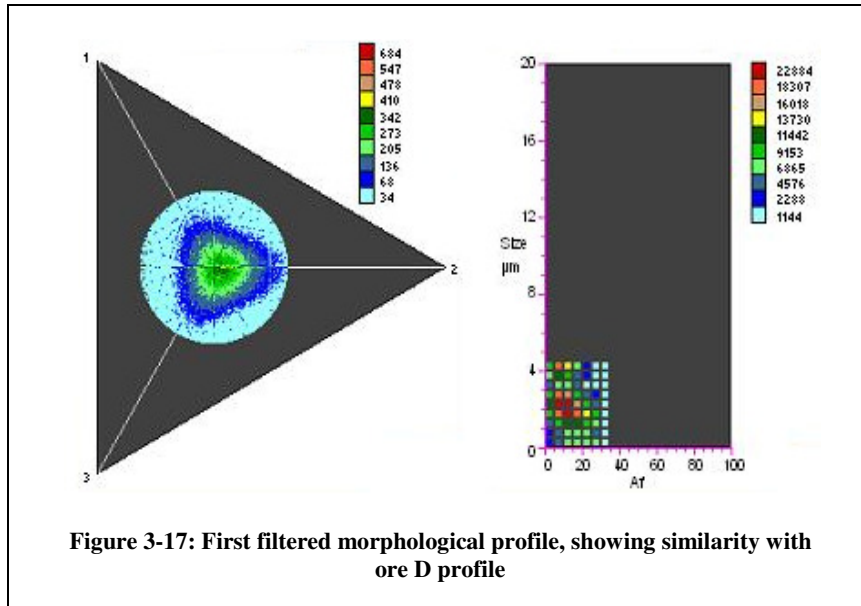
Flue Dust and Sinter Dust Mixture

The flue dust and sinter dust mixture also produced profiles (Figure 3-19) which looked similar to the individual flue dust profile. Particulates were present in every size, for both replicates, with A_f values of between 0 and 40. High concentrations of particulates were present at 7 µm, 8 µm and between 10 and 20 µm, with low A_f values, indicating very spherical particulates. This was also shown by the small red and blue circles on the centroid

plot. The replicate profiles were reproducible with similar numbers of particulates characterised.

Figure 3-19: Aspect profiles for flue dust mixed with sinter dust
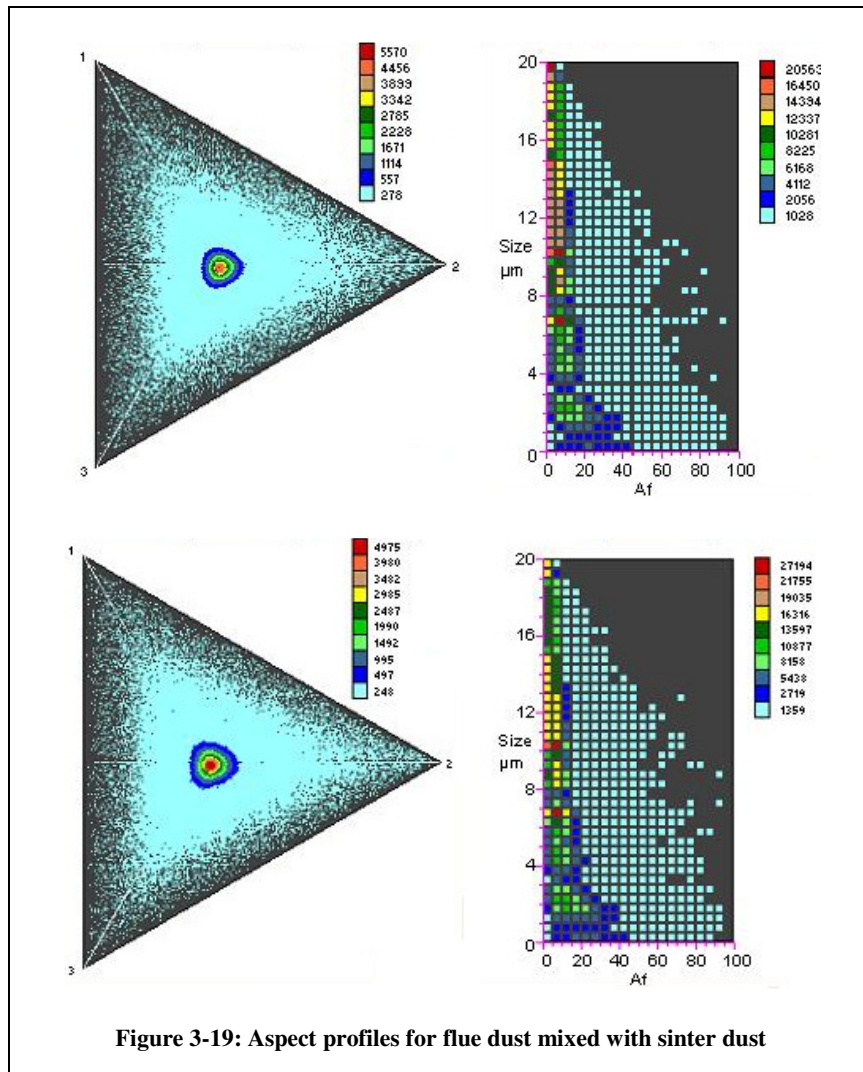
Due to the similarity of the mixed profile with the flue dust's profile, filtering was completed to extract a new profile, as shown in Figure 3-20. The plots were both filtered to show particulates between 0.5 µm and 4 µm with A_f values of between 0 and 30. This filtered fingerprint corresponded well with the individual sinter dust profile.

Figure 3-20: Filtered morphological profile, showing similarity with sinter dust profile
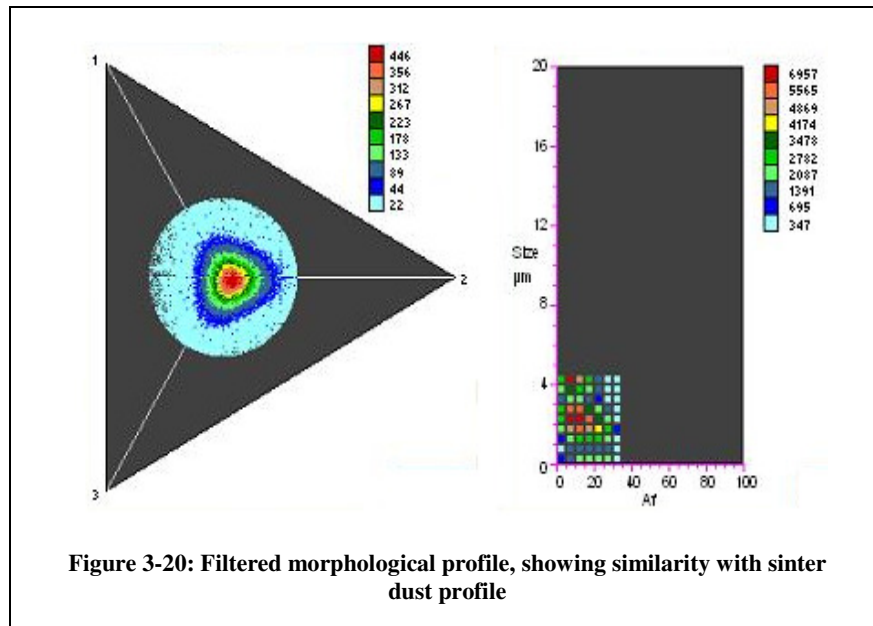
One possible issue with this material mixture was that the particulates seemed to be agglomerating together, which could have caused the high concentration of particulates above 10 µm. To determine if the particulates were agglomerating a further experiment should be completed.

The same mixture of materials should be placed within the drum and the drum rotated. Instead of rotating the drum for the full four minutes it should be rotated for one minute at a time, up to four minutes, and a small sample of the particulates taken from inside the drum after each minute. The four samples should then be examined using SEM. This would allow photographs to be taken of the sample, at a high magnification, and if agglomerates were present they could be seen on these photographs. By only rotating the drum for one minute at a time it could be determined at what point the particulates agglomerated during the experiment. Another option would to be to complete the experiment at a lower temperature and humidity to determine whether these parameters had an effect on the overall results.

The characterisation of the two binary mixes indicated that it was possible to both characterise mixes of different materials as well as extract unique and characteristic

morphological fingerprints from a mixed sample. Results are summarised in Table 3-5. To further enhance this work a larger range of binary mixes should be characterised.

Mixture	Size of largest concentration	Shape of largest concentration
Flue dust with ore D	7, 8 and 10 µm	Spherical particulates
Flue dust with sinter dust	7, 8 and 10 to 20 µm	Spherical particulates

Table 3-5: Summary of the morphological characterisation of two binary mixtures

3.3.4 Replicate Morphological Characterisation of Sinter Dust

Three replicate analyses were undertaken to clarify whether particulates that had not become airborne during a first experimental run could still become airborne with further agitation, as you would experience on site. The three replicates were also used to determine if any of the particulates which did become airborne, following further agitation, had the same or similar morphological characteristics as the particulates which had already been characterised. The morphological profiles obtained from the three replicate analyses are detailed in Figure 3-21. In general a decrease in the number of particulates characterised was seen for each replicate. This was because as each replicate was completed a smaller number of particulates were left in the drum for the next characterisation. This showed that with further agitation particulates may still become airborne. It was thought that this further agitation may cause an increase in the general size of particulates through agglomeration. However, since none of the replicates showed any non-background particulates present above 7 µm it is unlikely that agglomeration occurred within the RDS. In terms of the morphological profiles the centroid and contour plots from the first replicate are consistent with those previously obtained, as shown in Section 3.3.2. Particulates ranged from 0.5 µm to 7 µm with A_f values of 0 to 40 with a high concentration of asymmetric particulates visible at 1 µm. The second replicate showed the characterisation of a similar number of particulates, which were also asymmetric.

Although a high concentration of particulates was seen for the same parameters as the first replicate the size distribution was smaller, with the largest non-background particulates recorded at 3 µm. The third replicate indicated a decrease in the number of particulates characterised, which is shown in both the centroid and contour plots. However particulates of a similar shape and size to those present during the second replicate were characterised. The fact that no particulates were present in the second and third replicates above 3 µm in size indicated that all of the larger particulates must have become airborne and transported to the Aspect analyser during the first experimental run. Results are summarised in Table 3-6.
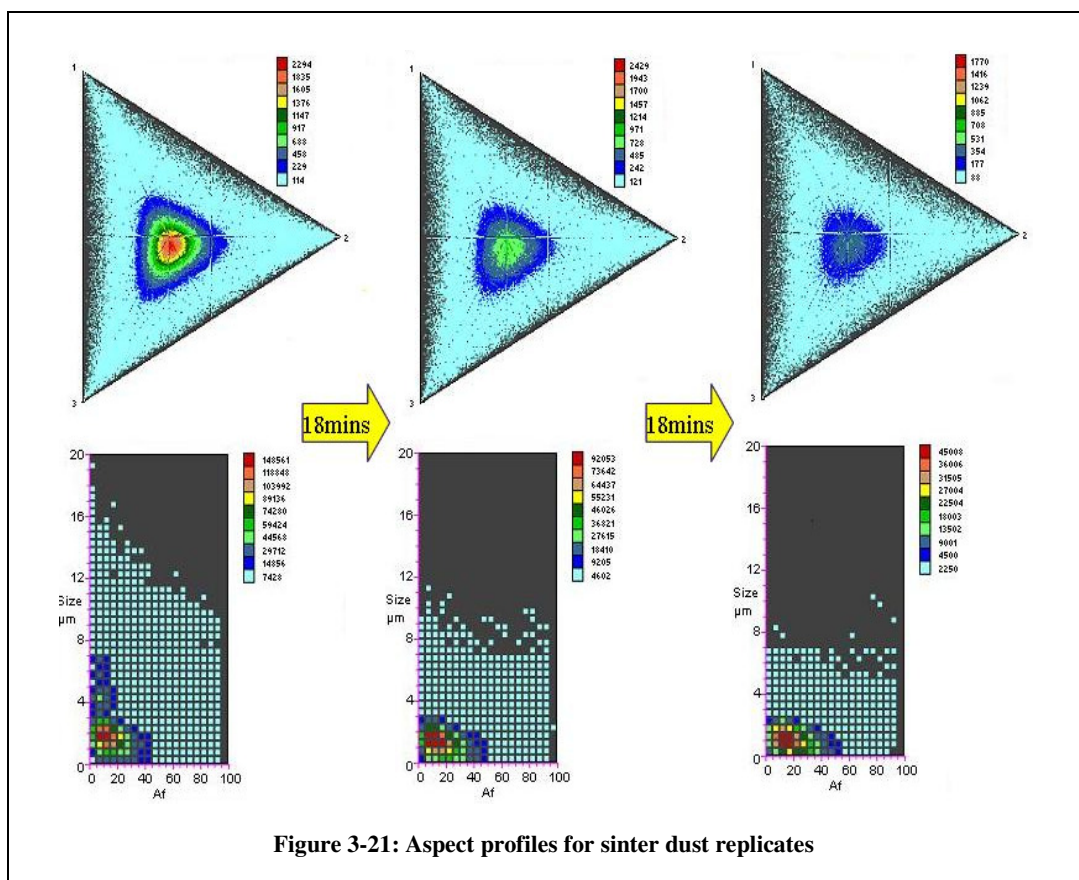
Figure 3-21: Aspect profiles for sinter dust replicates

Material	Size of largest concentration	Shape of largest concentration
Sinter dust replicates	1 µm	Asymmetric particulates

Table 3-6: Summary of the morphological characterisation of the replicate sinter dust experiments

3.4 Source Apportionment Study

The morphological profiles obtained during this work have been used to aid and complement a source apportionment study completed at the Tata Steel integrated steelworks in Scunthorpe. The sampling location was approximately 1.2 km north east of the steelworks and sampling was undertaken over nine days. Wind in this area generally originates from the south west, therefore making the sampling location ideal. The wind direction was recorded for the duration of the study. A map of the steelworks and the sampling location is shown in Figure 3-22.

Figure 3-22: Map of the sampling site in Scunthorpe, UK

1. Coke Plant A
2. Coke Plant B
3. Sinter Plant
4. Blast furnaces
5. BOS plant
6. Iron ore yards
7. Mills
8. Coal handling
9. Slag handling and processing
10. Material storage
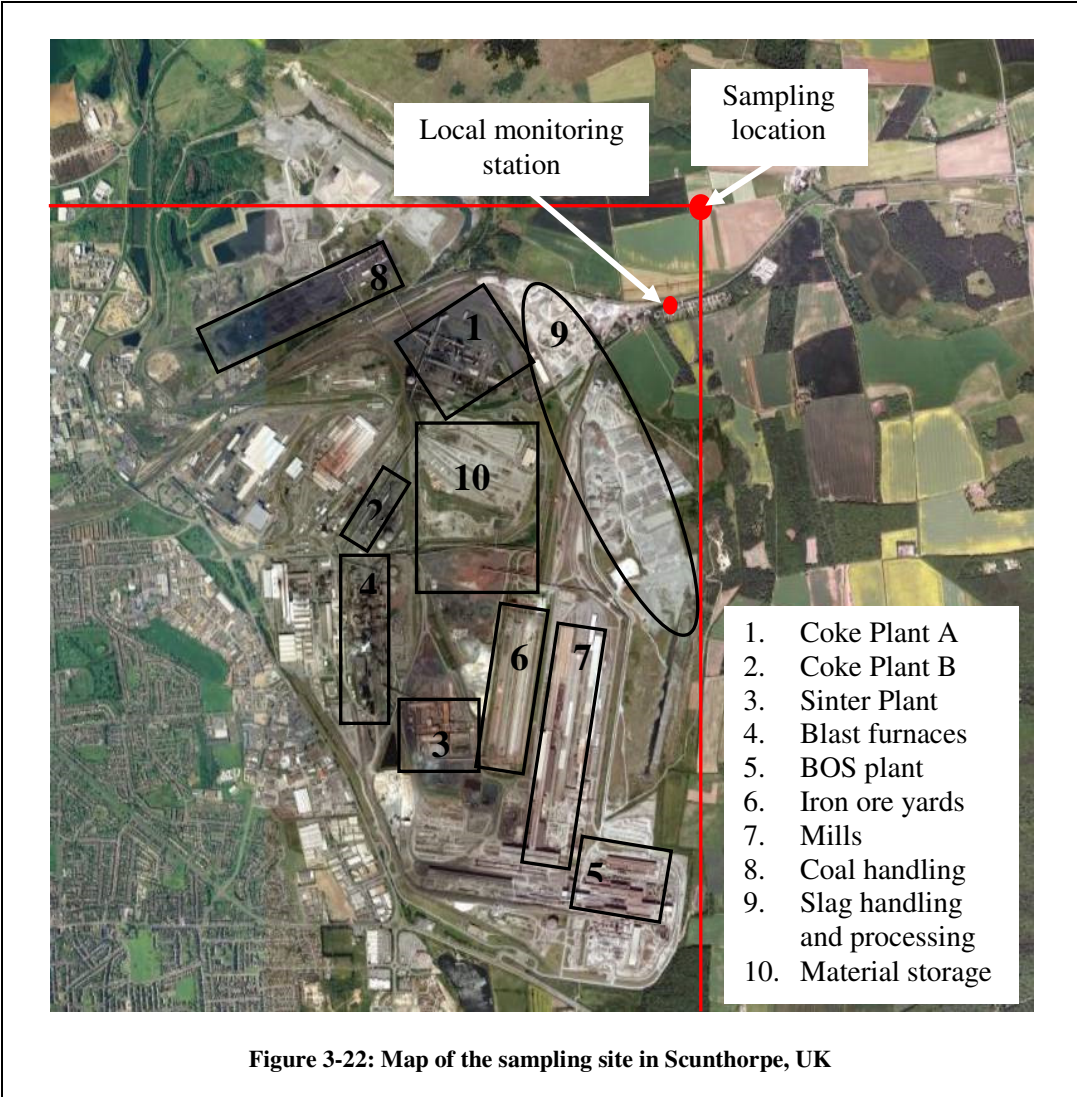
The temporal particulate concentration plots obtained during the study, showed a large number of peaks in the first five days with a reduced number of peaks between days six and nine, Figures 3-23 and 3-24. These temporal plots corresponded well with the wind data, which indicated that during days six to nine the majority of the wind was coming from the north east, rather than the integrated site.
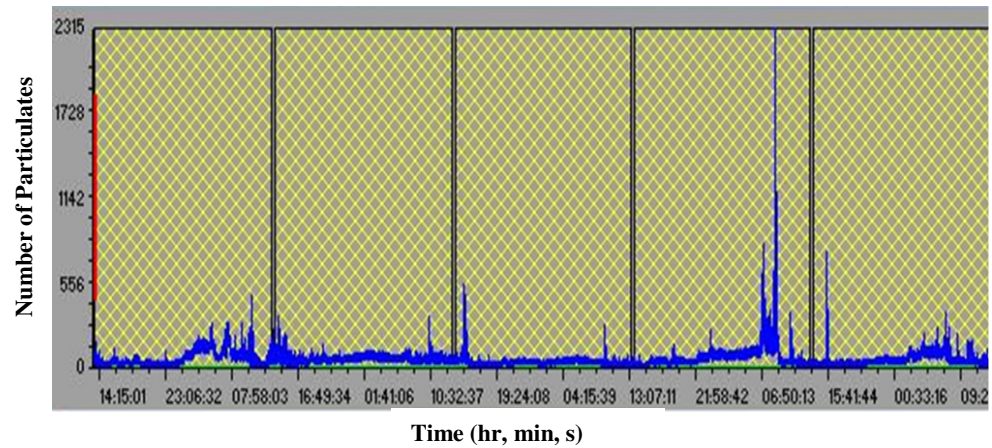
Figure 3-23: Temporal plot for days one to five, the black lines indicate the different days
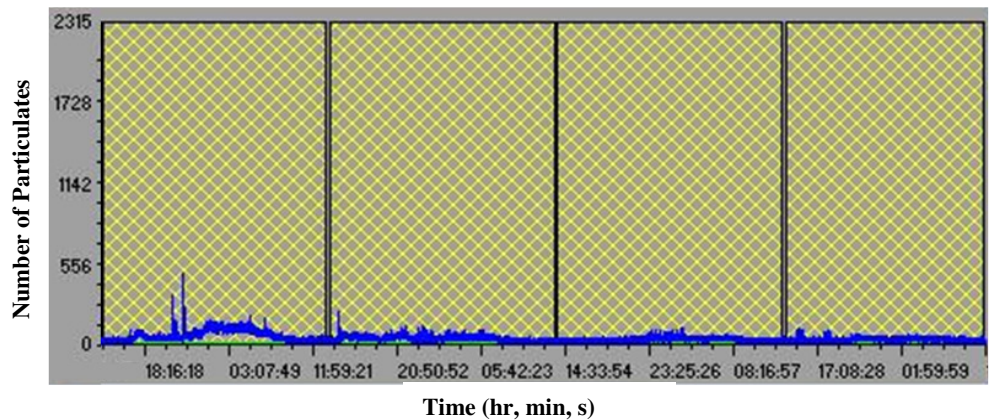
Figure 3-24: Temporal plot for days six to nine, the black lines indicate the different days

During the first five days both high numbers of particulates (peaks in temporal plots), as well as low numbers of particulates (troughs in temporal plots) were characterised. To allow the determination of the main particulate sources the times that the peaks occurred were noted and cross examined against the wind data and morphological profiles obtained both in

Section 3.3.2 and during a separate mobile laboratory trial. In general the particulates which were characterised during the study were very small, between 0.5 µm and 3 µm, and generally quite spherical, with some asymmetric particulates characterised. This indicated that the majority of the characterised particulates were generated by high temperature processes and this was confirmed by the mobile laboratory and wind data which pointed towards the blast furnace, the basic oxygen steelmaking plant and a road that is used to transport slag as the main sources of particulates. None of the peaks which were cross examined corresponded with the morphological profiles obtained in Section 3.3.2. This indicated two possibilities, firstly that two of the sources, the ore stockpiles and sinter plant, did not emit as many particulates as other sources. This is possible, since it is known that abatement procedures, such as the wetting of the stockpiles and electrostatic precipitators, are concentrated on these two areas of the steelworks. The second possibility is that the particulates from these sources had either been deposited before reaching the sampling site or were too high in the atmosphere to be sampled. This was discussed previously by Moreno, Jones and Richards.[16] They found that particulates from a steel plant could be found up to 50 km away from their source after remaining in the atmosphere for several days.[16] The Aspect is capable of detecting and characterising up to 20,000 particulates per second or 1,200 particulates per cubic centimetre of air. However, it can only sample this number of particulates if they are firstly present within the atmosphere and secondly if they are within the vicinity to the Aspect's inlet. For this study the sampling inlet was approximately one metre from the ground. To allow the sampling of particulates which have remained airborne, in future studies the inlet of the Aspect should be raised either by placing the Aspect on top of a building or using an extended sampling tube. Although the morphological profiles obtained in Section 3.3.2 were not of great use in this source apportionment work, the study has allowed proof of concept. It is also hoped that the RDS-Aspect method can be used to characterise a larger range of materials in future. This will therefore allow a database of morphological profiles to be developed which could then be used during future source apportionment studies.

3.5 Main Findings

An RDS has been successfully coupled to an Aspect morphology analyser and morphological profiles obtained for a control material, four individual materials and two binary mixes. Two replicates were completed for each of the materials and mixes, and comparisons between the replicates have been undertaken.

The control material was used to test the equipment set up. The sizes of the particulates determined corresponded well with the literature values, indicating that the RDS-Aspect method was capable of providing reliable results.

The four individual morphological profiles all showed diverse characteristics, and could be distinguished from each other. This capability could be of critical importance when completing on site analysis and source apportionment studies to allow the sources of characterised particulates to be determined. The morphological profiles, along with the chemical compositions obtained in Chapter Two, allowed a fuller understanding of the particulates composition.

The reproducibility of the individual morphological profiles was excellent. Similar numbers of particulates were characterised for each replicate and the profiles obtained were almost identical. This reproducibility indicated that the morphology of the particulates was consistent. The SEM photographs all indicated that the particulate morphologies determined using the Aspect were correct. Similarities were also seen between the shapes of particulates determined here and SEM photographs which were published in the literature. This signifies that the Aspect was correctly determining the morphologies of the particulates it characterised.

The characterisation of the two binary mixtures allowed the characterisation of material mixes as well as the opportunity to extract unique and characteristic morphological fingerprints from a mixed morphological profile. This knowledge that this extraction is possible would aid in on site source apportionment for diverse industries and materials.

The replicate analysis of sinter dust indicated that further agitation of the material did not change the particulates shape or size and it is unlikely that any agglomeration occurred. This indicated that morphological profiles of materials present on site are unlikely to change as they are further handled or moved. Therefore, the sources of particulates should be more easily determined on site as the particulates from a particular source will generally provide the same morphological profile as that which was obtained in a laboratory environment, using the RDS-Aspect method.

The source apportionment study has demonstrated that the use of an Aspect morphology analyser for source apportionment is possible and has allowed proof of concept. However, the sensitivity of the Aspect whilst completing source apportionment would have been reduced from the sensitivity which was obtained using the RDS method. The Aspect is capable of characterising up to 20,000 particulates per second, yet a much smaller number of particulates would have been present within the atmosphere at the source apportionment site. Therefore the number of particulates characterised would have been reduced and this may explain why it was not possible to obtain representative samples from all of the sources. Further development work, such as running the drum with a smaller sample weight to simulate conditions on site, could be carried out. Source apportionment studies using other light scattering techniques, such as APS and SMPS, could also be undertaken.

Although this work has shown that the RDS-Aspect method is successful, characterisation of other materials is needed to allow the development of a database of morphological profiles which could be used for onsite and source apportionment studies. In terms of the steel

making industry, materials from in and around an integrated steelworks should be collected and characterised, such as raw materials and dust from roads. To further enhance this work more materials could be collected from other industries as well as naturally occurring materials, such as sand and pollen.

The characterisation of more binary mixtures should also be completed as well as a small investigation into the agglomeration of particulates, as discussed in Section 3.3.4. This would allow a further insight into the possibility of extracting morphological fingerprints from a mixed profile as well as aiding the development of a database of typical material morphologies. The use of an artificial neural network should also be investigated. This would aid both in the examination of data and source apportionment studies. An artificial neural network allows a many part profile to be extracted into the individual parts. To do this the individual parts must first be 'fed' into the network. Then once the mixed profile is put through the network it can recognise the individual parts that make up the mixture and determine the probability that any of the individual parts are present within the mixture.

The Aspect can only characterise particulates between 0.5 µm and 20 µm. Therefore to allow the characterisation of particulates smaller than 0.5 µm and to obtain a full characteristic overview of these four materials an ELPI will be coupled to the RDS. The ELPI is able to characterise particulates as small as 0.029 µm as well as allowing the collection of particulates smaller than 10 µm to be collected onto substrates. These substrates will be gravimetrically analysed to obtain number and mass distributions and allow the determination of the mass fractionation of the particulates. Following gravimetric analysis the substrates will be digested and chemically analysed using an ICP-MS.

A novel experimental system for the characterisation of particulate matter from the iron and steel making process

M. Barker*[1], C.W. McLeod[1], D. Ciaparra[2], K. Jackson[2], D.R. Anderson[2] & D. Bard[3]

[1] Centre of Analytical Sciences, University of Sheffield
[2] Tata Steel RD&T, Swinden Technology Centre, Rotherham
[3] Health and Safety Laboratory, Harpur Hill, Buxton

1. Introduction

In view of the environmental and health implications that particulate matter (PM) can cause[1] the characterisation of the chemical and physical properties of particulates is of significant importance. To reduce the impacts of PM, the release of particulates into the atmosphere must be controlled by characterisation of PM sources. One source of PM in the iron and steel making industry is raw material stockpiles.

2. Methodology

A rotating drum sampler (RDS) has been directly coupled to both a three stage Dekati impactor and a Biral Aspect particle morphology analyser. Samples taken from stockpiles include two iron ores, a flue dust, an electrostatic precipitator dust, a coke breeze and an olivine. The Aspect is capable of providing real time morphological data by measuring irregularities in light scattering properties. The Dekati impactor collects size fractionated particulates onto three polycarbonate substrates, which may be analysed by inductively coupled plasma-mass spectrometry (ICP-MS), laser ablation-ICP-MS and SEM to obtain chemical and physical information.

Drum	4 minute run
	4 rpm rotation
Samples	6g of sample
	3 repeats per sample
Substrates	Weighed before and after use

3. Results

Morphological

Flue Dust

Light was scattered uniformly and there was a high concentration of PM with a low asymmetric factor, suggesting spherical particles were present. There was a large size distribution of PM, with a high concentration between 1 and 8 μm.

Ore F

Light was scattered non uniformly by flat faces on the PM suggesting the particles were asymmetric. There was a small size distribution of PM, with a high concentration between 2 and 5 μm.

Gravimetric

Both ores, the ESP dust and the coke breeze had high % of PM between 10-2.5 μm, whereas, the flue dust and the olivine had a high % of PM <1 μm. The smaller PM is more likely to become airborne from the stock piles, may impact locally and also be transported over longer distances.

5. Conclusions

• Characterisation of samples from the iron and steel making industry has been completed using the RDS coupled to a morphology analyser and a 3 stage impactor
• Each sample has a characteristic fingerprint, which may be used when characterising unknown samples

6. Further Work

• Analyse substrates using ICP-MS, Laser ablation-ICP-MS and SEM
• Compare results with those obtained from the bulk acid digestion and analysis of the raw materials by ICP-MS

7. References

1. K. Ravindra, Rev. Environ. Health, 2001, 16, 169-189
2. C. P. Lyons, J. Aerosol Sci., 1992, 23, S607-S61
3. J. M. Clark, Optically Based Biological and Chemical Sensing and Optically Based Materials for Defence, SPIE, Belgium, 2005

8. Acknowledgements

Work presented as a poster at the Royal Society of Chemistry, Young Members Symposium Manchester, UK, 2010. This poster was awarded a prize, by SCI, for collaboration between industry and academia

3.6 References

1.   J. F. Hamelmann and E. Schmidt, *KONA*, 2003, **21**, 7-18.
2.   E. Petavratzi, S. Kingman and I. Lowndes, *Minerals Engineering*, 2005, **18**, 1183-1199.
3.   C. A. Pope and D. W. Dockery, *Journal of the Air & Waste Management Association*, 2006, **56**, 709-742.
4.   K. Ravindra, A. K. Mittal and R. Van Grieken, *Review on Environmental Health*, 2001, **16**, 169-189.
5.   *Workplace atmospheres - Size fraction definitions for measurement of airborne particles,* BS EN 481, BSI, 1993.
6.   *Workplace atmospheres - Measurement of the dustiness of bulk materials - Requirements and reference test methods,* BS EN 15051, BSI, 2006.
7.   K. Jackson, PhD Thesis, University of Sheffield, 2009.
8.   H. Price, R. Arthur, K. Sexton, C. Gregory, B. Hoogendoorn, I. Matthews, T. Jones and K. BéruBé, *Journal of Toxicology and Environmental Health, Part A*, 2010, **73**, 355 - 367.
9.   J. P. Shi, A. A. Khan and R. M. Harrison, *The Science of the Total Environment*, 1999, **235**, 51-64.
10.   P. H. Kaye, E. Hirst, J. M. Clark and F. Micheli, *Journal of Aerosol Science*, 1992, **23**, 597-611.
11.   A. Jillavenkatesa, S. J. Dapkunas and L.-S. H. Lum, *NIST Recommended Practice Guide*, 2001, Special Publication 960-1.
12.   S. J. B. Reed, *Electron Microprobe Analysis and Scanning Electron Microscopy in Geology*, Cambridge University Press, Cambridge, 2005.
13.   R. J. Cheng, V. A. Mohnen, T. T. Shen, M. Current and J. B. Hudson, *Journal of the Air Pollution Control Association*, 1976, **26**, 787-790.
14.   N. Kaufherr and D. Lichtman, *Environmental Science & Technology*, 1984, **18**, 544-547.
15.   H. G. Siegrist Jr. and A. G. Wylie, *Environmental Research*, 1980, **23**, 348-361.
16.   T. Moreno, T. P. Jones and R. J. Richards, *Science of the Total Environment*, 2004, **334-335**, 337-346.
17.   E. Remoundaki, A. Bourliva, P. Kokkalis, R. E. Mamouri, A. Papayannis, T. Grigoratos, C. Samara and M. Tsezos, *Science of the Total Environment*, 2011, **409**, 4361-4372.
18.   www.malvern.com, Accessed 4th July 2013
19.   www.tsi.com, Accessed 4th July 2013
20.   *Scanning Mobility Particle Sizer Spectrometer, Model 3936, Specification Sheet*, TSI, 2012.
21.   *Aerodynamic Particle Sizer, Model 3321, Specification Sheet*, TSI, 2012.
22.   *Aspect User Manual*, Biral, 2010.
23.   K. Reid, A. T. Martin and J. M. Clark, *Journal of Aerosol Science*, 1992, **23**, S325-S328.
24.   E. Hirst and P. H. Kaye, *Journal of Geophysical Research*, 1996, **101**, 19231-19235.
25.   P. H. Kaye, *Measurement Science and Technology*, 1998, **9**, 141-149.
26.   J. M. Clark, M. J. Shelton, S. P. Evans, P. D. Smith, I. A. Simpson and P. H. Kaye, Optically Based Biological and Chemical Sensing and Optically Based Materials for Defence, Bruges, Belgium, 2005.
27.   C. P. Lyons, D. Mark, K. Y. K. Chung and G. Burdett, *Journal of Aerosol Science*, 1992, **23**, S607-S610.
28.   C. P. Lyons and D. Mark, *HSE Contract Research Report, 62/1994*, Warren Springs Laboratory, 1994.
29.   C.-J. Tsai, C.-H. Wu, M.-L. Leu, S.-C. Chen, C.-Y. Huang, P.-J. Tsai and F.-H. Ko, *Journal of Nanoparticle Research*, 2009, **11**, 121-131.

Chapter Four

Physical and elemental studies of particulates using an RDS-ELPI method and ICP-MS

4.1 Introduction

Particulates are a natural component of the atmosphere,[1] however anthropogenic particulates which are connected to human activities may also be present.[2] Natural sources of particulates include sea salt, forest fires and soil dust[2] whilst anthropogenic sources include industrial operations, transport and the burning of fossil fuels, such as wood burning in homes or barbeques.[3] Anthropogenic particulates have no boundaries and although they may be generated in a highly populated and industrialised area they can travel to remote regions. In general particulate emissions are decreasing, but their adverse effects are likely to remain for the near future. The reason for the decrease in these emissions is due to the introduction of air quality standards. These standards establish maximum allowable concentrations for a number of pollutants, such as particulates, and also assist in the development and implementation of environmental protection regulations and policies.[4]

The current European air quality limit values for PM_{10}, were widely exceeded throughout Europe in 2010.[5] As well as the effects they have on human health, discussed in previous chapters, particulates can also have adverse effects on the climate and ecosystems as outlined in Table 4-1.[5] On 7th May 2013, the PM_{10} concentration, as a running 24 hour mean, for Sheffield town centre was 23 µg/m^3. DEFRA use a band system to judge the levels of air pollution. This concentration for Sheffield town centre was within the 'low' band as it was below the European air quality limit.[6]

Health effects	Environmental effects	Climate effects
- Cardiovascular and lung diseases - Heart attacks - Affect the central nervous and reproductive systems - Cancer	- Affect animals in the same way as humans - Plant growth - Ecosystem processes - Reduced visibility - Damage to buildings	- Net cooling or warming - Changed rainfall patterns

Table 4-1: Adverse particulate effects[5]

These adverse effects, especially those to the climate, are controlled by a range of properties such as particulate size, chemical composition and number concentration. To understand these effects the chatacterisation of the properties of airborne particulate is of upmost importance.[7]

There are a range of methods used to determine particulate size, which are detailed in Table 4-2. The fast mobility particle sizer, operates in a similar way to the SMPS, described in Chapter Three. It uses multiple electrometers for particulate detection which allows rapid size distribution measurements, with a one second resolution.[8]

Dynamic light scattering can also be used to determine particulate size, specifically nanosized particulates. A number of dynamic light scattering instruments are commercially available, including the 90 Plus, manufactured by Brookhaven instruments and the LAS, manufactured by TSI. The 90 Plus is able to characterise nanosized particulates that are in suspension. Applications include the characterisation of polymer latexes, pharmaceutical preperations, paints, pigments, emulsions as well as cosmetic formulations.[9] If the particulates of interest cannot be put into suspension and a laser scattering technique is required, a laser aerosol spectrometer, manufactured by TSI, may be used. The LAS uses dynamic light scattering to complete both indoor and outdoor air quality measurements as well as exposure monitoring and is capable of quickly characterising particulates between 90 nm and 7.5 µm.

Technique	Size Range	Operating mode	Strengths	Limitations
FMPS, TSI	5.6 nm to 560 nm	On line	Real time size measurements, Easy set up	Small size range, Will only run unattended for up to twelve hours
90 Plus, Brookhaven	1 nm to 6 µm	Off line	Good reliability and reproducibility Large range of applications	Particulates must be in a suspension, Long measurement time, 1 to 2 minutes
LAS, TSI	90 nm to 7.5 µm	On or Off line	Quick measurement time, less than a second, Large range of applications	Small size range Dry sample characterisation only
MOUDI, M125, AP	10 nm to 18 µm	On or Off line	Broad size range, Impactor rotates for better particulate distribution	Flow rate unchangeable, No online measurements
Gravimetric impactor, Dekati	0.2 µm to 2.5 µm	On line	Can replace a standard filter holder, High flow rate, 70 L/min and high sample yield	Only collects particulates on 4 stages, No online measurements
ELPI, Dekati	30 nm to 10 µm	On or Off line	Provides number-size distributions in real time, Unattended operation possible	Lots of training required Dry sample characterisation only

Table 4-2: Techniques for characterising the size of particulates[8-13]

To allow the simultaneous determination of particulate size distributions, as well as the collection of particulates onto substrates, cascade impaction may be used. The use of impaction to collect particulates onto substrates was first discussed by May in 1945.[14] May developed a instrument which used four stages with progressively smaller jets and a compressed air unit to sample both windborne and stationary aerosols.[14] This technique has been developed over the years and there are now a range of commercially available instruments which use cascade impaction, such as the MOUDI, manufactured by MSP.[10] The MOUDI differs from normal cascade impactors in that each stage is rotated relative to the stages above and below it to allow uniform distribution of the impacting particulates.[15]

A large range of other cascade impactors, such as the gravimetric impactor and the ELPI are manufactured by Dekati.[16] The gravimetric impactor allows particle size distribution measurements to be undertaken and is generally used for automotive research. It collects particulates onto four stages with cut off diameters of 2.5 µm, 1.0 µm, 0.5 µm, 0.2 µm. However this impactor can only collect particulates for further gravimetric analysis and does not allow real time measurements to be conducted. To allow real time particulate size measurements an ELPI may be used. The ELPI was first designed and developed at Tampere University of Technology, in 1992, by Keskinen, Pietarinen and Lehtimäki.[17] Although the use of electrical detection had been previously discussed by Tropp, Kuhn and Brock in 1980,[18] Keskinen, Pietarinen and Lehtimäki were the first to combine electrical real time detection with low pressure impaction allowing a much larger size range of particulates, 30 nm to 10 µm, to be characterised than previous impactors.[17] The method showed good potential for the measurement of submicrometer size distributions and the ELPI is now commercially manufactured by Dekati.[16] In 2000, Marjamäki, Keskinen, Chenm and Pui[19] completed a performance evaluation of the ELPI. They calibrated both the impactor and the charger before completing characterisation of a generated monodisperse aerosol. The results were compared to those obtained when using the same method with an SMPS. There was a good agreement

between the distributions obtained from each of the instruments indicating that the real time size distributions obtained when using the ELPI were valid.[19]

Although the ELPI can provide real time number-size distributions it also allows the collection of particulates onto substrates. These substrates can be analysed gravimetrically, through weighing and re-weighing, they and the particulates contained on the substrates, may also be chemically characterised. Both indirect and direct characterisation may be undertaken using techniques such as ICP, XRF and LA-ICP. This chapter will focus on indirect analysis using ICP-MS.

When using an indirect analysis technique, the sample of interest must be in a liquid form. The solid sample must be completely dissolved and the elements of interest released into solution.[20] A popular method for the digestion of solids is to use a microwave assisted reaction system. Microwave systems are closed systems, which can withstand high pressures and temperatures to allow greater digestion efficiency than other digestion methods. Once digested samples may be elementally characterised using techniques such as ICP-AES and ICP-MS. ICP techniques possess a high detection power and can be used for simultaneous multielement analysis.[21] From the initial development of the ICP discharge in 1961,[22] ICP instruments are now commercially available from a range of companies.

The digestion and consecutive analysis of ELPI substrates, using ICP-MS, was described by Price, Arthur, Sexton, Gregory, Hoogendoorn, Matthews, Jones and BéruBé, in 2010.[23] Particulate collection was completed using an ELPI located in an urban air traffic canyon (in Swansea) and in a rural location (the Brecon Beacons). Sampling was completed using aluminium substrates for ten weeks in Swansea and for three weeks in the Beacons. However, the samples collected from the Beacons were unusable due to an atypical dust storm, originating from the Sahara, a bonfire and a power failure. Substrates were digested and chemically characterised using ICP-MS. Elements analysed included cadmium, chromium, cobalt, copper,

iron, lead, magnesium, manganese, nickel, vanadium and zinc. Consistent daily profiles were found, with a steep increase in particulate number concentrations during morning rush hour. By examining the morphology of the particulates, by using SEM, some of the sources were determined allowing source apportionment to be completed.[23]

This chapter will discuss the coupling of an RDS with an ELPI to allow physical characterisation of four samples obtained from an integrated steelworks, ore D, ore F, flue dust and sinter dust. The ELPI will allow real time distributions to be obtained whilst also allowing the collection of particulates onto polycarbonate substrates. Following gravimetric analysis, the polycarbonate substrates will be digested, using a microwave system, and the resulting digests analysed by ICP-MS.

4.2 Experimental

4.2.1 Reagents and Materials

Four materials, ore D, ore F, flue dust and sinter dust, were studied using the RDS-ELPI method. These materials were chemically and morphologically characterised in Chapters Two and Three, respectively. Their chemical compositions and morphologies are listed in Table 4-3.

Element	Ore D (µg/g)	Ore F (µg/g)	Flue dust (µg/g)	Sinter dust (µg/g)
Ba	91.4 ± 3	66.2 ± 4	102 ± 2	167 ± 6
Cd	<LOD	<LOD	7.65 ± 0.2	45.2 ± 2
Co	19.9 ± 1	15.5 ± 0.5	131 ± 2	11.2 ± 0.5
Cr	18.7 ± 0.2	35.2 ± 1	238 ± 9	136 ± 4
Cu	10.1 ± 0.3	8.27 ± 0.7	316 ± 26	200 ± 12
Fe	932171 ± 14253	885057 ± 63852	534122 ± 33183	690894 ± 19345
K	52.3 ± 6	81.9 ± 7	3382 ± 256	15822 ± 942
Mn	2836 ± 158	1461 ± 50	8227 ± 320	3527 ± 175
Ni	21.5 ± 0.7	8.66 ± 0.5	305 ± 6	89.4 ± 5
Pb	5.99 ± 0.3	7.53 ± 0.5	3112 ± 66	2275 ± 84
V	27.7 ± 1	52.0 ± 3	377 ± 12	64.2 ± 3
Zn	20.8 ± 0.7	11.1 ± 3	9885 ± 171	159 ± 6
Morphology	Asymmetric	Both asymmetric and spherical	Spherical	Asymmetric
Particulate size	2 µm	2, 7 and 11 µm	7 µm	1 to 3 µm

Table 4-3: Chemical and morphological composition of materials

Each material was sieved, using a 45 µm sieve, to minimise the agglomeration of particulates. The four materials were stored separately, in glass bottles and analysed directly. Approximately ten grams of ore D, ore F and sinter dust were used for charging the RDS, however only five grams of flue dust were used due to its dustiness. Titanium dioxide (manufactured by Huntsman Pigments, Stockton-on-Tees, UK) was used as a control material to confirm that the equipment was set up and functioning correctly. A number of direct tests, with varying weights of titanium dioxide, were completed.

For the ICP-MS analysis of the substrates a calibration set containing seven multielement solutions was prepared from one 10 mg/L multielement stock solution (PlasmaCal multielement standard, 500 mL, 5 % HNO_3). The seven calibration solutions had concentrations of 5 µg/L, 10 µg/L, 20 µg/L, 50 µg/L, 100 µg/L, 200 µg/L and 500 µg/L. A multielemental QC solution, 20 µg/L, was also prepared (Aristar, multielement calibration standard 2, 100 mL, 5 % HNO_3). All solutions were made up using one percent nitric acid (Aristar, VWR). The elements were copper, iron, lead, magnesium, manganese, vanadium and zinc.

4.2.2 Substrates

25 mm poreless polycarbonate substrates were used within the ELPI. They were weighed before and after use by a Mettler MT5 balance. Before any weighing took place, the substrates were left to equilibrate for two hours in a temperature and humidity controlled room. Unless being used within the impactor, the substrates were all stored in single Petri dishes. For every thirteen substrates that were used, one unused substrate was kept aside to use as a blank. This blank substrate was weighed and re-weighed at the same time as the thirteen substrates it was paired with. It was then used to subtract any weight gain or loss of the substrates themselves. The performance and the calibration of the balance were assessed using a check weight (27.486 mg) before any weighing commenced.

4.2.3 Instrumentation

The RDS, as used in Chapter Three, was also used for the experiments within this chapter. Again foams were not used to establish dustiness indices of solid materials, as stated in BS 15051,[24] but instead the drum's rotation was used to simulate material handling processes. Coupled to the RDS was an ELPI, manufactured by Dekati and shown in Figure 4-1.

Figure 4-1: Electrical low pressure impactor
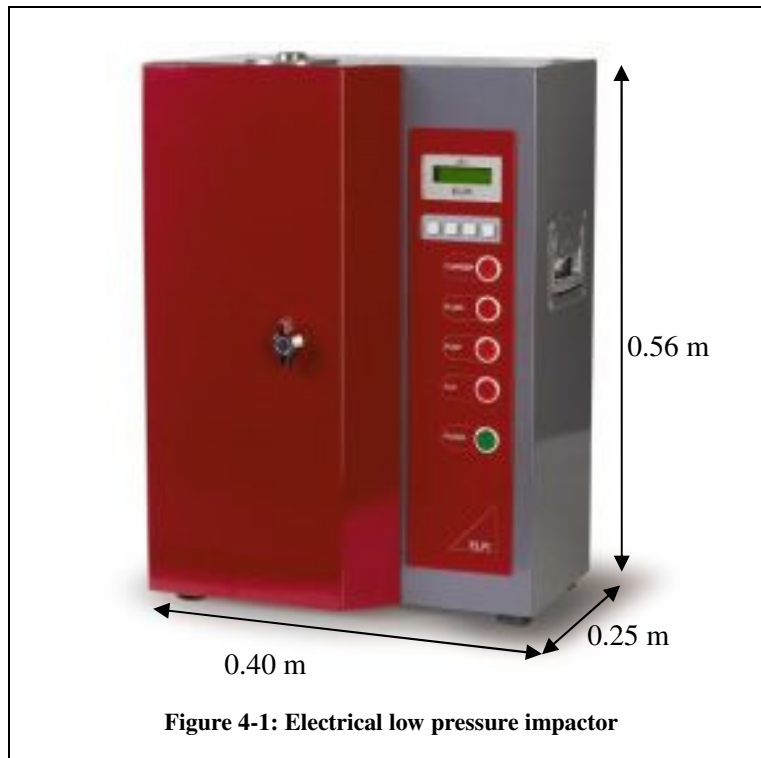
The ELPI is a low pressure impactor which allows the real time measurement of particulate size distribution and concentration. By electrically charging the particulates it characterises it is able to count them as well as determine which of the thirteen electrically isolated stages they land upon. These electrically isolated stages each hold a 25 mm substrate and collect particulates between 30 nm and 10 µm. The counting of particulates is generally preferred to gravimetric analysis of the substrates as it provides highly precise results. The low pressure is generated by a pump that operates at a flow rate of 30 L/min. The air pressure within the impactor decreases as the orifices between each stage decrease, causing particulates to lose momentum and impact on a stage. The largest orifices are located at the top of the impactor, with the smallest orifices at the bottom.[13] The cut off points for the thirteen stages are listed in Table 4-4.

Stage	Cut off point (μm)
1	0.0285
2	0.0562
3	0.0937
4	0.156
5	0.262
6	0.383
7	0.615
8	0.950
9	1.60
10	2.40
11	4.01
12	6.60
13	9.98

Table 4-4: ELPI cut off points[13]

To connect the RDS to the ELPI a freely rotating connector and one metre of conductive silicone tubing, with an internal diameter of 28 mm, was used. To prevent particle deposition or settling in the tubing, a minimal length, of one metre, was used and sharp bends were avoided. This setup is detailed in Figure 4-2.
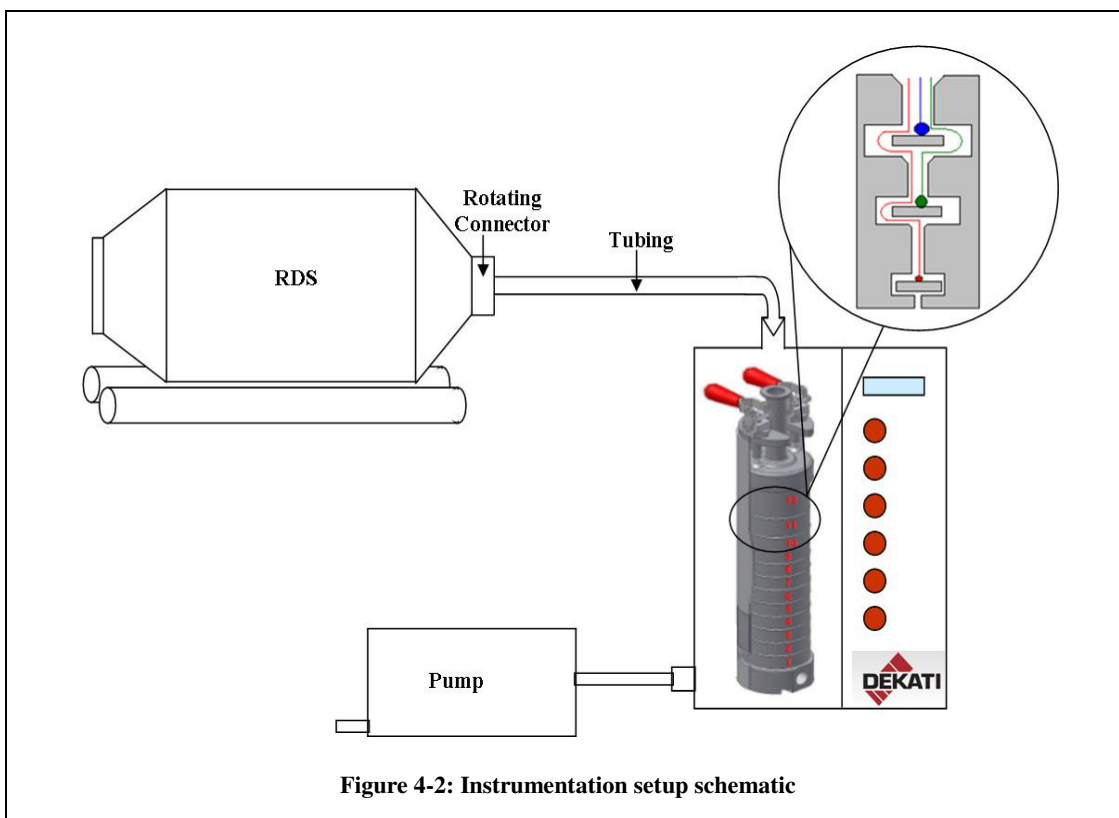
Figure 4-2: Instrumentation setup schematic

4.2.4 Procedures

After coupling the RDS to the ELPI, the drum was charged with the material of interest and then sealed with technostat filter material. Technostat was used to stop any particulates entrained within the atmospheric air entering the drum and at the same time stop any generated particulates from exiting the drum and entering the atmosphere. The pre-weighed 25 mm substrates were loaded into the thirteen impactor stages and the impactor was positioned within the ELPI. The ELPI was then flushed with laboratory air for ten minutes and the system was zeroed to ensure a low and stable background reading was obtained. The ELPI software was started and data was recorded for exactly one minute prior to the simultaneous starting of the RDS rotation and the ELPI pump. The ELPI pump operated at a flow rate of 30 L/min. The RDS was rotated for four minutes, at a rate of four revolutions per minute. Once the four minutes was over, both the ELPI pump and the RDS rotation were stopped. The ELPI software was left to record data for at least another minute to confirm that the background had returned to the same level as was obtained before commencement of the experiment. The ELPI was then disconnected from the RDS and the remaining dust was allowed to settle. During this time, the thirteen substrates were removed from the impactor stages and placed in separate Petri dishes for storage before being re-weighed. This remaining dust was disposed of and the RDS, along with the impactor and its stages were taken to a fume cupboard for cleaning. They were all rinsed once with water and twice with isopropanol before being left to air dry. Each experiment was completed in duplicate. The replicates were completed on two different days but at similar temperatures and relative humidities, approximately 20 ℃ and 45 %. As a separate one day study, completed at a temperature of 19 ℃ and a relative humidity of 70 %, three replicates were completed in quick succession. Ten grams of sinter dust was used, in total, for the three replicates. This was charged into the drum at the start of the first replicate and no extra material was added during the further two replicates. A gap of eighteen minutes was left between each replicate to allow the impactor and its stages to be cleaned and the thirteen substrates changed, the RDS was not cleaned between each replicate. During these eighteen minutes, the RDS rotation was stopped and the ELPI pump and software were switched off.

4.2.5 Multielement Analysis of ELPI Substrates

Following the re-weighing of the substrates, after their use within the ELPI impactor, the first twelve substrates from each experiment were digested and chemically analysed using ICP-MS. Digestion was completed using a microwave system. Each substrate was placed, using metal tweezers, into the digestion vessel followed by the addition of 4 mL of nitric acid and 1 mL of hydrochloric acid. Each digestion set included nine substrates, one acid blank and one SRM, NIST 1648a, urban particulate matter. Four blank substrates were also digested to determine their elemental concentrations. Table 4-5 details the microwave method used.

Step	Power (W)	% Power	Ramp time (min)	Digest Time (min)	Temp (^{0}C)	Pressure (psi)
1	1600	100	20	10	140	400

Table 4-5: Microwave method used for digestion

After the digestion process and once the vessels had cooled, the vessels were rinsed with high purity de-ionised water (18.2 MΩ.cm). The digestion solutions were transferred to 50 mL sample tubes and made up to 30 mL with high purity water. The majority of the solutions were analysed directly. The only exception to this was the SRM digestion solutions which were diluted, using high purity water (18.2 MΩ.cm), by a factor of twenty before analysis. Analysis was performed using an Agilent 7500ce ORS ICP-MS with operating conditions as listed in Table 4-6. The ICP-MS was fitted with a collision cell to reduce isotopic interferences.

Plasma power	1.55 kW
Carrier gas flow	0.85 L/min
Make up gas flow	0.2 L/min
Integration time	0.5 seconds
Sampling depth	8 mm

Table 4-6: ICP-MS operating conditions

4.3 Results and Discussion

4.3.1 Initial Studies

Initially the physical characterisation of titanium dioxide was completed. This was to confirm whether the coupling of the two instruments, the RDS and the ELPI, had been completed successfully.

Number distributions, such as the one shown in Figure 4-3, were provided by the ELPI software. These distributions plot the number of particulates per cm^3 over the aerodynamic diameter of the particulates. Therefore the graph in Figure 4-3 indicates a large proportion of particulates at approximately 0.05 µm, followed by a general decrease in particulate number up to 0.5 µm, where a slight increase is seen, before a tailing off in particulate number up to 3 µm. Gravimetric analysis of the substrates allows mass distributions to be plotted in the same way.

Figure 4-3: Example number distribution plot
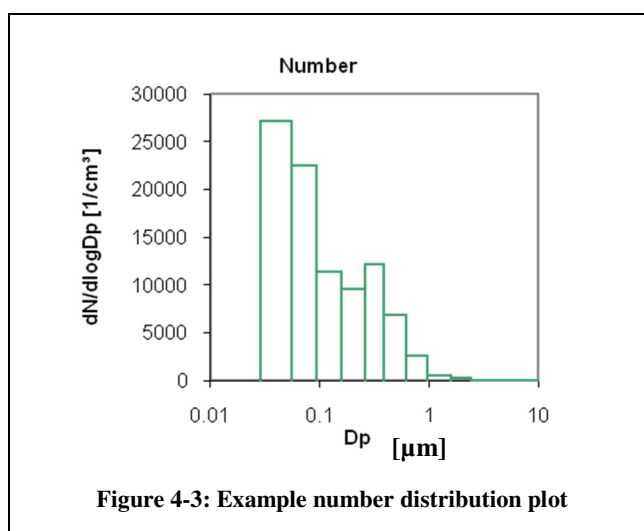
Four experiments, using different masses of titanium dioxide were completed on the same day. The four masses used were 10 g, 5 g, 2.5 g and 1 g. Four different masses were tested because, when using the larger masses, the particulate detectors were overloaded and, therefore, to get accurate results the mass of control material was reduced. The four different experiments all produced similar number distributions (Figure 4-4), with peaks in particulate number at comparable diameters. The first peak at 0.05 µm was always the largest. A decrease in

particulate number was then seen down to 0.1 µm where very few particulates were present. An increase in particulate number was then seen with a peak at 0.5 µm to 0.8 µm. This was followed by a tailing off in particulate number up to 5 µm. There was a general decrease in the number of particulates as the mass used for the experiments also decreased, which was to be expected.

Figure 4-4: ELPI profiles for TiO₂. 10 g (top left), 5 g (top right), 2.5 g (bottom left) and 1 g (bottom right). Dp is in µm.
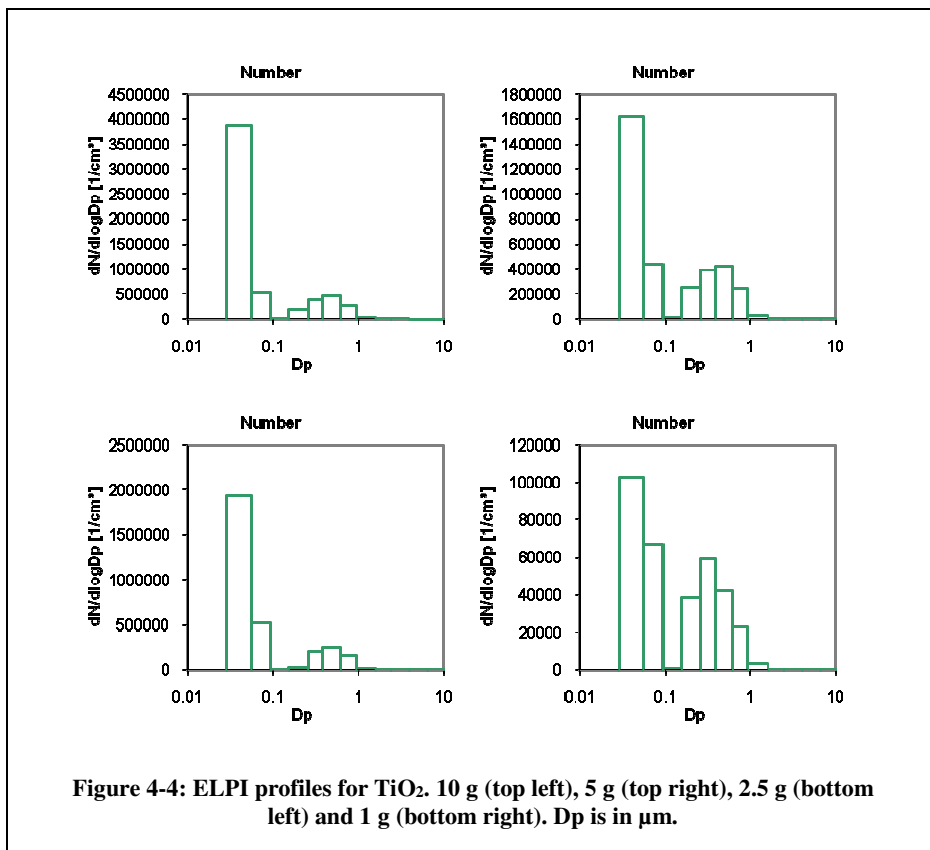
Comparisons cannot be made with the manufacturer's data, as no particulate size data was provided. The peaks viewed at 0.5 µm agreed with the results obtained when using the RDS-Aspect method, discussed in Section 3.3.1. Comparisons could be made in relation to previous research completed by Tsai et al.[25] where size distribution measurements were completed using a scanning mobility particle sizer and an aerodynamic particle sizer. The median diameters obtained were 0.37 µm and 0.86 µm respectively.[25] Although the results obtained here were not the same as the results obtained by Tsai et al., similarities could be seen. Full comparisons were not expected because the materials were not the same. Results are summarised in Table 4-7.

Material	Size of largest concentration
Titanium Dioxide	0.05 µm

Table 4-7: Summary of the physical characterisation of the control material

The successful physical characterisation of the titanium dioxide control material confirmed that the configured RDS-ELPI system was functioning as expected. Results corresponded well with those previously obtained indicating that the RDS-ELPI method was giving sensible results.

4.3.2 Physical Characterisation of Materials

The physical characterisation of the four materials will now be discussed. The overall gravimetric analysis will be discussed first followed by the examination of both the mass and number distributions for each individual material.

Gravimetric Analysis

The total particulate mass collected on the substrates, for each replicate, has been determined and is plotted in Figure 4-5. The masses for each substrate and the particulates collected upon them are shown in the Appendix. Ore D replicates indicated excellent reproducibility, with similar masses obtained for each, 0.083 mg and 0.085 mg. The reproducibility for the other materials was poor and the obtained masses were inconsistent (Table 4-8). Although the materials are homogenous on a large scale, the differences in masses could represent heterogeneities on the small scale. The slight differences in laboratory temperature and humidity could have also affected the overall results.
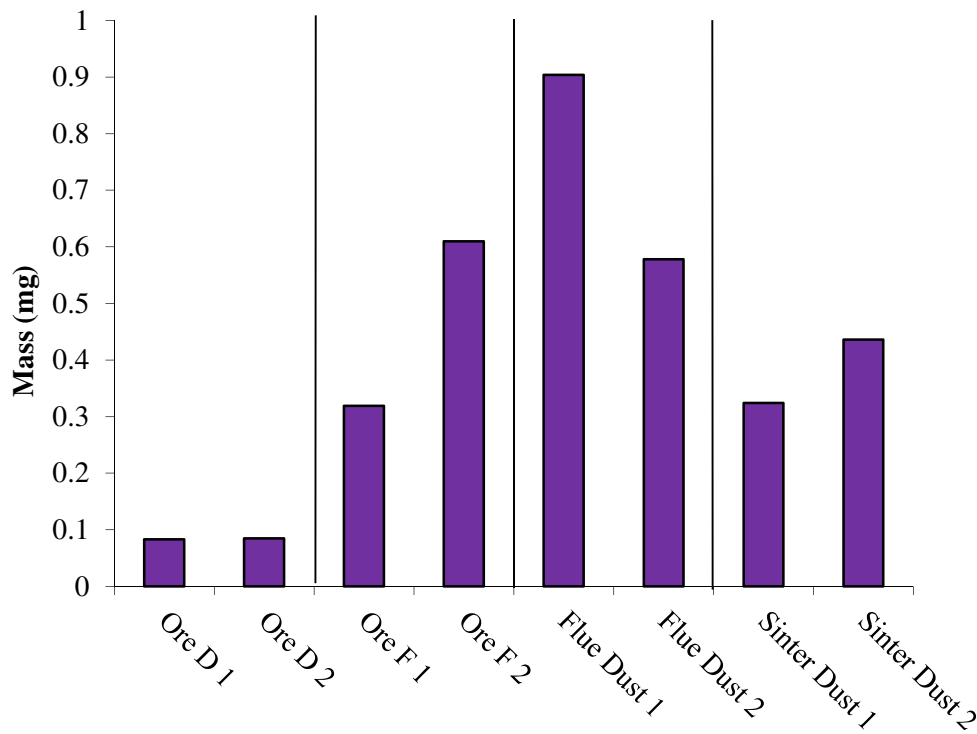
Figure 4-5: Total particulate masses collected with the ELPI

Material	Replicate one	Replicate two
Ore D	0.083 mg	0.085 mg
Ore F	0.319 mg	0.610 mg
Flue dust	0.904 mg	0.578 mg
Sinter dust	0.324 mg	0.436 mg

Table 4-8: Summary of the particulate masses collected for each replicate

The mass fractionation of the particulates was also determined, as shown in Figure 4-6. All four materials showed similar mass fractionation profiles between replicates. Three of the materials, ore F, flue dust and sinter dust indicated high percentages of particulates on stages nine to twelve, 1.60 µm to 6.60 µm. This was to be expected because particulates collected upon these stages are larger, and therefore heavier, than the smaller, and lighter, particulates, which were collected on the lower stages. Ore D indicated high percentages of particulates on stages five to seven, corresponding to diameters of 0.262 µm to 0.950 µm. This indicates that there were a large proportion of particulates between these diameters present in the ore D material. Although

different to the other materials, this information might be helpful when examining mixtures of materials in real sampling scenarios.

Figure 4-6: Total percentage mass fractionation when using the ELPI
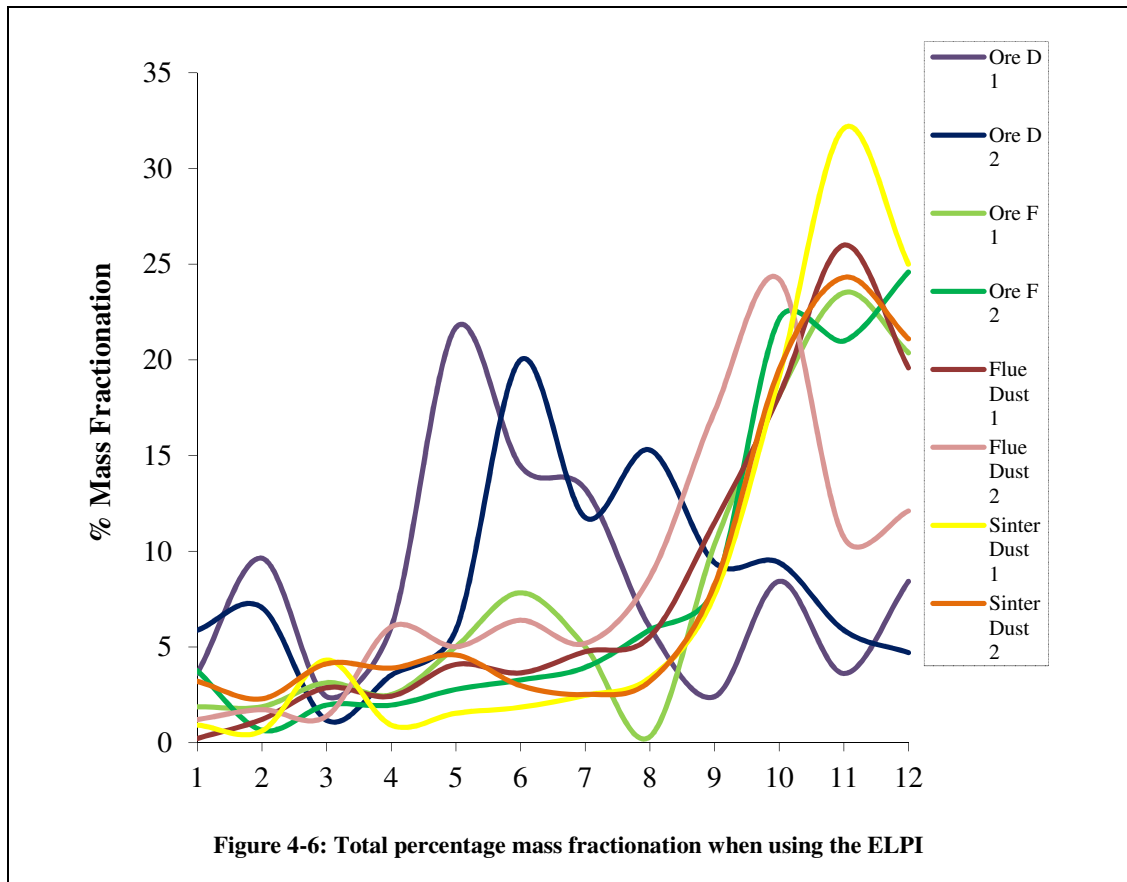
Ore D

The number and mass distributions for ore D are presented in Figures 4-7 and 4-8, respectively. Both replicates indicated a range of particulates with differing diameters and masses. The highest number concentration of particulates was present at approximately 0.05 µm, followed by a small decrease in particulate number. This was followed by another peak in number concentration at 0.5 µm and a final tailing off of particulates. Both replicates indicated similar numbers of characterised particulates, pointing to good reproducibility.

Figure 4-7: Number distributions for ore D
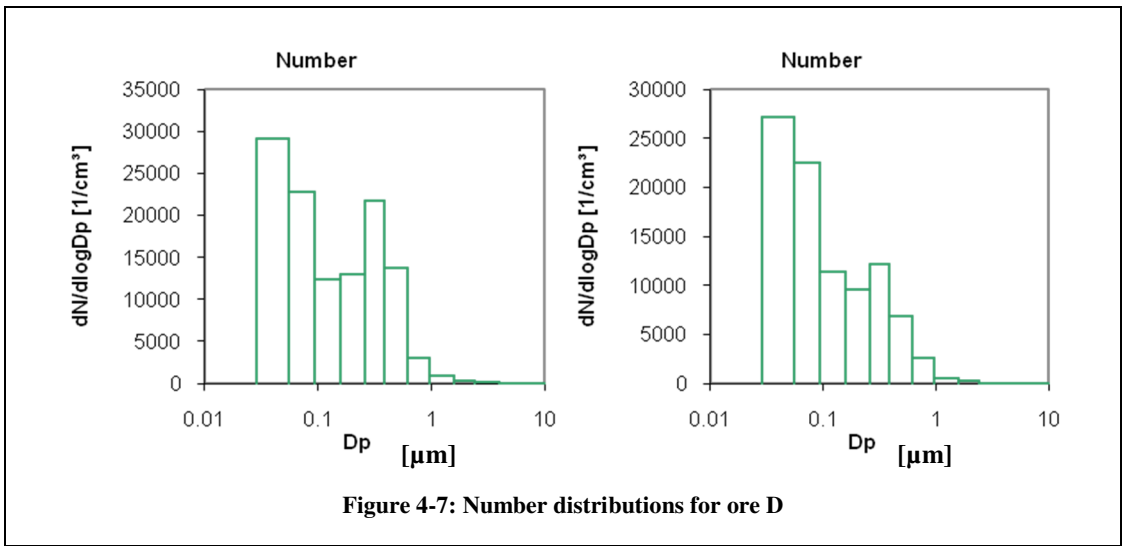
The mass distributions indicated a peak in concentration at 0.4 µm, this is the largest peak, rather than the second largest as shown in the number distributions. This is because, although there were a large proportion of particulates present at 0.05 µm, they would have been lighter than the particulates at 0.4 µm, therefore producing a smaller peak. The reproducibility of the two replicates is generally good with increases in mass present at similar particulate diameters.

Figure 4-8: Mass distributions for ore D
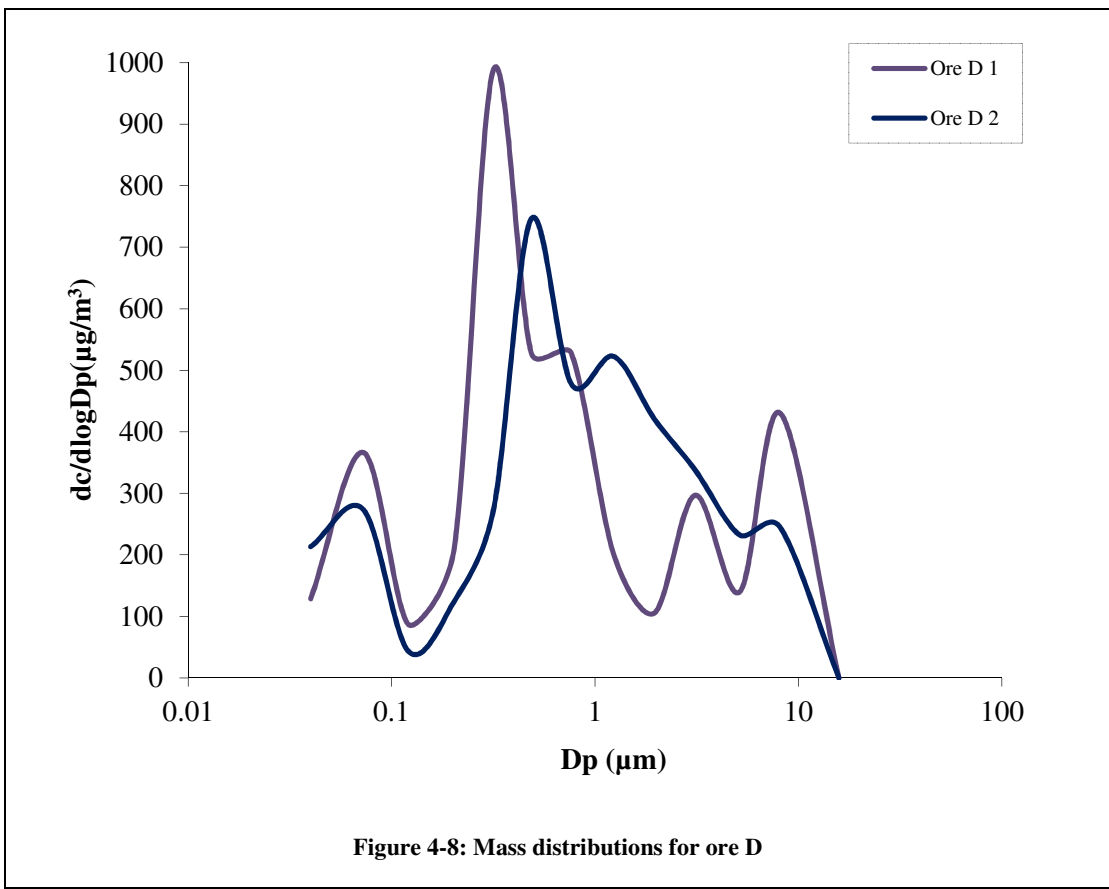
Ore F

Ore F produced quite different number and mass distributions to ore D as shown in Figures 4-9 and 4-10, respectively. Although a high number concentration was still visible at 0.05 µm, the number of particulates present above 0.1 µm was much smaller and tailed off quicker. The number of particulates present in general was larger than ore D, indicating a much dustier material. Replication was very good, with both replicates producing almost identical number distributions.

Figure 4-9: Number distributions for ore F
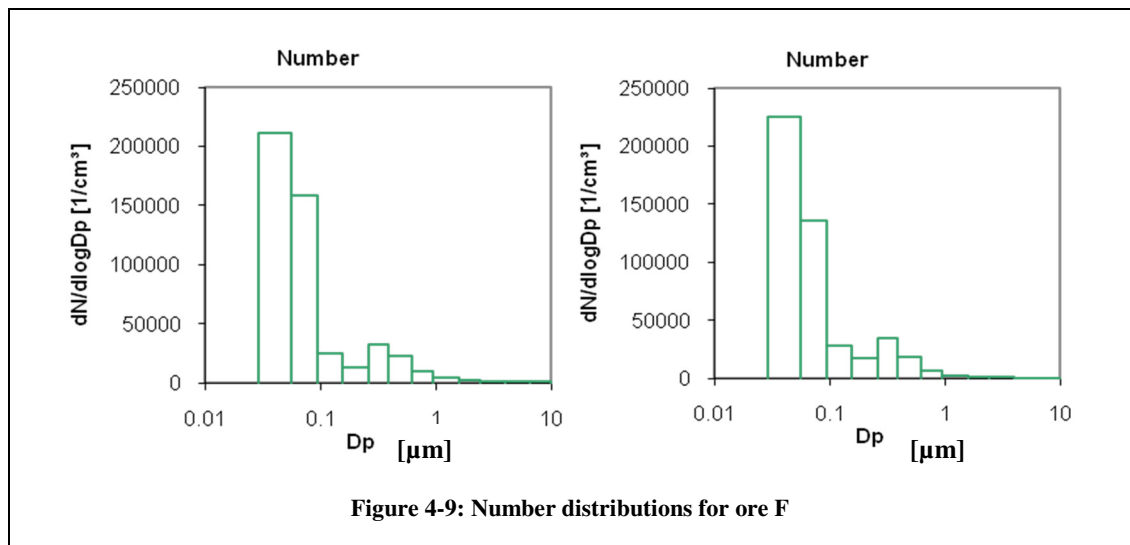
The peaks in the mass distributions for ore F were opposite to those seen in the number distributions. This indicated that although there was a large number of particulates present below 0.1 µm they would have been very light and not contributed greatly to the overall mass of the particulates characterised. There was a difference in the mass of particulates between replicates, however, peaks were seen at the same diameter in each, 8.12 µm.

Figure 4-10: Mass distributions for ore F
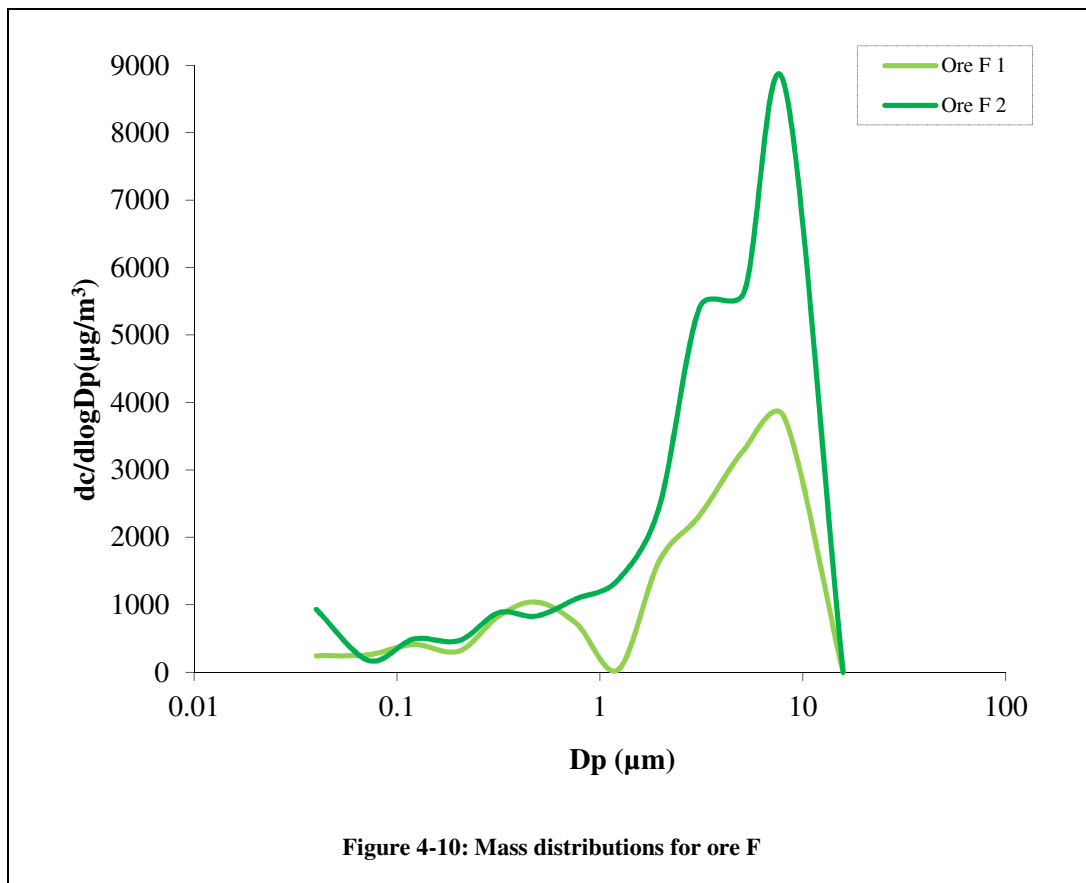
Flue Dust

The flue dust number distributions, Figure 4-11, indicated that a very large number of small particulates were present within the material at approximately 0.05 µm. A smaller peak was viewed at 0.08 µm, followed by a tailing off in particulate number concentration, which was not seen for either of the ores. The number of particulates characterised, in general, was a lot larger than seen for either of the ores, even with a reduced initial mass of five grams.

Figure 4-11: Number distributions for flue dust
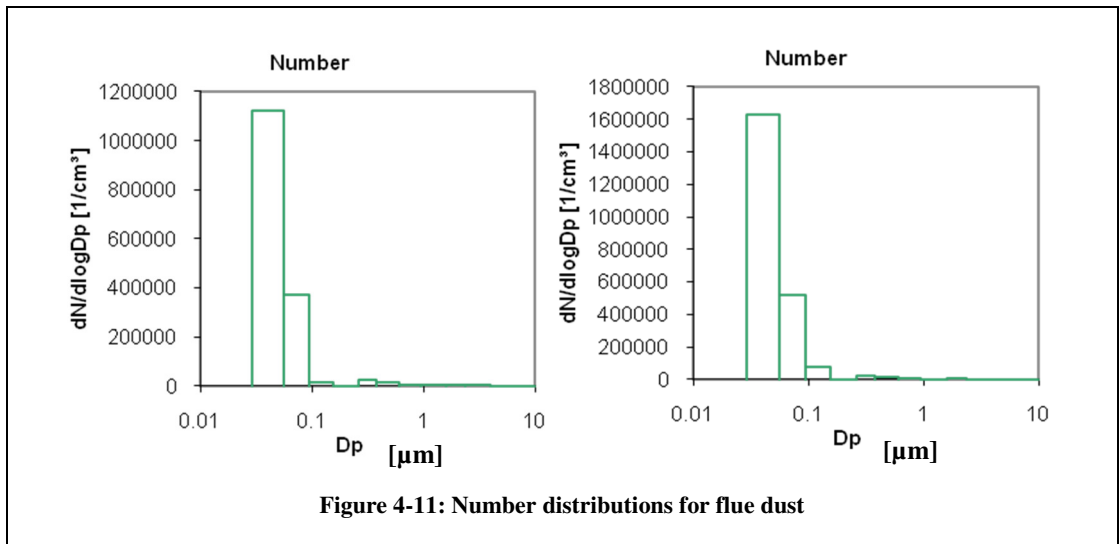
The mass distributions for the flue dust material, Figure 4-12, were very similar to those obtained for ore F. This again indicated that although a large proportion of the material contained very small particulates the larger particulates, at 8.12 µm, were heavier and therefore contributed more to the overall mass.

Figure 4-12: Mass distributions for flue dust
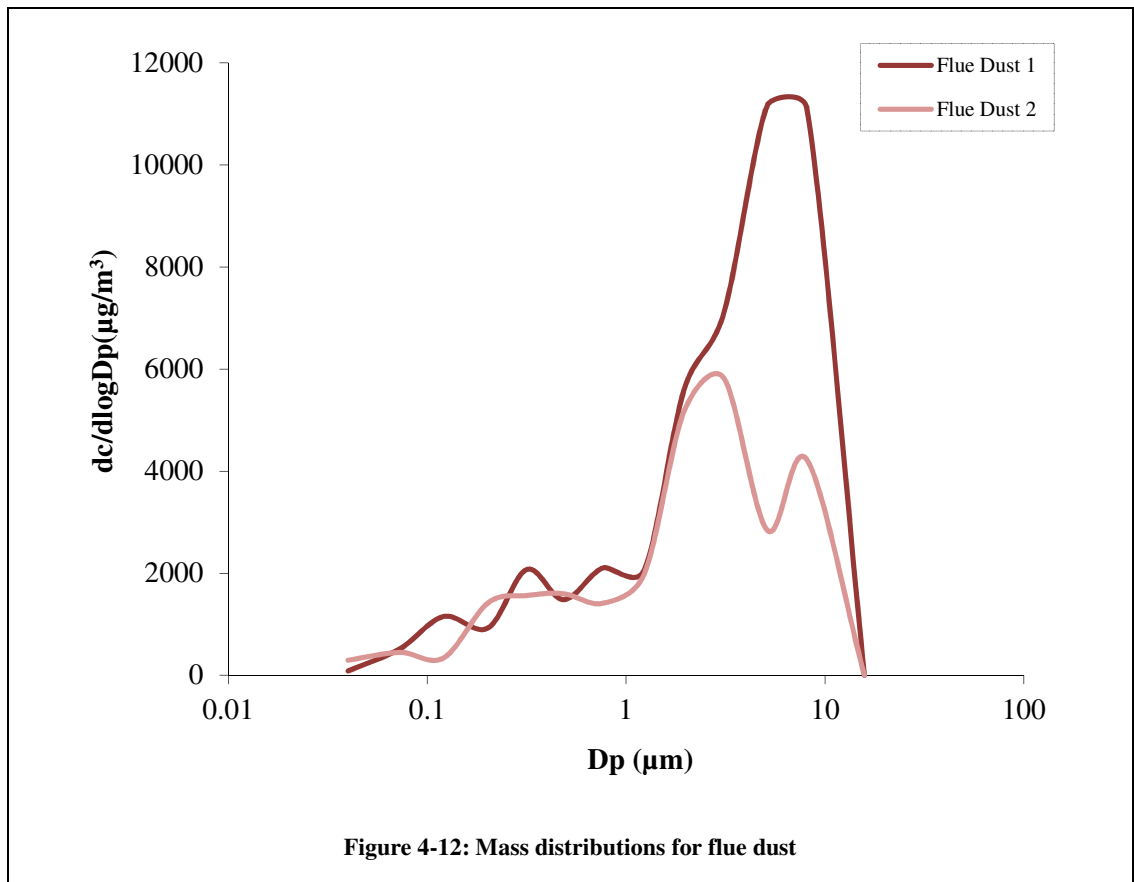
Sinter Dust

The sinter dust showed good similarities between both replicates for number and mass distributions as indicated in Figures 4-13 and 4-14. In similarity with the flue dust a large proportion of the particulates were present at 0.5 µm followed by a large decrease in particulate number above 0.1 µm. However rather than a tailing off in particulate number, seen for flue dust, a slight increase in number concentration was seen at 0.3 µm to 0.5 µm followed by a tailing off.

Figure 4-13: Number distributions for sinter dust
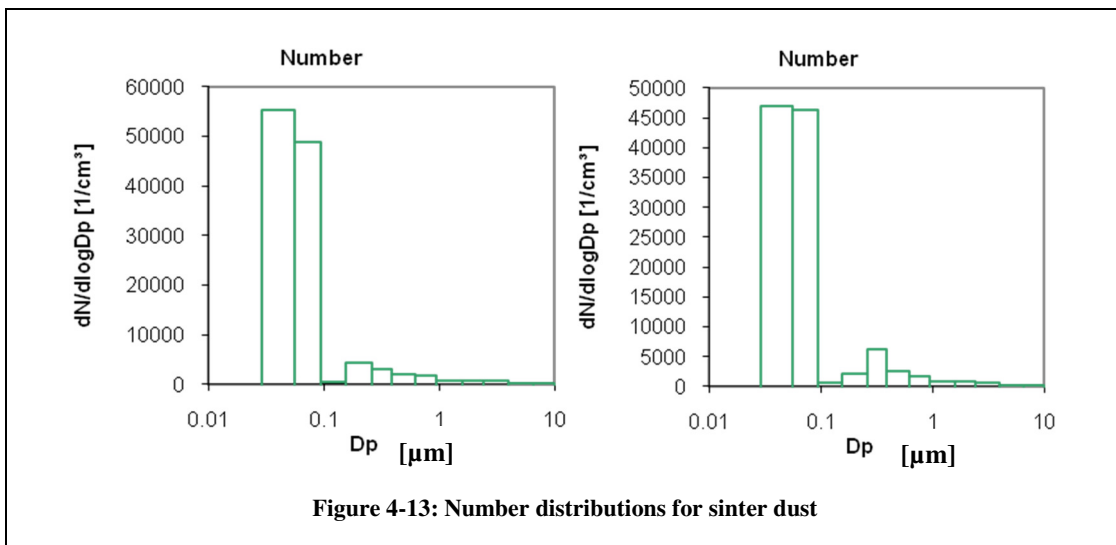
Both mass distributions show similarities with the flue dust mass distribution. As with the ore F and flue dust distributions the largest proportion of particulates was present on the higher ELPI stages, with diameters of 8.12 µm

Figure 4-14: Mass distributions for sinter dust
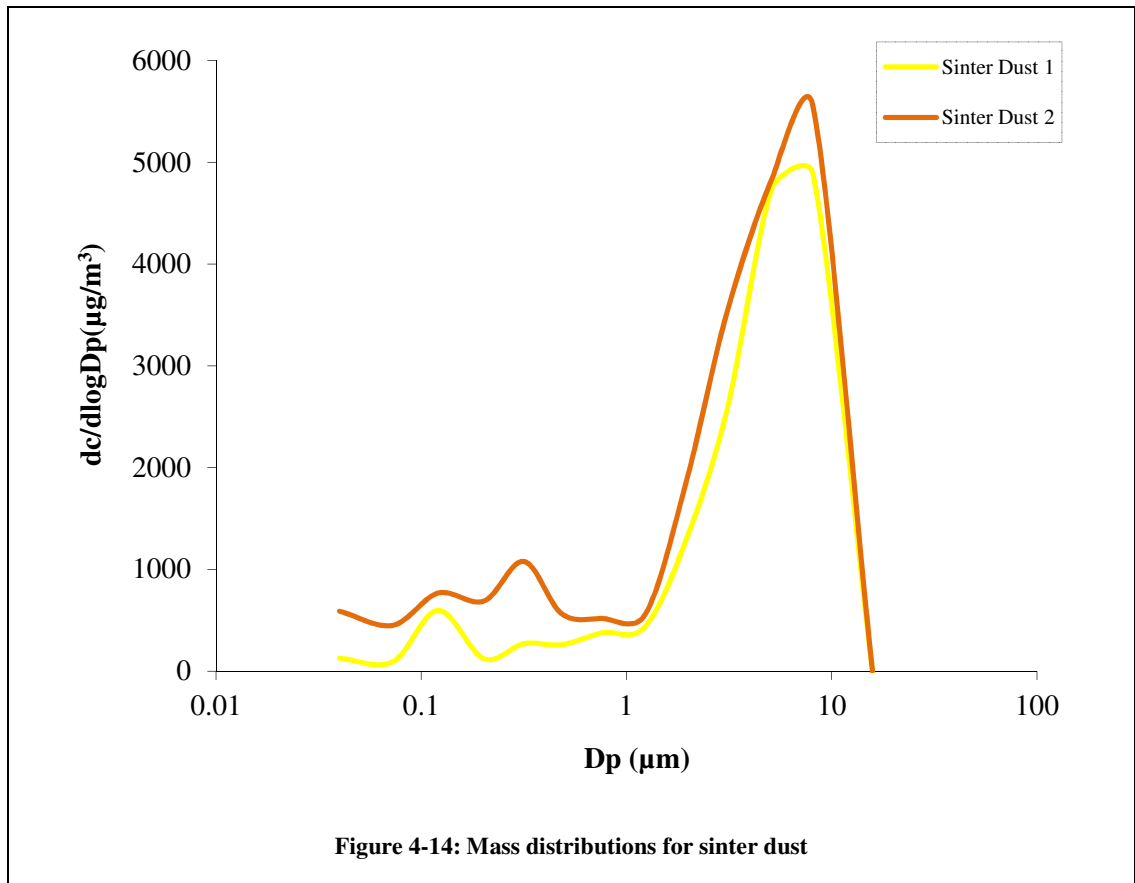
Apart from ore D, the other three materials showed some similarities in the number and masses of particulates present within the material characterised. There were also some differences, especially in the concentrations of particulates between 0.1 µm and 1 µm, which allowed comparisons to be made. These differences could also help when extracting fingerprints from mixed profiles in future studies. The results for each of the four materials are summarised in Table 4-9.

Material	Size of largest number concentration	Size of largest mass concentration
Ore D	0.05 µm	0.4 µm
Ore F	0.05 µm	8.12 µm
Flue dust	0.05 µm	8.12 µm
Sinter dust	0.05 µm	8.12 µm

Table 4-9: Summary of the physical characterisation of the four materials

4.3.3 Replicate Characterisation of Sinter Dust

Three replicate analyses were carried out to understand if, with increased agitation, more particulates could become airborne and whether their physical characteristics would change. The number distributions obtained from the three replicate analyses are detailed in Figure 4-15.

The number distribution from the first replicate profile was similar to that obtained previously and discussed in Section 4.3.2. The number distribution from the second replicate showed the presence of particulates at similar sizes and in similar proportions to the first replicate, however there was a reduction in the number of particulates. The third number distribution again indicated a reduction in particulate number but also showed a change in the size of particulates characterised. The first peak, at 0.05 µm, was a lot smaller that the second peak and there was also a peak visible at 0.1 µm which was not present previously. The peak at 0.1 µm may have only been present due to the large number of particulates in the first two replicates drowning out this peak and it could, therefore, only be seen once the number of particulates decreased. The general decrease in particulate number was expected because as each replicate was completed a smaller number of particulates would then remain in the drum for the next replicate. This illustrated that further agitation would allow particulates to become airborne. A summary of the experiment is detailed in Table 4-10.

Figure 4-15: Number distributions for sinter dust replicates
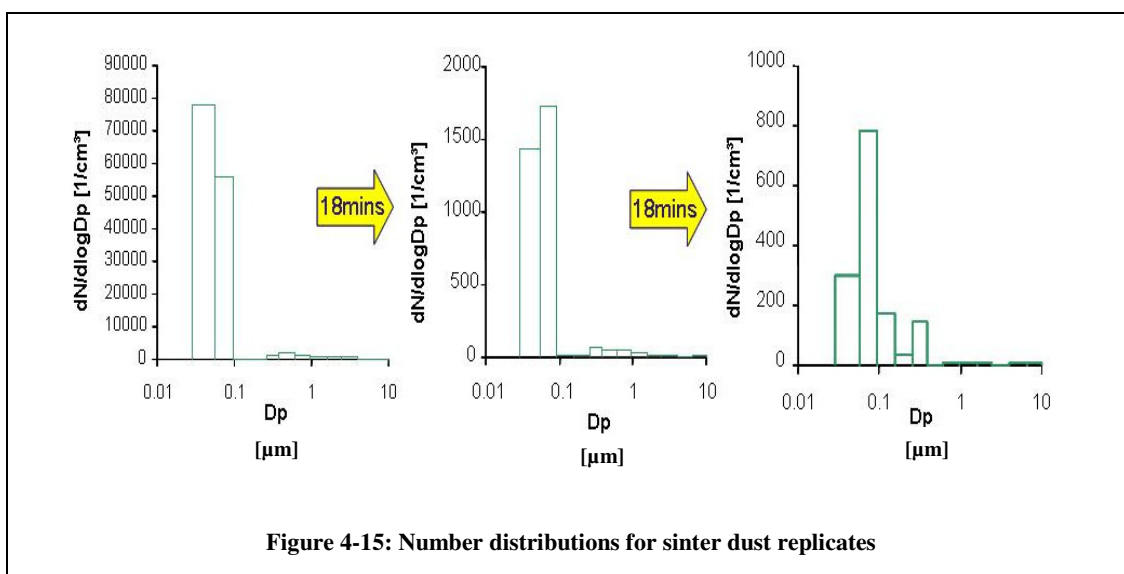
Material	Size of largest concentration
Sinter Dust Replicate One	0.05 µm
Sinter Dust Replicate Two	0.08 µm
Sinter Dust Replicate Three	0.08 µm

Table 4-10: Summary of the physical characterisation of the replicate sinter dust experiments

4.3.4 Multielemental Analysis of ELPI Substrates

Following the gravimetric analysis of the ELPI substrates, the substrates were digested and analysed, using ICP-MS, alongside a quality control solution and a standard reference material. Seven elements were chosen for analysis, copper, iron, lead, magnesium, manganese, vanadium and zinc. These were chosen since it was known that they were mostly known to be present within the materials and they were also present within the SRM.

The QC solution (20 µg/L) was analysed following the measurement of every six solutions, to check on the reliability of the calibration and for instrumental drift. The precision of the measurements could be determined by examining the RSD values. All the values were below five percent, indicating excellent precision over the ten replicates. The results are presented in Table 4-11.

Element	Reference (µg/L)	QC Results (µg/L)	RSD (%)
Cu 63	20	19 ± 1.01	5.23
Fe 56	20	18 ± 0.25	1.32
Mg 24	20	19 ± 0.57	2.96
Mn 55	20	19 ± 0.39	2.04
Pb 208	20	17 ± 0.84	4.76
V 51	20	19 ± 0.32	1.66
Zn 66	20	21 ± 0.81	3.80

Table 4-11: QC Results (n=10)

Digestion and analysis of five replicates of SRM 1648a was completed to establish the reliability of the digestion and the overall accuracy of the method. Results are listed in Table 4-12. All of the SRM recoveries were greater than 90 percent indicating a reliable digestion and accuracy. The RSD values were generally below ten percent apart from one, copper at 11.7 percent, which was considered acceptable. All but two of the elemental concentrations were within the limits specified by the SRM certificate. The exceptions were lead and zinc where values were both above the certified allowable limit. These biases were most likely due to contamination, possibly from the digestion vessel.

Element	Certified Value (µg/g)	Obtained Value (µg/g)	% Recovery	RSD (%)
Cu 63	610 ± 70	643 ±75	105	11.7
Fe 56	39200 ± 2100	40187 ± 3616	103	9.00
Mg 24	8130 ± 120	7646 ± 694	94	9.08
Mn 55	790 ± 44	786 ± 50	99	6.32
Pb 208	6550 ± 330	7408 ± 290	113	3.92
V 51	127 ± 11	115 ± 10	90	8.68
Zn 66	4800 ± 270	5410 ± 172	113	3.18

Table 4-12: SRM Results (n=5)

The limit of detection is defined as "the concentration, derived from the smallest measure, which can be detected with reasonable certainty for a given analytical procedure."[26] One percent nitric acid was analysed ten times and the results used to determine the detection limits through 3σ, Table 4-13. In general, the limits of detection were below 0.9 ng/g for all elements, expect iron and magnesium, where detection limits were 3.27 ng/g and 1.39 ng/g, respectively. These increased limits did not affect any of the iron results, however, four of the substrates for ore F, produced elemental concentrations below the limit of detection for magnesium. These four substrates were located on stages nine to twelve of the ELPI where fewer particulates were expected to collect. It is, therefore, understandable that these concentrations were below the limits, especially when a number of other elements produced concentrations below the limits of detection on these four substrates. In general a proportion of elemental concentrations were below the limits of detection, typically lead, vanadium and zinc. Some of these were expected

due to their elemental concentration within the original solid material, determined in Chapter Two and detailed in Table 4-3. Within the original material these elements reported the smallest concentrations out of all the elemental concentrations which were determined. The limits of detection were compared with those obtained by Jackson, in a similar study, completed in 2009.[27] All limits obtained here were smaller than those obtained by Jackson. This was because this work involved the use of a collision cell to remove interferences, whereas Jacksons work did not. The lower detection limits also indicated that there was no contamination present. One option to allow the determination of all elemental concentrations with this type of material would be to load the substrates more heavily with particulates. To do this either more of the material of interest could be placed within the rotating drum or sampling could be completed for longer, allowing more time for the particulates to become airborne within the rotating drum and be collected onto the substrates within the ELPI.

All of the blank substrates which were analysed reported concentrations which were below the limits of detection. This indicated that only trace concentrations were present within the substrates and they would therefore not affect the concentrations of the elements within the particulates.

Element	1	2	3	4	5	6	7	8	9	10	Mean	Standard deviation	LOD	Jackson *et al.* LOD[27]
Cu 63	0.218	0.063	0.065	0.137	0.031	0.097	0.117	0.008	0.051	0.088	0.088	0.060	**0.181**	1.88
Fe 56	0.251	0.367	3.81	0.267	0.436	0.565	1.05	0.361	0.614	0.231	0.796	1.08	**3.27**	17.8
Mg 24	0.472	0.446	0.352	0.466	0.205	0.491	0.061	0.043	2.47	0.074	0.508	0.713	**2.14**	3.00
Mn 55	0.167	0.075	0.059	0.147	0.041	0.060	0.098	0.031	0.034	0.133	0.085	0.049	**0.148**	0.23
Pb 208	0.074	0.058	0.016	0.034	0.014	0.008	0.008	0.020	0.046	0.007	0.029	0.023	**0.071**	0.93
V 51	0.069	0.025	0.011	0.047	0.011	0.007	0.019	0.001	0.007	0.061	0.026	0.024	**0.073**	0.06
Zn 66	0.302	1.05	0.406	0.239	1.02	0.324	0.350	0.369	0.438	0.357	0.487	0.297	**0.892**	19.2

Table 4-13: Analytical values for nitric acid and limits of detection (µg/L)

Multielement analysis of the substrates obtained during the RDS-ELPI trial has been successfully completed. Four sets of substrates have been characterised, one set from each of the four materials, ore D, ore F, flue dust and sinter dust. When chemically characterised using ICP-MS all four of the materials indicated very high concentrations of iron and high concentrations of magnesium and manganese. All other elements within the two iron ores gave concentrations below 80 µg/g with both dusts reporting concentrations generally below 20 µg/g, apart from zinc.

A number of different steps were completed to determine the elemental concentrations in both µg/L and µg/g. The results provided by the ICP were in µg/L. To obtain the results listed in this chapter the averaged results from the digestion blanks were taken away from the ICP results to account for any contamination with the digestion vessels. These results are listed in Tables 4-16, 4-18, 4-20 and 4-22. To change these results into µg/g, as listed in Tables 4-17, 4-19, 4-21 and 4-23, the weight of the substrate and the mass of particulates collected upon them were taken into consideration.

Only one substrate digestion and analysis was completed per material, and therefore, it was not possible to comment critically on method repeatability for these materials. Comparisons with other studies are also not easy, as those which used similar methods, reported experimental data for emissions associated with roadways.[23, 28] Mass balance calculations have been completed to allow comparisons between the masses of particulates collected on the substrates for each material (gravimetric analysis) and the masses of elements determined for on each substrate. The element masses, determined using the calculation in Table 4-14, were all smaller than the masses of particulates collected upon the twelve substrates (Table 4-15). Elemental masses for ore F, flue dust and sinter dust were all of the same order of magnitude, with ore D reporting a mass one order of magnitude lower. However, the mass of particulates collected for ore D was also one order of magnitude lower, therefore, this was to be expected. Results from the ICP-MS analysis of the four sets of ELPI substrates are now discussed separately.

Ore D, stage one	
Cu 63 (µg/g)	-
Fe 56 (µg/g)	132
Mg 24 (µg/g)	10.7
Mn 55 (µg/g)	3.60
Pb 208 (µg/g)	-
V 51 (µg/g)	0.630
Zn 66 (µg/g)	10.0
Sum of elemental concentrations for substrate one = Total elemental concentration (µg/g)	157
Mass of particulates on substrate one, from gravimetric analysis (g)	5×10^{-6}
Total elemental concentration x particulate mass = Total elemental mass, converted in ng	**0.785 ng**

This calculation was completed for all twelve substrates and the total elemental concentrations from each substrate were added together to provide the elemental masses for each material.

Table 4-14: Example elemental mass calculation

Material	Gravimetric Mass	Elemental Mass
Ore D	85 µg	70.1 ng
Ore F	610 µg	4243 ng
Flue Dust	904 µg	1819 ng
Sinter Dust	436 µg	7688 ng

Table 4-15: Gravimetric and elemental mass for all four materials

Ore D

Elemental results for ore D are tabulated in Tables 4-16 and 4-17. Results for each element will be discussed separately and are graphed in Figures 4-16 and 4-17. The overall total mass of all the analysed elements collected upon the twelve substrates was 70.1 ng which was three orders of magnitude smaller than the mass of particulates collected on the substrates, 85 µg. This indicated that although a range of elements was analysed, some with high concentrations, for example iron, there was a large proportion of elements which were not analysed which could

have contributed to the overall elemental mass. It also indicated that the particulates contained upon the substrates may not have been fully digested and were therefore not analysed by the ICP. Replicate digestions and analyses of other substrates could help to clarify this.

Elemental results for copper were generally all below 4.19 µg/g, which was seen on stage twelve. The lowest concentration was given on stage eleven, 1.18 µg/g. Stages one to three and five gave concentrations below the limit of detection which was 0.181 µg/L.

Iron was the most concentrated element with all substrates reporting concentrations above 132 µg/g (Figure 4-16). The least concentrated substrate was found on stage one, followed by a general increase in iron concentration up to stage six, where the highest concentration of iron was found, 1353 µg/g. A general decrease in concentration was then seen down to stage ten with a levelling off in concentration, at 300 µg/g to 400 µg/g for stages eleven and twelve. The high concentration of iron on stage four corresponded with the mass distributions obtained for ore D, Figure 4-8, as did the slight increase in concentration from stage eleven to twelve.

Figure 4-16: Iron distribution for ore D
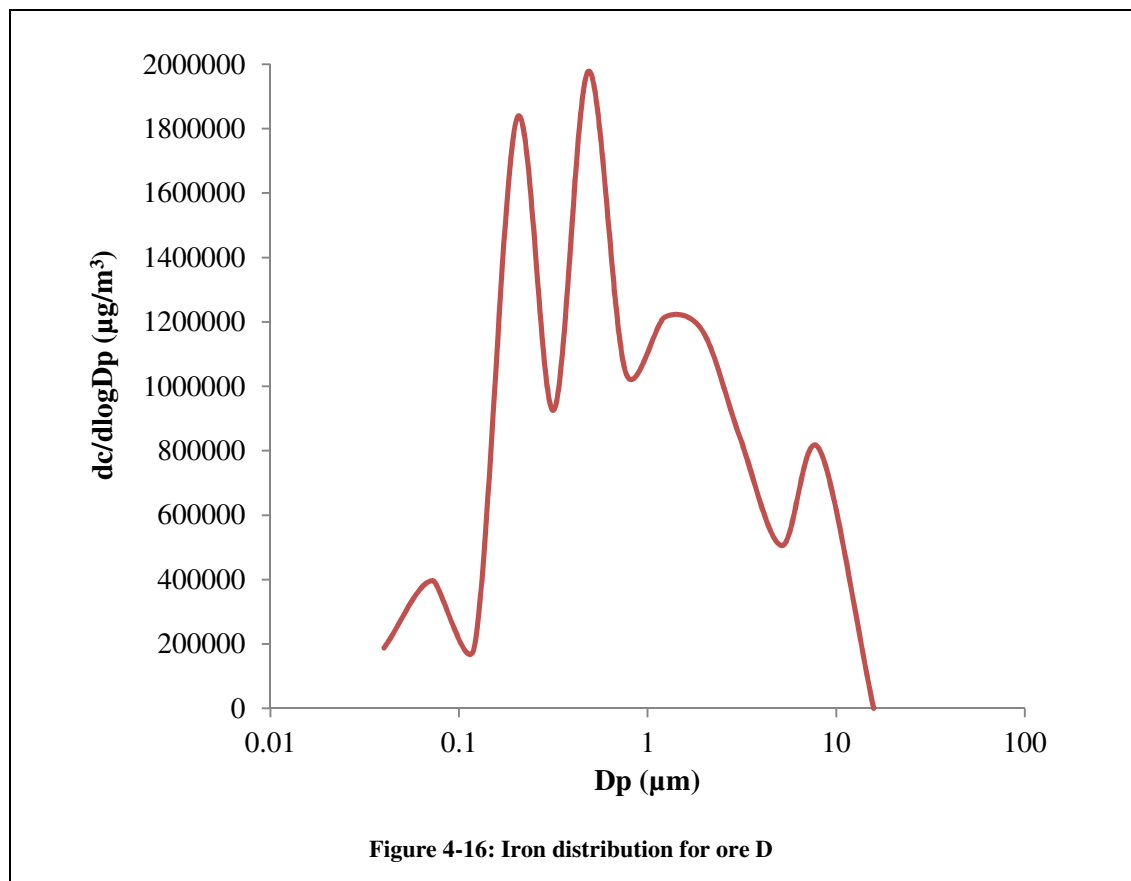
Element	1	2	3	4	5	6	7	8	9	10	11	12
Cu 63 (µg/L)	<0.181	<0.181	<0.181	0.609	<0.181	0.324	0.352	0.437	0.312	0.239	0.233	0.819
Fe 56 (µg/L)	27.0	55.4	24.0	283	97.9	237	133	183	125	108	64.4	77.2
Mg 24 (µg/L)	2.20	3.91	1.84	2.19	2.80	3.48	<2.14	7.28	3.16	4.22	3.17	3.59
Mn 55 (µg/L)	0.739	0.936	0.892	3.15	4.29	16.5	6.30	7.41	4.91	3.53	1.83	1.27
Pb 208 (µg/L)	<0.071	<0.071	<0.071	<0.071	<0.071	<0.071	<0.071	<0.071	<0.071	<0.071	<0.071	<0.071
V 51 (µg/L)	0.128	0.316	0.314	0.696	<0.073	0.357	<0.073	0.090	0.231	0.257	0.227	0.189
Zn 66 (µg/L)	2.05	<0.891	<0.891	<0.891	1.18	12.6	<0.891	4.40	1.95	<0.891	<0.891	1.17

Table 4-16: Elemental analysis of substrates for ore D (µg/L)

Element	1	2	3	4	5	6	7	8	9	10	11	12
Cu 63 (µg/g)	-	-	-	2.87	-	1.85	1.74	2.16	1.67	1.31	1.18	4.19
Fe 56 (µg/g)	132	261	134	1335	508	1353	655	906	668	595	326	395
Mg 24 (µg/g)	10.7	18.4	10.3	10.3	14.5	19.8	-	36.0	16.9	23.2	16.1	18.4
Mn 55 (µg/g)	3.60	4.40	4.99	14.9	22.2	94.2	31.1	36.7	26.2	19.4	9.25	6.47
Pb 208 (µg/g)	-	-	-	-	-	-	-	-	-	-	-	-
V 51 (µg/g)	0.630	1.48	1.75	3.28	-	2.04	-	0.450	1.24	1.42	1.15	0.970
Zn 66 (µg/g)	10.0	-	-	-	6.10	71.8	-	21.8	10.4	-	-	5.96
Sum of elemental concentrations (µg/g)	157	285	151	1366	550	1543	688	1004	725	640	354	544
Mass of particulates on substrate (g)	5×10^{-6}	6×10^{-6}	1×10^{-6}	3×10^{-6}	5×10^{-6}	2×10^{-5}	1×10^{-5}	1×10^{-5}	8×10^{-6}	8×10^{-6}	5×10^{-6}	4×10^{-6}
Total elemental concentration x particulate mass = Total elemental mass, converted into ng	0.785	1.71	0.151	4.10	2.75	26.2	6.88	13.0	5.80	5.12	1.77	1.72

Total concentration of all analysed elements on the twelve filters, 7894 µg/g

Total elemental masses added together to give the total mass of all analysed elements on the twelve filters, **70.1 ng**

Table 4-17: Elemental and fractionation results for substrates for ore D

The magnesium concentration was at a maximum on stage eight, 36.0 µg/g, and although it was smaller than the iron concentration it showed that a large proportion of magnesium was present within the particulates of this size. The lowest concentrations were seen on stages three and four, both reporting the same concentration of 10.3 µg/g. Stage seven gave a concentration below the limit of detection, 2.14 µg/L.

In general manganese concentrations were below 40 µg/g, apart from the highest concentration which was seen on stage six, 94.2 µg/g. The lowest concentration was given on stage one, 3.60 µg/g. The manganese concentrations corresponded well with the mass distribution as well as the copper concentrations, as seen in Figure 4-17.

For lead, no stages reported concentrations above the limit of detection, 0.071 µg/L, indicating that only trace amounts of lead were present within the particulates.

A mix of vanadium concentrations were seen, with two stages, five and seven, reporting concentrations below the detection limit, 0.073 µg/L, and most stages reporting concentrations below 2 µg/g. However substrates from stages four and six reported concentrations of 3.28 µg/g and 2.04 µg/g, respectively, which corresponded well with the high concentration seen for copper, iron and manganese.

Six substrates reported zinc concentrations which were below the limit of detection, 0.891 µg/L, stages two to four, seven, ten and eleven. The highest zinc concentration was seen on stage six, 71.8 µg/g, which corresponded with the high concentrations seen for copper, iron, manganese and vanadium. The lowest concentration was given on stage twelve, 5.96 µg/g.

Figure 4-17: Elemental distributions for ore D
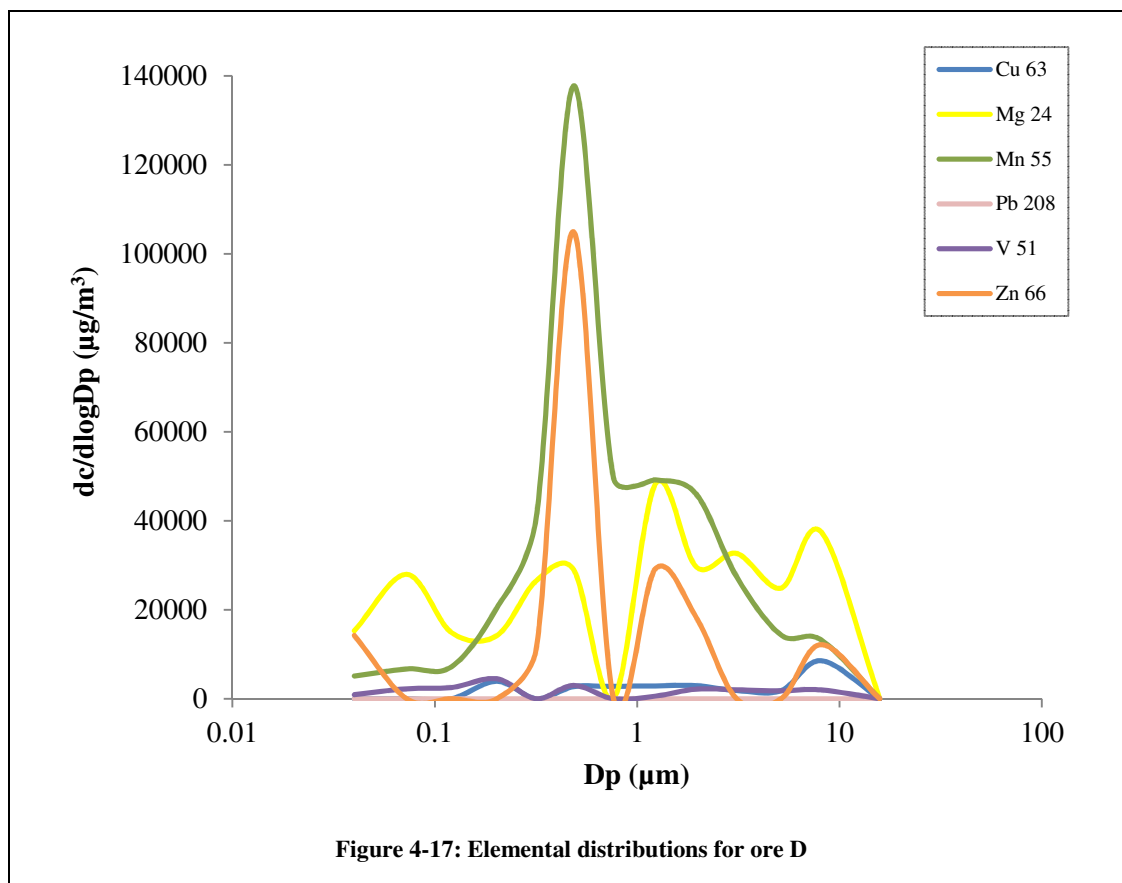
In general peaks in concentration were seen on stage six, which corresponded well with the mass distributions. Iron, cobalt, copper, magnesium and manganese also all exhibited a further peak in concentration at 8.12 µm which corresponded to a smaller peak seen in the two mass distributions. This indicated that an increase in elemental concentration did correspond to an increase in particulate mass.

Ore F

The elemental results from the analysis of the ore F substrates are listed in Tables 4-17 and 4-18. Distributions will be discussed by element. The total mass of the analysed elements collected upon the twelve substrates was 4243 ng, two orders of magnitude smaller than the mass of the particulates weighed on the substrate, 610 µg. Again further replicates digestions and analyses should be completed, especially concentrating on the analysis of a larger range of elements.

Copper showed an increase in concentration on stage ten, at 1.65 µg/g. Eight of the substrates, from stages one to three, five to seven and eleven to twelve, reported concentrations below the detection limit, 0.180 µg/L.

As expected iron was the most concentrated element, with the lowest concentration on stage two at 123 µg/g. The greatest concentration of iron was present, on stage twelve, at 11005 µg/g. This was followed by stages ten and eleven which also had increased iron concentrations of 9014 µg/g and 8963 µg/L, respectively. The elemental distribution, Figure 4-18, corresponded well with the mass distributions, Figure 4-10.

Element	1	2	3	4	5	6	7	8	9	10	11	12
Cu 63 (µg/L)	<0.181	<0.181	<0.181	0.297	<0.181	<0.181	<0.181	0.494	0.871	0.340	<0.181	<0.181
Fe 56 (µg/L)	24.9	23.1	81.1	223	274	231	390	341	469	1859	1699	1986
Mg 24 (µg/L)	<2.14	<2.14	<2.14	47.5	18.6	6.02	3.00	<2.14	<2.14	3.87	2.98	4.62
Mn 55 (µg/L)	0.999	1.36	4.14	8.91	10.83	9.45	16.8	11.8	14.9	60.5	45.6	41.5
Pb 208 (µg/L)	<0.071	<0.071	<0.071	<0.071	<0.071	<0.071	<0.071	<0.071	<0.071	0.370	0.192	0.267
V 51 (µg/L)	<0.073	<0.073	<0.073	0.511	0.088	0.167	0.146	<0.073	<0.073	0.184	0.142	0.164
Zn 66 (µg/L)	<0.891	<0.891	2.49	<0.891	3.00	7.24	1.47	<0.891	<0.891	1.29	<0.891	0.955

Table 4-17: Elemental analysis of substrates for ore F (µg/L)

Element	1	2	3	4	5	6	7	8	9	10	11	12
Cu 63 (µg/g)	-	-	-	1.67	-	-	-	0.30	0.52	1.65	-	-
Fe 56 (µg/g)	130	123	448	1252	1381	1138	1820	204	281	9014	8693	11005
Mg 24 (µg/g)	-	-	-	267	93.93	29.7	14.0	-	-	18.8	15.2	25.6
Mn 55 (µg/g)	5.21	7.26	22.9	50.1	54.6	46.6	78.5	7.10	8.92	294	233	230
Pb 208 (µg/g)	-	-	-	-	-	-	-	-	-	1.79	0.981	1.48
V 51 (µg/g)	-	-	-	2.87	0.445	0.822	0.681	-	-	0.894	0.724	0.906
Zn 66 (µg/g)	-	-	13.8	-	15.1	35.7	6.84	-	-	6.28	-	5.29
Sum of elemental concentrations (µg/g)	135	131	484	1573	1545	1251	1920	212	291	9336	8943	11268
Mass of particulates on substrate (g)	2×10^{-5}	4×10^{-6}	1×10^{-5}	1×10^{-5}	2×10^{-5}	2×10^{-5}	2×10^{-5}	4×10^{-5}	5×10^{-5}	1×10^{-4}	1×10^{-4}	2×10^{-4}
Total elemental concentration x particulate mass = Total elemental mass, converted into ng	3.11	0.522	5.81	18.9	26.3	25.0	46.1	7.62	14.2	1260	1145	1690

Total concentration of all analysed elements on the twelve filters, 37089 µg/g

Total elemental masses added together to give the total mass of all analysed elements on the twelve filters, **4243 ng**

Table 4-18: Elemental and fractionation results for substrates for ore F

Figure 4-18: Iron distribution for ore F
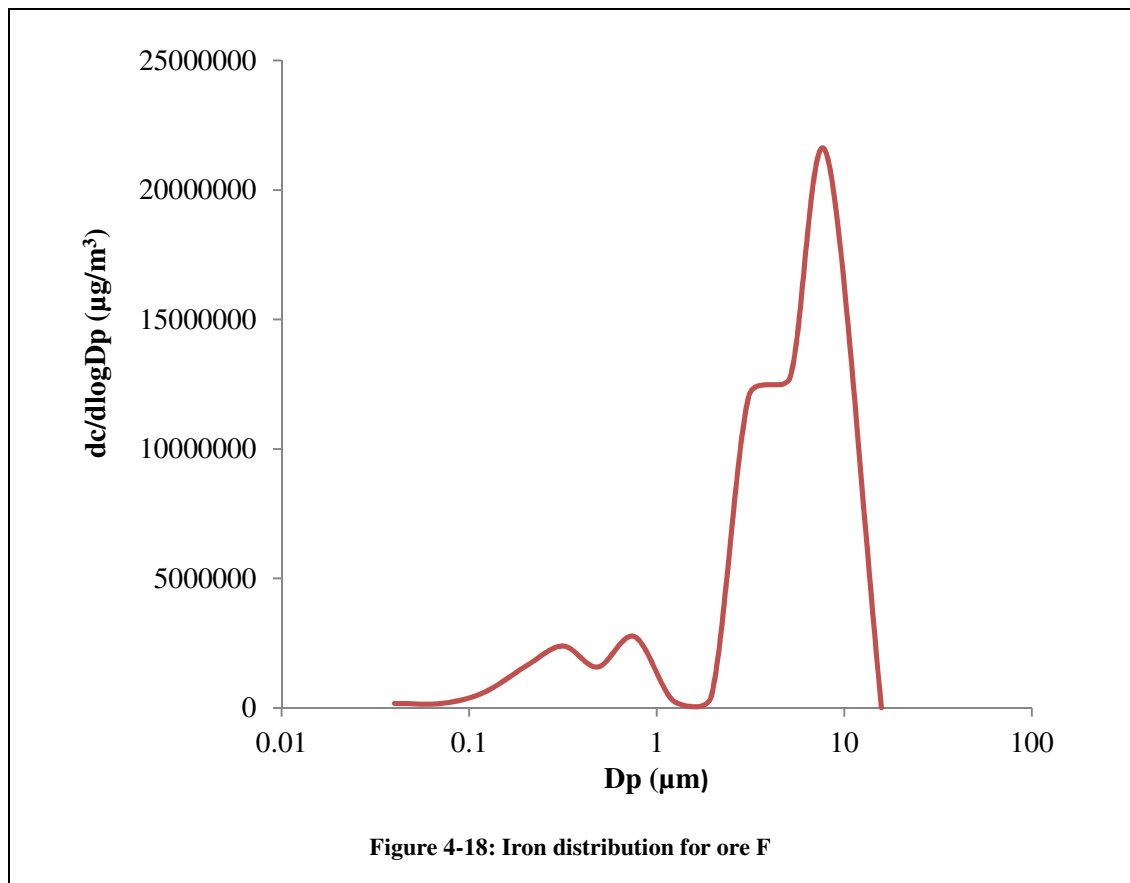
Magnesium concentrations varied, with five substrates, one to three, eight and nine reporting concentrations below the limit of detection, 2.14 µg/L. Stage four indicated the highest concentration at 267 µg/g and stage seven indicated the lowest detectable concentration, 14.0 µg/g.

Manganese concentrations showed similar trends to the iron concentrations, as shown in Figure 4-19. Stage one reported the lowest concentration, 5.12 µg/g, and substrate ten the largest concentration, 294 µg/g. Stages eleven and twelve also gave increased concentrations of 233 µg/g and 230 µg/g, respectively.

Only three stages, ten to twelve, reported concentrations of lead that were above the limit of detection, 0.071 µg/L. These concentrations varied from 0.981 µg/g to 1.79 µg/g.

Vanadium concentrations were undetectable for substrates from stages one to three and eight to nine. There was an increase in concentration for stage four as seen for manganese. The other stages all reported concentrations below 1.0 µg/g.

The results for zinc differed to what was seen for other elements. The main peak in concentration was seen on stage two, 13.8 µg/g, compared to stage four as seen previously. Stage one also reported zinc concentrations below the limit of detection, 0.891 µg/L, which corresponded well with the concentrations observed for the other elements.

Figure 4-19: Elemental distributions for ore F
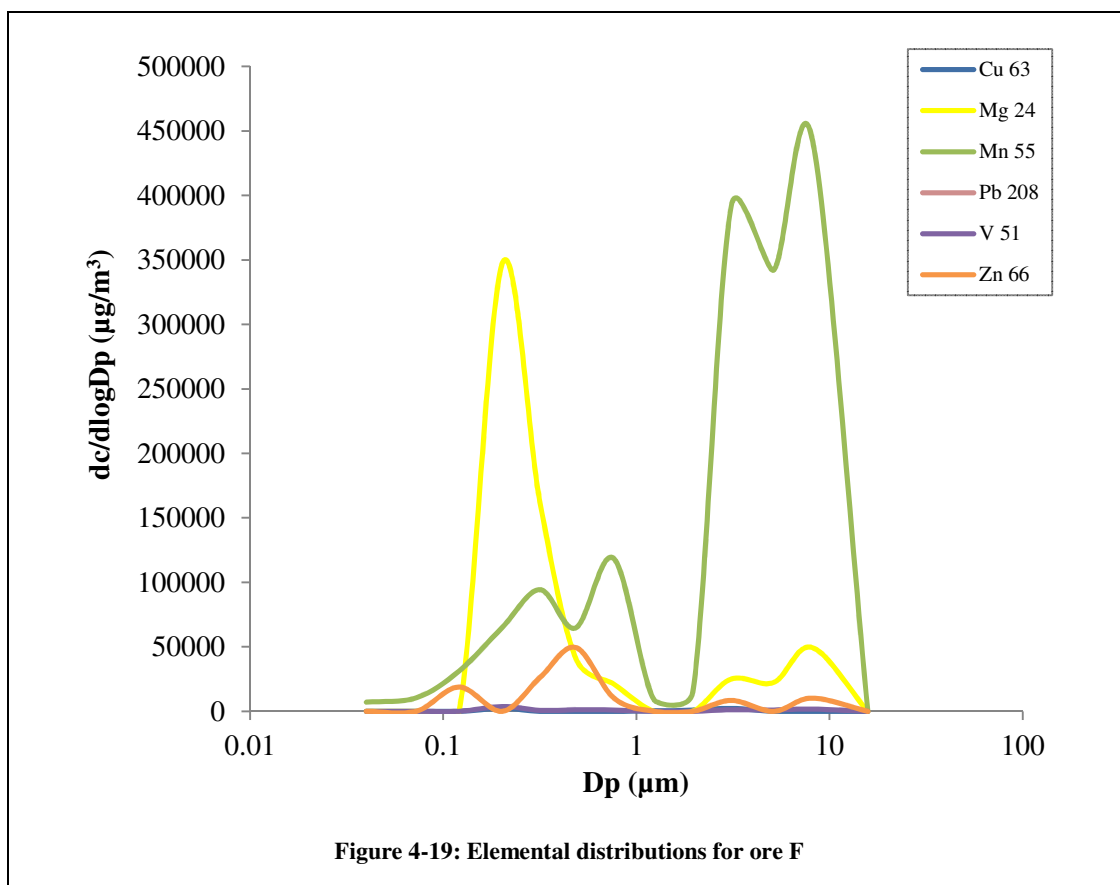
Overall the iron elemental results for ore F corresponded well with mass distributions, indicating that a large proportion of the particulates contained high concentrations of iron. Manganese also showed a peak in concentration for stages eleven and twelve like both the iron and mass distributions. Cobalt and lead were only present in trace concentrations. Zinc was the only element to display a different elemental distribution which may have been due to its trace concentration within ore F itself.

Flue Dust

Elemental results from the analysis of the flue dust substrates are tabulated in Tables 4-19 and 4-20. The overall mass of the analysed elements collected upon the twelve substrates was 7688 ng. This was the same order of magnitude as seen for ore F, 4243 ng, indicating that overall similar elemental masses were obtained for both materials. No elements indicated concentrations below their relative limits of detection, indicating generally high elemental concentrations.

Copper reported concentrations between 2.93 µg/g, stage five, and 17.7 µg/g, stage eleven as was seen for the two iron ores. This corresponded well with the mass distribution shown in Figure 4-12.

As with copper, the highest iron concentration was present on stage eleven, 12590 µg/g, again corresponding with the mass distribution. The lowest concentration was given on stage one, 478 µg/g, which is most likely due to the smaller size of the particulates. The concentrations on the other stages varied with a number of increases and decreases seen over the twelve stages, Figure 4-20.

Element	1	2	3	4	5	6	7	8	9	10	11	12
Cu 63 (µg/L)	0.644	1.67	0.712	1.05	0.623	0.956	0.770	0.823	1.85	2.73	3.45	2.16
Fe 56 (µg/L)	86.1	150	264	291	162	407	44.2	369	998	1496	2454	2031
Mg 24 (µg/L)	28.0	10.0	11.0	11.1	6.83	10.0	16.4	9.90	25.9	39.5	52.3	30.0
Mn 55 (µg/L)	1.69	3.50	6.25	7.02	3.44	7.16	0.694	8.69	23.6	34.3	50.0	33.6
Pb 208 (µg/L)	1.74	3.86	6.30	6.96	3.69	7.27	0.490	8.57	25.1	35.3	51.4	27.4
V 51 (µg/L)	0.311	0.022	0.392	0.428	0.222	0.536	0.167	0.499	1.28	1.77	2.35	1.48
Zn 66 (µg/L)	5.36	15.1	19.9	21.6	10.6	22.5	15.9	26.4	69.7	97.5	133	72.5

Table 4-19: Elemental analysis of substrates for flue dust (µg/L)

Element	1	2	3	4	5	6	7	8	9	10	11	12
Cu 63 (µg/g)	3.58	8.85	3.54	5.14	2.93	5.39	3.85	4.40	10.15	13.43	17.7	11.2
Fe 56 (µg/g)	478	797	1313	1427	764	2297	221	1971	5487	7349	12590	10497
Mg 24 (µg/g)	155	53.2	52.2	54.4	32.1	56.5	81.7	52.9	143	194	269	155
Mn 55 (µg/g)	9.40	18.6	31.1	34.4	16.2	40.4	3.47	46.4	130	168	257	174
Pb 208 (µg/g)	9.68	20.4	31.3	34.1	17.3	41.0	2.45	45.8	138	174	264	142
V 51 (µg/g)	1.73	0.119	1.95	2.10	1.04	3.02	0.835	2.67	7.01	8.70	12.1	7.63
Zn 66 (µg/g)	29.8	80.1	98.9	106	49.8	127	79.5	141	383	479	682	375
Sum of elemental concentrations (µg/g)	688	978	1532	1663	883	2571	393	2265	6298	8386	14090	11361
Mass of particulates on substrate (g)	2×10^{-6}	1×10^{-5}	3×10^{-5}	2×10^{-5}	4×10^{-5}	3×10^{-5}	4×10^{-5}	5×10^{-5}	1×10^{-4}	2×10^{-4}	2×10^{-4}	2×10^{-4}
Total elemental concentration x particulate mass = Total elemental mass, converted into ng	1.38	10.8	39.8	36.6	32.7	84.8	16.9	113	655	1375	3311	2011

Total concentration of all analysed elements on the twelve filters, 51106 µg/g

Total elemental masses added together to give the total mass of all analysed elements on the twelve filters, **7688 ng**

Table 4-20: Elemental and fractionation results for substrates for flue dust

Figure 4-20: Iron distribution for flue dust
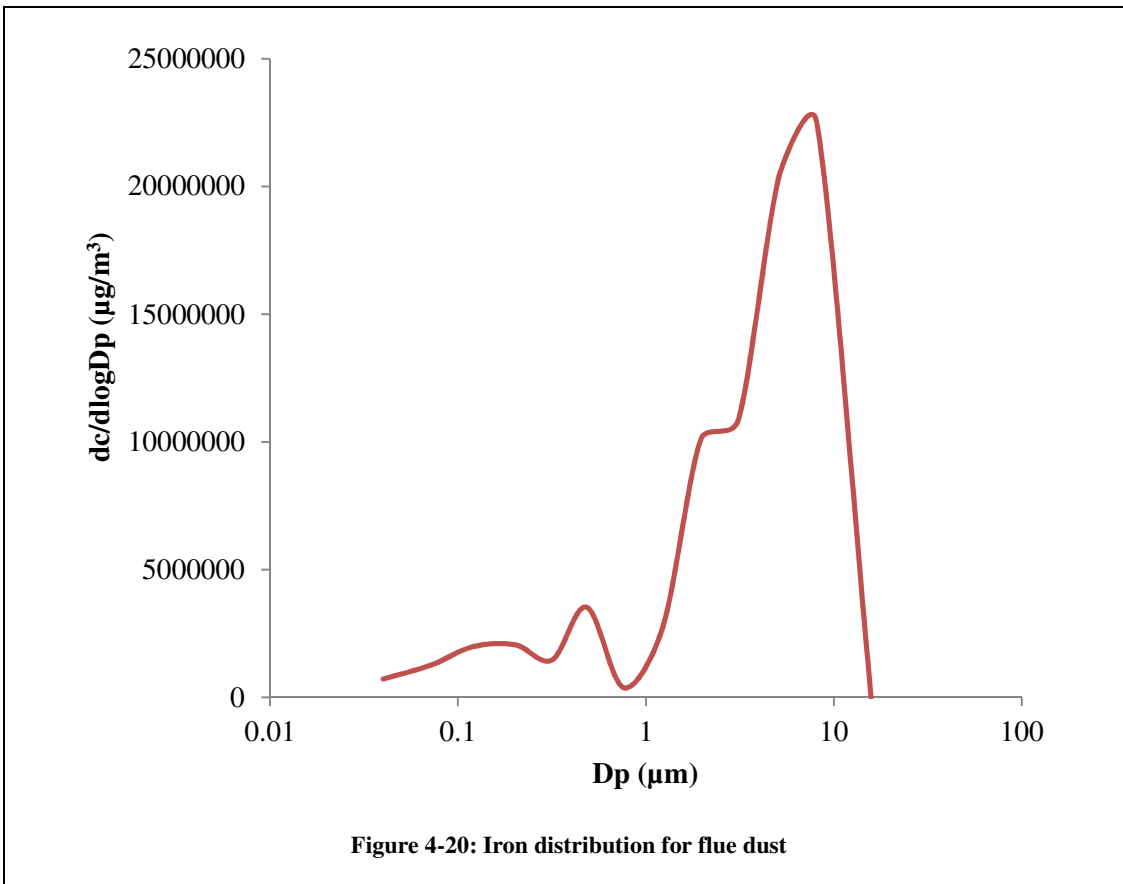
The highest magnesium concentration was given on stage eleven, 269 µg/g. Like copper the lowest concentration was on stage five, 32.1 µg/g, which indicated that these two elements were related to each other in terms of their concentration within the dust particulates. This may be due to similar concentrations within the blast furnace, where this dust was obtained from.

As with other elements, such as copper and iron, manganese indicated a high concentration for stage eleven, 257 µg/g. The lowest concentration was given on stage seven, 3.47 µg/g/

Lead concentrations followed the same pattern as the manganese concentrations, as seen in Figure 4-21, with an increased concentration on stage eleven, 264 µg/g, and the lowest concentration on stage seven, 2.45 µg/L. This can be seen in Figure 4-21.

For vanadium, generally trace concentrations were observed, with the highest occurring on stage eleven, 12.07 µg/g. All other substrates indicated concentrations below 9 µg/g with stage two giving the lowest, 0.12 µg/g.

Zinc concentrations are graphed in Figure 4-21. Concentrations were observed to be between 29.7 µg/g, stage one, and 682 µg/g, stage eleven. This corresponded well with the iron concentrations, shown in Figure 4-20, indicating that the two elements were related in their proportions within the material.

Figure 4-21: Elemental distributions for flue dust
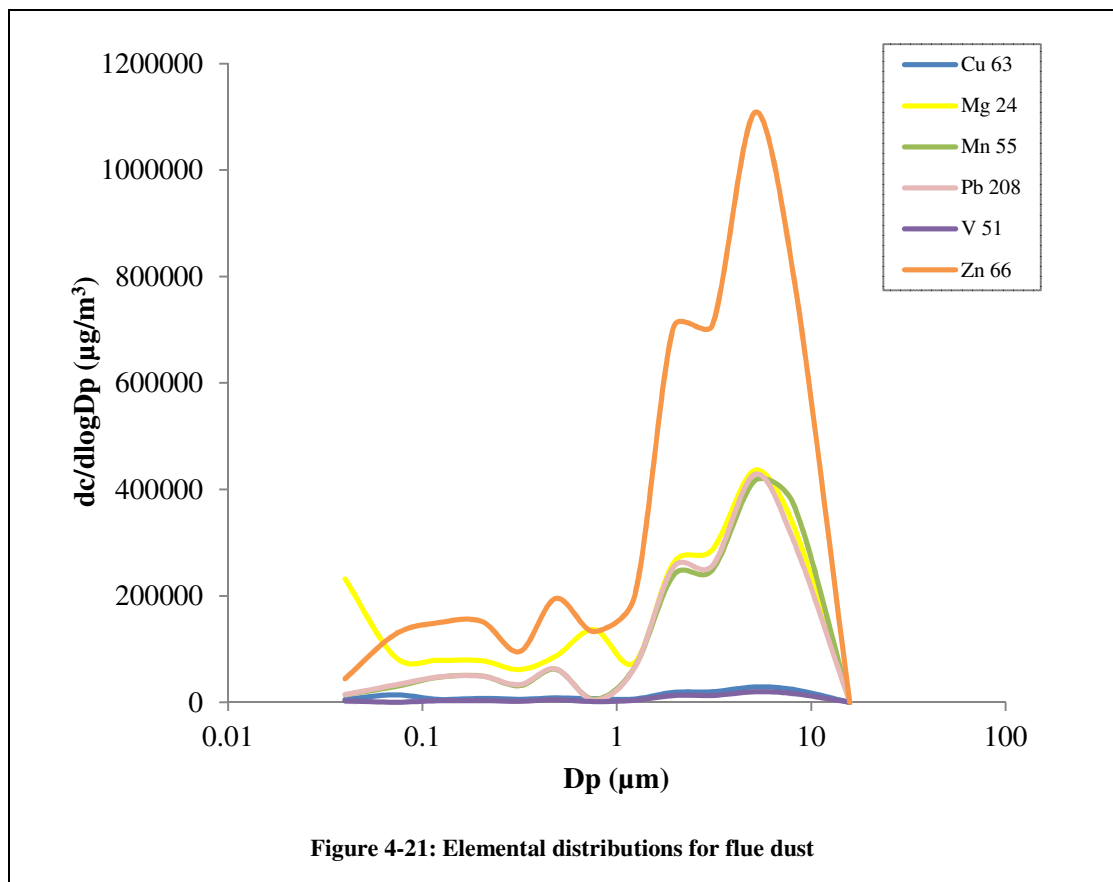
The flue dust elemental distributions, Figures 4-20 and 4-21, all showed a large peak in concentration for stage eleven, 5.14 µm, which corresponded well with the mass distributions in Figure 4-12. This indicated that the flue dust material contained large particulates which had relatively high elemental concentrations. Most elements also showed a peak in concentration at 0.49 µm, stage six, which corresponded well with the mass distribution. Iron was the most concentrated element within the material.

Sinter Dust

The elemental results for sinter dust are listed in Tables 4-21 and 4-22. The overall total concentration of all the analysed elements collected upon the twelve substrates was 1819 ng. This mass was two orders of magnitude lower than the mass of particulates collected upon the substrates, 436 µg.

Six substrates reported concentrations below the limit of detection for copper, 0.181 µg/L, with other substrates generally reporting concentrations below 2 µg/g. The highest concentration was found on stage three, 2.96 µg/g. This corresponded well with a small peak in the mass distribution, Figure 4-14, indicating that a proportion of the smaller particulates contained a high concentration of copper.

For iron, a general increase in concentration was seen from stage one, 130 µg/g, to stage eleven, 6687 µg/g, with only one slight decrease at stage six to 264 µg/g. The concentration also decreased between stages eleven and twelve, to 4803 µg/g. The peaks in the iron elemental distribution (Figure 4-22) are almost identical to the mass distributions, shown in Figure 4-14, with both distributions indicating peaks at 8.12 µm. This indicated that iron was the element with the highest concentration within the material.

Element	1	2	3	4	5	6	7	8	9	10	11	12
Cu 63 (µg/L)	0.259	0.267	0.514	0.212	<0.181	<0.181	<0.181	<0.181	<0.181	0.264	0.483	<0.181
Fe 56 (µg/L)	26.7	25.8	59.3	60.6	74.6	53.0	86.4	166	329	1041	1364	1029
Mg 24 (µg/L)	3.33	2.47	4.04	2.04	2.46	1.39	4.82	7.65	10.1	26.2	31.6	21.5
Mn 55 (µg/L)	1.09	0.449	0.940	0.925	1.27	0.683	1.09	2.09	4.12	13.2	17.5	11.7
Pb 208 (µg/L)	0.340	0.294	0.383	0.098	0.079	<0.071	<0.071	<0.071	0.157	1.65	1.82	1.52
V 51 (µg/L)	<0.073	<0.073	<0.073	<0.073	<0.073	<0.073	<0.073	<0.073	0.098	0.294	0.398	0.231
Zn 66 (µg/L)	1.693	1.16	9.10	1.07	1.02	<0.891	<0.891	0.584	1.24	6.42	5.83	4.77

Table 4-21: Elemental analysis of substrates for sinter dust (µg/L)

Element	1	2	3	4	5	6	7	8	9	10	11	12
Cu 63 (µg/g)	1.26	1.51	2.96	1.10	-	-	-	-	-	1.44	2.37	-
Fe 56 (µg/g)	130	145	342	316	353	264	428.04	891	1812	5690	6687	4803
Mg 24 (µg/g)	16.14	13.9	23.3	10.6	11.7	6.92	23.9	41.1	55.5	143	155	100
Mn 55 (µg/g)	5.29	2.53	5.42	4.82	5.99	3.40	5.38	11.21	22.7	71.9	85.8	54.3
Pb 208 (µg/g)	1.65	1.66	2.21	0.513	0.373	-	-	-	0.866	8.99	8.95	7.07
V 51 (µg/g)	-	-	-	-	-	-	-	-	0.543	1.61	1.95	1.08
Zn 66 (µg/g)	8.19	6.54	52.5	5.56	4.81	-	-	3.14	6.86	35.1	28.6	22.2
Sum of elemental concentrations (µg/g)	162	172	428	339	375	274	457	946	1899	5953	6970	4988
Mass of particulates on substrate (g)	1×10^{-5}	1×10^{-5}	2×10^{-5}	2×10^{-5}	2×10^{-5}	1×10^{-5}	1×10^{-5}	1×10^{-5}	4×10^{-5}	9×10^{-5}	2×10^{-4}	9×10^{-5}
Total elemental concentration x particulate mass = Total elemental mass, converted into ng	2.27	1.72	7.70	5.76	7.51	3.57	5.03	13.25	68.35	506	739	459

Total concentration of all analysed elements on the twelve filters, 22962 µg/g

Total elemental masses added together to give the total mass of all analysed elements on the twelve filters, **1819 ng**

Table 4-22: Elemental and fractionation results for substrates for sinter dust

Figure 4-22: Iron distribution for sinter dust
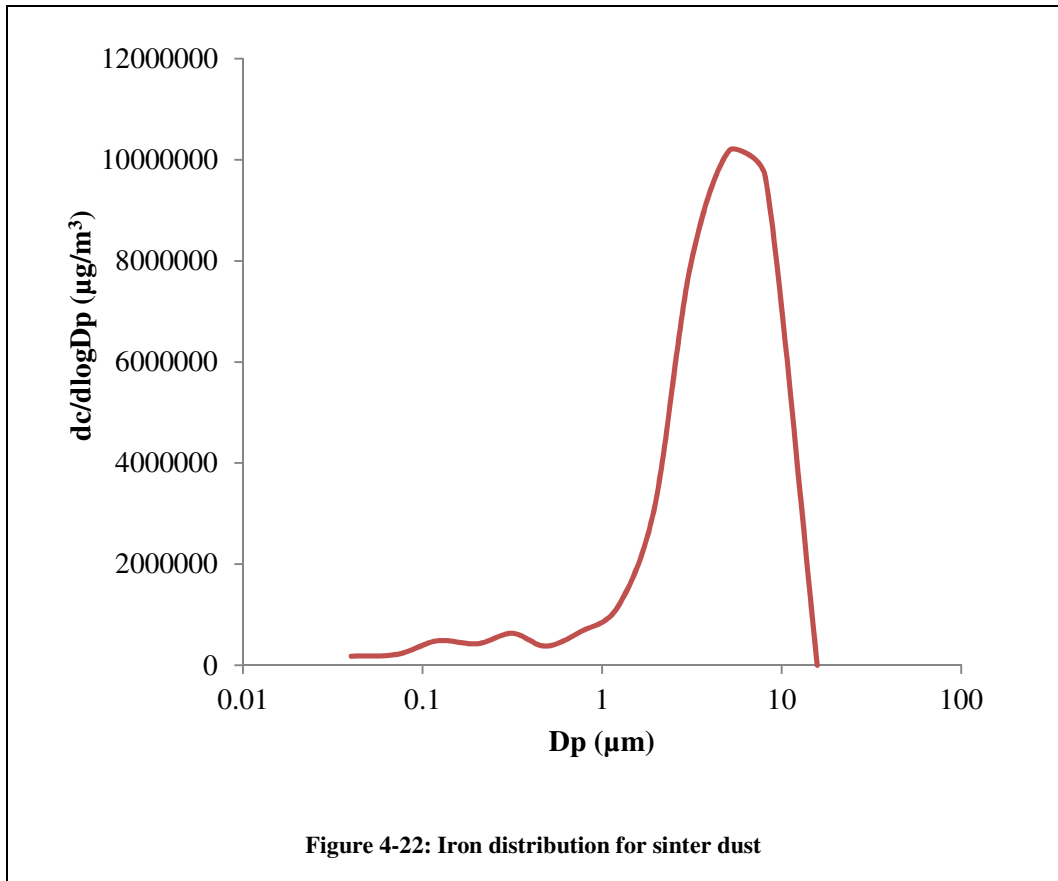
Magnesium also reported its highest concentration on stage eleven, 155 µg/g. The lowest concentration was seen on stage six, 6.92 µg/g, the same stage where a dip in the iron concentration was seen. Stages one to five showed steady concentrations of between 10 µg/g and 23 µg/g.

Manganese reported much lower concentrations than magnesium, however, by examining Figure 4-23, it can be seen that they both follow a similar pattern. The highest concentration was seen on stage eleven, 85.8 µg/g, with the lowest on stage two, 2.53 µg/g. A dip in concentration was again seen for stage six to 3.40 µg/g.

Both magnesium and manganese, Figure 4-23, showed very similar distributions to iron. This indicated that these two elements contributed greatly to the overall chemical composition of the sinter dust particulates.

Figure 4-23: Elemental distributions for sinter dust
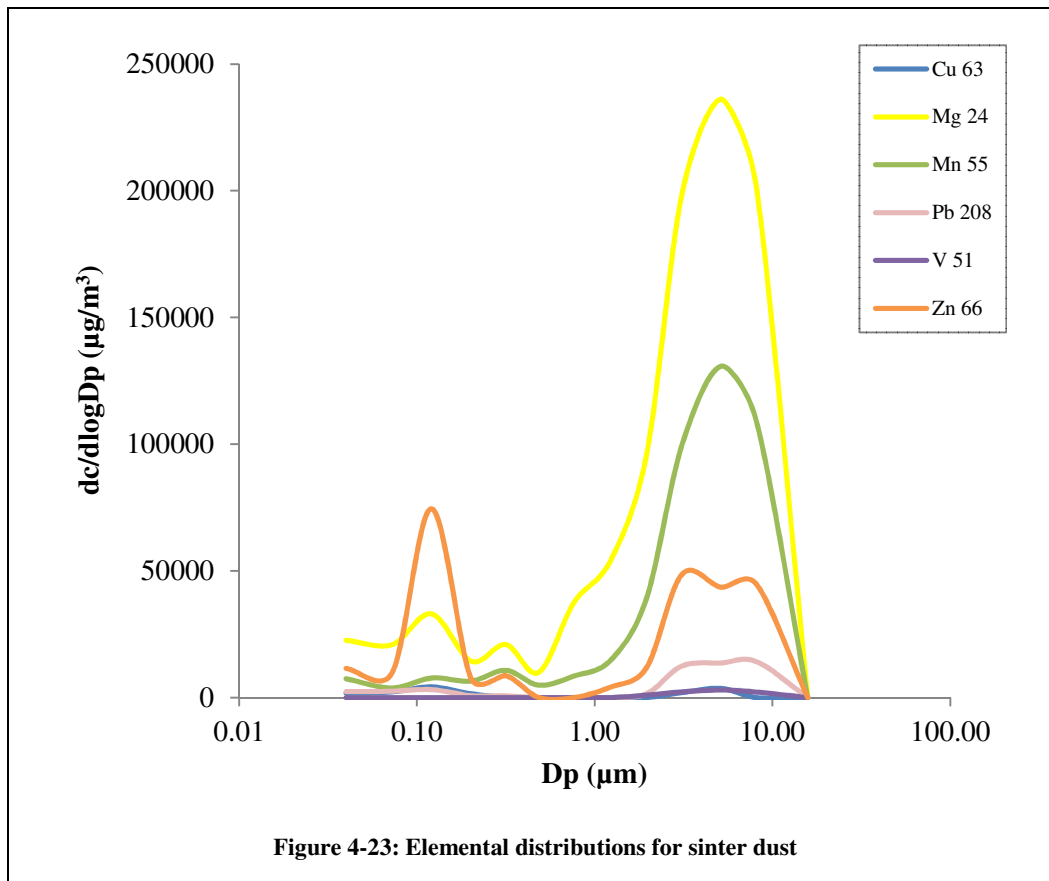
Stages one to five reported lead concentrations between 0.37 µg/g and 2.21 µg/g. Stages six to eight reported concentrations below the limit of detection, 0.071 µg/L. Stage nine reported a concentration of 0.89 µg/g, followed by stages ten to twelve which all reported concentrations of approximately 7 µg/g to 9 µg/g. This agreed with the results obtained for a number of other elements where larger concentrations were seen on higher stages.

Vanadium concentrations were below the limit of detection, 0.073 µg/L for stages one to eight. Trace concentrations of vanadium were then seen on stages nine to twelve, between 0.54 µg/g, stage nine, to 1.95 µg/g, stage eleven.

Zinc showed a large increase in concentration between stage two (6.54 µg/g) and stage three (52.47 µg/g). The substrates from the other lower stages all generally reported concentrations of between 4 µg/g and 8 µg/g, with stage six and seven reporting

concentrations below the limit of detection, 0.891 µg/L. Stages ten to twelve again reported an increase in concentration, up to approximately 30 µg/g.

For the sinter dust substrates a number of peaks in concentration, especially for magnesium, manganese and iron, mirror those seen in Figure 4-14, the sinter dust mass distributions. This indicates that they are key components of the material and also shows that the results obtained here are trustworthy.

Overall the chemical and elemental analysis of the ELPI substrates was successful. High concentrations of iron were found on the majority of the substrates which was to be expected. In general the iron concentrations followed the same patterns as the number and mass distributions, with increased concentrations corresponding to increases in the collected masses on the substrates. This was also seen for other elements such as magnesium and manganese. Although some results were reported to be below the limits of detection by refining the method, it should be possible to determine concentrations for all elements. Further replicate analyses are also needed to confirm the mass balance of elements determined on the twelve substrates.

4.4 Main Findings

The successful coupling of a rotating drum and an ELPI has been completed followed by the digestion and elemental analysis of the ELPI substrates. Four materials have been characterised independently to obtain gravimetric data as well as number, mass and elemental size distributions.

The use of titanium dioxide as a control material allowed the equipment set up to be tested. Four different experiments, using varying weights of material, all provided similar number-size distributions which also showed some similarities with literature values. This initial study demonstrated that the RDS-ELPI method was capable of providing reliable results.

The physical characterisation of the four materials, ore D, ore F, flue dust and sinter dust, was performed in duplicate with many similarities seen between the replicates. This indicated good reproducibility could be obtained when using the RDS-ELPI method. In future more replicates could be completed to confirm the results obtained in this chapter.

All four materials showed similarities in their number distributions, with high number concentrations seen at 0.05 µm for all of the materials. However some differences could be seen in their mass distributions, especially for ore D. Ore D indicated high masses of particulates at 0.4 µm, with smaller peaks at 0.07 µm and 8.12 µm, whereas the other four materials had high mass concentrations at 8.12 µm, with smaller peaks at 0.32 µm. This difference would help when extracting characteristic fingerprints from mixed profiles, since the ore D profile could be easily located.

The replicate analyses of the sinter dust material illustrated a general decrease in the number of particulates that became airborne as a result of extending the period of

agitation. It also indicated that further agitation of a material would allow particulates to become airborne when on site. These particulates may not be present in high concentrations, but may still contribute to an industrial sites emission data.

There were clear differences in the particulate diameters obtained in this chapter and those obtained when using the RDS-Aspect method. This was because the ELPI is more effective at analysing particulates below 0.5 µm in diameter, whereas the Aspect has better capabilities for particulates larger than 0.5 µm. Therefore the particulate diameters from the two different methods cannot truly be compared, but do allow an overall picture of each material to be obtained.

The ICP-MS analysis of the ELPI substrates has allowed the elemental concentrations of particulates present on the substrates to be determined. Analysis of a 20 ng/L QC and a standard reference material, NIST 1648a, was also undertaken and in general good accuracy and precision were reported for these reference samples.

The obtained limits of detection were lower than those reported in other literature.[27] A number of elements, generally lead, vanadium and zinc, reported concentrations below their respective limits of detection, therefore, to allow the determination of these elements in future work the filters could be loaded with more particulate material. The volume of high purity water used (30 mL) for dilution prior to analysis could also be reduced.

The determination of elemental concentrations was successful with some distributions, especially for iron, corresponding well with the number and mass size distributions. The elemental mass balances were all smaller than the masses of particulates collected upon the substrates. Therefore further studies are required, which include the analysis of a wider range of elements.

As well as allowing proof of concept this study has allowed particulate chemical information to be obtained and a fuller understanding of the four materials has been acquired. To allow further comparisons to be made and more conclusions to be drawn from these results replicate digestions and analyses should be completed.

Future work should also involve the collection of a reference material onto substrates using the RDS-ELPI setup. This would allow the reference material to have been through all of the same steps as the materials in question rather than just the digestion and analysis procedure. An alternative option to solution ICP-MS would be LA-ICP-MS. This would reduce the analysis time since pre-digestion would not be required and substrates could be analysed directly.

The next two chapters will discuss the consecutive coupling of a laser ablation unit to the Aspect morphology analyser and the ELPI to allow the physical characterisation of a laser generated aerosol. By applying the same method used in this chapter, substrates from the ELPI will also be chemically characterised.

Development and validation of a novel experimental system for physical characterisation of particulate matter

M. Barker*[1], C.W. McLeod[1], D. Ciaparra[2], K. Jackson[2] & D.R. Anderson[2]
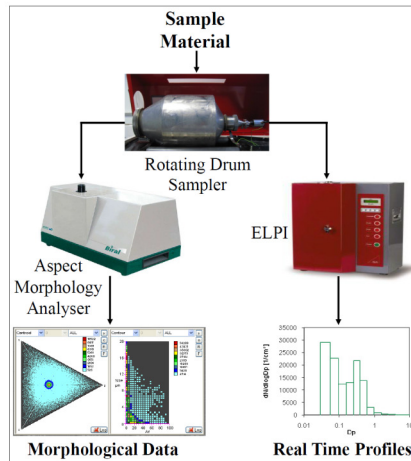[1] Centre of Analytical Sciences, University of Sheffield, S3 7HF, UK
[2] Group Environment, Tata Steel Europe, Swinden Technology Centre, Rotherham, S60 3AR, UK
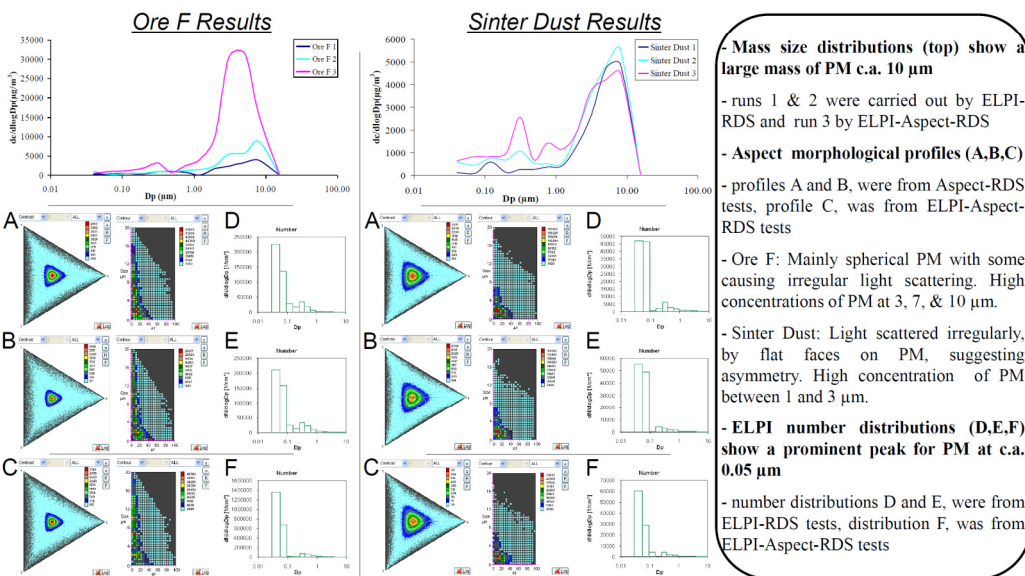
1. Introduction

Workplace exposure to particulate matter (PM) can be a health risk, especially if it is able to penetrate into the respiratory system (Petavratzi *et al*., 2005). Both the shape and size of PM determines how far along the respiratory tract it can penetrate and also its rate of removal. One known source of PM within the iron and steel making industry is the handling and stockpiling of raw materials. To help further understand such sources of PM and develop abatement procedures, full characterisation must be completed.

2. Methodology

An Aspect morphology analyser and an ELPI have been coupled, both individually and simultaneously, to a rotating drum sampler (RDS). This unique set up allows the determination of real time morphological information for particulates 0.5 μm to 20 μm in diameter and number and mass size distributions for particulates 30 nm to 20 μm in diameter. Four granular samples, two Brazilian iron ores, a blast furnace flue dust and a sinter dust, originating from an integrated steelworks have been tested. Two replicates were completed for each sample with three instrument conformations, i.e. ELPI-RDS, Aspect-RDS and ELPI-Aspect-RDS. Each run lasted four minutes and 16 rotations of the drum were completed in this time. Poreless polycarbonate substrates (25 mm) were used within the ELPI.

Sample Material → Rotating Drum Sampler → Aspect Morphology Analyser → Morphological Data; ELPI → Real Time Profiles

3. Results and Discussion

Ore F Results

Sinter Dust Results

- **Mass size distributions (top) show a large mass of PM c.a. 10 μm**

- runs 1 & 2 were carried out by ELPI-RDS and run 3 by ELPI-Aspect-RDS

- **Aspect morphological profiles (A,B,C)**

- profiles A and B, were from Aspect-RDS tests, profile C, was from ELPI-Aspect-RDS tests

- Ore F: Mainly spherical PM with some causing irregular light scattering. High concentrations of PM at 3, 7, & 10 μm.

- Sinter Dust: Light scattered irregularly, by flat faces on PM, suggesting asymmetry. High concentration of PM between 1 and 3 μm.

- **ELPI number distributions (D,E,F) show a prominent peak for PM at c.a. 0.05 μm**

- number distributions D and E, were from ELPI-RDS tests, distribution F, was from ELPI-Aspect-RDS tests

4. Conclusions

Both instruments have been successfully coupled to the RDS, however if coupled simultaneously (ELPI-Aspect-RDS) changes in concentrations could be seen. Materials showed some similarities in their shape but had very different size distributions. Replicates produced similar profiles. As part of further work a mix of materials will be tested to determine whether individual material characteristics are retained.

5. References

Petvratzi, E., Kingman, S., Lowndes, I.(2005) *Minerals Engineering*, **18**, 1188-1199

6. Acknowledgements

Work presented as a poster at the European Aerosol Conference, Manchester, UK, 2011.

This poster was also a finalist in the Royal Society of Chemistry ChemCareers Postgraduate Competition.

4.5 References

1. R. N. Reeve, *Environmental Analysis*, John Wiley & Sons, Chichester, 1994.
2. W. C. Hinds, *Aerosol Technology*, 2nd edn., Wiley and Sons, New York, 1999.
3. S.-H. Lee and H. C. Allen, *Analytical Chemistry*, 2011, **84**, 1196-1201.
4. R. Bargagli, *Trace Elements in Terrestrial Plants*, Springer, Berlin, 1998.
5. *Air Quality in Europe - 2012 Report*, European Environment Agency,Copenhagen, 2012.
6. http://uk-air.defra.gov.uk/air-pollution/daqi, Accessed 4th July 2013
7. K.-P. Hinz and B. Spengler, *Journal of Mass Spectrometry*, 2007, **42**, 843-860.
8. *Fast Mobility Particle Sizer Spectrometer, Model 3091, Specification Sheet*, TSI, 2012.
9. *90Plus, Nanoparticle Size Analyzer Specification Sheet*, Brookhaven Instruments, 2013.
10. *Aerosol Instruments Product Guide*, MSP Corporation, 2008.
11. *Laser Aerosol Spectrometer, Model 3340, Specification Sheet*, TSI, 2012.
12. *Gravimetric Impactor Brochure*, Dekati, 2010.
13. *ELPI User Manual*, Dekati Ltd, 2008.
14. K. R. May, *Journal of Scientific Instruments*, 1945, **22**, 187-195.
15. V. A. Marple, K. L. Rubow and S. M. Behm, *Aerosol Science and Technology*, 1991, **14**, 434-446.
16. www.dekati.com, Accessed 4th July 2013
17. J. Keskinen, K. Pietarinen and M. Lehtimäki, *Journal of Aerosol Science*, 1992, **23**, 353-360.
18. R. J. Tropp, P. J. Kuhn and J. R. Brock, *Review of Scientific Instruments*, 1980, **51**, 516-520.
19. M. Marjamäki, J. Keskinen, D.-R. Chen and D. Y. H. Pui, *Journal of Aerosol Science*, 2000, **31**, 249-261.
20. K. J. Lamble and S. J. Hill, *Analyst*, 1998, **123**, 103R-133R.
21. M. Thompson, *Handbook of Inductively Coupled Plasma Spectrometry*, 2nd edn., Blackie, Glasgow, 1989.
22. T. Reed, *Journal of Applied Physics*, 1961, **32**, 821-824.
23. H. Price, R. Arthur, K. Sexton, C. Gregory, B. Hoogendoorn, I. Matthews, T. Jones and K. BéruBé, *Journal of Toxicology and Environmental Health, Part A*, 2010, **73**, 355 - 367.
24. *Workplace atmospheres - Measurement of the dustiness of bulk materials - Requirements and reference test methods,* BS EN 15051, BSI, 2006.
25. C.-J. Tsai, C.-H. Wu, M.-L. Leu, S.-C. Chen, C.-Y. Huang, P.-J. Tsai and F.-H. Ko, *Journal of Nanoparticle Research*, 2009, **11**, 121-131.
26. http://goldbook.iupac.org/, Accessed 4th July 2013
27. K. Jackson, PhD Thesis, University of Sheffield, 2009.
28. G. C. Lough, J. J. Schauer, J.-S. Park, M. M. Shafer, J. T. DeMinter and J. P. Weinstein, *Environmental Science & Technology*, 2004, **39**, 826-836.

Chapter Five

Morphological studies of laser generated particulates using LA-Aspect methods

5.1 Introduction

LA is a reliable sampling technique, generally used with ICP spectrometry for analysis of solid samples.[1] By firing a short-pulsed high power laser onto a material, a finite amount of the material is converted instantaneously into its vapour phase constituents[2] which when transported to the ICP by a carrier gas permits elemental analysis. Since laser ablation and LA-ICP-MS were first discussed in 1985[3] it is now considered a "well accepted analytical technique for in situ trace element analysis".[4] A large range of materials have been characterised using laser ablation techniques including minerals, such as magnetite[5] and granite,[6] biological samples, such as brain tissue[7] and tumours[8] and particulate matter contained upon substrates.[9-12] Although laser ablation has mainly been used to allow the elemental characterisation of solid samples the aerosol generated along with the particulates contained within it may be physically characterised.

The first paper to complete a detailed investigation of the nature of the particulates produced through laser ablation was published in 1990.[13] Thompson, Chenery and Brett had noticed that there had been a shortfall in the previous research and decided to examine the material produced by and the processes involved in ablation using a ruby laser (694 nm). The investigation focused on the morphology of the ablated particulates, which were collected onto a substrate for examination using SEM. A selection of materials, with different characteristics were ablated, including aluminium, a stainless steel and a ceramic material. All were polished before ablation was performed. Ablation

took place in an argon atmosphere, with a flow rate of 1 L/min. A single substrate was placed at the exit of the ablation cell to allow the collection of the particulates.

The particulates collected upon the substrate represented 20 to 30 percent of the laser generated aerosol. The other particulates either remained trapped within the chamber or were too large to be carried to the exit of the chamber. There would have been only a low number of these larger particulates but they would have contributed greatly to the total percentage. The ablation and subsequent SEM analysis of the aluminium and steel materials indicated that a large number of spherical particulates ranging from 1 µm to 10 µm in size had been generated. When ablating the ceramic material two different populations of particulates were generated. The first population consisted of spheres less than 4 µm in size, the second consisted of angular particulates. The morphological results pointed towards three different processes occurring during ablation which are described below:

- A plume of plasma is formed within 100 µs of the start of the ablation, which condenses to form an amorphous material, less than 1 µm in diameter, which is efficiently transported by the carrier gas.

- For metallic materials spherical particulates are formed from the melting of the material which are then removed from the crater. Their transport efficiency depends upon the particulate size.

- For brittle materials, such as a ceramic, angular particulates are generated not through melting but through thermal or mechanical shock which causes the material to chip and fragment. The chemical composition of these particulates should be similar to that of the original ablated material.

In conclusion Thompson, Chenery and Brett were able to successfully complete morphological characterisation of both metallic and non-metallic materials and determine how each type of generated particulate was formed.[13] Since the publication of this first paper in 1990,[13] a range of other papers have been published which have discussed and completed morphological characterisation of laser generated aerosols, Table 5-1.

Various techniques have been employed for morphological characterisation including cavity ring down laser absorption spectroscopy,[14] DMA,[15] SEM, TEM[16-20] and laser light scattering.[21-25]

In 2005 Kuhn et al.[26] completed an off line study into particle size distributions of laser generated aerosols. A laser ablation unit, with an ArF 193 nm laser, was used to ablate a range of metal materials including a NIST brass SRM. The aerosol particulates generated through ablation were collected onto polycarbonate substrates using a low pressure impactor. For impaction 1 L/min of helium was used along with 9 L/min of laboratory air. The particulates upon the substrates were then characterised by SEM. As well as being collected onto substrates, a proportion of the generated aerosol was simultaneously analysed by a DMA and an OPC to determine electrical mobility diameters and particle counts, respectively. The OPC characterised particulates between 65 nm and 1000 nm, whilst the DMA characterised particulates between 20 nm and 660 nm. The particulates collected were mainly spherical with a diameter of 1500 µm, however, chain like agglomerates were seen on one of the stages, with a 30 nm cut off point. The DMA and OPC reported high concentrations of agglomerated particulates between 230 nm and 300 nm and 85 nm and 90 nm, respectively. The OPC also indicated high concentrations of particulates at 650 nm in diameter. The three measurement techniques were able to provide complementary information on the laser generated particulates. The study's downfall was that the microscopy analysis was completed off line, meaning a slow and labour intensive process.[26]

Authors	Date	Laser used	Material/s	Characterisation technique	Comments
Chenery, Hunt and Thompson[17]	1992	Two ruby lasers (694 nm, 347 nm) and one Nd:YAG laser (532 nm)	Pyrite and Olivine	SEM	Found large differences between the properties of particulates generated from different materials
Whitlock and Frick[15]	1994	KrF, 284 nm	Aluminium, ceramic and polymer	DMA	Found each material responded differently when ablated and created different sized particulates
Jeong, Borisov, Yoo, Mao and Russo[25]	1999	Nd:YAG, 266 nm	Glass	Optical particle counter	Found more particulates were generated as more ablations were completed on one position
Seto, Kawakami, Suzuki, Hirasawa, Kano, Aya, Sasaki and Shimura[27]	2001	Nd:YAG, 532 nm	Silicon and titanium dioxide	DMA, SEM and TEM	Generated mainly spherical particulates, with some agglomerates
Bulatov, Khalmanov and Schechter[14]	2003	Nd:YAG, 1064 nm	Aluminium, gold, silver and zinc	Cavity ring down spectroscopy	First use of cavity ring down spectroscopy for morphological characterisation of laser generated aerosols
Košler, Wiedenbeck, Wirth, Hovorka, Sylvester and Míková[28]	2005	Nd:YAG, 266 nm	Silicate glass and zircon	Laser light scattering and SEM	Found laser ablation of similar materials can produce particulates with different size distributions
Holá, Konečna, Mikuška, Kaiser and Kanický[29]	2010	Nd:YAG, 213 nm	Tungsten carbide, steel and glass	Laser light scattering and SEM	Found that the production of particulates is dependent on the materials composition and structure
Glaus, Kaegi, Krumeich and Günther[30]	2010	ArF, 193 nm and Ti:sapphire, 795 nm and 265 nm	Brass, steel, zircon, glass and iron and lead sulphides	SEM and TEM	Found aerosols generated by different lasers had different morphological properties

Table 5-1: Summary of articles discussing LIBS aerosol analysis

As seen in Table 5-1 and also discussed in a review paper completed by Hergenröder[31] in 2006, a large proportion of the morphological analysis of laser generated aerosols is completed off line using microscopy or imaging techniques. Off line analysis can be slow and labour intensive whereas on line analysis allows particulates to be characterised almost instantaneously.[32] In this context research using the Aspect will allow the real time morphological characterisation of laser generated aerosols to be completed. This is the first time that the Aspect instrument has been coupled to a laser ablation unit to characterise laser generated aerosols. Comparisons will also be made between the wavelength of the lasers as well as the atmosphere used for the ablation of the materials.

Lasers operating at different wavelengths have previously been used for the ablation of materials. One paper which compared three laser wavelengths, produced by the same laser, was written by Guillong, Horn and Günther in 2003.[33] LA-ICP-MS was used and the three compared wavelengths were 266 nm, 213 nm and 193 nm. The sizes of the generated particulates were determined using a laser light scattering instrument. Guillong, Horn and Günther found that the shortest wavelength, 193 nm, produced generally small particulates, from 60 nm to 150 nm in diameter, which in turn allowed more stable analytical signals to be realised. The other two wavelengths produced particulates much larger in size, generally from to 60 nm to at least 1000 nm, which reduced the detection power of LA-ICP-MS.[33]

The laser ablation and analysis of materials is generally completed under either atmospheric conditions or in an inert atmosphere. The use of different atmospheres for ablation has been explored to determine how variations in ablation environment could affect the obtained results. One review completed in 2010 by Effenberger Jr. and Scott[34] focused on the performance of a LIBS system in reduced pressure environments as well as in gases other than air. One of the reviewed papers, written by Iida in 1990,[35] found

that LIBS emission intensities of iron were greater when the ablation was completed in argon rather than air. Another of the reviewed papers, Aguilera and Aragon[36] found that during the ablation of steel, using a LIBS system, the use of an argon atmosphere resulted in higher plasma temperatures with a slower decay than when using an air atmosphere. Günther and Heinrich[37] investigated the use of a helium and argon atmosphere for use with LA-ICP-MS. They found that using a flow of 1.2 L/min of helium would allow the most reproducible and intense signals as the particulate transport was improved.[37] None of the studies into ablation atmospheres commented upon the sizes of the particulates generated and thus comparisons will not be possible.

It is hoped that this chapter will provide new insights into how different experimental parameters can affect the particulates generated by the laser ablation technique. Two Nd:YAG laser ablation units, operating at 1064 nm and 266 nm, will be coupled to an Aspect morphology analyser to generate aerosols for on line and real time morphological characterisation. The respective methods will be known as LA (1064 nm)-Aspect and LA (266 nm)-Aspect. Previous research[33] has indicated that smaller particulates would be produced when using a laser with a lower wavelength. Thus it is expected that when using the 266 nm laser for ablation, rather than the 1064 nm laser, the generated particulates will be smaller in diameter. Studies completed previously have also shown that argon is the preferred method for ablation, generally providing more reproducible results than other atmospheres. This hypothesis will be tested by completing the characterisation of six different materials using the 1064 nm laser in both argon and laboratory air atmospheres. Results obtained in each of the atmospheres will be evaluated and morphological profiles from each of the six materials will be compared.

Bleiner[38] simulated the effect of a laser pulse onto a flat surface and the formation of a crater. For this study laser shots will be fired in triplicate onto one position on each material.

Using Bleiner's research, as a guide, it is expected that as more shots are fired onto the same position the crater will become larger and deeper, since a flat surface is no longer being fired upon. Each material should also form slightly different craters due to the different physical properties of all the materials.

5.2 Experimental

5.2.1 Materials

Six materials, high purity carbon rod, high purity zinc, boron nitride, a polyethylene lid from a sample tube, a carbon steel certified reference material (BAS, SS-CRM 457-2) and a glass reference material (NIST 612) have been studied using both the LA (1064 nm)-Aspect and LA (266 nm)-Aspect methods. The six materials were chosen for their different physical and chemical properties and compositions, some of these are detailed in Table 5-2. The carbon steel was also used for method development. All materials were ablated directly without any sample preparation.

Property	Carbon rod	Zinc	Boron nitride	Polethylene	Carbon steel	Glass
Melting point (ºC)	3675	420	3000	110	1400	1500
Boiling point (ºC)	4200	907	3273	-	2850	2300
Thermal conductivity (W/mK)	140	116	25	0.46	43	1.05

Table 5-2: Physical properties of the six materials

5.2.2 Instrumentation

Four different instrument configurations were used for the characterisation of the laser generated aerosols. Three of these configurations involved the use of a LIBS unit manufactured by Applied Photonics (Skipton, UK) shown in Figure 5-1. This schematic shows the laser head, external sample chamber and the modified internal sample chamber, other components, not shown in the schematic, include the laser power supply, the spectrometer console and a laptop. Since the LIBS generated spectra were only required for method development and not for morphological characterisation the LIBS

unit was mainly used as a laser ablation unit, known from this point onwards as the LA (1064 nm) unit.

Figure 5-1: LA (1064 nm) Instrument[39]

The laser head was used to focus the laser beam onto the material of interest as well as to collect the plasma light for transmission to the three spectrometers. The head also held a small camera to assist with the positioning of the material. The power for the laser head was provided by the laser power supply which also stopped the laser head from overheating. The Nd:YAG laser operated at the fundamental wavelength of 1064 nm.[40]

The external sample chamber contained a breadboard plate which was attached to a manual three-axis translation stage which allowed 50 mm of travel in each axis. Laser safety glass was used to stop any laser light from exiting the sample chamber. The interlock and its override unit were operated through both the sample chamber and the laser power supply. If the interlock was 'on' the laser would only fire if the sample

chamber door was shut. If the interlock was turned 'off' the laser would become active with the sample chamber door open, allowing an open beam configuration. This research was completed with the interlock on at all times, reducing the safety category of the laser system from Class four to Class one.

The internal sample chamber was attached to the breadboard plate of the external sample chamber. It was originally a laser ablation cell and was modified by Applied Photonics specifically for this research. Two extra ports were added to facilitate entry of a carrier gas stream (normally argon) which would transport the ablated particulates from the internal chamber (Figure 5-2) to the Aspect. The original ports were joined together by a 20 cm length of PVC tubing (0.32 cm internal diameter) to make sure no particulates or carrier gas escaped into the external sample chamber or laboratory atmosphere.

Figure 5-2: Internal sample chamber[39]
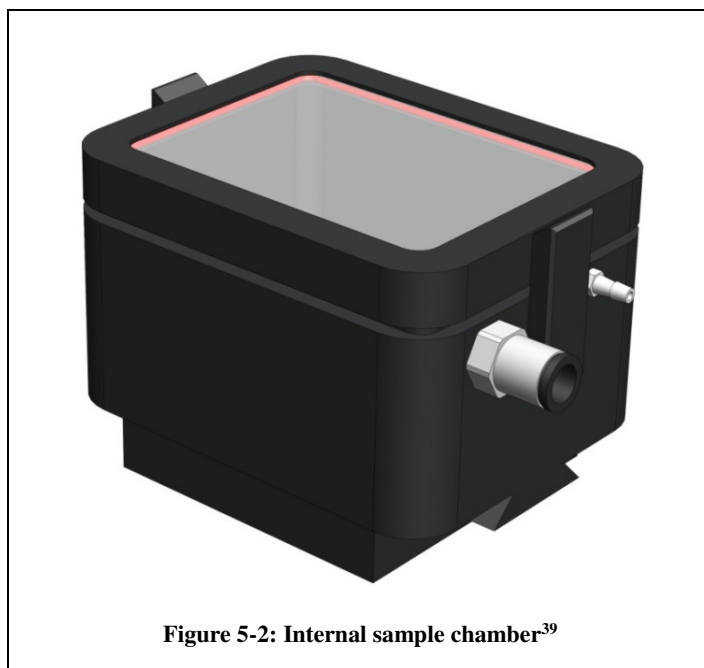
The first of the four experimental configurations is illustrated in Figure 5-3. This configuration was used for initial signal stability studies. It connected a cylinder of argon, via a regulator and PVC tubing (1.5 m in length), to the LA (1064 nm) unit, and

the internal sample chamber. All measurements were completed at a pressure of 0.5 bars.

**Figure 5-3: Argon-LA (1064 nm) configuration**
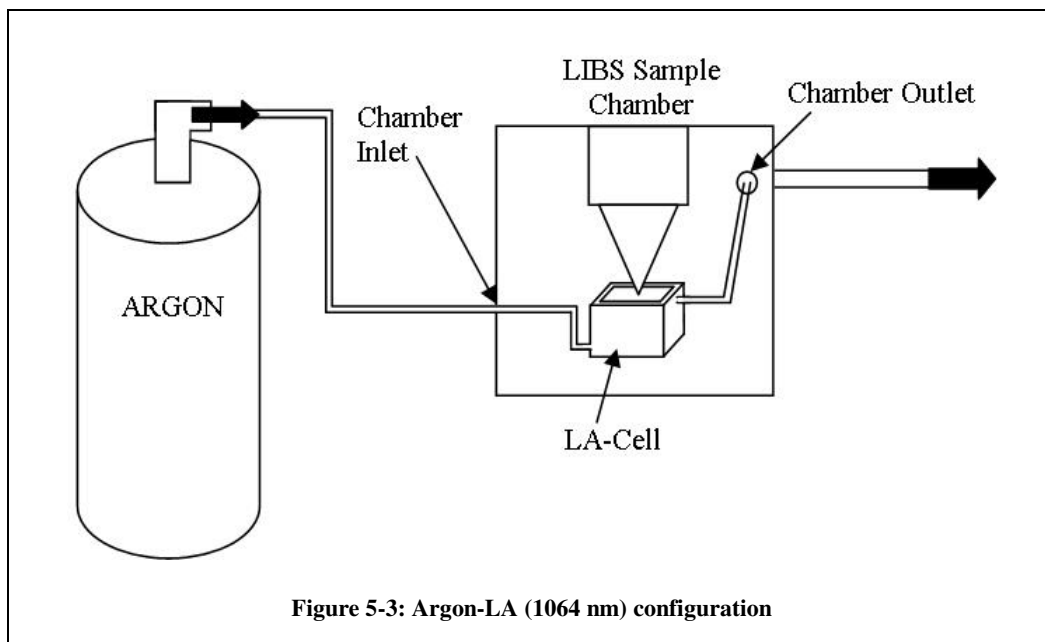
The next two experimental configurations utilised the Aspect morphology analyser, which was used in Chapter Three, and required a flow rate of 7 L/min to operate. Two different atmospheres were investigated when using each of these configurations, an argon atmosphere and a laboratory air atmosphere.

To reach and maintain the required gas flow rate, when using the argon atmosphere, one option was to just use argon, as was seen in Figure 5-3. An argon flow rate of 7 L/min could not be achieved at low pressure (0.5 bar) and an increased pressure, which allowed a flow rate of 7 L/min, would have been too high for the internal sample chamber to withstand. Therefore when using an argon atmosphere a regulator, connected to the argon gas cylinder, and a flow meter were used to control the pressure and flow of argon to the LA (1064 nm) unit. Argon was delivered to the internal sample chamber at a pressure of 0.5 bars and a flow of 1.7 L/min. To permit the flow rate to reach 7 L/min before the Aspect morphology analyser, a small plastic tee piece was inserted into the one meter length of conductive silicon tubing which connected the LA

(1064 nm) unit and the Aspect. This allowed the flow rate to be 'made up' to the required 7 L/min flow using laboratory air. A similar set up was used by Kuhn et al. in 2005.[26]

When using a laboratory air atmosphere no make-up gas was required. Hence, 7 L/min of laboratory air passed all the way through the internal sample chamber, through one meter of sealed conductive silicon tubing and onto the Aspect. Thus, the only difference between the two configurations was the tubing that connected them. Both configurations are detailed in Figures 5-4 and 5-5, respectively.

Figure 5-4: LA (1064 nm)-Aspect argon configuration

Figure 5-5: LA (1064 nm)Aspect laboratory air configuration
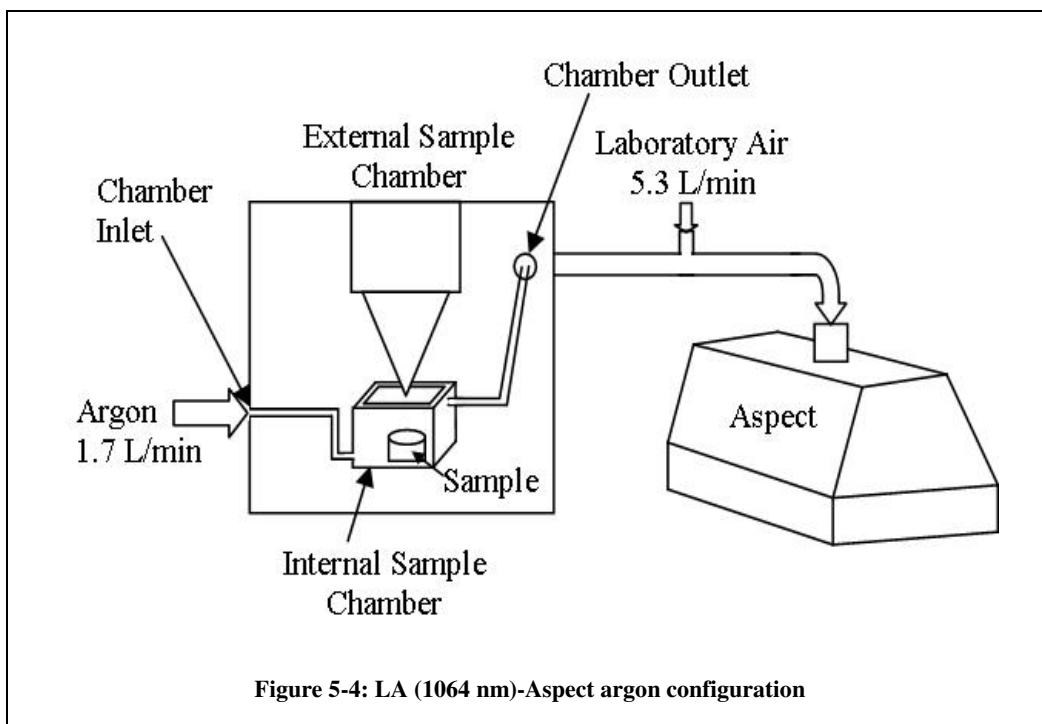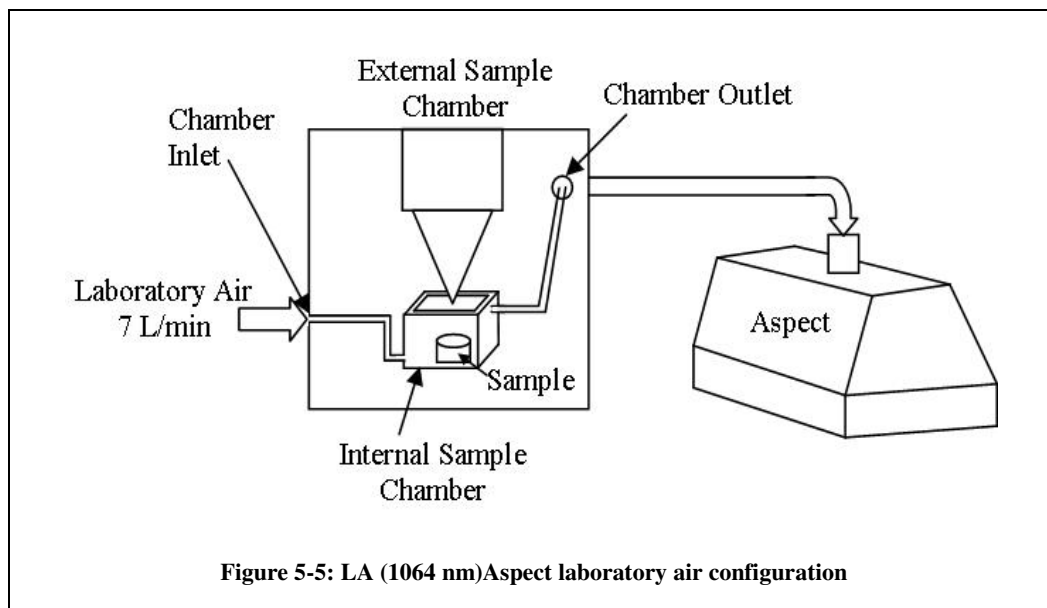
A further configuration consisted of a commercial LA (266 nm) unit, LAX 200, Cetac Technologies (Nebraska, USA), coupled to the Aspect morphology analyser, illustrated in Figure 5-6. The Cetac Nd:YAG laser operated at a wavelength of 266 nm. An argon flow rate of 1.7 L/min at 0.5 bars was used with laboratory air as the make-up gas. Conductive silicon tubing (length one metre), connected the LA (266 nm) system to the Aspect morphology analyser.

Figure 5-6:LA (266 nm)-Aspect configuration, with laboratory air carrier gas
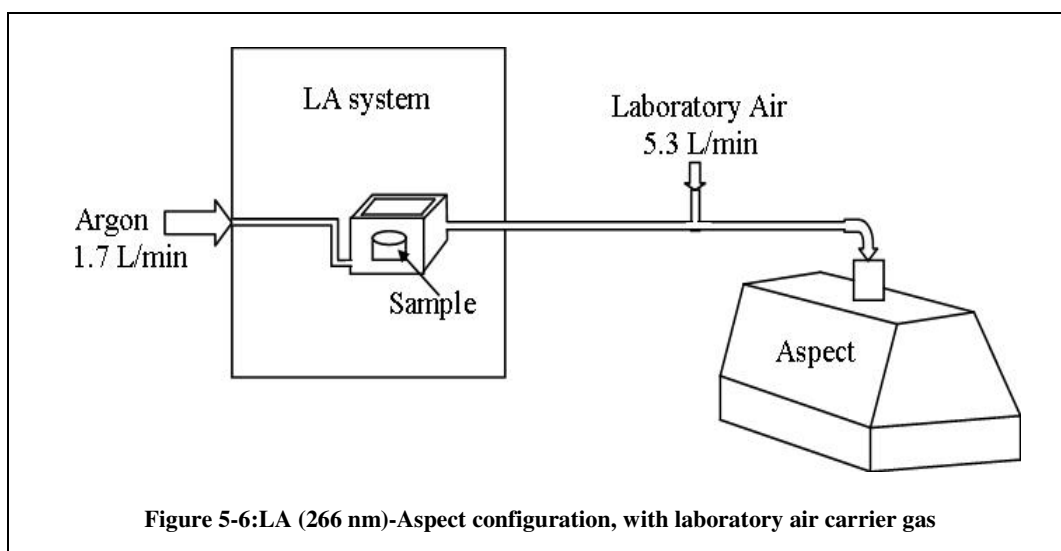
5.2.3 Procedures

For each different instrument configuration a different procedure was used. These will now each be discussed separately.

Signal Stability Studies

Using the Argon-LA (1064 nm) configuration, illustrated in Figure 5-4, initial studies were performed at specific experimental conditions. A range of parameters were studied and in addition to morphological characterisation elemental spectra were also obtained for each parameter set. The obtained spectra were examined to determine the optimum conditions for ablation. The parameters which were altered included the argon flow rate, the number of laser shots, laser repetition rate and the Q switch delay, which controlled the laser energy. One ablation was completed per measurement and the measurements were done in duplicate. Background measurements were taken every time any parameter was changed.

Twelve measurements, lettered M to Y and shown in Table 5-3, were originally completed to deduce the best Q switch delay, flow rates and repetition rates. Ten laser shots were completed for each of these first twelve measurements.

Parameter	M	N	P	Q	R	S	T	U	V	W	X	Y
Q switch delay (µs)	300	250	200	300	250	200	300	250	200	300	250	200
Laser shots	10	10	10	10	10	10	10	10	10	10	10	10
Repetition rate (Hz)	10	10	10	10	10	10	5	5	5	5	5	5
Flow rate (L/min)	0.85	0.85	0.85	1.7	1.7	1.7	0.85	0.85	0.85	1.7	1.7	1.7

Table 5-3: Parameter set one used for signal stability studies

A further series of measurements was then completed. Five measurements, in duplicate were taken in this series, Z1, Z5, Z10, Z25 and Z50, each with its own background.

Table 5-4 indicates the parameters used for each measurement. This completed the initial method development studies for the LA (1064 nm)-Aspect method with an argon atmosphere.

Parameter	Z1	Z5	Z10	Z25	Z50
Q switch delay (μs)	200	200	200	200	200
Laser shots	1	5	10	25	50
Repetition rate (Hz)	5	5	5	1	1
Flow rate (L/min)	1.7	1.7	1.7	1.7	1.7

Table 5-4: Parameter set two used for signal stability studies

LA (1064 nm)–Aspect Method Development

Using the carbon steel material, systematic experiments, whereby one parameter was changed at a time, were undertaken. The parameters which were studied included the Q switch delay time, the repetition rate, the number of laser shots and the number of conditioning shots. The parameters used for each experiment are listed in Table 5-5. A flow rate of 1.7 L/min of argon, at a pressure of 0.5 bars, was used with a make-up gas of laboratory air. To determine the best parameter the argon emission peak was monitored, on the obtained spectra, as well as the number of particulates characterised by the Aspect.

Parameter		Delay, μs	Conditioning shots	Repetition Rate, Hz	Laser shots
Delay, μs	A	150	50	5	10
	B	200	50	5	10
	C	250	50	5	10
Conditioning shots	A	200	10	5	10
	B	200	25	5	10
	C	200	50	5	10
	D	200	100	5	10
Repetition rate, Hz	A	200	50	1	10
	B	200	50	2	10
	C	200	50	5	10
	D	200	50	10	10
	E	200	50	20	10
Laser shots	A	200	50	5	1
	B	200	50	5	5
	C	200	50	5	10
	D	200	50	5	25

Table 5-5: Method development experimental parameters for LA (1064 nm)-Aspect

To obtain a background for each experiment the argon was turned on and allowed to flow through the whole configuration. The Aspect was then turned on and a background reading was taken for one minute. After one minute the LA (1064 nm) laser was fired and a morphological profile of the ablated particulates was obtained. Once the number of analysed particulates had returned to the background level and remained stable for at least one minute the Aspect was turned off. This was repeated twice more for the same location before moving on to the next parameter set.

LA (1064 nm)-Aspect Analysis of CRMs

Following the completion of the method development the six materials were ablated and the laser generated aerosol was morphologically characterised. The LA (1064 nm) parameters, which were chosen following the method development were a Q switch

delay (which controlled laser power) of 150 μs, 25 conditioning shots and 25 laser shots which were completed at a repetition rate of 10 Hz (25 laser shots in 2.5 seconds). When using an argon atmosphere the argon flow rate was 1.7 L/min at a pressure of 0.5 bars. The laser energy was 105 mJ.

The material of interest was placed inside the internal sample chamber, the internal chamber was sealed and the door of the external sample chamber was closed to activate the interlock. If using argon the cylinder was turned on and left for five minutes to allow any laboratory air to exit the internal chamber. Following this, the Aspect was turned on and a steady state background, of the chosen atmosphere, was maintained for one minute before ablation was commenced and particulates were generated. The laser generated particulates exited the internal sample chamber and flowed along the metre long conductive silicon tube before being characterised by the Aspect. After the ablation had finished and all particulates had been characterised the number of particulates returned to the background level. Once this background level had remained stable for at least one minute, the Aspect was turned off. The same procedure was used for both the laboratory air and argon atmospheres.

Six locations were ablated on each material, three in a laboratory air atmosphere and three in an argon atmosphere. Three ablations were completed on each location. To determine reproducibility the eighteen ablations on each material were duplicated on a different day to the original set of ablations. The temperature and humidity of the laboratory, in which the work was completed, was recorded twice daily.

LA (266 nm)-Aspect Method Development

In a similar way to the LA (1064 nm)-Aspect method development, systematic experiments were also performed for the LA (266 nm) configuration, as shown in Table 5-6. The carbon steel served as a development material and the parameters which were varied included laser energy, repetition rate and number of laser shots. A flow rate of 1.7 L/min of argon, at a pressure of 0.5 bars, was used with a make-up gas of laboratory air.

Parameter		Energy, %	Repetition rate, Hz	Laser shots
Energy, %	A	25	10	500
	B	50	10	500
	C	75	10	500
	D	100	10	500
Repetition rate, Hz	A	100	5	500
	B	100	10	500
	C	100	20	500
Laser shots	A	100	10	250
	B	100	10	300
	C	100	10	400
	D	100	10	500

Table 5-6: Method development experimental parameters for LA (266 nm)-Aspect

A one minute background reading was obtained for each experiment. Next the laser was fired and the laser generated aerosol was characterised by the Aspect. The Aspect was turned off only after the number of analysed particulates had returned to the background level and remained stable for at least one minute. Each experiment was repeated twice more on the same location before moving on to the next parameter set.

LA (266 nm)-Aspect CRM analysis

Following the method development, four of the materials were ablated in an argon atmosphere and the resultant laser generated aerosols were morphologically characterised. For the polyethylene and glass materials, ablation was completed only in a laboratory air atmosphere. This was because the laser unit developed an irreparable fault before ablation of these two materials, in an argon atmosphere, could be completed. The parameters which were used for all ablations were 500 laser shots at 100 percent energy, with a repetition rate of 10 Hz (500 laser shots in 50 seconds). This corresponded to a laser energy of 7.5 mJ. When using an argon atmosphere the argon flow rate was 1.7 L/min at a pressure of 0.5 bars.

The material of interest was placed inside the ablation cell and the cell was sealed. The door of the unit was then closed to activate the interlock. When using argon the cylinder was turned on and left for five minutes to allow any laboratory air to exit the LA (266 nm) ablation cell. The Aspect was then turned on and a steady state background was maintained for one minute before commencing ablation. Ablation of the material of interest resulted in the generation of a particulate aerosol stream which was morphologically characterised by the Aspect. Following this measurement and once the background level had returned and remained stable for at least one minute, the Aspect was turned off.

Three locations were ablated on each material, with three ablations completed on each location. This study was used to compare particulates generated at the different laser wavelengths (266 nm compared with 1064 nm) and therefore no replicates were completed. The temperature and humidity of the laboratory was recorded daily.

5.3 Results and Discussion

5.3.1 Initial Studies

A range of studies were performed under different experimental conditions. To achieve effective ablation conditions the variation of the following parameters was completed, argon flow rate, the number of laser shots, the laser repetition rate and the Q switch delay, which controlled the laser energy. One spectrum was recorded per measurement and each measurement was done in duplicate. Background spectra were taken every time a parameter was changed.

For eight of the twelve original measurements (M, N, Q, R, T, U, W and X) emission signals corresponding to argon emission lines were not observed This was due to the use of relatively high Q switch delays of 250 µs to 300 µs, which related to low energies. By using a low energy laser for ablation the energy applied to the argon atoms would not have been high enough to overcome the ionisation potential of argon, thus not ejecting any electrons or allowing the excited state to become populated.[41]

For the other four measurements (P, S, V and Y) a Q switch delay of 200 µs was used which resulted in a prominent argon signal to be seen at 415.86 nm. Of the four measurements two of them were completed with an argon flow rate of 0.85 L/min and the other two at 1.7 L/min. The repetition rates were varied between 5 and 10 Hz for each argon flow rate.

Both of the measurement Y replicate analyses (200 µs delay, 10 laser shots, 5 Hz, 1.7 L/min) gave the most intense argon peaks at 415.86 nm and therefore the parameters used for this measurement were used for a further series of measurements where the number of laser shots was varied (Z1, Z5, Z10, Z25 and Z50). By completing this extra

series of measurements it was found that as more laser shots were completed the speed of the analysis slowed greatly. For Z25 and Z50, the repetition rate had to be lowered to 1 Hz due to the increased time taken to acquire data from the spectrometers.

Argon peaks were seen in the spectra, at 415.86 nm, for all measurements except Z1. However, the peaks for Z5 and Z10 were quite small. This would have been expected for the Z5 measurement but since the Z10 measurement had the same parameters as measurement Y, completed previously, then a larger peak should have been seen.

The peak heights for the Z measurements are shown in Table 5-7. For Z25 and Z50 the peaks were proportional to each other in size as well as being proportional to the peak heights seen previously for measurement Y.

Measurement	Peak height 1	Peak height 2
Z5	355	382
Z10	506	469
Y (same parameters as Z10)	1939	1486
Z25	3741	4181
Z50	8848	8936

Table 5-7: Argon peak heights for Z measurements

The data and the spectra generated indicated that the set up of the LA (1064 nm) system with the integrated sample chamber was successful. The peak heights indicated that there was a good correlation between measurements completed with 10 laser shots or more. This was a sign of good signal stability when using the LA (1064 nm) unit and also allowed an insight into which conditions could be used for further LA (1064 nm) related studies. Due to the time taken for Z50 to be completed, 50 seconds, the most practical parameters, from the Z25 measurement, were 200 µs delay, 25 laser shots, 1 Hz and 1.7 L/min of argon, since they allowed a strong emission peak to be obtained in

a reasonable time of 25 seconds. Following this initial study the development of the LA (1064 nm)-Aspect method was commenced.

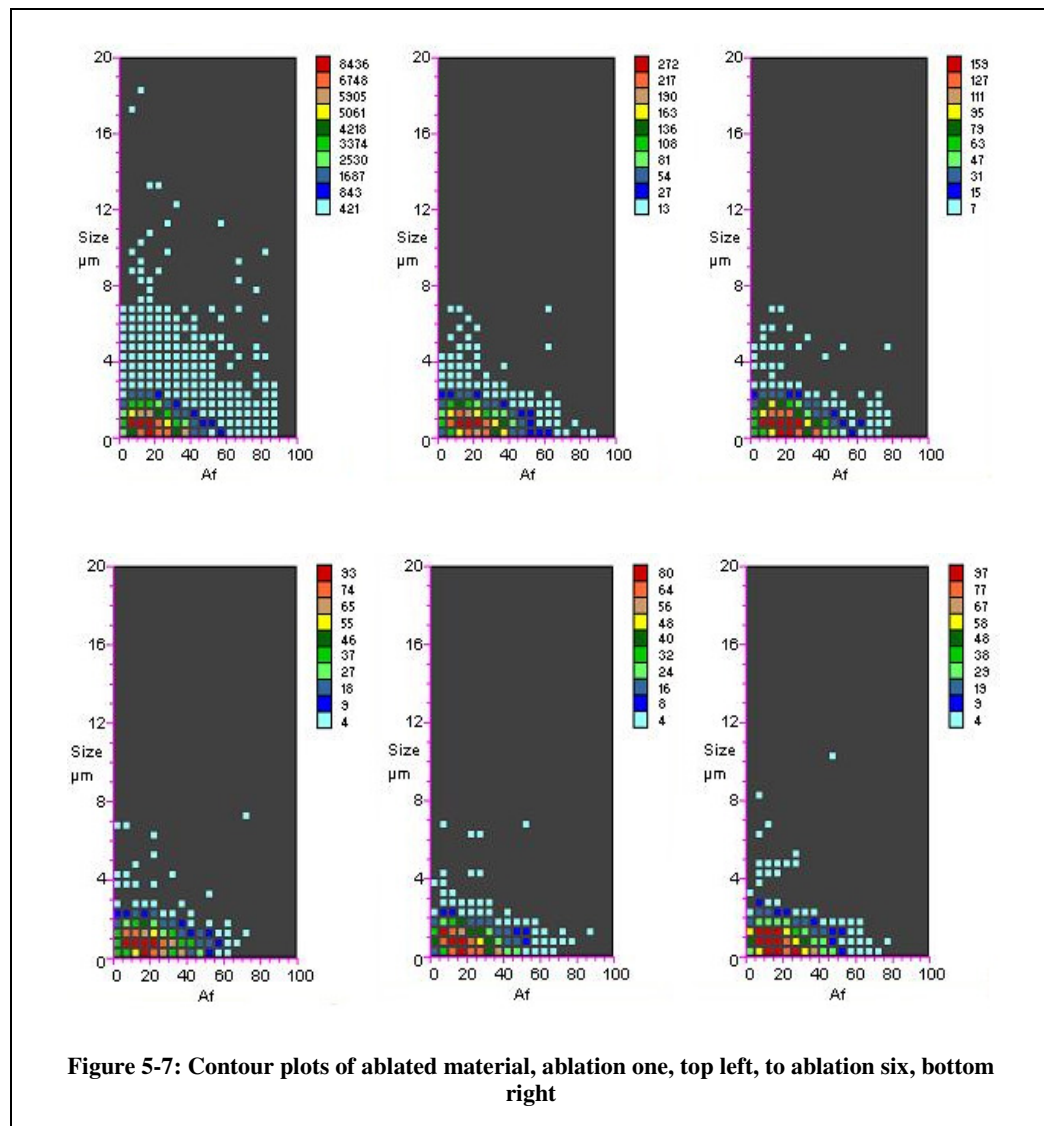## 5.3.2 LA (1064 nm)-Aspect Method Development

Each of the LA (1064 nm) parameters, as specified in Table 5-5, was varied and ablation was completed using each parameter set. For all of the spectra obtained from the differing parameter sets, the argon peak, at 415.86 nm, and the related peak heights were recorded and compared for intensity and reproducibility. The number of particulates produced and the morphological profiles were also examined for reproducibility. The parameter set which gave the most reproducible results was chosen for further testing together with the parameter set used in the initial signal stability studies (Section 5.3.1). The argon flow rate was kept constant at 1.7 L/min and the carbon steel was used for all experiments. Three analyses per parameter set were completed.

- Set One: 150 µs delay, 25 laser shots, 10 Hz, 25 conditioning shots
- Set Two: 200 µs delay, 25 laser shots, 1 Hz, 25 conditioning shots

Parameter set one produced spectra with the most intense and reproducible argon peaks, as shown in the Appendix. This parameter set also generated the largest number of particulates, as determined by the Aspect. A larger number of particulates were preferable because it would allow morphological characterisation to be completed more easily.

Next six ablations on the same location of the carbon steel were completed to check whether the Aspect morphological profiles were reproducible for parameter set one. Results are shown in Figure 5-7. Although the number of particulates was found to

decrease, as more ablations were undertaken, the shapes and sizes of the ablated matter were consistent and reproducible throughout the six analyses. Therefore parameter set one, 150 µs delay, 25 laser shots, 10 Hz, 25 conditioning shots, was chosen for the next stage of work.

Figure 5-7: Contour plots of ablated material, ablation one, top left, to ablation six, bottom right

5.3.3 *Morphological Analysis Using the LA (1064 nm)-Aspect Method*

The six different materials were ablated and morphological profiles of the respective laser generated aerosols were generated. Photomicrographs of the craters formed during ablation were also taken and are shown alongside their relevant morphological profiles.

The transit time for particulates from the LA (1064 nm) unit to the Aspect sample chamber was between eight and twelve seconds. This was determined by recording the time the laser was fired and then examining the temporal plot, obtained from the Aspect software, to find at what time particulates were detected by the Aspect. The difference in the two times equated to the particulate transit time. The range of times was due to the different sizes and therefore masses of the particulates. Lighter and smaller particulates took less time to reach the Aspect than larger and heavier particulates.
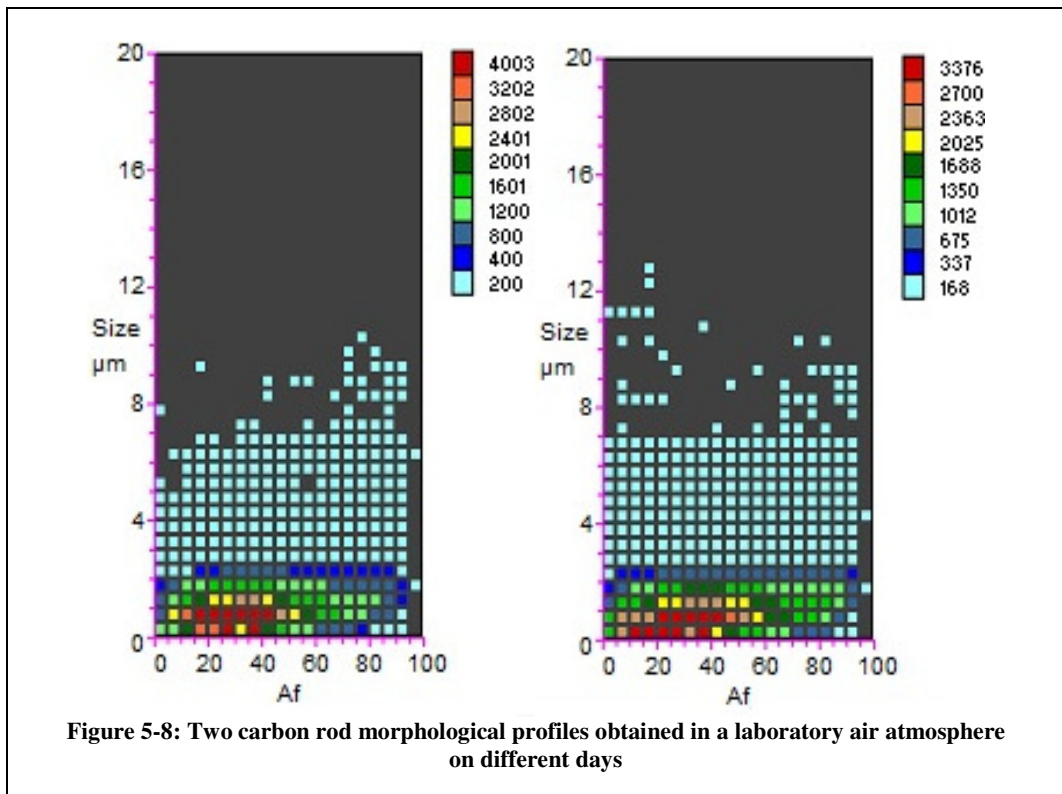
Results from the six materials will be discussed in terms of replicate comparisons, the effect of multiple ablations on a single location as well as the examination of any relationships between the morphological profiles obtained for each of the different materials.
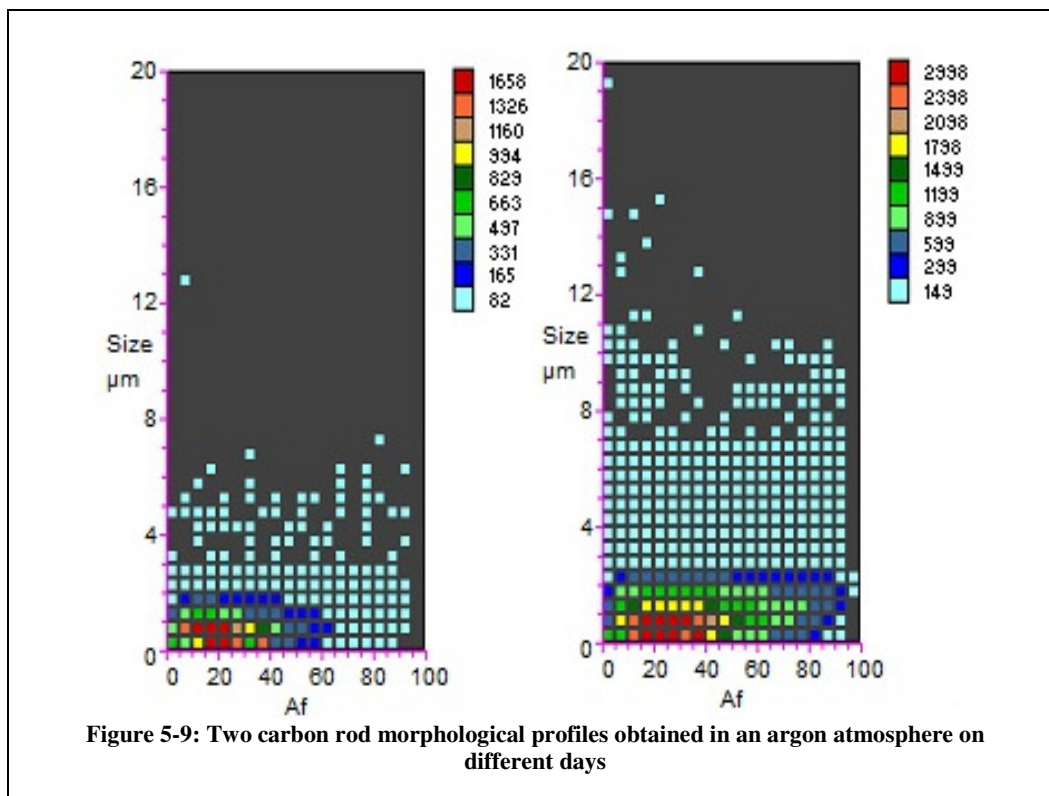
Carbon Rod

All of the carbon rod morphological profiles, whether obtained in a laboratory air or argon atmosphere, showed significant concentrations of particulates which were fibrous in shape (Figures 5-8 and 5-9). The highest concentrations of particulates within the laser ablated aerosol were present between A_f values of 10 and 40, particulate numbers of 1658 to 4003, showing asymmetry and the occurrence of faces and edges on the particulates. The morphological profiles all showed a small spread of particulate sizes,

with no non-background particulates present above 3 µm. High concentrations tended to appear at approximately 0.5 µm to 1 µm in size.

In general little variation was observed in the morphological profiles as more ablations were completed on one location. However a decrease in the number of particulates produced was noticeable. This was most likely due to a crater being formed as more ablations were completed on the same position. The formation of a crater would cause the laser to become slightly defocused, therefore less material would be ablated and the number of particulates generated would decrease. To avoid this in future experiments the laser could be refocused after each ablation on one position.

Figure 5-8: Two carbon rod morphological profiles obtained in a laboratory air atmosphere on different days

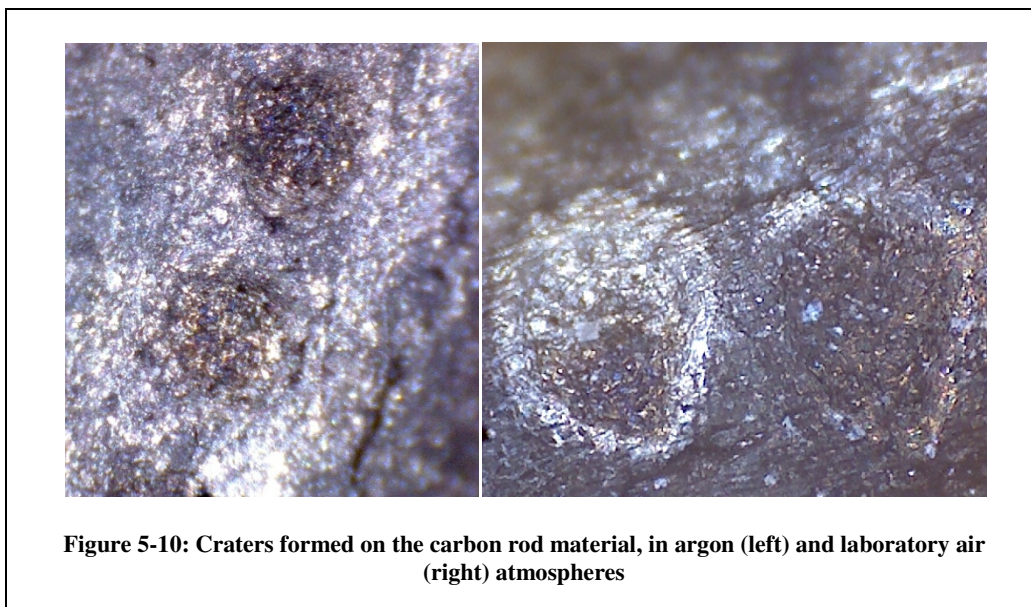**Figure 5-9: Two carbon rod morphological profiles obtained in an argon atmosphere on different days**

The morphological profile replicates differed slightly from each other. For the first set of profiles there were some obvious differences between the ablated particulates generated in each of the two atmospheres. Although similarities could be seen between the two plots, such as high concentrations of particulates at the same size and A_f values, the spread of particulate shapes was a lot larger when using the laboratory air atmosphere. The replicates, completed on different days in both atmospheres, showed very little differences. The spread of particulates was similar, with the only difference being that there were higher concentrations of particulates, around 4000 rather than 2500, spread over a greater range of A_f values, present when using a laboratory air atmosphere. The differing replicate results may have been related to the backgrounds recorded by the Aspect or the different positions of the ablation locations.

Photomicrographs of the carbon rod craters are shown in Figure 5-10. The craters appeared to be quite similar, however, the ones generated in a laboratory air atmosphere were slightly larger, 0.78 mm, than the ones generated in an argon atmosphere, 0.55 mm

and 0.37 mm. Due to the carbon rod's high melting point, 3675 ºC, the material would have undergone thermal shock. However since it also had a high thermal conductivity of 140 W/mK the heat would not have been retained and the particulates would have quickly fragmented. This is the possible cause behind the fibres.

Figure 5-10: Craters formed on the carbon rod material, in argon (left) and laboratory air (right) atmospheres
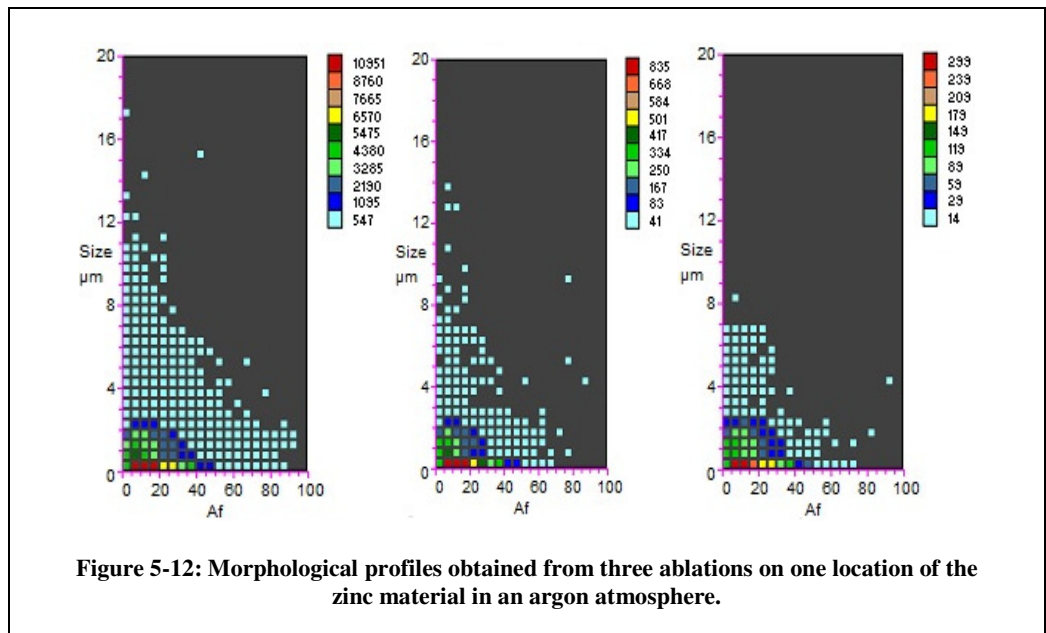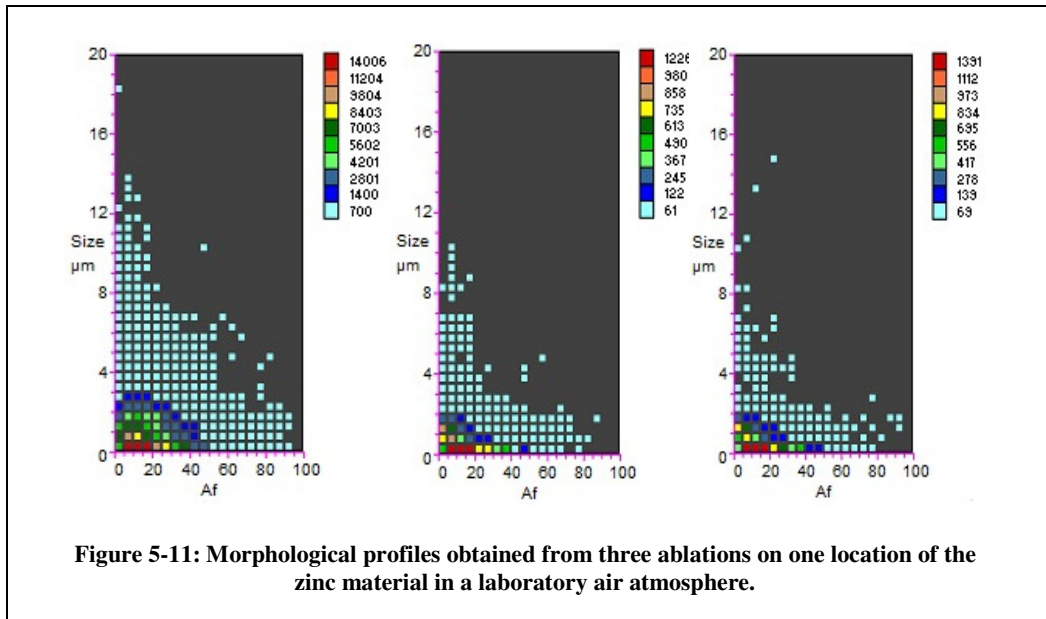
High Purity Zinc

The morphological profiles, obtained from the high purity zinc ablation, differed greatly to those obtained from the carbon rod characterisation. For zinc, a much smaller spread of data was observed with the highest concentrations of particulates present at 0.5 µm and between A_f values of 5 and 20. Generally no particulates were seen which were larger than 3 µm or reported an A_f value greater than 50. This indicated the presence of small spherical particulates, unlike the fibrous particulates seen in the carbon rod morphological profiles. The presence of spherical particulates was most likely due to the material melting, due to its low melting point of 420 ºC, rather than undergoing thermal shock like the carbon rod material.

The laser generation of zinc particulates was undertaken by Gonzalez et al. in 2008.[42] Gonzalez et al. completed the ablation of a zinc SRM using a 266 nm pulsed laser and

collected the laser generated zinc particulates onto substrates before completing characterisation with SEM. When using a femto second laser pulse (150 fs) they generated spherical particulates approximately 0.5 µm in diameter,[42] which corresponded well with the results obtained here.

Similar morphological profiles were obtained for the two replicates in both atmospheres, indicating good reproducibility. In comparison to the carbon rod morphological profiles, the zinc morphological profiles acquired in each of the atmospheres were very similar, although some differences could be viewed in the way the characteristics of the laser generated particulates changed as the number of shots on a single location increased. For example, when using a laboratory air atmosphere the first ablation produced a larger range of particulates than the second and third ablations at the same location. However, when using an argon atmosphere the three profiles obtained when ablating the same location were quite similar, with the most obvious difference being a decrease in the number of particulates, from 10951 to 299. This is shown in Figures 5-11 and 5-12. One possible reason for this is the fact that the argon atmosphere was more controllable than the laboratory air atmosphere. Also, very few background particulates were present for the argon atmosphere, compared to the laboratory air background. This increase in background particulates and the "unstable nature" of the atmosphere for the laboratory air ablations may have altered the morphological profiles obtained for the high purity zinc material.

Figure 5-11: Morphological profiles obtained from three ablations on one location of the zinc material in a laboratory air atmosphere.

Figure 5-12: Morphological profiles obtained from three ablations on one location of the zinc material in an argon atmosphere.

Photomicrographs of the high purity zinc craters are shown in Figure 5-13. The craters generated in the different atmospheres were similar in size, 0.96 mm for argon and 1.2 mm for laboratory air but they looked quite different. When using a laboratory air atmosphere the crater appeared to be more uniform. This may have been due to the thermal conductivity of the ablation atmosphere. Air has a greater thermal conductivity than argon and therefore cooled quicker, leading to a shorter plasma lifetime.[34] This in

turn would have meant that the material was melting for a shorter time period and produced a more uniform crater.
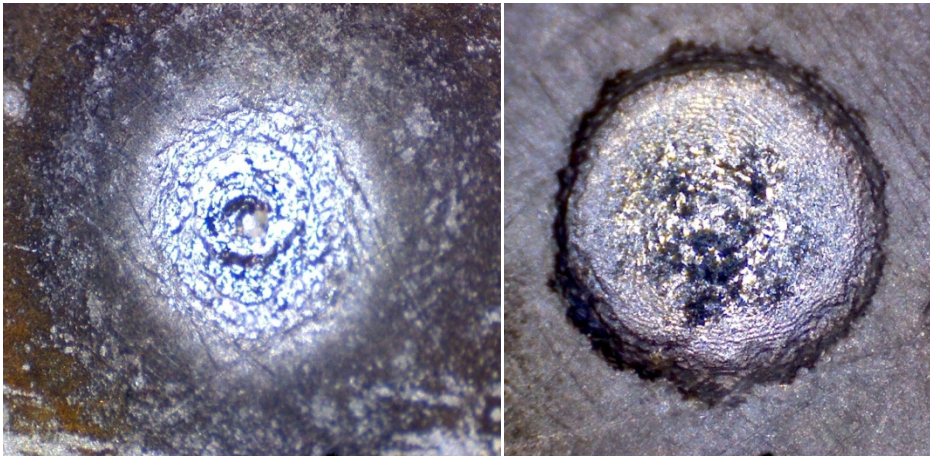

Figure 5-13: Craters formed on the high purity zinc material, in argon (left) and laboratory air (right) atmospheres

Polyethylene

Particulates were present up to 4.5 µm in size in all of the morphological profiles for the polyethylene material, with a proportion of these profiles indicating the presence of particulates up to 7 µm in size. The highest concentration of particulates, 814 particulates for laboratory air and 1182 particulates for argon, was seen at 1.5 µm, with an A_f value of 10, indicating that small symmetrical particulates were the main component of the aerosol generated for this material. This corresponded well with Thompson, Chenery and Brett's[13] findings and the melting point of the material. Thompson, Chenery and Brett found that metallic materials produced small spherical particulates due to melting. This material had a lower melting point (110 ºC) than the high purity zinc material (420 ºC) and it is therefore likely that this material underwent a similar process.

Photomicrographs of the polyethylene craters are shown in Figure 5-14. The crater produced when using an argon atmosphere was twice the size of that produced when
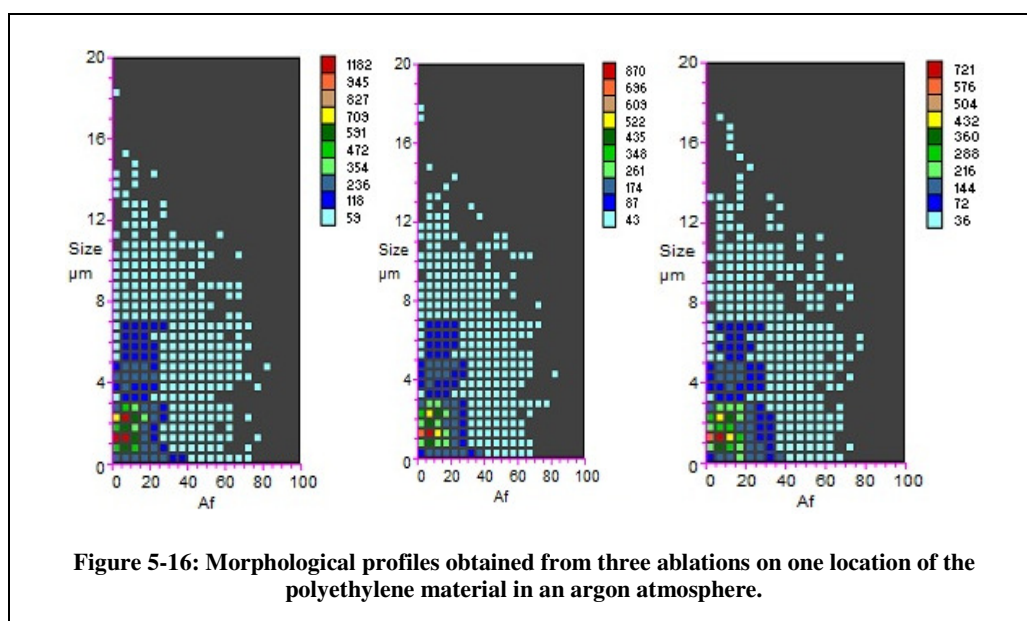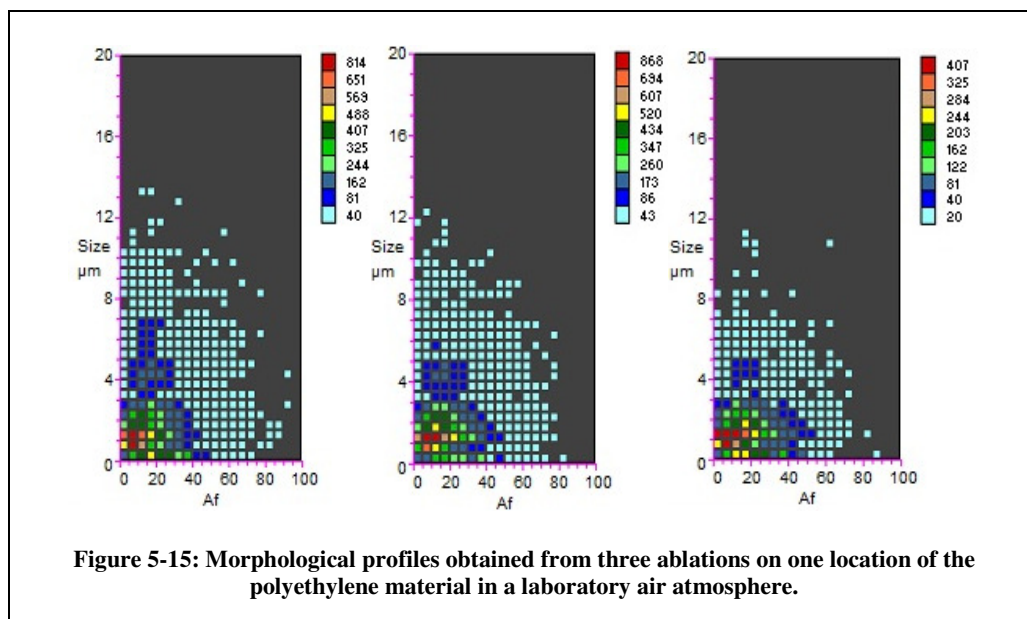
using a laboratory air atmosphere, 1.07 mm and 0.52 mm, respectively. Again, as with the high purity zinc material, the laboratory air crater was more uniform than the argon crater due to a shorter plasma lifetime, melting the material for a shorter time period.

Figure 5-14: Craters formed on the polyethylene material, in argon (left) and laboratory air (right) atmospheres
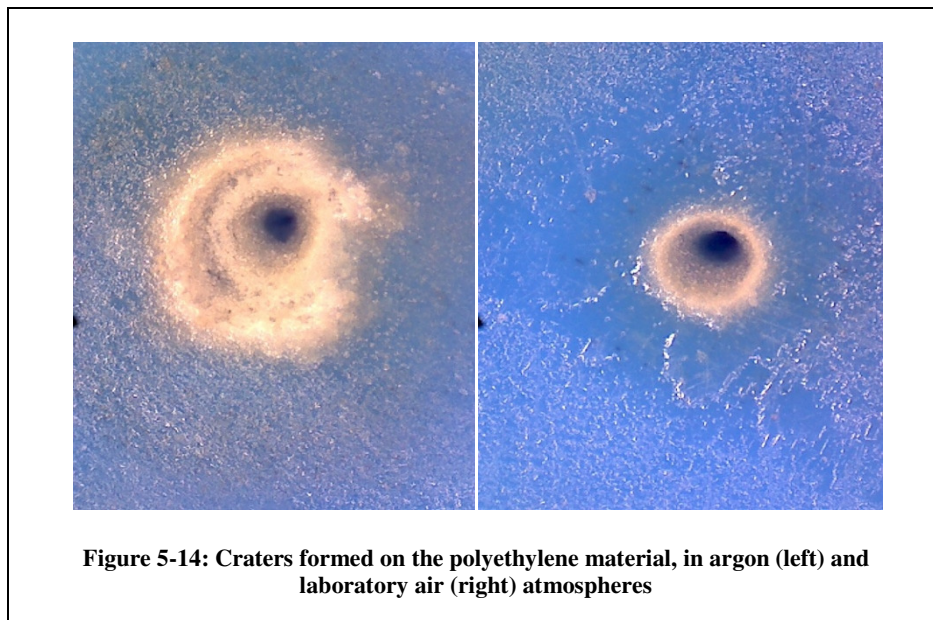
When using the laboratory air atmosphere all of the morphological profiles, including the replicate profiles, generally indicated that no particulates were present within the laser generated aerosol with an A_f value greater than 50. The only three exceptions, showed particulates present at 55 or 60 on the A_f scale. When using an argon atmosphere none of the morphological profiles showed particulates present within the aerosol above 40 on the A_f scale. This indicated that no fibrous particulates were present, as in the carbon rod materials and that a proportion of particulates generated by the ablations were asymmetric, causing the Aspect laser light to be scattered irregularly.

The two replicate morphological profiles obtained were comparable and therefore showed good reproducibility. For both argon atmosphere replicates the three ablations completed on one location showed similar profiles, with the most obvious difference being the decrease in particulate number concentration, from 1182 particulates to 721 particulates, as seen in Figure 5-15. As previously discussed this may have been due to the generation of a crater and the slight defocusing of the laser. When using the

laboratory air atmosphere as more ablations were completed on the same one location, the shape and size of the particulates produced did alter slightly, as seen in Figure 5-16. This indicated that the more controllable argon atmosphere resulted in more reproducible morphological profiles. There was also a smaller variation in the number of particulates, from 814 to 407, rather than 1182 to 721 as was seen for the argon atmosphere.

Figure 5-15: Morphological profiles obtained from three ablations on one location of the polyethylene material in a laboratory air atmosphere.

Figure 5-16: Morphological profiles obtained from three ablations on one location of the polyethylene material in an argon atmosphere.

Carbon Steel

The morphological profiles obtained from the ablation of the carbon steel were similar to the high purity zinc particulate morphological profiles, in that they both showed the presence of small spherical particulates within the laser ablated aerosol. This was due to them both having a metallic nature and generally low melting points. When compared to the high purity zinc profiles the carbon steel morphological profiles consistently showed a high concentration of laser ablated particulates, approximately 800 particulates in both atmospheres, at 1 µm, with an A_f of 10. In some of the morphological profiles large concentrations of particulates were also seen at other sizes and A_f values, but with less consistency. The majority of the obtained profiles showed a small spread of particulates, no greater than 3 µm in size and no higher than 50 on the A_f scale. This indicated the presence of small particles which had some symmetry but that also had faces and edges which were scattering the Aspect laser light irregularly. Morphological profiles obtained both in the laboratory air and argon atmospheres are shown in Figures 5-17 and 5-18, respectively.
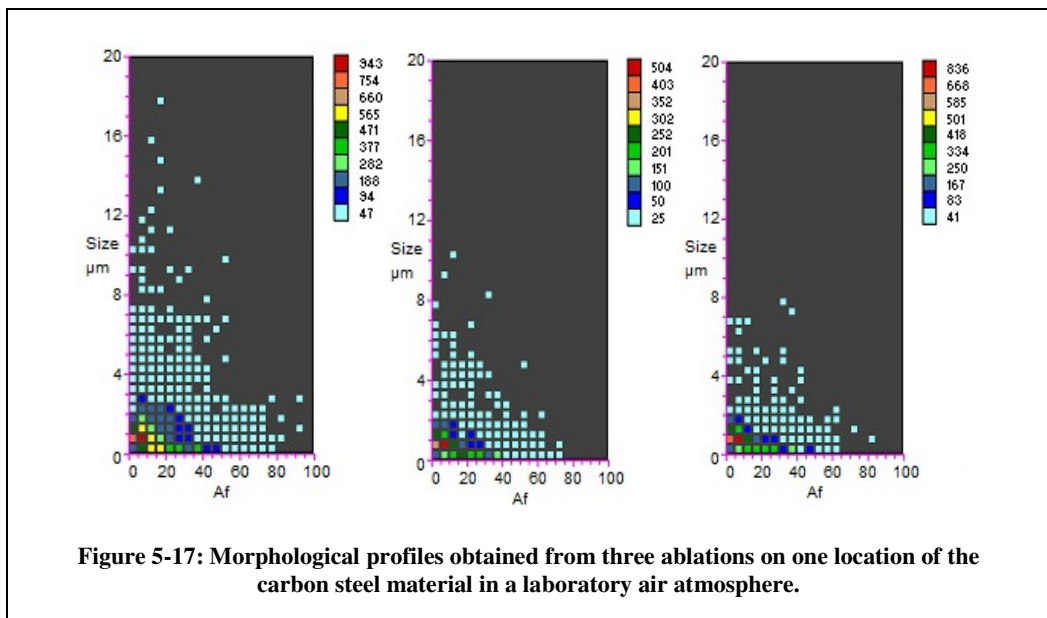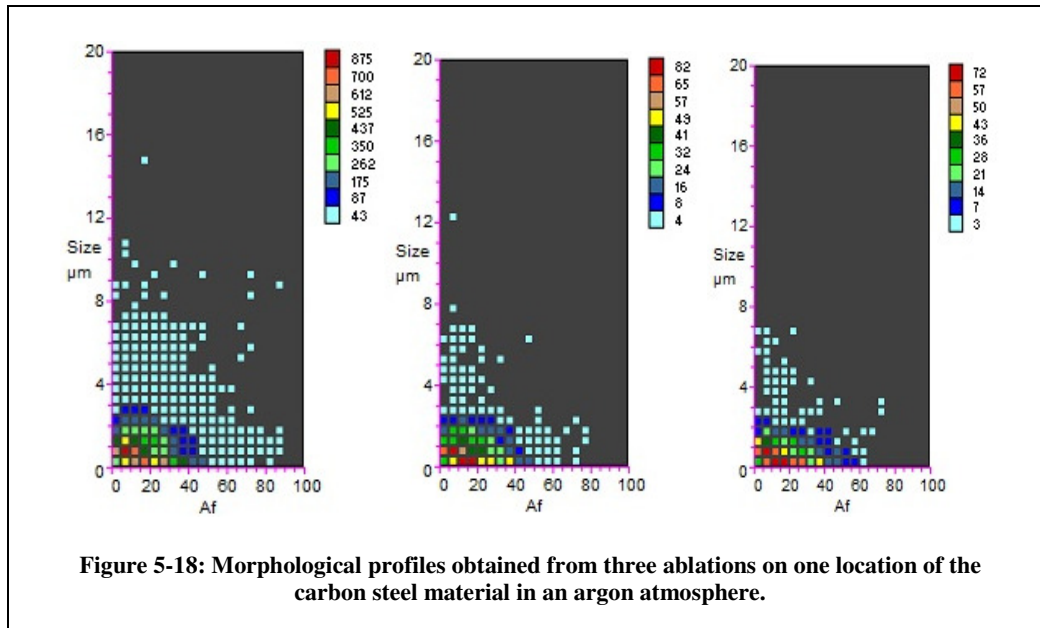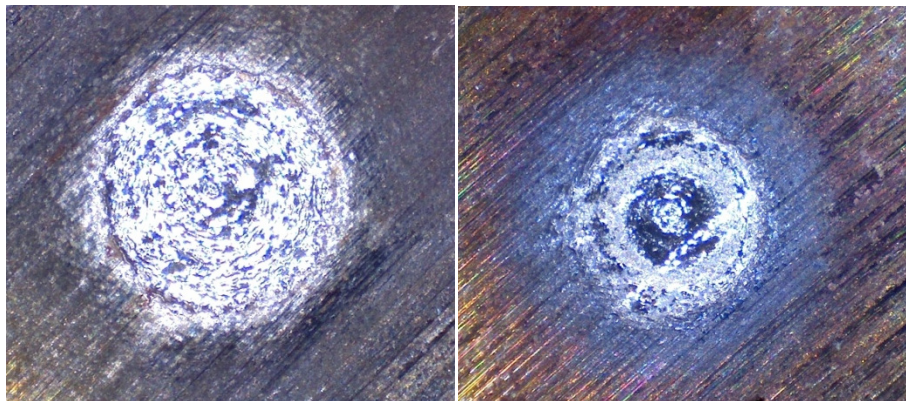

Figure 5-17: Morphological profiles obtained from three ablations on one location of the carbon steel material in a laboratory air atmosphere.

Figure 5-18: Morphological profiles obtained from three ablations on one location of the carbon steel material in an argon atmosphere.

The carbon steel material showed the most variation between replicates. Although most of the laser generated particulates were within the limits previously mentioned the particulate number concentrations differed greatly, especially when using an argon atmosphere (875 particulates to 82 particulates). The differing profiles were a sign of poor reproducibility which was not seen with the other four materials. The major difference between this material and the other four was the varied chemical composition. The carbon steel material contained a greater number of elements than the other three materials, especially trace elements. Although it is not known for definite, this may have been a reason for the differing morphological profiles produced by the ablated carbon steel particulates. Further studies should be completed into other similar materials to confirm this.

Photomicrographs of the carbon steel craters are shown in Figure 5-19. The crater produced in an argon atmosphere was slightly larger (0.93 mm) than that produced in a laboratory air atmosphere (0.70 mm), most likely due to the prolonged plasma lifetime when using an argon atmosphere.

Figure 5-19: Craters formed on the carbon steel material, in argon (left) and laboratory air (right) atmospheres

Boron Nitride

The morphological profiles of the aerosol from the boron nitride, varied depending on the atmosphere. When using a laboratory air atmosphere, some similarities could be seen with the profiles obtained from the ablation of the polyethylene material, however, in the case of the boron nitride a larger spread of particulates was observed. For example, high concentrations of particulates were present between 0.5 and 2.5 µm, with A_f values of 15 to 25. Lower concentrations were seen up to 7 µm and up to 80 on the A_f scale.

When using an argon atmosphere, a much smaller spread of particulates was observed and the morphological profiles obtained were almost identical to the high purity zinc profiles. The main difference was that for boron nitride higher numbers of particulates were characterised. For the boron nitride high particulate concentrations, 15724 particulates for laboratory air and 7779 particulates for argon, were noted at 0.5µm with A_f values of between 10 and 20. Lower concentrations, 1572 particulates for laboratory air and 777 particulates for argon, were generally present up to 3 µm in diameter with A_f values up to 60.

Photomicrographs of the boron nitride craters are shown in Figure 5-20. The two craters were quite different in both shape and size. The crater formed in an argon atmosphere was 0.83 mm in diameter and quite spherical, whilst the crater generated in a laboratory air atmosphere was 1.02 mm in diameter and oval in shape. The boron nitride material would have undergone thermal shock, due to its high melting point of 3000 ºC, therefore causing the material to fragment and chip rather than produce spherical particulates.
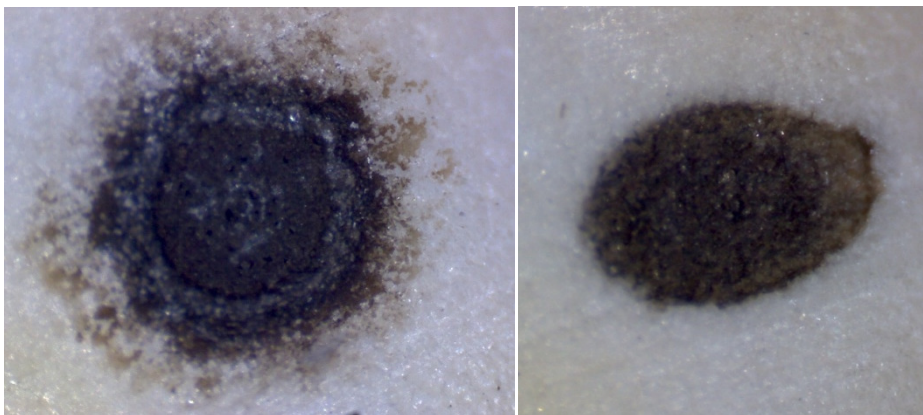
Figure 5-20: Craters formed on the boron nitride, in argon (left) and laboratory air (right)

As more ablations were completed for a single location, in either atmosphere, few differences were seen in the morphological profiles. This can be seen in Figures 5-21 and 5-22. The morphological profiles obtained from the replicate analyses were also comparable to the original profiles, despite a change in the humidity within the laboratory. The only slight difference was a change in the number of aerosol particulates characterised, from 15724 to 16209 for laboratory air and from 7779 to 5408 for argon, which was also seen for the other four materials.

Figure 5-21: Morphological profiles obtained from three ablations on one location of the boron nitride in a laboratory air atmosphere.

Figure 5-22: Morphological profiles obtained from three ablations on one location of the boron nitride in an argon atmosphere.
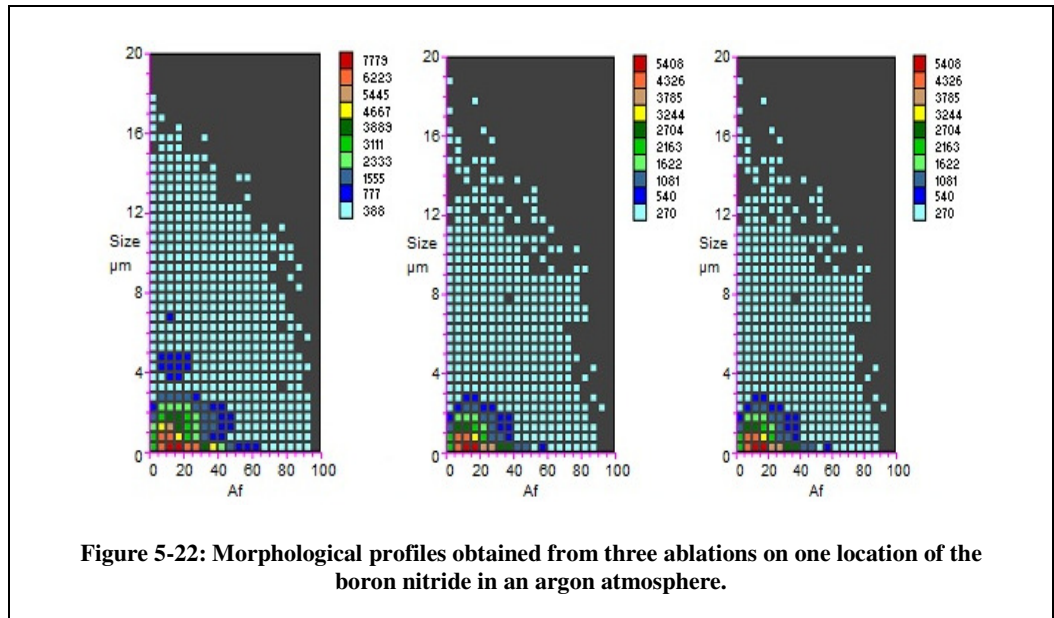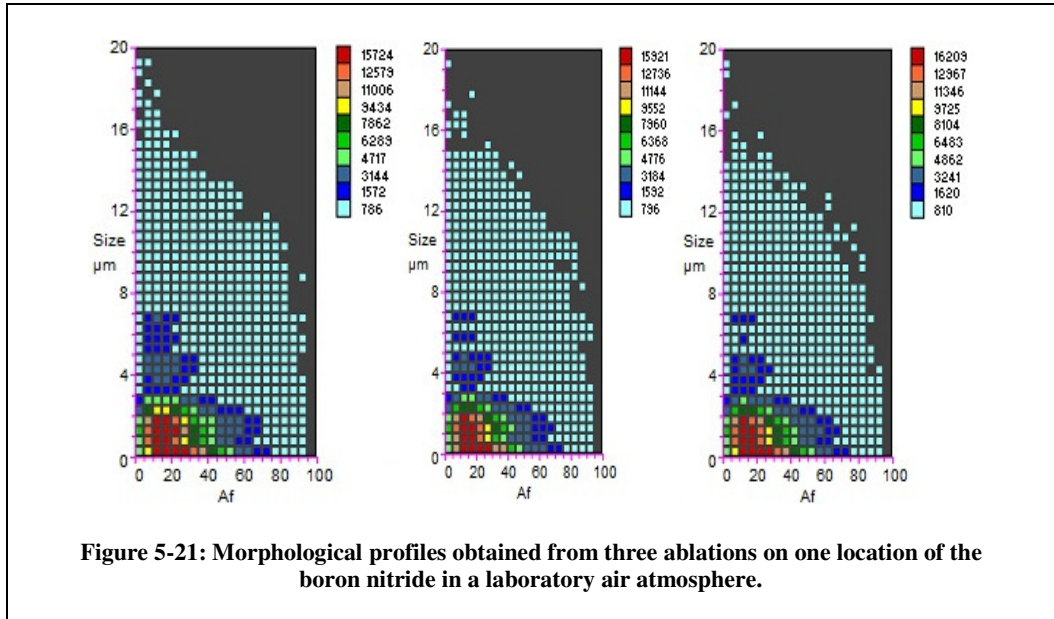
Glass

Ablation of the glass material was unsuccessful. The glass material was transparent to the laser light[43] and therefore did not absorb it. This meant that no particulates were generated and hence, no morphological profiles were obtained from this material.

In summary, morphological profiles have been successfully obtained for five of the six materials and the results are presented in Table 5-8. For the carbon rod, high purity zinc and the boron nitride, the size of the largest concentrations of particles was 0.5 µm whereas the equivalent sizes for the polyethylene and the carbon steel were 1.5 µm and 1 µm, respectively. Relatively high concentrations of spherical particulates were seen for high purity zinc, polyethylene and carbon steel whereas the boron nitride indicated high concentrations of asymmetric particulates. Unlike any other material the carbon rod material yielded high concentrations of fibrous particulates. Some of these results are consistent with the findings of Thompson, Chenery and Brett, 1990.[13] Both metallic materials, high purity zinc and carbon steel, produced spherical particulates, whilst boron nitride, a brittle material generated asymmetric particulates. The other two materials, the carbon rod and the polyethylene did not fall within the descriptions of the three processes for laser ablation, discussed in Section 5.1, however these processes could be used to help explain the results. The carbon rod material was not metallic and had a high melting point, 3765 º C, therefore undergoing thermal shock. The high thermal conductivity meant that the material did not hold the heat and therefore fibrous particulates were generated as the laser interacted with the material. This also explained why the two different materials containing carbon, carbon rod and carbon steel, generated different shaped particulates. The metallic content of the carbon steel had caused it to melt whereas the carbon rod was not metallic and did not melt. The polyethylene was a non brittle, non metallic material. It would have melted easily like the metallic materials, having a melting point of 110 ºC, thus producing spherical particulates.

| Material	Size of largest concentration	Shape of largest concentration
Carbon rod	0.5 µm	Fibrous particulates
High purity zinc	0.5 µm	Spherical particulates
Polyethylene	1.5 µm	Spherical particulates
Carbon steel	1 µm	Spherical particulates
Boron nitride	0.5 µm	Asymmetric particulates
Glass	-	-

Table 5-8: Summary of the morphological characterisation of the six materials, using the LA (1064 nm)-Aspect method

The profiles have been compared with each other and their reproducibility discussed. It has been found that, in general, an argon atmosphere gave place to more stable results compared to that for laboratory air. Analysis of diverse materials with different chemical compositions could be completed in future to confirm this. The morphology of the particulates generated when using the LA (266 nm)-Aspect method will now be discussed as well as the method development for this coupling.

5.3.4 LA (266 nm)-Aspect Method Development

Method development for the LA (266 nm)-Aspect method was completed by varying each of the key experimental parameters, as detailed in Table 5-6. The carbon steel and an argon atmosphere were used for all experiments. The number of particulates measured by the Aspect was used to compare the different parameter sets. The most reproducible particulate numbers were obtained from only one of the parameter sets and therefore that set was chosen for further investigation. The parameters were 500 laser shots at 100 percent energy, with a repetition rate of 10 Hz (500 laser shots in 50 seconds). The argon flow rate was 1.7 L/min at a pressure of 0.5 bars.

Using the chosen parameters, six ablations were completed for one location of the carbon steel. Results are presented in Figure 5-23. Apart from the first ablation, the particulate number generally remained quite stable (generally around 1200 particulates) and a high concentration of particulates at 0.5 µm and an A_f of 15 to 25 was noted for all six ablations. This indicated good reproducibility and these parameters were thus chosen for the ablation of the six materials using the LA (266 nm)-Aspect method.

Figure 5-23: Contour plots of ablated material, ablation one, top left, to ablation six, bottom right
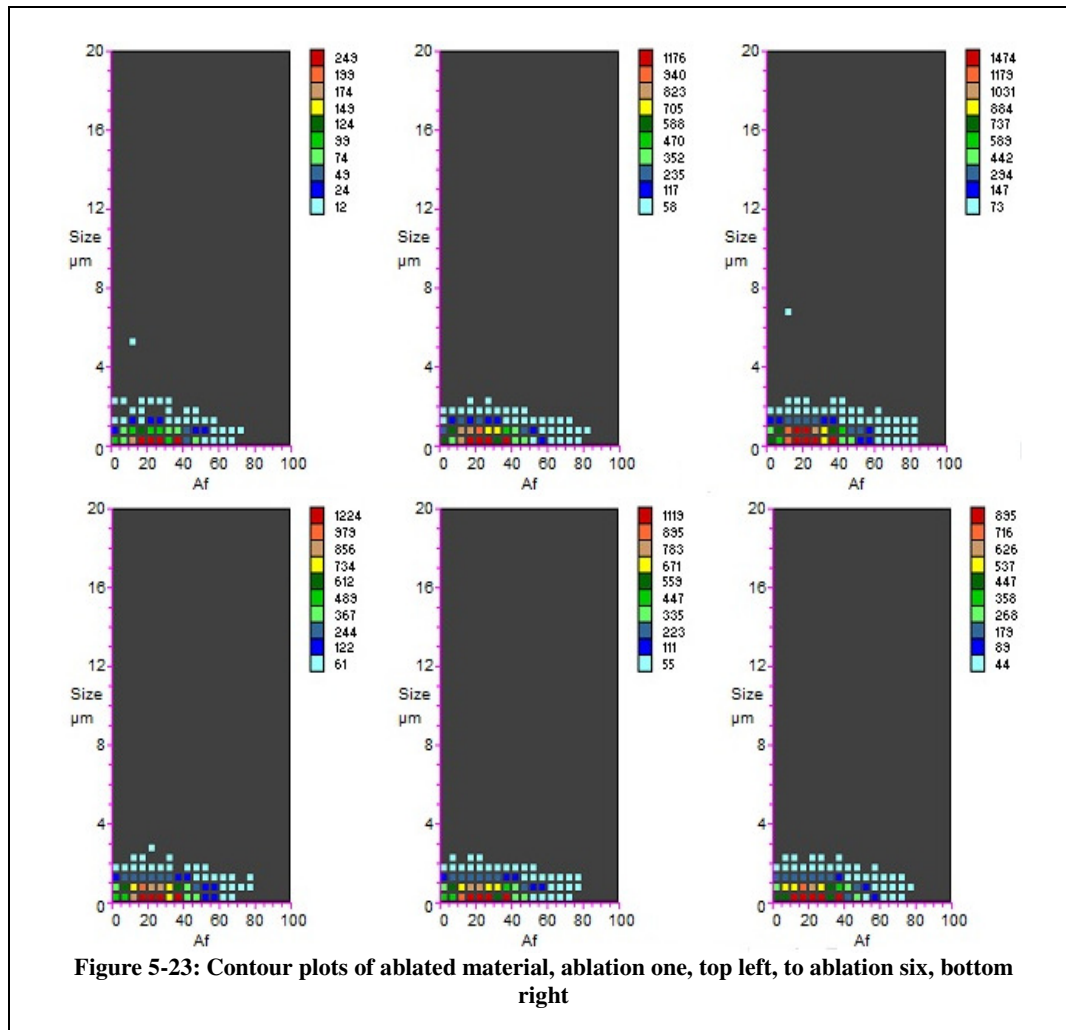
5.3.5 *Morphological Analysis Using the LA (266 nm)-Aspect Method*

Following completion of the method development and after selection of the operating parameters, 500 laser shots at 100 percent energy (7.5 mJ), with a repetition rate of 10

Hz (500 laser shots in 50 seconds), the ablation of the six materials and consecutive characterisation of the resulting particulates contained within the generated aerosols was performed. Morphological profiles for four of the materials were obtained for an argon atmosphere, however, a laboratory air atmosphere was used for both the polyethylene and glass materials because the laser unit developed an irreparable fault before ablation of these two materials, under argon, could be finished.

In general the transit time for the generated particulates was between eight and ten seconds. The transit time was determined by recording the time at which the laser was fired and then examining the temporal plot, obtained from the Aspect software, to see at what time particulates were detected by the Aspect. The transit time was the difference between the two recorded times. The most likely reason for the variation in transit times for different materials was the size and mass of the generated particulates. Lighter and smaller particulates would take less time to reach the Aspect than larger and heavier particulates, following ablation.

Photomicrographs of the craters formed during ablation were also taken and are shown alongside their relevant morphological profiles which will be examined separately for each of the six materials.

Carbon rod

The carbon rod morphological profiles obtained when using the LA (266 nm)-Aspect method, showed some similarities with one of the morphological profiles obtained when using the LA (1064 nm)-Aspect method with an argon atmosphere. However the morphological profiles could definitely be distinguished from each other. The spread of particulates characterised, and therefore generated, when using the LA (266 nm)-Aspect technique was much smaller than when using the LA (1064 nm)-Aspect method.

In general no particulates exceeded 2 µm in size and were no greater than 65 on the A_f scale. The highest concentrations of particulates (6132 to 2935 for the three ablations) were present at 1 µm with A_f values of between 20 and 30, indicating the presence of larger and more spherical particulates than characterised previously. This disagrees with what was found by Guillong, Horn and Günther in 2003.[33] They found that using a laser of lower wavelength, 193 nm, produced particulates which were smaller in diameter than those produced by lasers with higher wavelengths of 213 nm and 266 nm. To confirm whether the results obtained in this study were analogous with those obtained by Guillong, Horn and Günther and to also allow more comparisons to be undertaken, further ablations should be completed.

Overall, there was a slight decrease in the number of particulates characterised over the three ablations, from 6132 to 2935, but in general the particulate shape and size remained the same. Three different locations on the carbon rod were ablated. The morphological profiles obtained from the replicates were very similar to those shown in Figure 5-24, indicating excellent reproducibility.

Figure 5-24: Morphological profiles obtained from three ablations on one location of the carbon rod material in an argon atmosphere using the LA (266 nm)-Aspect method
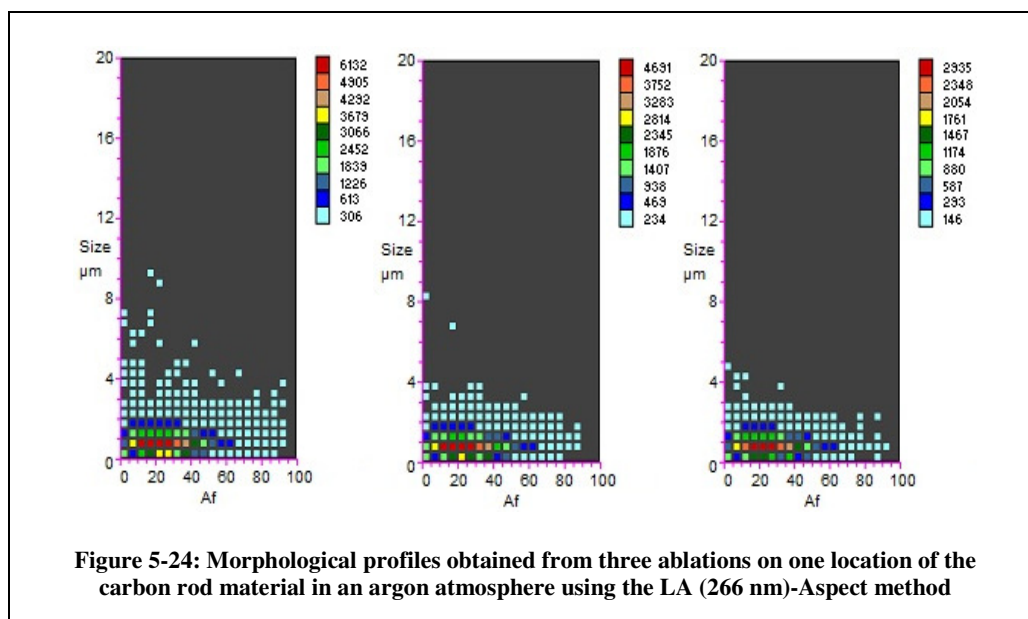
A photomicrograph of the carbon rod craters is shown in Figure 5-25. The craters were similar in shape and size to each other, between 0.20 mm and 0.30 mm, but were

smaller in diameter than those generated when using the LA (1064 nm) laser, 0.37 mm to 0.78 mm. This was possibly due to the lower energy of the laser which was used and would have influenced the overall laser fluence.
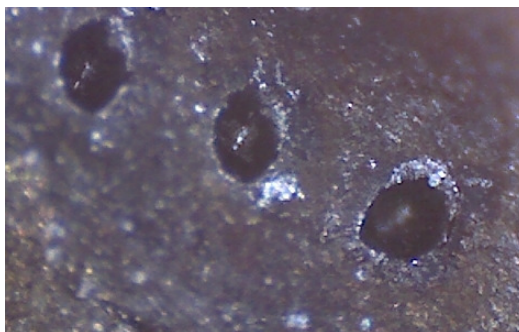
Figure 5-25: Craters formed on the carbon rod material, in an argon atmosphere

High Purity Zinc

Morphological profiles obtained from the ablation of the high purity zinc material and subsequent characterisation of the resulting aerosol are shown in Figure 5-26. The profiles differ greatly from those obtained for the carbon rod when using the LA (266 nm)-Aspect method, however they showed some similarities with the high purity zinc profiles obtained when using the LA (1064 nm)-Aspect method.
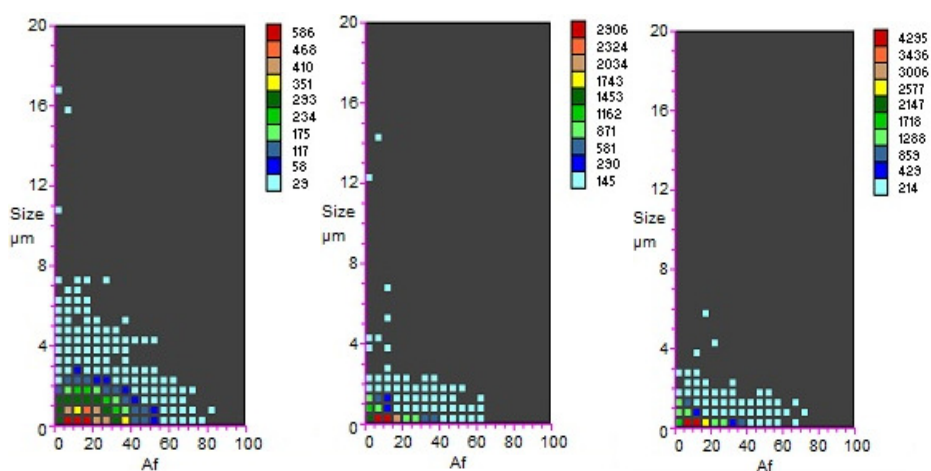
Figure 5-26: Morphological profiles obtained from three ablations on one location of the zinc material in an argon atmosphere using the LA (266 nm)-Aspect method

As with the morphological profiles shown in Figure 5-13, high concentrations of particulates were seen at 0.5 µm, with A_f values of 10 to 15 for all three ablations on the same location. As more ablations were completed the spread of particulates decreased and the number of particulates characterised increased, from 586 to 4295. This was also seen for ablation at the other two locations on the zinc material. These results corresponded with the findings discussed by Jeong et al. in 1999.[25] Using a 266 nm Nd:YAG laser, they fired five single pulse, each of 5 ns in length, onto a glassy material in an argon atmosphere. They found that the first ablation produced a smaller number of particulates than any other further ablations on the same position and that ideally the material should be conditioned prior to ablation to allow representative results to be obtained.[25]

A photomicrograph of one of the high purity zinc craters is shown in Figure 5-27. The crater shown was 0.33 mm in diameter, again a lot smaller than the ones generated when using the LA (1064 nm)-Aspect method, which were between 0.96 mm and 1.2 mm. This was most likely due to the decreased energy of the laser used, 7.5 mJ compared with 105 mJ which would have affected the overall laser fluence, therefore causing the laser to interact differently with the material.[44]
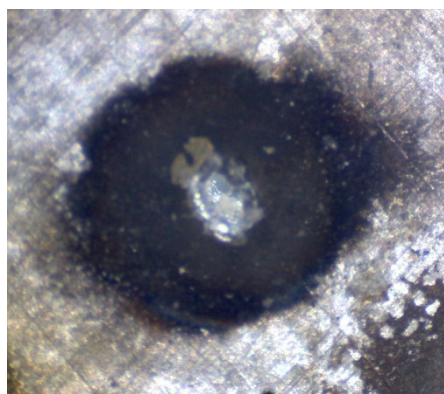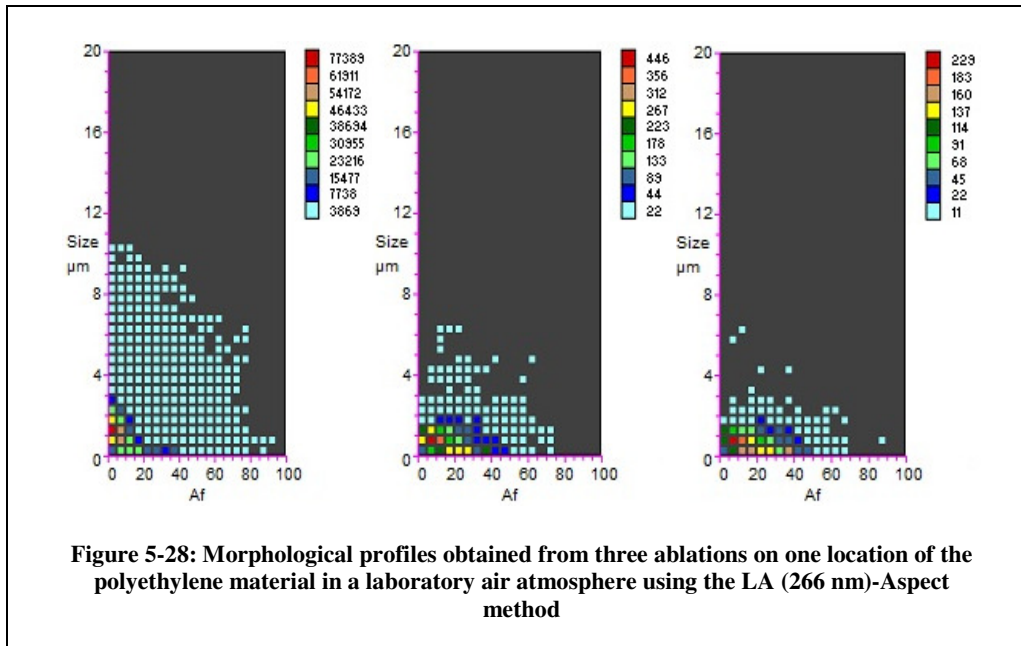

Figure 5-27: A crater formed on the high purity zinc material, in an argon atmosphere

Polyethylene

The polyethylene morphological profiles, shown in Figure 5-28, were obtained in a laboratory air atmosphere. The morphological profiles varied greatly from those obtained when using the LA (1064 nm)-Aspect method and were also dissimilar to any other profiles obtained when using the LA (266 nm)-Aspect method. The morphological profile obtained from the first ablation indicated the presence of particulates with different characteristics to those seen in the profiles from the second and third ablations. For the first ablation a high concentration of particulates, 7738, could be seen at 1.5 µm with an A_f of 5, which indicated the presence of very small, spherical particulates. However for the second and third ablations on the same location the particulates became less spherical with high concentrations, 446 particulates and 289 particulates, respectively, present at 1 µm and an A_f value of 10. The spread of particulates also changed. Instead of a wider range of sizes (0.5 µm to 3 µm) over a relatively narrow spread of A_f values (0 to 40), particulates with a larger spread of A_f values (0 to 50) were seen over a smaller size range (0.5 µm to 2 µm). These results indicated that during the first ablation the material was melted, generating spherical particulates, for the second and third ablations the material was starting to fragment slightly rather than melt, causing less spherical particulates to be generated. This linked in well with what was described by Jeong et al.[25], who found that the particulates generated from the second and any subsequent ablations differed to those generated by the first ablation.

Figure 5-28: Morphological profiles obtained from three ablations on one location of the polyethylene material in a laboratory air atmosphere using the LA (266 nm)-Aspect method

A photomicrograph of the polyethylene craters is shown in Figure 5-29. The craters were both 0.24 mm in diameter, indicating good reproducibility, however, as with the carbon rod and high purity zinc materials they were smaller than the craters generated when using the LA (1064 nm)-Aspect method, which were between 0.52 mm and 1.07 mm, due to the lower energy of the laser used.

Figure 5-29: Craters formed on the polyethylene material, in a laboratory air atmosphere
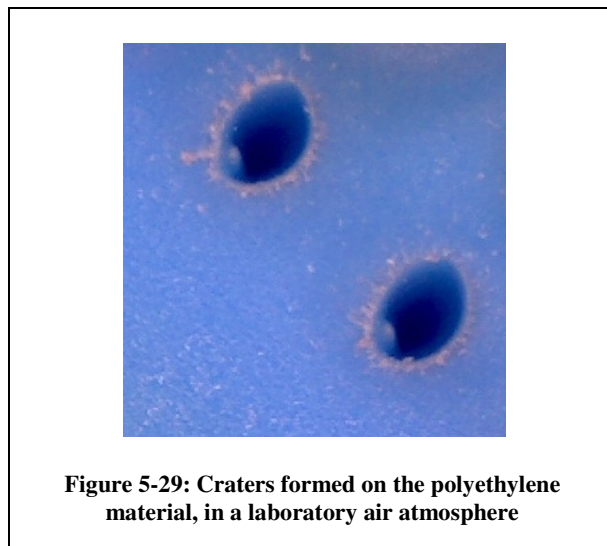
Carbon Steel

Morphological profiles obtained for the characterisation of the carbon steel indicated the presence of small particulates, between 0.5 µm and 1.5 µm, with a range of shapes, A_f values being from 0 up to 65. For all three of the morphological profiles, shown in Figure 5-30, high concentrations of particulates (236, 582 and 768 particulates) were present at 0.5 µm with A_f values of between 20 and 30. This demonstrated that a large proportion of particulates present within the laser generated aerosol were asymmetric, with faces and edges, which were scattering the Aspect laser light irregularly. The morphological profiles obtained for the ablations completed on the other two locations on the same material were comparable to those shown here, therefore indicating good reproducibility.

Some similarities could be seen between the morphological profiles obtained here and those obtained when using the LA (1064 nm)-Aspect method, especially the third profile shown in Figure 5-18. However, the profiles were easily distinguishable from each other. This may have been due to the chemical composition of the carbon steel material. Each of the many elements present would have interacted differently to ablation by the laser. This fact, as well as the lower energy used would have affected the shape and the size of the particulates generated overall.

Figure 5-30: Morphological profiles obtained from three ablations on one location of the carbon steel material in an argon atmosphere using the LA (266 nm)-Aspect method
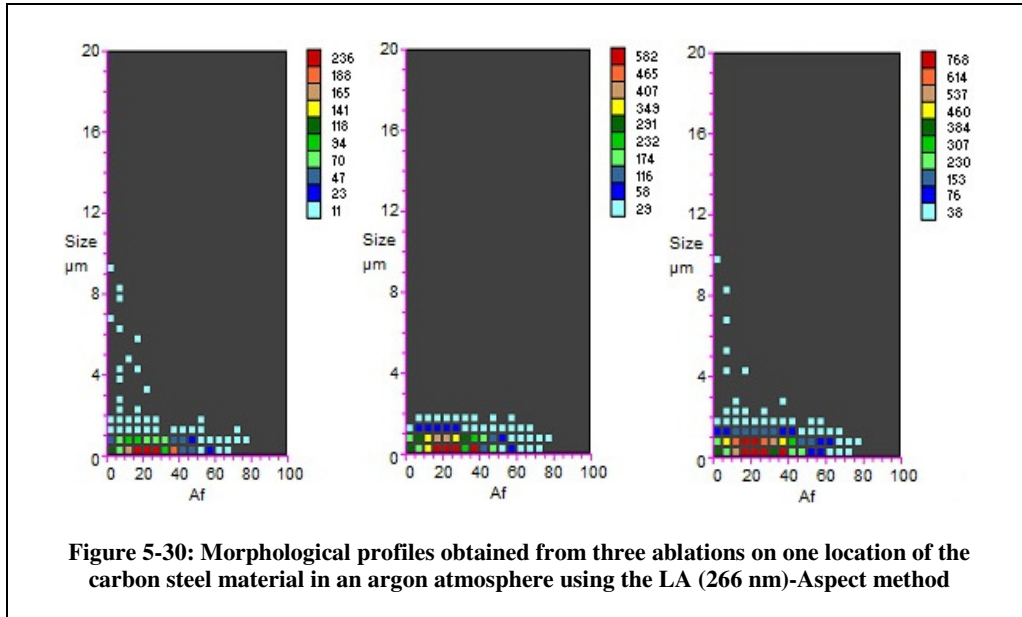
A photomicrograph of the carbon steel craters is shown in Figure 5-31. Both craters were the same size, 0.26 mm, indicating excellent reproducibility between the different ablations. Again these were smaller than those obtained when using the LA (1064 nm)-Aspect method, due to a decreased laser fluence, which affected the laser material interaction.[44]

Figure 5-31: Craters formed on the carbon steel material, in an argon atmosphere
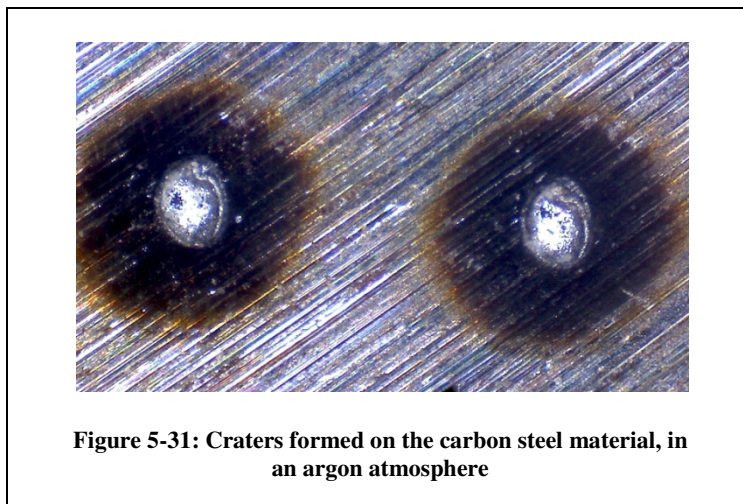
Boron Nitride

The morphological profiles for boron nitride, Figure 5-32, showed some resemblance to the profiles obtained when using the LA (1064 nm)-Aspect method, as shown in Figure 5-22. The shapes and sizes of the characterised particulates were similar, 0.5 µm in size and with A_f values of between 15 and 20, indicating large concentrations of small asymmetric particulates. The morphological profiles obtained when using the LA (266 nm)-Aspect method did show a slightly larger spread of particulates, with a larger range of sizes at higher A_f values. This indicated that the high melting point of the material (3000 ºC), caused it to undergo thermal shock rather than melting. Therefore when using a laser with a lower wavelength and therefore a lower penetration depth, the particulates which were produced had a range of shapes due to the chipping and fragmenting of the same position on multiple occasions.

Figure 5-32: Morphological profiles obtained from three ablations on one location of the boron nitride in an argon atmosphere using the LA (266 nm)-Aspect method
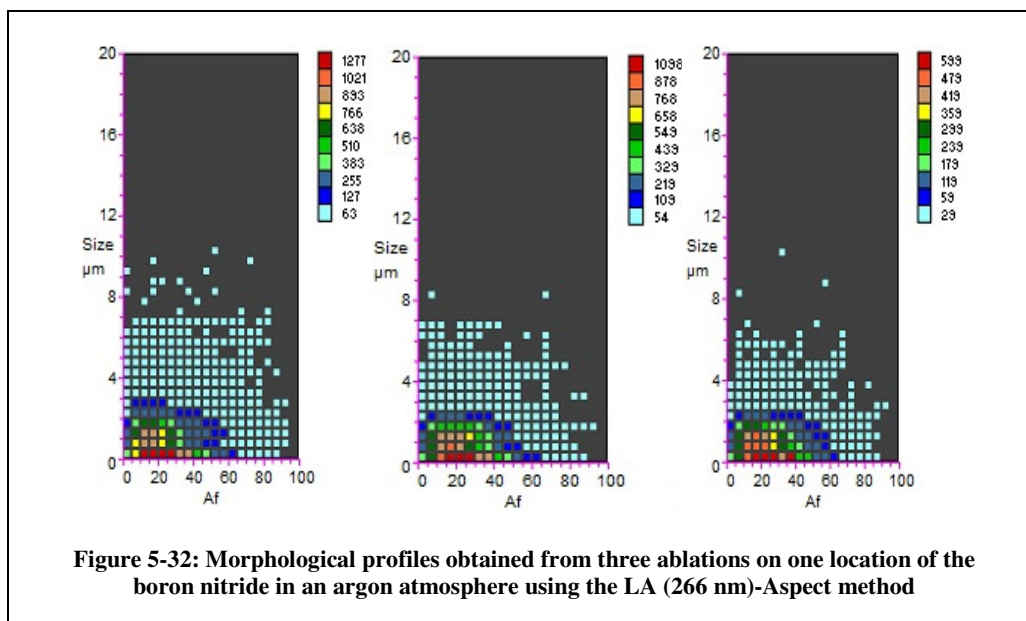
For the three ablations, performed at the same location, there was a general decrease in particulate number (from 1277 to 599), which was also noted for most of the other materials, but not a change in the particulate shape and size, indicating good reproducibility. A photomicrograph of the boron nitride craters is shown in Figure 5-33. Both craters were much smaller than those generated when using the LA (1064 nm)-

Aspect method, at 0.24 mm and 0.30 mm, due to the decreased laser energy. They were a similar shape to those seen when using the laboratory air atmosphere. This indicated that the 266 nm laser possibly had a short plasma lifetime.
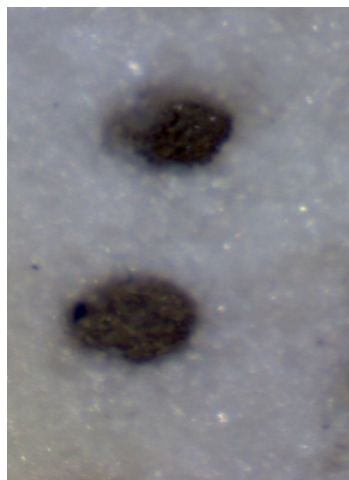
Figure 5-33: Craters formed on the boron nitride, in an argon atmosphere

Glass

The LA (266 nm)-Aspect method permitted successful ablation of the glass material in a laboratory air atmosphere. This indicated that the energy of the LA (266 nm) laser was absorbed by the glass material, unlike when using the LA (1064 nm) laser. Since no morphological profiles for the glass material were obtained when using the LA (1064 nm)-Aspect method comparisons cannot be made between the results from each method.

The morphological profiles obtained, from the three ablations on one location, are shown in Figure 5-34. As more ablations were completed on the same location the number of particulates decreased, from 64166 to 1182, and their shape and size changed quite dramatically. The first ablation indicated a very small spread of particulates, with a high concentration (64166) of spherical particulates present at 1.5 µm. The morphological profiles from the second and third ablations, completed on the same location, both had a much wider spread of particulates with high concentrations of

particulates (2426 and 1182, respectively) at 1 µm with A_f values of 10 to 20. This may have been due to the first ablation conditioning the surface and therefore the particulates from the first ablation may not have been representative of the actual material. No replicate locations were ablated on the glass material and therefore it is not possible to discuss the reproducibility of the results.

Figure 5-34: Morphological profiles obtained from three ablations on one location of the glass material in a laboratory air atmosphere using the LA (266 nm)-Aspect method
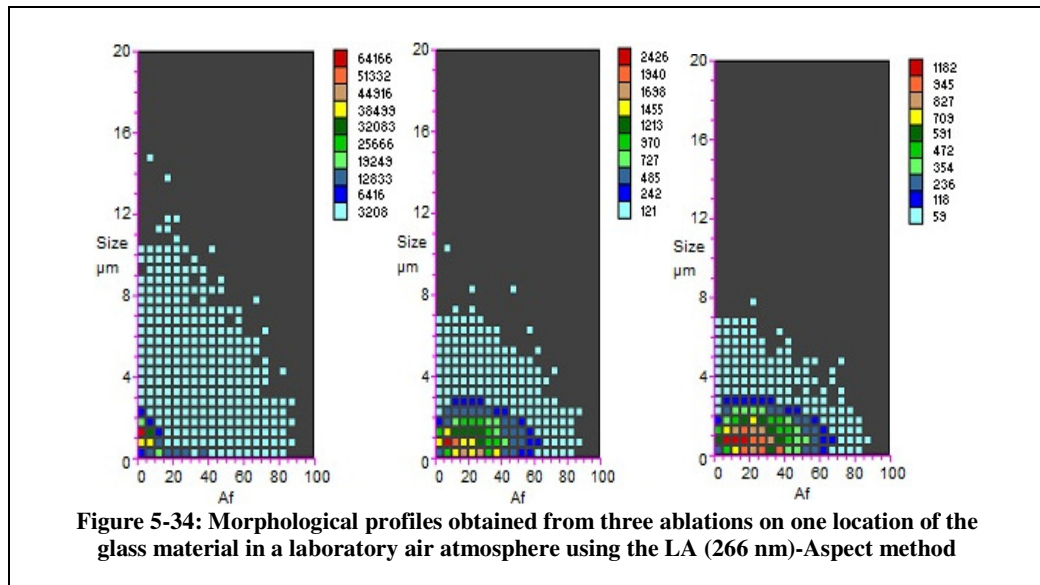
The LA (266 nm)-Aspect method allowed morphological profiles of the laser generated particulates to be obtained for all six materials, mainly using an argon atmosphere. Different profiles were obtained for each of the different materials, demonstrating that the materials all responded differently to the laser ablation process. For example, some of the materials, high purity zinc and boron nitride, produced profiles which were similar to those obtained when using the LA (1064 nm)-Aspect method, however, other materials, such as the polyethylene and the carbon steel, produced profiles which were different to those obtained previously. Nevertheless, this method did allow morphological profiles to be obtained for the glass, although some further studies are needed for this material to determine the reproducibility of the results. No photomicrographs were obtained for the glass material.

The overall results are tabulated in Table 5-9, alongside the results obtained from the use of the LA (1064 nm)-Aspect method. Three materials, the high purity zinc, the carbon steel and boron nitride, reported high concentrations of generated particulates at 0.5 µm, with the other three, the carbon rod, polyethylene and glass, materials reporting high concentrations at 1 µm. Apart from the high purity zinc, the polyethylene and the glass materials, which showed a presence of spherical particulates, all other materials indicated that asymmetric particulates were generated by ablation.

The results indicated that the high purity zinc and the polyethylene were readily melted, generating spherical particulates, whilst the boron nitride underwent thermal shock, resulting in the generation of asymmetric particulates. The production of asymmetric particulates by the carbon rod material was partially expected. Although no fibrous particulates were generated, as seen for the LA (1064 nm)-Aspect method, the particulates did have a large range of A_f values, 0 to 60, indicating that the fibrous nature of the particulates could still be observed. As discussed previously the dominant process for the carbon steel was a thermal shock event rather than melting, to generate non spherical particulates. The majority of the glass' generated particulates were asymmetric, indicating that the material also underwent thermal shock. This was to be expected as the glass was a non metallic, brittle material.

Material	Size of largest concentration: LA (266 nm)	Shape of largest concentration: LA (266 nm)	Size of largest concentration: LA (1064 nm)	Shape of largest concentration: LA (1064 nm)
Carbon rod	1 µm	Asymmetric particulates	0.5 µm	Fibrous particulates
High purity zinc	0.5 µm	Spherical particulates	0.5 µm	Spherical particulates
Polyethylene	1 µm	Spherical particulates	1.5 µm	Spherical particulates
Carbon steel	0.5 µm	Asymmetric particulates	1 µm	Spherical particulates
Boron nitride	0.5 µm	Asymmetric particulates	0.5 µm	Asymmetric particulates
Glass	1 to 1.5 µm	Mix of spherical and asymmetric particulates	-	-

Table 5-9: Summary of the morphological characterisation of the six materials, using both LA-Aspect methods

5.4 Main Findings

This work has allowed the characterisation of aerosols generated from the laser ablation of six different materials using two lasers of different wavelengths, 1064 nm and 266 nm. Two different ablation atmospheres were also compared when using the LA (1064 nm)-Aspect method.

For the carbon rod, the high purity zinc and the polyethylene materials the most reproducible morphological profiles were obtained when using an argon atmosphere. The boron nitride showed good reproducibility in both atmospheres and the carbon steel material gave relatively poor reproducibility in both atmospheres. This indicated that an argon atmosphere was preferred from the standpoint of achieving reproducible ablation profiles, as was hypothesised in Section 5.1.

The laser generated aerosols generally produced different morphological profiles. This was partly due to the different physical properties, structures and chemical compositions of the materials. The metallic materials tended to produce spherical particulates due to melting of the material being a dominant process during ablation, whilst the boron nitride produced asymmetric particulates due to the fragmentation of the material. The soft nature of the polyethylene caused it to melt and therefore produce spherical particulates whilst the carbon rod, a non metallic and soft material, but with relatively high melting and boiling points, produced fibrous particulates.

The LA (266 nm)-Aspect method provided the opportunity to clarify whether the morphological profiles of each material were affected by the wavelength of the laser used for ablation. For the high purity zinc, polyethylene and boron nitride materials the morphological profiles obtained when using the two different laser methods were very similar, although for the carbon rod and carbon steel differences in the shape and size of

the generated particulates were evident in their respective profiles. This indicated that for these two materials it was possible that the wavelength of the laser affected the morphology of the laser generated particulates.

In general the majority of the particulates generated were quite similar in size to the particulates generated when using the LA (1064 nm) laser. However, a number of the materials reported large numbers of particulates with a diameter of 0.5 µm. This could indicate that there were also a large proportion of particulates below 0.5 µm in size and this could be where the difference in laser wavelength could be seen. To confirm this further studies will be completed using an ELPI.

Photomicrographs were obtained for five of the six materials, excluding glass. The photomicrographs allowed the craters to be fully examined and their diameters measured. In general differences were seen between the two atmospheres when using the LA (1064 nm)-Aspect method. This was most likely due to the differing thermal conductivities of the gases which lead to a shorter plasma lifetime when using a laboratory air atmosphere.[34] Good reproducibility was seen when using the LA (266 nm)-Aspect method with similar sized craters generated for replicate ablations. However all of the generated craters were smaller when using the lower wavelength laser. This was most likely due to the lower energy of the laser used, which would have also decreased the laser fluence and affected the interaction between the laser and the material. Future work should allow comparisons of lasers with more similar energies to confirm whether this parameter may have affected the overall crater size and therefore the shape and size of the generated particulates.

This research has demonstrated that the experimental systems configured have for the first time been used to study the morphological characteristics of laser generated aerosols. The shape and size of particulates generated by laser ablation may now be

easily characterised using either of the methods discussed within this chapter. The morphological profiles which were obtained also indicated that the ablation of a material did not just produce small spherical particulates but, for example, when ablating high purity carbon, can generate fibrous particulates. This was earlier shown by Thompson, Chenery and Brett[13] who found that the nature of a material, such as whether it was metallic or brittle, could influence the shape of the particulates generated through laser ablation.

The LA-Aspect approach could be very useful when characterising an unknown material, as well as determining how a material may react to undergoing laser ablation since both methods provide the ability to determine particulate number, shape and size distributions simultaneously in a short space of time. If ablation was being undertaken to produce particulates for analysis, by ICP for example, it would be useful to know the size of the particulates, which would be generated by the laser, as this may affect the overall analysis, as pointed out by Guillong, Horn and Günther in 2003.[33] They found that smaller particulates allowed more stable spectra to be obtained compared to the spectra obtained when larger particulates were analysed by the ICP.[33]

In future the characterisation of more materials, with varying chemical and physical compositions should be completed, whilst also completing more replicate analyses of the materials discussed within this chapter. Detailed studies on how the laser fluence could affect particulate morphology, together with research into femto second lasers, which are being increasingly used in analytical and material science, should also be completed. This would provide a more complete understanding of how different materials interact with high energy laser radiation as well as an insight into the composition of the particulates which can be generated.

The final stage in this work is to complete the coupling of the LA (1064 nm) unit to the

ELPI. The laser generated particulates can then be analysed in real time as well as being

collected onto substrates This will allow the chemical composition of the particulates to

be determined as well as allowing gravimetric analysis to be completed.

5.5 References

1.   R. Thomas, *Spectroscopy*, 2002, **17**, 26-33.
2.   R. E. Russo, X. Mao, H. Liu, J. Gonzalez and S. S. Mao, *Talanta*, 2002, **57**, 425-451.
3.   A. L. Gray, *Analyst*, 1985, **110**, 551-556.
4.   M. Guillong and D. Günther, *Journal of Analytical Atomic Spectrometry*, 2002, **17**, 831-837.
5.   P. Nadoll and A. E. Koenig, *Journal of Analytical Atomic Spectrometry*, 2011, **26**, 1872-1877.
6.   K. Novotný, J. Kaiser, M. Galiová, V. Konečná, J. Novotný, R. Malina, M. Liška, V. Kanický and V. Otruba, *Spectrochimica Acta Part B: Atomic Spectroscopy*, 2008, **63**, 1139-1144.
7.   J. S. Becker, M. Zoriy, J. S. Becker, J. Dobrowolska and A. Matusch, *Journal of Analytical Atomic Spectrometry*, 2007, **22**, 736-744.
8.   J. A. T. Pugh, A. G. Cox, C. W. McLeod, J. Bunch, B. Whitby, B. Gordon, T. Kalber and E. White, *Journal of Analytical Atomic Spectrometry*, 2011, **26**, 1667-1673.
9.   C.-F. Wang, S.-L. Jeng, C. C. Lin and P.-C. Chiang, *Analytica Chimica Acta*, 1998, **368**, 11-19.
10.   S. Gligorovski, J. T. van Elteren and I. Grgic, *Science of the Total Environment*, 2008, **407**, 594-602.
11.   S. Tanaka, N. Yasushi, N. Sato, T. Fukasawa, S. J. Santosa, K. Yamanaka and T. Ootoshi, *Journal of Analytical Atomic Spectrometry*, 1998, **13**, 135-140.
12.   W. Chung, V. N. Sharifi, J. Swithenbank, O. Osammor and A. Nolan, *Modern Applied Science*, 2008, **2**, 17-32.
13.   M. Thompson, S. Chenery and L. Brett, *Journal of Analytical Atomic Spectrometry*, 1990, **5**, 49-55.
14.   V. Bulatov, A. Khalmanov and I. Schechter, *Analytical and Bioanalytical Chemistry*, 2003, **375**, 1282-1286.
15.   R. R. Whitlock and G. M. Frick, *Journal of Materials Research*, 1994, **9**, 2868-2872.
16.   D. Bleiner and P. Gasser, *Applied Physics*, 2004, **79**, 1019-1022.
17.   S. Chenery, A. Hunt and M. Thompson, *Journal of Analytical Atomic Spectrometry*, 1992, **7**, 647-652.
18.   J. H. Yoo, S. H. Jeong, X. L. Mao, R. Greif and R. E. Russo, *Applied Physics Letters*, 2000, **76**, 783-785.
19.   C. Liu, X. L. Mao, S. S. Mao, X. Zeng, R. Greif and R. E. Russo, *Analytical Chemistry*, 2003, **76**, 379-383.
20.   H.-R. Kuhn and D. Günther, *Analytical and Bioanalytical Chemistry*, 2005, **383**, 434-441.
21.   H.-R. Kuhn, M. Guillong and D. Günther, *Analytical and Bioanalytical Chemistry*, 2004, **378**, 1069-1074.
22.   M. L. Alexander, M. R. Smith, J. S. Hartman, A. Mendoza and D. W. Koppenaal, *Applied Surface Science*, 1998, **127–129**, 255-261.
23.   D. J. Figg, J. B. Cross and C. Brink, *Applied Surface Science*, 1998, **127–129**, 287-291.
24.   H.-R. Kuhn and D. Gunther, *Journal of Analytical Atomic Spectrometry*, 2004, **19**, 1158-1164.
25.   S. H. Jeong, O. V. Borisov, J. H. Yoo, X. L. Mao and R. E. Russo, *Analytical Chemistry*, 1999, **71**, 5123-5130.
26.   H.-R. Kuhn, J. Koch, R. Hergenroder, K. Niemax, M. Kalberer and D. Günther, *Journal of Analytical Atomic Spectrometry*, 2005, **20**, 894-900.

27. T. Seto, Y. Kawakami, N. Suzuki, M. Hirasawa, S. Kano, N. Aya, S. Sasaki and H. Shimura, *Journal of Nanoparticle Research*, 2001, **3**, 185-191.
28. J. Košler, M. Wiedenbeck, R. Wirth, J. Hovorka, P. Sylvester and J. Míkova, *Journal of Analytical Atomic Spectrometry*, 2005, **20**, 402-409.
29. M. Holá, V. Konečná, P. Mikuška, J. Kaiser and V. Kanický, *Spectrochimica Acta Part B: Atomic Spectroscopy*, 2010, **65**, 51-60.
30. R. Glaus, R. Kaegi, F. Krumeich and D. Günther, *Spectrochimica Acta Part B: Atomic Spectroscopy*, 2010, **65**, 812-822.
31. R. Hergenröder, *Spectrochimica Acta Part B: Atomic Spectroscopy*, 2006, **61**, 284-300.
32. K.-P. Hinz and B. Spengler, *Journal of Mass Spectrometry*, 2007, **42**, 843-860.
33. M. Guillong, I. Horn and D. Günther, *Journal of Analytical Atomic Spectrometry*, 2003, **18**, 1224-1230.
34. A. Effenberger Jr. and J. R. Scott, *Sensors*, 2010, **10**, 4907-4925.
35. Y. Iida, *Spectrochimica Acta Part B: Atomic Spectroscopy*, 1990, **45**, 1353-1367.
36. J. A. Aguilera and C. Aragón, *Applied Physics A: Materials Science & Processing*, 1999, **69**, S475-S478.
37. D. Günther and C. A. Heinrich, *Journal of Analytical Atomic Spectrometry*, 1999, **14**, 1363-1368.
38. D. Bleiner, *Spectrochimica Acta Part B: Atomic Spectroscopy*, 2005, **60**, 49-64.
39. A. Whitehouse, *Personal Communiation*, Applied Photonics, 2012.
40. *LIBSCAN, Modular LIBS System, User's Manual*, Applied Photonics, 2010.
41. F. Anabitarte, A. Cobo and J. M. Lopez-Higuera, *ISRN Spectroscopy*, 2012, **2012**, 12.
42. J. J. Gonzalez, C. Liu, S.-B. Wen, X. Mao and R. E. Russo, *Talanta*, 2007, **73**, 567-576.
43. R. Feng, *Geochimica et Cosmochimica Acta*, 1994, **58**, 1615-1623.
44. F. Brygo, C. Dutouquet, F. Le Guern, R. Oltra, A. Semerok and J. M. Weulersse, *Applied Surface Science*, 2006, **252**, 2131-2138.

Chapter Six

Physical and elemental studies of laser generated particulates using a LA-ELPI method and ICP-MS

6.1 Introduction

To allow the full characterisation of laser generated aerosols, not only does their shape and size need to be considered but also their chemical composition. In several studies a laser ablation unit has been connected to an ICP spectrometer to determine a particulate's elemental concentration.[1-5] However, when using an LA-ICP method it is possible that fractionation may occur. There are three forms of fractionation, laser induced, transport induced and ICP-induced. These fractionation effects have been discussed by Koch et al. in 2004[6] and are outlined here.

- Laser induced: generation of non-stoichiometric aerosol particulates formed during ablation

- Transport induced: selective particulate deposition due to diffusion and gravitational settling

- ICP-induced: non complete atomisation of transported particulates (also discussed by Hattendorf, Latkoczy and Günther in 2003[7])

Koch et al. discussed the need to quantitatively investigate the three fractionation forms to allow the fractionation of particulates to be reduced when using LA-ICP techniques. To do this they characterised aerosols generated through the laser ablation of a brass material by collecting particulates using a Dekati twelve stage low pressure impactor.

They chose to use a cascade impactor over light scattering methods, such as optical particulate counting or differential mobility analysis. This was because the cascade impactor allowed a larger range of different sized particulates to be characterised, 30 nm to 10 µm, whilst also collecting them for further chemical characterisation.

Using a Ti:sapphire 775 nm laser Koch et al. generated particulates from a brass material in both helium and argon atmospheres, with a flow rate of 1 L/min. Both nano and femtosecond pulses were applied to the sample to allow comparisons to be undertaken. The impactor was placed after the ablation cell followed by a vacuum pump. The flow rate of the vacuum pump was 10 L/min and therefore a 'make up' gas of filtered air was used for the additional 9 L/min needed. This was added between the ablation cell and the impactor. Following the collection of the laser generated particulates onto 25 mm substrates the substrates were digested and an aliquot of the solution pipetted onto a glass support. The residue was then analysed using XRF. They found that using a femtosecond laser pulse generated particulates with a mean diameter of 10 nm. However, a nanosecond laser pulse generated larger particulates, generally in the micrometer range. They also found that smaller particulates contained a greater proportion of zinc than the larger particulates which contained higher concentrations of copper.[6] This research illustrated the need to use impaction over other techniques if a larger size range and the collection of particulates is required. Particulate collection allows the elemental composition of the generated particulates to be obtained whilst also permitting particulates to be sorted into size categories. This would mean that it could be determined whether larger particulates contained more elements, with greater concentrations, than smaller particulates and vice versa. A number of other studies which have used impaction to collect and characterise laser generated particulates are detailed in Table 6-1.

Authors	Date	Laser Used	Materials	Impaction Technique	Comments
Outridge, Doherty and Gregorie[13]	1997	Nd:YAG, 1064 nm	Glass and phosphorised copper	One in-line 47 mm filter (0.2 µm pore size)	Research into the fractionation of laser generated particulates
Jaworski, Hoffman and Stephanowitz[14]	2002	Nd:YAG, 355 nm	Brass alloy	11 stage cascade impactor with 7 mm graphite impaction disks	Development of a technique for the elemental analysis of size sorted laser generated particulates
Kuhn and Günther[15]	2003	Nd:YAG, 266 nm and ArF 139 nm	Brass	Polyethylene filter box with 25 mm substrates (0.22 µm pore size)	Collection of laser generated particulates onto substrates, followed by analysis using SEM and ICP-MS
Liu, Mao, González and Russo[16]	2005	Nd:YAG, 266 nm	Brass alloy	PIXE cascade impactor	Used the cascade impactor to capture particulates below a set cut off point and eliminate ICP-MS signal fluctuations
Glaus, Koch and Günther[17]	2012	Diode pumped solid state laser, 532 nm	Glass, gold and ceramic	One in line 13 mm substrate (0.4 µm pore size)	Development of a portable LA system where laser generated particulates were collected onto a single substrate then analysed by SEM

Table 6-1: Previous research on laser generated aerosols using impaction techniques

The studies listed in Table 6-1 used a number of impaction techniques to collect particulates for characterisation. Since 1945, when impaction was first discussed,[8] a large number of instruments have now been made commercially available to allow the collection of particulates onto substrates. A proportion of impaction instruments are manufactured by Dekati (Finland)[9-12] including the ELPI used in Chapter Four.

The first paper to describe the use of impaction for laser generated particulates was published in 1996 by Outridge, Doherty and Gregoire.[18] A Q-switched Nd:YAG laser, 1064 nm, was used to ablate three different materials, glass, a copper coin and an Arctic walrus tooth. The laser generated particulates were captured on an in-line 47 mm filter with 0.2 µm pores. Twenty different sites on each of the materials were ablated and the filters stored in polycarbonate Petri dishes. Following their use each filter was analysed using SEM. Table 6-2 indicates the results for each material.

Material	Shape of generated particulates	Size of generated particulates
Glass	Mainly spherical, some asymmetric	0.9 µm to 2 µm
Copper coin	Spherical	Not reported
Walrus tooth	Mixture of spherical and asymmetric	2 µm to 25 µm

Table 6-2: Results of Outridge, Doherty and Gregoire paper[18]

Outridge, Doherty and Gregoire concluded that the technique had been successful but future work would be required to quantify the extent of the fractionation during ablation and transport. To do this, filters would be placed at varying distances from the ablation cell to collect particulates. These filters would then be digested and chemically characterised using ICP-MS. This additional work was completed in 1997 and is summarised in Table 6-1.

Chapter Five discussed the morphology of laser generated particulates. Only a small size range of particulates was studied (0.5 µm to 20 µm) and elemental characterisation was not

performed. Therefore, to gain a more complete understanding of the particulates generated through laser ablation they must be physically and chemically characterised. Hence, this chapter will discuss the use of an impactor to collect laser generated particulates onto substrates whilst completing physical characterisation in real time. The substrates will then be chemically analysed using ICP-MS.

Previous research was completed concerning the digestion of ELPI substrates by Jackson and co-workers in 2009.[19, 20] In this study an ELPI was coupled to a rotating drum sampler to obtain information regarding the chemical and physical properties of particulate matter from iron ores. Particulate matter was collected onto both polycarbonate substrates and aluminium foils. Analysis of these substrates was then completed using solution ICP-MS, scanning electron microscopy and gravimetric analysis. Indirect chemical analysis of the polycarbonate filters using hot block digestion and solution ICP-MS allowed concentrations of the major elements, iron and manganese, to be determined. Other elements were not present in high enough concentrations to allow chemical analysis. SEM analysis of both the polycarbonate substrates and the aluminium foils allowed images of the particulates collected to be obtained.[19]

In 2011, Hsieh et al. used an ELPI to collect airborne particulate matter in Taiwan, followed by the direct analysis of the substrates using LA-ICP-MS.[5] The collection of particulates was completed for twelve hours. This study concentrated on the collection and subsequent analysis of the particulates using LA-ICP-MS as well as the generation of LA-ICP-MS standards for calibration. It was concluded that the ELPI/LA-ICP-MS method allowed elemental and quantitative analysis of particulates to be completed.[5]

Here, an ELPI will be coupled to a LA (1064 nm) unit, used in Chapter Five. This method will be known as LA (1064 nm)-ELPI. Four materials will be ablated to produce laser generated aerosols and the particulates contained within the aerosols will be collected onto 25 mm poreless polycarbonate substrates. The substrates will then be gravimetrically analysed to allow

mass distributions to be determined. Finally the substrates will be digested and analysed by ICP-MS, apart from boron which will be analysed using ICP-AES, to establish elemental concentrations of the collected particulates. As an argon atmosphere was found to provide the most reproducible results in Chapter Five, therefore, this gas is used for all work in this chapter.

High concentrations of small particulates (0.5 µm in size) were seen when previously examining the carbon rod, high purity zinc, carbon steel and boron nitride materials in Chapter Five. It is, therefore, expected that current studies will generate large proportions of particulates which are small in diameter, generally below 0.5 µm. For three of the materials, the high purity zinc, the carbon steel and the boron nitride, the main constituents of that material will be chemically characterised and it is anticipated that the elemental distribution plots will show similar characteristics to the mass distribution plots obtained from the gravimetric analysis of the ELPI substrates.

6.2 Experimental

6.2.1 Reagents and Materials

Four materials, high purity carbon rod, high purity zinc, a carbon steel certified reference material (BAS, SS-CRM 457-2) and boron nitride, were characterised using the LA (1064 nm)-ELPI method. The main morphological features of the four materials, determined in Chapter Five, as well as the melting points, boiling points and thermal conductivities of the materials, are summarised in Table 6-3.

Material	Melting point (ºC)	Boiling point (ºC)	Thermal conductivity (W/mK)	Size of largest concentration	Shape of largest concentration
Carbon Rod	3675	4200	140	0.5 µm	Fibrous particulates
High Purity Zinc	420	907	116	0.5 µm	Spherical particulates
Carbon Steel	1400	2850	43	1 µm	Spherical particulates
Boron Nitride	3000	3273	25	0.5 µm	Asymmetric particulates

Table 6-3: Summary of the morphological characterisation of the six materials, using the LA (1064 nm)-Aspect method

The calibration standards were prepared using the same method as detailed in Section 4.2.1, with the inclusion of boron. The substrates, as used in Chapter Four were also used within this work.

6.2.3 Instrumentation

The LA (1064 nm)-ELPI method used a similar instrumental configuration to that described for the LA (1064 nm)-Aspect method, with the Aspect instrument being replaced with the ELPI

unit (used in Chapter Four) and its external pump. The same tubing, a one meter length of conductive silicon tubing, was used as well as an argon atmosphere, operating at a flow of 1.7 L/min and a pressure of 0.5 bars. A 'make up' gas of laboratory air was used to achieve the ELPI pump flow rate of 30 L/min. The use of the 'make up' gas was described by Koch, von Bohlen, Hergenröder and Niemax.[6] Figure 6-1 illustrates the instrumental configuration.

Figure 6-1: LA (1064 nm)-ELPI configuration
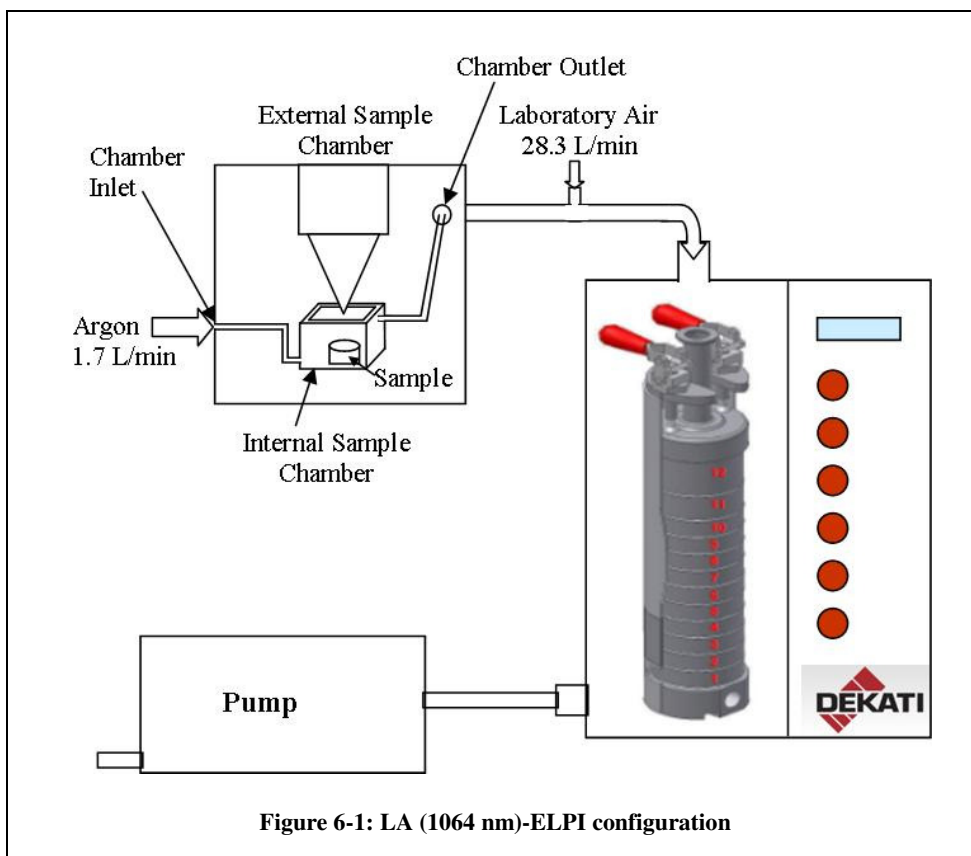
6.2.4 Procedure

Following the coupling of the LA (1064 nm) unit to the ELPI, the material of interest was placed within the internal sample chamber. The thirteen pre-weighed 25 mm substrates were loaded into the impactor stages and the impactor was positioned within the ELPI. The ELPI was flushed for ten minutes with laboratory air and then zeroed to ensure a low and stable background reading was obtained. The ELPI software was started and data was recorded for exactly one minute. The argon gas was then turned on and background data was recorded for another minute before turning on the ELPI pump. Shots were then fired onto the material of interest. The LA (1064 nm) parameters were a laser energy of 105 mJ, a Q switch delay of 150

μs, 25 conditioning shots and 25 laser shots at a repetition rate of 10 Hz (25 laser shots in 2.5 seconds). Twenty five different positions on each material were ablated. This number of shots and positions were chosen since it meant that particulates were generated for approximately four minutes, the time used for the RDS-ELPI study, as discussed in Chapter Four.

Once all shots had been fired the ELPI pump was left on for another minute to allow all of the generated particulates to be drawn to the impactor. Following this, the pump was turned off and the software left to record data for a further minute so that the particulate concentration had returned to the background level. The impactor was then removed from the ELPI and the thirteen substrates collected into separate Petri dishes for storage, before re-weighing commenced. The temperature and humidity of the laboratory was recorded for each experiment. This study was undertaken to demonstrate proof of concept and therefore replicates were not performed.

The gravimetric and multielement analysis of the ELPI substrates was completed using the same methods as detailed in Sections 6.2.2 and 4.2.5 respectively. Substrates from the boron nitride were also analysed for boron using a Spectro Ciros Vision ICP-AES and the 208.959 nm line.

6.3 Results and Discussion

6.3.1 Physical Characterisation of Materials

All four materials were physically characterised using the LA (1064 nm)-ELPI method. The results from the gravimetric analysis will be considered first followed by comparisons of the mass and number distributions obtained for each individual material.

Gravimetric Analysis

Gravimetric analysis was completed for all four sets of substrates and the overall results are plotted in Figure 6-2. The results for each substrate are listed in the Appendix. Only one experiment was completed per material and therefore the reproducibility cannot be discussed. A range of particulate masses were determined for each of the materials, from 0.084 mg, for the carbon rod, to 0.187 mg, for boron nitride. This, when combined with the number distributions, seen in Figures 6-4, 6-6, 6-8 and 6-10, indicated that although the same number of shots was fired onto each material different numbers of particulates were emitted from the ablation of each material, causing the variation in masses. This also confirmed what was seen in Chapter Five where different numbers of generated particulates were seen for each of the morphological profiles for each material. The varying particulate masses signified that each of the materials reacted differently to ablation. Thomson, Chenery and Brett[21] discussed the processes which occur in laser ablation and these have been applied to determine why different masses were collected. The carbon rod material had a high melting point of 3675 ℃. This meant that the material would not have melted but would have undergone thermal shock, generating particulates through fragmentation. The materials high thermal conductivity, 140 W/mK would have meant that it would have conducted heat and not retained it therefore only allowing a small number of particulates to be generated. Both the high purity zinc and the carbon steel materials were metallic, with melting points below 2000 ℃, therefore when the laser was fired onto them they melted, both easily producing a similar number of particulates. Boron nitride was a brittle material with a high melting point, 3000 ℃, therefore it underwent thermal shock when the

laser was fired onto it. Unlike the carbon rod, boron nitride had a low thermal conductivity, 25 W/mK. This meant that it retained heat causing the fragmentation of the material to continue and producing the most particulates of the four materials, 0.187 mg.

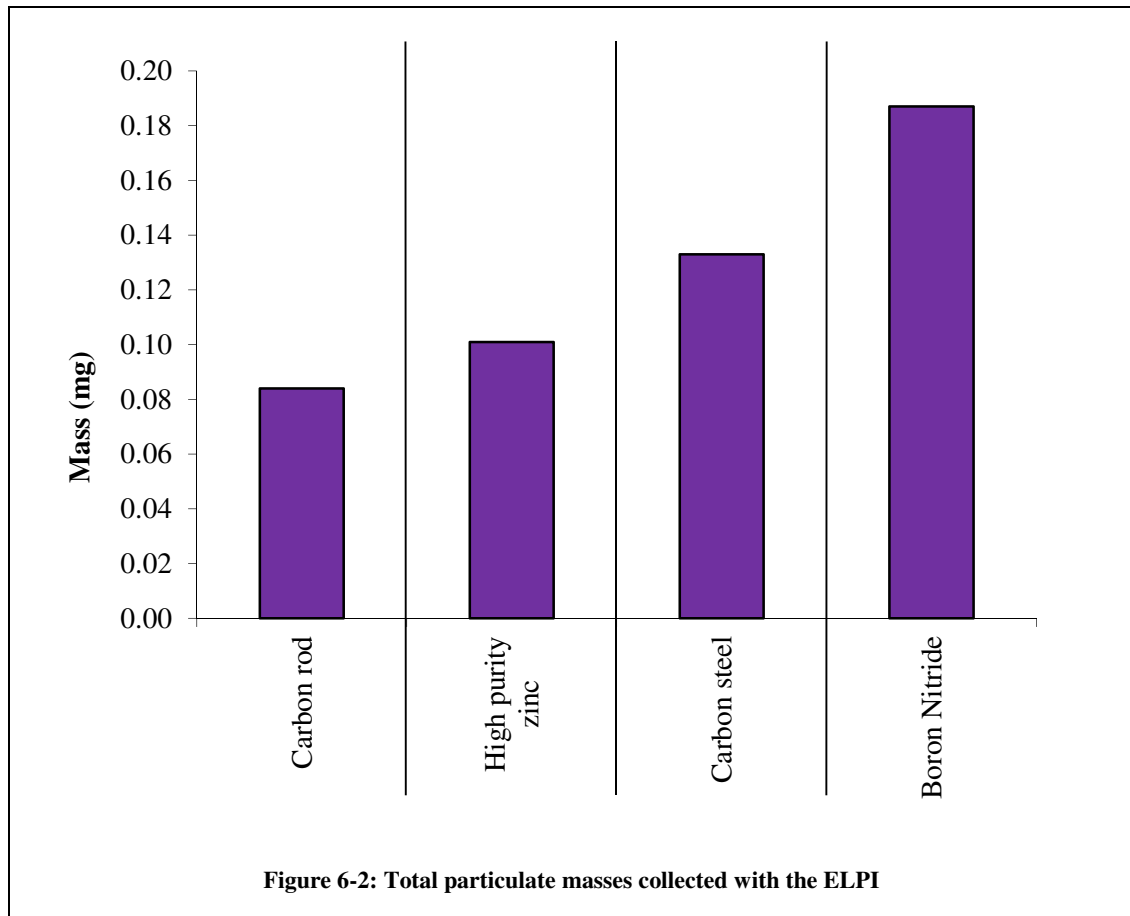**Figure 6-2: Total particulate masses collected with the ELPI**

Figure 6-3 indicates the mass fractionation of the particulates. Each material showed slightly different mass fractionation. For the high purity zinc and the boron nitride materials, in particular, over 50 percent of the particulates were found on stages one to three, 0.0285 µm to 0.0937 µm, with the other 50 percent spread over stages four to twelve, 0.156 µm to 9.98 µm. This illustrated that a very large proportion of the generated particulates had small diameters and were therefore able to pass through most of the impactor to settle on the lower stages. For the other two materials, the carbon rod and the carbon steel, the particulates were spread over the twelve stages quite evenly, with no individual stage holding more than 15 percent of the collected particulates showing that the particulates generated had a range of different sizes from 0.0285 µm to 9.98 µm.

Overall these results illustrated that although some of the materials underwent the same processes the particulates which were generated using the same method, melting or thermal shock, were not necessarily produced with the same size ranges. This indicated that the composition of the material may also play a part in the laser material interaction, especially since the two carbon containing materials produced similar mass fractionation profiles.

Figure 6-3: Total percentage mass fractionation when using the ELPI
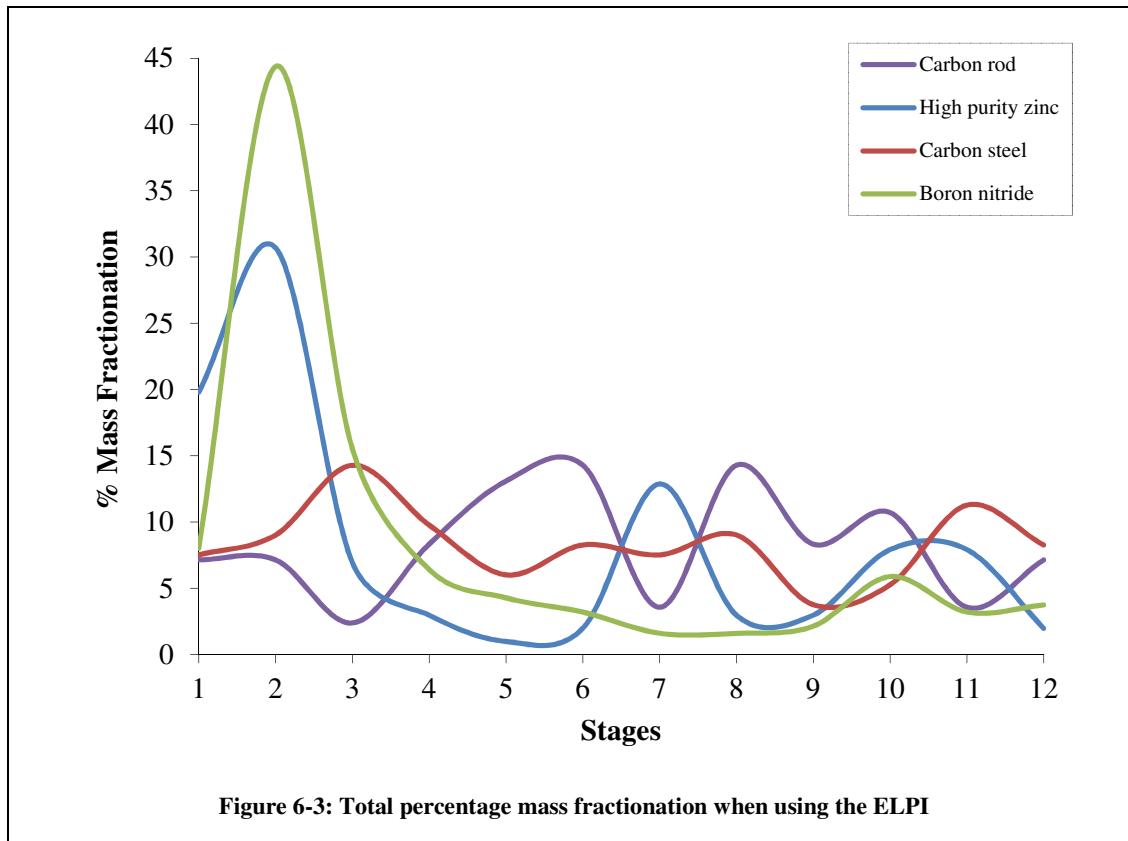
Carbon Rod

The number and mass distributions obtained from the characterisation of the carbon rod material are shown in Figures 6-4 and 6-5. The ELPI number distribution indicated a large peak in particulate number at 0.05 µm, followed by a steady decrease in the number of particulates down to 1 µm. The mass distribution was quite different to the number distribution, with variations in particulate mass as the particulate size increased. The largest peak was seen at 0.32 µm, followed by three smaller peaks at 1.23 µm, 3.10 µm and 8.12 µm. There was also a smaller peak at 0.07 µm, which corresponded to that seen in the number distribution. This illustrated that although there were a large number of particulates, 800,000, with a diameter of

0.05 µm, they would have been quite light and therefore did not contribute to the overall mass as much as the larger and heavier particulates. The large mass of particulates at 8.12 µm may have been due to agglomeration of the smaller particulates, which would have started within the ablation cell immediately after the formation of the smaller particulates.[22] Jackson and Günther[23] found that small particulates are generally formed from the condensation of the vapour phase, whilst larger particulates are formed from direct ejection.[23] Another explanation for the low number of smaller particulates could have been that, for the carbon rod material, the number of particulates formed through condensation was low and more fragmented particulates were directly ejected from the material, when undergoing thermal shock.

Figure 6-4: Number distribution for carbon rod

Figure 6-5: Mass distribution for carbon rod
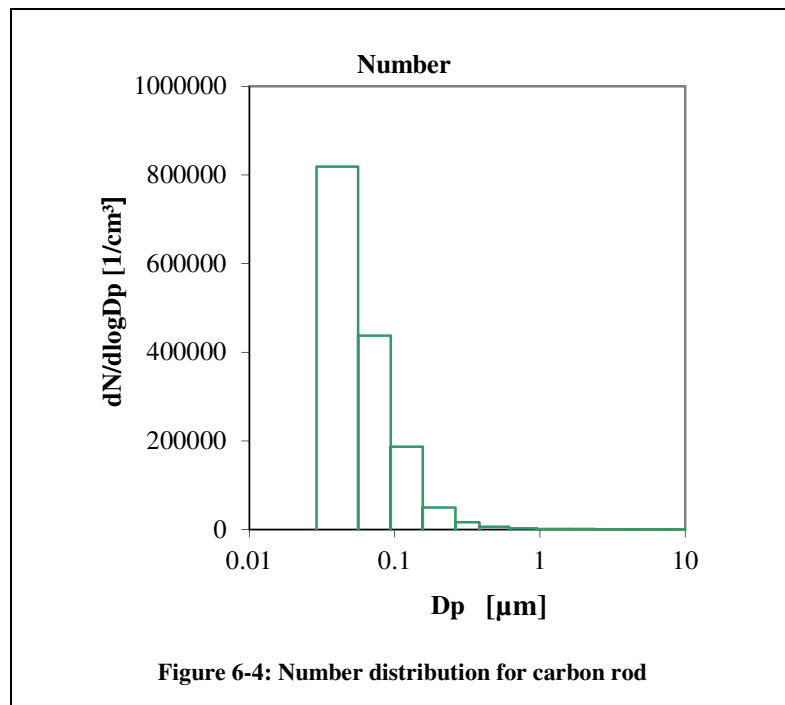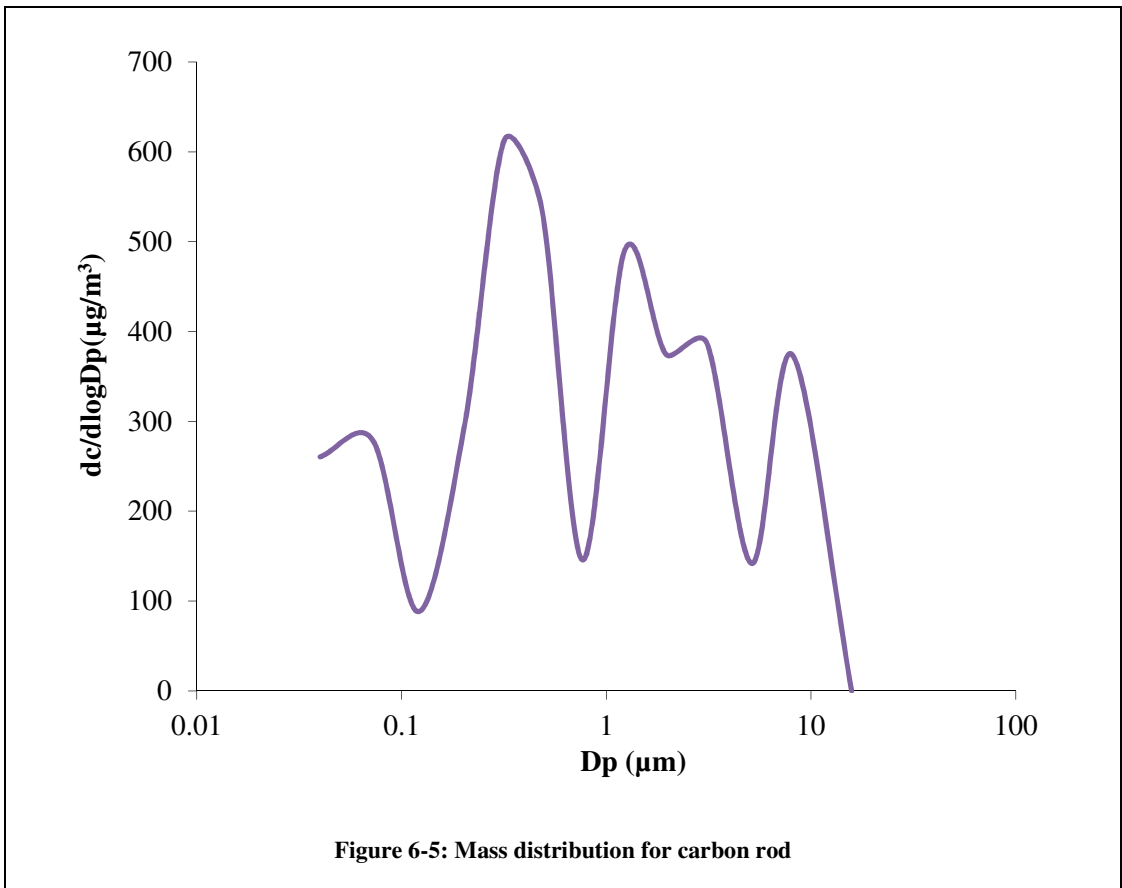
High Purity Zinc

The number distribution obtained from the characterisation of the high purity zinc material is shown in Figure 6-6. As with the carbon rod material, the largest peak in particulate number was seen at 0.05 µm. However the spread of particulates was smaller, with very few particulates present with a diameter greater than 0.5 µm. In general the number of particulates with a diameter of 0.5 µm was a lot greater than the number characterised for the carbon rod material, 13,500,000 for zinc compared to 800,000 for carbon rod. This showed that the ablation of the high purity zinc material produced a much greater number of particulates than when ablating the carbon rod material. This was possibly due to the metallic nature of the material, which would have caused the surface to rapidly melt on ablation, especially given high purity zinc's low melting point of 420 ℃. This would have allowed the generation of a large number of particulates produced directly from the liquefied material.[24]

Figure 6-6: Number distribution for high purity zinc
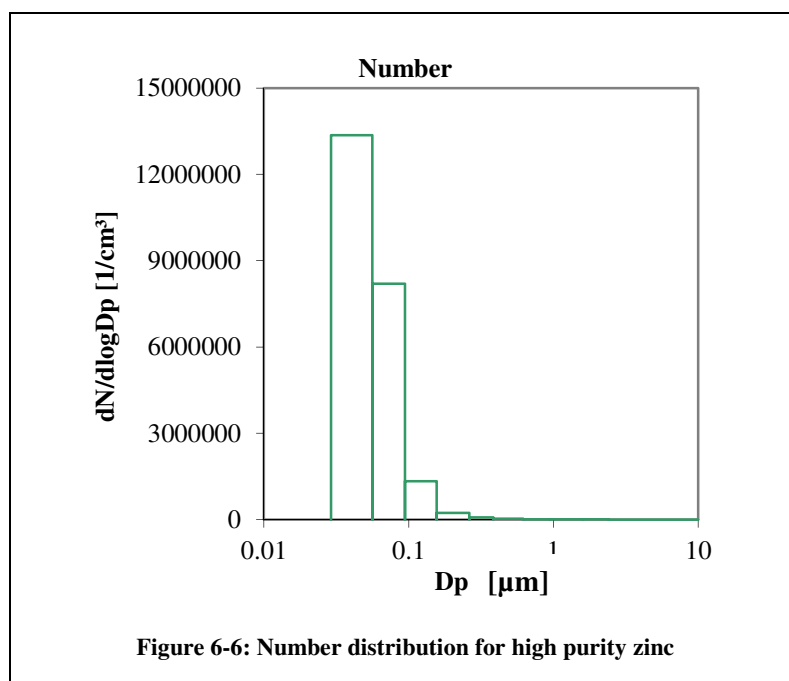
The mass distribution for high purity zinc is shown in Figure 6-7. The largest peak in mass was seen at 0.07 µm, which corresponded well with the number distribution. This confirmed that there was a very large number of small particulates present within the laser generated aerosol. Unlike the number distribution, the spread of particulates was larger, with peaks seen at both 0.76 µm and 3.10 µm. This indicated that although there was a small number of particulates present, with a diameter greater than 0.5 µm, they were quite heavy, causing the peaks in the mass distribution.
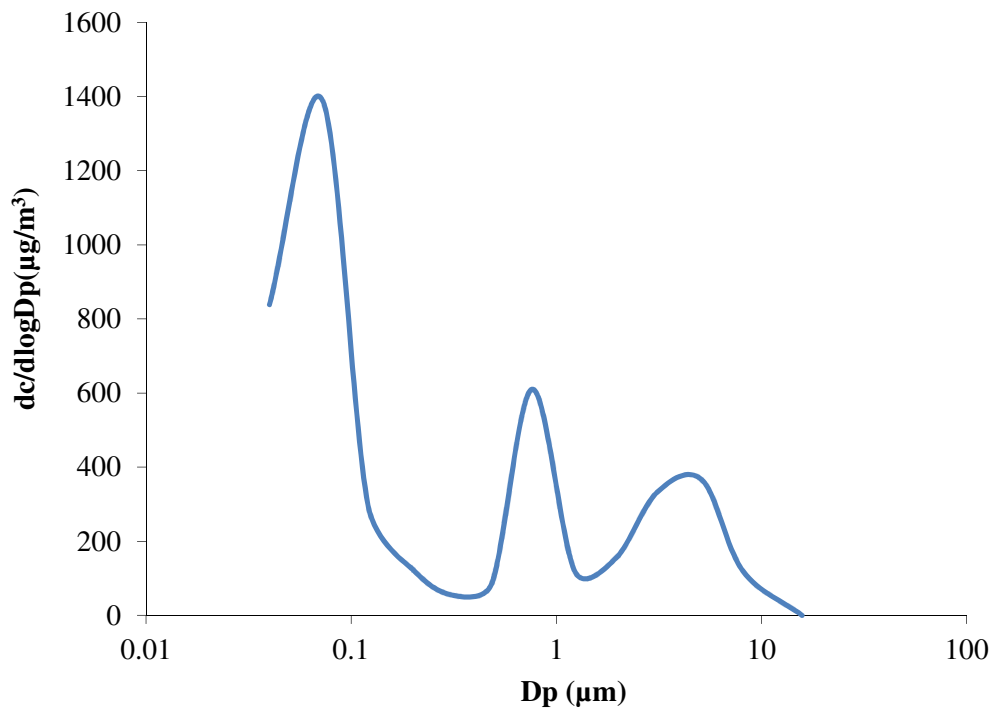
Figure 6-7: Mass distribution for high purity zinc

Carbon Steel

Number and mass distributions for the carbon steel are illustrated in Figures 6-8 and 6-9, respectively. As with the first two materials the number distribution for the carbon steel indicated a large number of particulates present, approximately 2,500,000, with a diameter of 0.05 μm. This peak was followed by a sharp decrease in particulate number, to 500,000 particulates with a diameter of 0.08 μm, and a general levelling out from 0.3 μm onwards. The number of particulates generated from the ablation of the carbon steel was smaller than that generated from the ablation of the high purity zinc material, 2,500,000 compared with 13,500,000. The carbon steel was a metallic material like the high purity zinc and therefore would have undergone melting when subjected to the laser. However, the carbon steel's melting point was higher than the high purity zinc's, 1400 ºC compared with 420 ºC. Hence, it would not have melted as easily and fewer particulates would have been produced, from the liquefied material, indicating that ablation was not as effective for the carbon steel as it was for the high purity zinc.

Figure 6-8: Number distribution for carbon steel
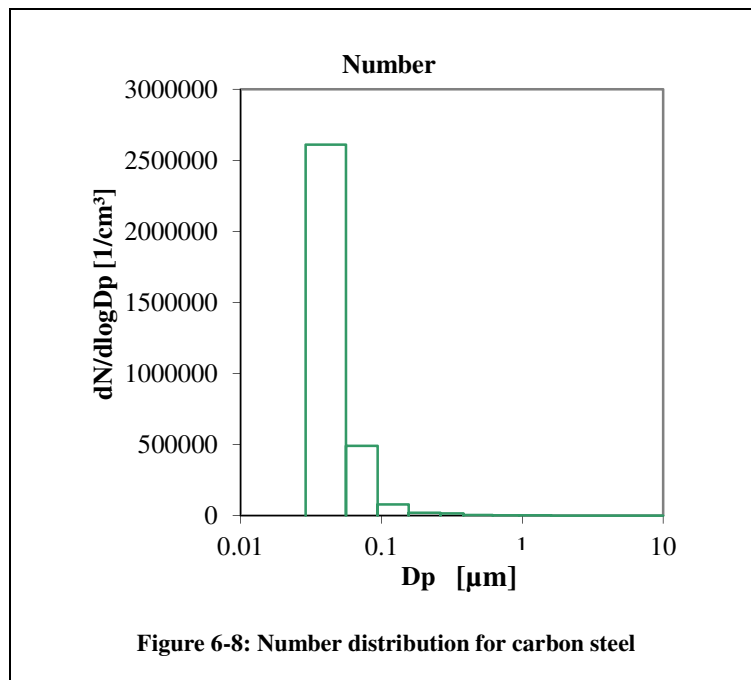
The mass distribution showed two main peaks, at 0.12 µm and 5.14 µm, with a plateau in the middle. This indicated that although there was a large number of very small particulates present within the laser generated aerosol, they were not the greatest contributor to the overall mass of particulates collected upon the twelve substrates. The second peak at 5.14 µm also confirmed that although there were not many particulates present within this size range, they were heavy and therefore contributed greatly to the overall particulate mass. The mass distribution obtained for the carbon steel showed some similarities with the carbon rod mass distribution indicating that the carbon content of the materials may have affected the laser materials interaction.

Figure 6-9: Mass distribution for carbon steel
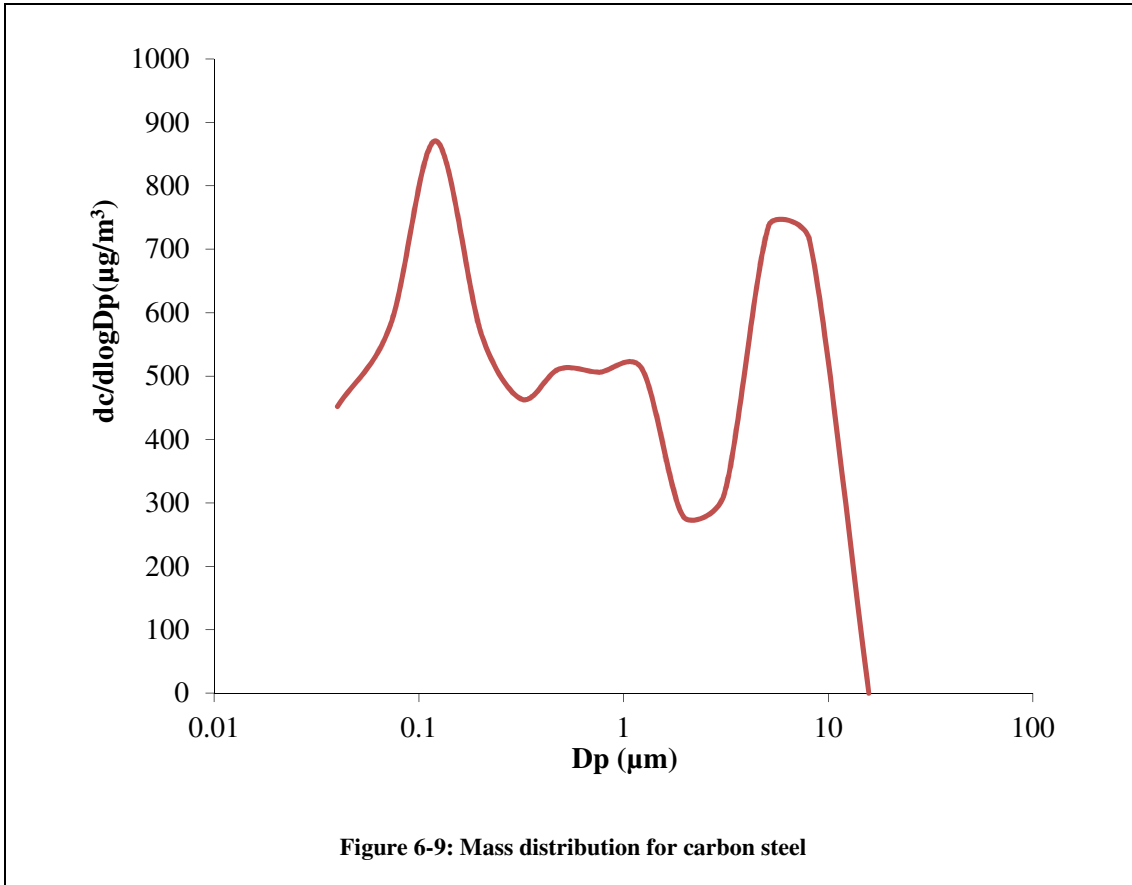
Boron Nitride

The number distribution for the boron nitride material, Figure 6-10, was quite different to the distributions obtained for the other three materials. As seen for the other materials, there was a large peak at 0.05 µm (12,000,000 particulates), although, rather than being followed by a sharp decrease in particulate number there was a further large peak present at 0.08 µm, 10,500,000 particulates. This indicated that a very large number, up to 22,500,000, of the generated particulates were below 0.1 µm in size. This was confirmed by the mass distribution.

The mass distribution, Figure 6-11, illustrated a peak in particulate mass at 0.07 µm. This was the only prominent peak seen in the distribution and was therefore a sign that a large proportion of the particulates generated through the ablation of the material were small in size and thus contributed greatly to the overall mass. This large number of small particulates was most likely due to the materials brittle nature and high melting point of 3000 ºC. Rather than melt, like the two metallic materials, the material would have fragmented due to thermal shock. The boron

nitride's smaller particulates were possibly formed through condensation as described by Jackson and Günther.[23]

Figure 6-10: Number distribution for boron nitride

Figure 6-11: Mass distribution for boron nitride
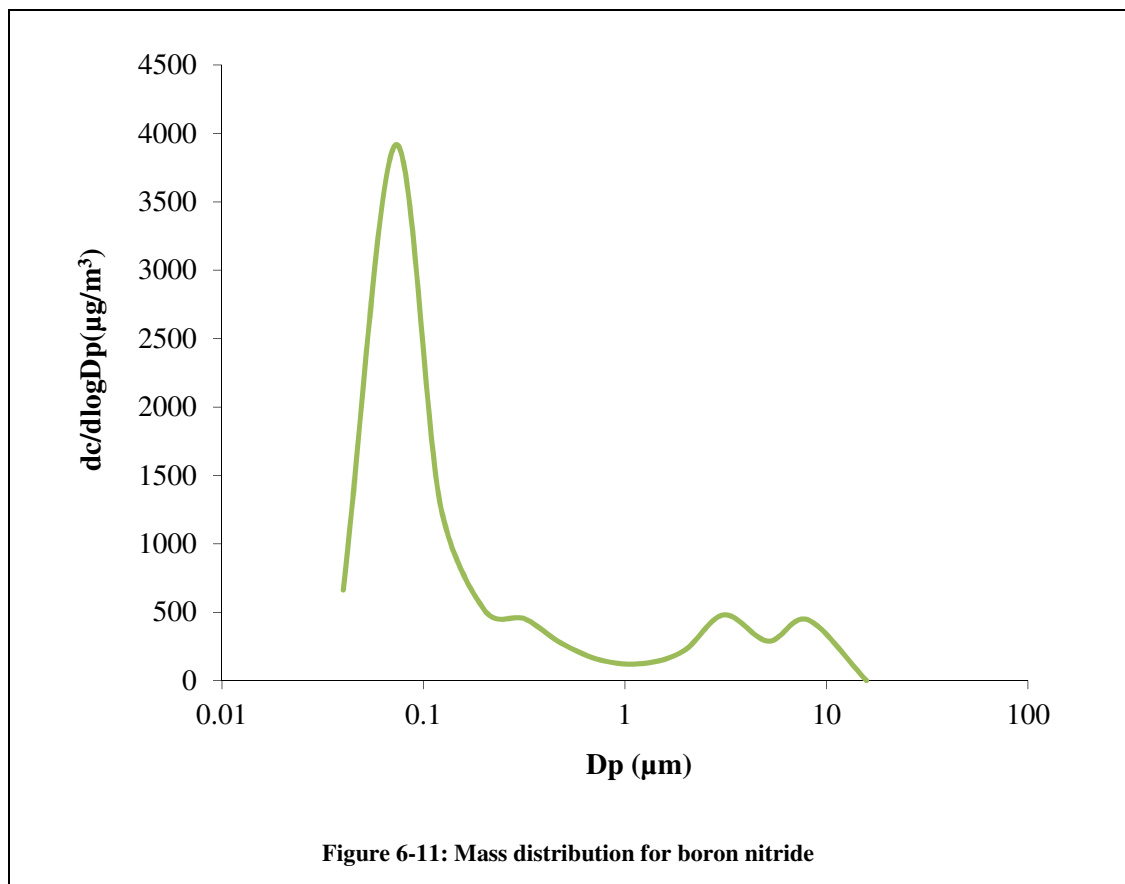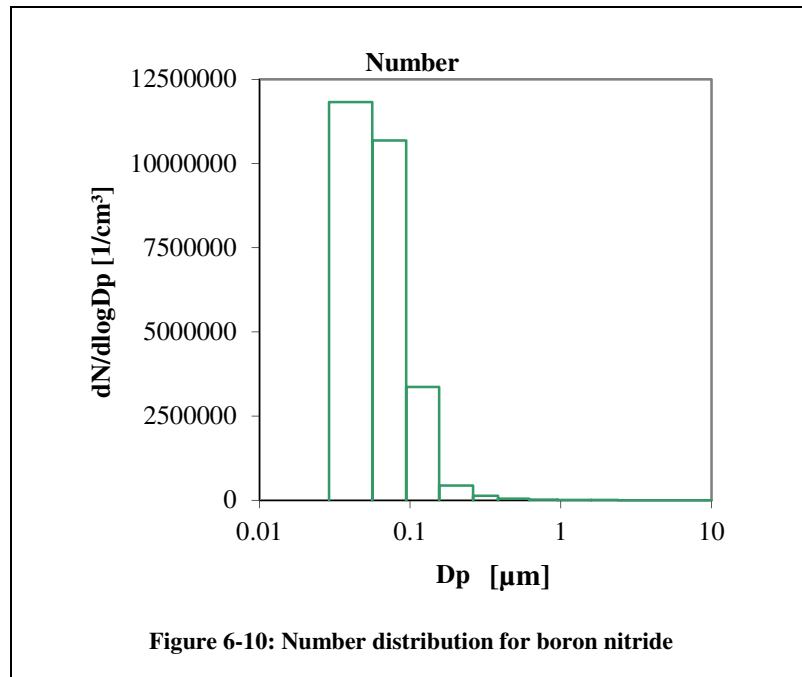
The physical characterisation of the laser generated aerosols has been completed and although three of the four materials produced similar number distributions a range of different mass distributions were obtained, Table 6-5. This indicated that the particulates generated through the ablation of the four different materials did not all have the same physical characteristics as each other. As expected large proportions of particulates which were below 0.5 µm in size were produced for all four materials. However, different numbers of particulates were generated, due to differences in the laser-material interaction processes for the four materials. The boron nitride material produced the largest number of particulates smaller than 0.08 µm in diameter, 22,500,000, which was most likely due to the condensation of the vapour phase. The high purity zinc and carbon steel materials generated the second and third highest numbers of particulates, 13,500,000 and 2,500,000, respectively, due to the melting of the material surface during ablation. Although both metallic, zinc produced more particulates than carbon steel since it had a lower melting point and therefore would have become liquefied more easily, allowing the production of more particulates.[24] The carbon rod generated the smallest number of particulates with a diameter of 0.5 µm, 800,000. This was most likely due to agglomeration of the smaller particulates, which had been generated through condensation of the vapour phase.

Material	Size of largest number concentration	Size of largest mass concentration
Carbon rod	0.05 µm	0.32 µm
High purity zinc	0.05 µm	0.07 µm
Carbon steel	0.05 µm	0.12 µm
Boron nitride	0.05 µm	0.07 µm

Table 6-5: Summary of the physical characterisation of the four materials

6.3.2 Multielemental Analysis of ELPI Substrates

Following gravimetric analysis, digestion and multielemental analysis of the LA (1064 nm)-ELPI substrates was performed. A quality control solution, 20 µg/L, and an SRM, NIST 1648a were also analysed. The elements analysed were boron, copper, iron, manganese, vanadium and

zinc. Boron, iron and zinc were chosen as they were major elements within three of the materials being characterised. The other three elements, copper, manganese and vanadium, were chosen since they were present within the SRM and it was of interest to see whether these trace elements could be reliably measured in the ELPI digests.

The analysis of the QC solution produced good recoveries which are listed in Table 6-6. The recoveries indicated that the calibration solutions were precise and reliable elemental concentrations had been obtained for the substrate analysis. All of the RSD values were below three percent, indicating excellent precision over the ten replicates. The boron QC was only analysed once, hence, there is no associated RSD value.

Element	Reference (µg/L)	QC Results (µg/L)	RSD (%)
B 208.959	20	19	-
Cu 63	20	20 ± 0.38	1.88
Fe 56	20	19 ± 0.29	1.54
Mn 55	20	20 ± 0.44	2.16
V 51	20	21 ± 0.42	2.03
Zn 66	20	19 ± 0.26	1.36

Table 6-6: QC Results (n=10)

The digestion and analysis of four SRM 1648a replicates was completed to establish the reliability of the analyses. Results are listed in Table 6-7. In general recoveries were above 95 percent, except for vanadium which gave recoveries of 88 percent. All four of the replicates reported concentrations for vanadium which were below the certified value but they were still within the certified limits. These low percentage recoveries obtained indicated that there may have been a problem with the digestion of the SRM and that in future hydrofluoric acid should be used to allow the full digestion of the substrates.

All, but one, of the elemental concentrations were within the limits specified by the SRM certificate, with zinc being the only exception. The obtained value for zinc was above the

certified value, which was most likely due to contamination from the digestion vessels. The RSD values were all below nine percent which was a sign of good precision and repeatability.

Element	Certified value (µg/g)	Obtained value (µg/g)	% Recovery	RSD (%)
Cu 63	610 ± 70	614 ±11	101	1.76
Fe 56	39200 ± 2100	37189 ± 1139	95	3.06
Mn 55	790 ± 44	819 ± 14	104	1.66
V 51	127 ± 11	111 ± 9	88	8.52
Zn 66	4800 ± 270	5167 ± 3	108	3.37

Table 6-7: SRM Results (n=4)

To determine the limits of detection of the method, one percent nitric acid was analysed ten times and the results used to calculate the detection limits through 3σ. The limits of detection, along with the concentrations of the ten replicates, are reported in Table 6-8. In general, the detection limits were below 1.0 µg/L. There were two exceptions to this, boron and iron which reported limits of 5.53 µg/L and 1.92 µg/L, respectively. Most of the key elements gave detectable results but for all of the materials, a number of substrates, gave concentrations for vanadium which were below the limits of detection, 0.046 µg/L.

These results will be discussed further when examining the findings from each material individually, but in brief the limits of detection were all lower than those obtained by Jackson[19] who also digested ELPI substrates, in a similar study, as described in Section 6.1. As previously mentioned the limits of detection were lower than those obtained by Jackson due to the use of a collision cell within the ICP-MS.

One option to allow a more sensitive determination of trace elemental concentrations would be to complete more laser shots on the material of interest, therefore allowing more particulates to be generated for collection upon the ELPI substrates. If more particulates were present upon each substrate, the overall concentration of each element would be increased.

Jaworksi, Hoffmann and Stephanowitz[14] compared the number of ablation shots onto a brass material. They found no more than 500 shots were needed, to allow particulate detection with ICP-MS. This study indicated that although 500 shots permitted the determination of the major elements within their brass material i.e. copper, zinc and lead, there is a need to complete further tests into the number of shots fired onto a material to allow trace and ultra trace elemental concentrations to be determined.

Element	1	2	3	4	5	6	7	8	9	10	Mean	Standard Deviation	LOD (3σ)	Jackson et al. LOD[19]
B 208.95	8.17	9.90	10.3	9.23	13.3	9.57	9.50	6.90	8.83	6.80	9.24	1.84	**5.53**	-
Cu 63	0.045	0.084	0.013	0.023	0.018	0.021	0.023	0.025	0.024	0.024	0.030	0.020	**0.062**	1.88
Fe 56	0.181	1.30	0.208	0.083	0.118	0.676	1.66	0.663	0.447	1.86	0.692	0.639	**1.92**	17.8
Mn 55	0.052	0.134	0.031	0.036	0.073	0.114	0.051	0.042	0.027	0.050	0.061	0.035	**0.107**	0.23
V 51	0.050	0.018	0.016	0.026	0.002	0.038	0.026	0.004	0.006	0.022	0.021	0.015	**0.046**	0.06
Zn 66	1.88	1.41	1.33	1.25	0.881	0.954	0.963	0.961	0.955	0.897	1.15	0.322	**0.966**	19.2

Table 6-8: Analytical values for nitric acid and limits of detection (µg/L)

The elemental results for the analysis of the individual substrates will now be discussed. To obtain these results, the same process used in Chapter Four was used here. Again the blank substrates reported concentrations below the limit of detection and therefore they did not affect the elemental results for the four materials. Since only one substrate set was obtained for each material it was not possible to report on the repeatability of the results. Thus, to allow some comparisons, mass balance calculations have been performed to compare the mass of particulates collected, obtained through gravimetric analysis, with the sum of the individual element masses determined to be present upon each set of substrates. All four materials reported mass balances which were smaller than the gravimetric masses, as shown in Table 6-9. The elemental mass balances for the carbon rod and carbon steel were of the same magnitude, whilst the elemental masses for the high purity zinc and the boron nitride were one order of magnitude greater. The mass balance results indicate a very poor mass recovery. One possible reason for this is that only five elements were analysed. All of the materials, especially the carbon steel, would have contained other elements which were not analysed and could have accounted for a proportion of the difference in masses. To rectify this in the future a larger number of elements should be analysed. Another possible reason for the decreased elemental mass balance is the incomplete digestion of the substrates as was seen for vanadium in the SRM analysis. To allow the full digestion of the substrates hydrofluoric acid should be used in future studies, and the temperature and pressure at which the digestion was completed at could also be increased. Finally, replicates should be completed to check the reliability of the mass balance calculations.

Material	Gravimetric mass	Elemental mass balance
Carbon rod	84 μg	9.93 ng
High purity zinc	101 μg	155 ng
Carbon steel	133 μg	11.8 ng
Boron nitride	187 μg	208 ng

Table 6-9: Gravimetric and elemental mass balances

Carbon Rod

The carbon rod elemental results, illustrated in Tables 6-10 and 6-11, indicated generally low trace elemental concentrations, below 25 µg/g, apart from iron where concentrations ranged from 17.4 µg/g up to 438 µg/g. The mass distribution plot, Figure 6-5, generally did not correlate with the elemental size distribution plots, Figures 6-12 to 6-14, indicating that the analysed elements were not the main particulate constituent and were only present at trace concentrations. Since the carbon content was not determined this result was to be expected. The total sum of all individual elements was 9.93 ng, four orders of magnitude smaller than the gravimetric mass, 84 µg. This was possibly due to the fact that the carbon elemental content was not determined, as carbon would have accounted for a large proportion of the material weight. It also indicates the need to analyse for more trace elements and refine the digestion procedure.

Only one stage, stage nine, reported a concentration below the limit of detection for copper, 0.062 µg/L. Most other stages indicated copper concentrations between 0.415 µg/g and 2.32 µg/g, apart from stage three. The substrate from stage three reported a high concentration of 5.43 µg/g, as seen in Figure 6-12. This was the only peak in concentration seen for copper.

Iron gave the highest concentrations of any of the elements analysed, as seen in Figure 6-13. Concentrations ranged from 17.4 µg/g to 438 µg/g with no stages having values below the limit of detection, 1.92 µg/L. The highest concentration, 438 µg/g, was seen on stage ten which did possibly correlate with a peak in the number distribution, Figure 6-5. The lowest concentration was seen on stage three, 17.4 µg/g.

Element	1	2	3	4	5	6	7	8	9	10	11	12
Cu 63 (µg/L)	0.116	0.317	1.07	0.363	0.215	0.176	0.487	0.157	<0.062	0.347	0.083	0.124
Fe 56 (µg/L)	14.2	8.16	3.44	6.45	5.43	10.5	75.1	15.6	3.50	82.5	11.8	26.7
Mn 55 (µg/L)	0.114	0.356	0.116	0.191	0.163	0.307	0.147	0.327	<0.107	0.418	0.177	0.415
V 51 (µg/L)	0.401	<0.0461	0.364	0.341	0.347	0.319	0.374	0.281	0.199	0.472	0.101	0.356
Zn 66 (µg/L)	<0.966	<0.966	<0.966	<0.966	<0.966	<0.966	<0.966	4.60	<0.966	<0.966	4.90	<0.966

Table 6-10: Elemental analysis of substrates for carbon rod

Element	1	2	3	4	5	6	7	8	9	10	11	12
Cu 63 (µg/g)	0.623	1.79	5.43	1.98	1.02	1.00	2.32	0.798	-	1.84	0.415	0.708
Fe 56 (µg/g)	76.2	46.1	17.4	35.2	25.8	59.7	365	79.3	18.8	438	59.02	152
Mn 55 (µg/g)	0.611	2.01	0.589	1.04	0.777	1.74	0.711	1.66	-	2.22	0.886	2.36
V 51 (µg/g)	2.15	-	1.85	1.86	1.65	1.82	1.82	1.43	1.07	2.51	0.503	2.03
Zn 66 (µg/g)	-	-	-	-	-	-	-	23.4	-	-	24.5	-
Sum of elemental concentrations (µg/g)	79.6	49.9	25.3	40.1	29.3	64.3	369	107	19.9	445	85.3	157
Mass of particulates on substrate (g)	6×10^{-6}	6×10^{-6}	2×10^{-6}	7×10^{-6}	1×10^{-5}	1×10^{-5}	3×10^{-6}	1×10^{-5}	7×10^{-6}	9×10^{-6}	3×10^{-6}	6×10^{-6}
Total elemental concentration x particulate mass = Total elemental mass, converted into ng	0.478	0.299	0.051	0.281	0.322	0.771	1.11	1.28	0.139	4.00	0.256	0.944

Total concentration of all analysed elements on the twelve filters, 1472 µg/g

Total elemental masses added together to give the total mass of all analysed elements on the twelve filters, **9.93 ng**

Table 6-11: Elemental and fractionation results for substrates for carbon rod

Figure 6-12: Iron distribution for carbon rod
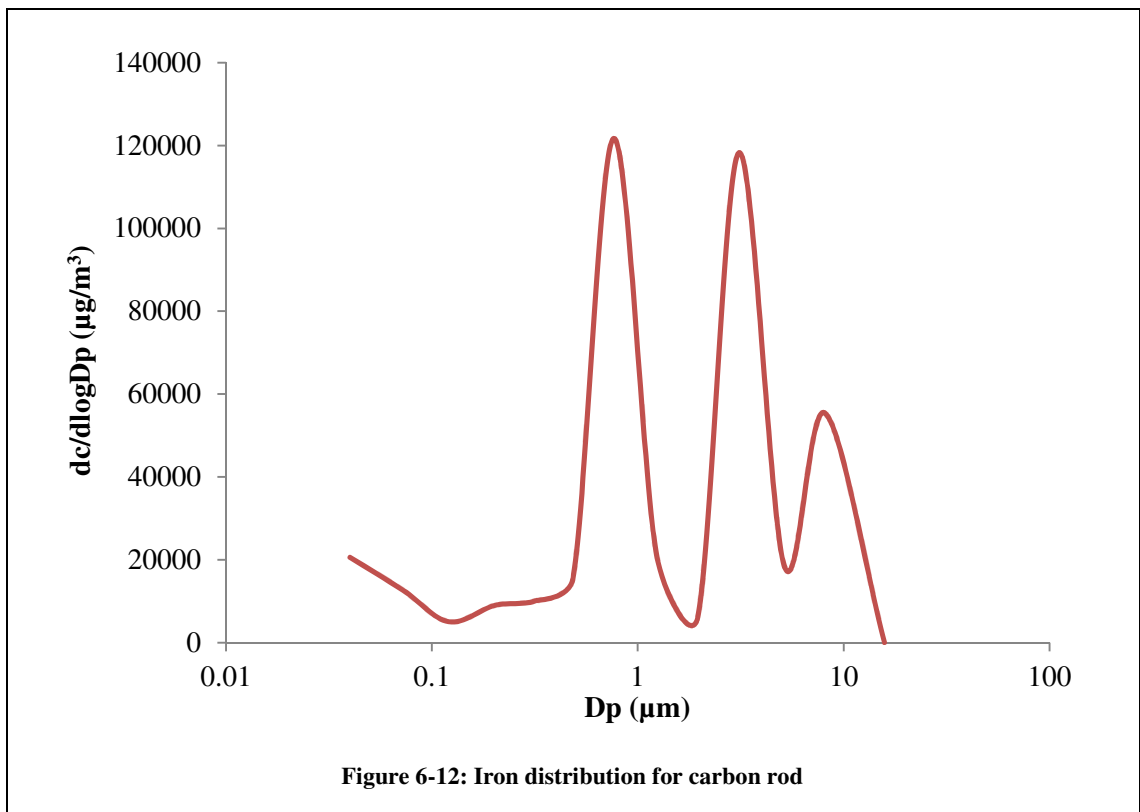
Three noticeable peaks in the manganese concentration were seen for stages two, ten and twelve. For these three stages the concentrations rose from approximately 2.01 µg/g to approximately 2.36 µg/g. Only stage nine gave a concentration which was below the limit of detection of 0.107 µg/L.

The vanadium concentrations followed a similar pattern to manganese, with peaks in concentration for stages ten and twelve, 2.51 µg/g and 2.03 µg/g, respectively. Only stage two had a concentration which was below the limit of detection, 0.046 µg/L, as shown in Figure 6-13. These results indicated that there was a correlation between these two elements and that they may have reacted in the same way to ablation.
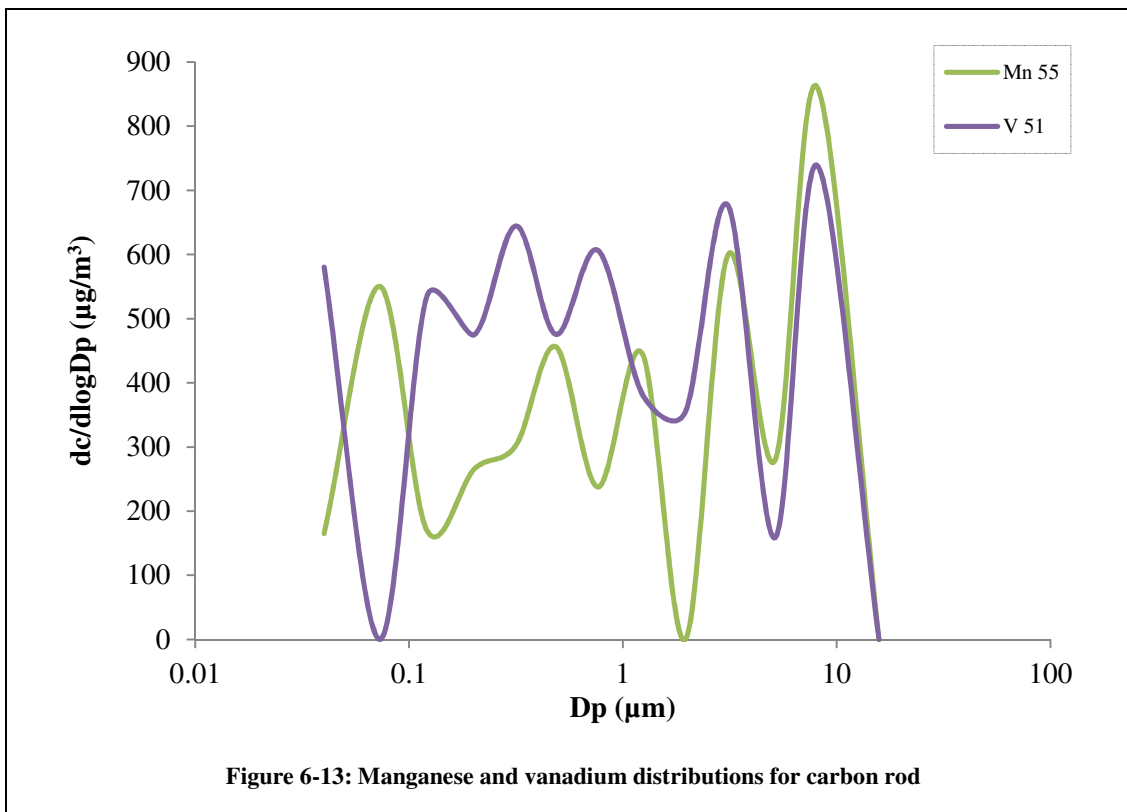
Figure 6-13: Manganese and vanadium distributions for carbon rod

The majority of the twelve stages gave zinc concentrations which were below the limit of detection, 0.97 µg/L, with positive results only being obtained for stages eight and eleven. The peak for stage eleven, at 24.5 µg/g, as seen in Figure 6-14, corresponded well with peaks in concentration seen for other elements, such as manganese and vanadium.

Figure 6-14: Copper and zinc distributions for carbon rod
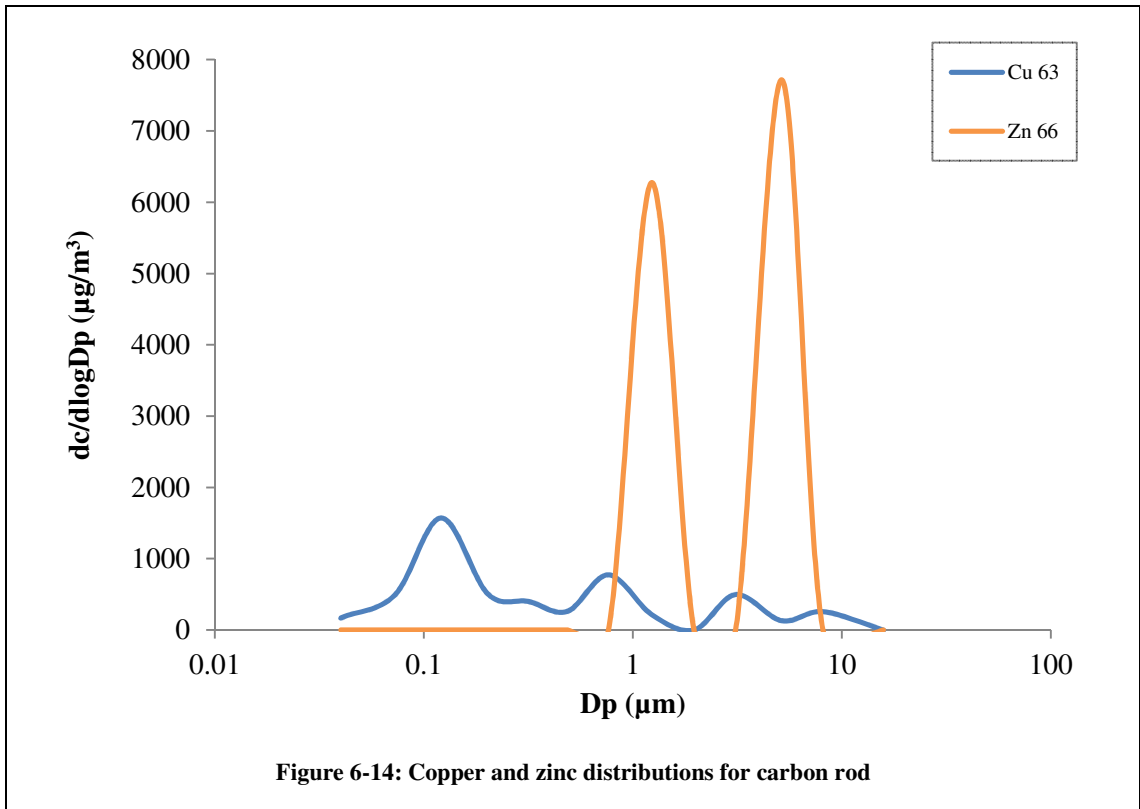
Overall, for the carbon rod material the highest elemental concentrations were seen on stages ten and twelve which corresponded to particulate diameters of 2.40 µm and 6.60 µm respectively. The peaks in concentration for stage twelve corresponded well with the peak in the mass distribution, Figure 6-5. For the majority of the elements, the lowest trace concentrations (including values less than the limit of detection) occurred on stage nine. A dip in the mass distribution was also seen for stage nine, indicating that few particulates were generated in the size range, 1.60 µm to 2.40 µm.

High Purity Zinc

As expected, and as shown in Tables 6-12 and 6-13, the ELPI substrates from the ablation of the high purity zinc material showed high concentrations of zinc upon all substrates, as well as some high iron concentrations on a number of the substrates. The total sum of the individual elements was 155 ng, which was three orders of magnitude smaller than the particulate gravimetric mass, 101 µg. This indicated that a high proportion of elements contained within the particulates were not measured by the ICP-MS. This would need to be rectified for any future work by analysing a larger number of elements, using hydrofluoric acid for digestion and completing replicates for comparison. Overall the zinc masses made up for 87 percent of the total elemental mass balance, with the other six elements combined making up the other 13 percent of the mass balance.

Trace concentrations of copper ranged from 0.518 µg/g, on stage six to 5.50 µg/g on stage two. Both stages five and twelve reported concentrations were below the limit of detection, 0.062 µg/L.

Iron was the second most concentrated element however, for two stages, three and nine, concentrations were below the limit of detection, 1.92 µg/L. The highest concentration occurred for stage twelve, 264 µg/g, an elevated concentration was also seen for stage six, 139 µg/g. The elemental distribution showed good correlation with the mass distribution indicating that it contributed greatly to the overall particulate composition.

Element	1	2	3	4	5	6	7	8	9	10	11	12
Cu 63 (µg/L)	0.540	1.04	0.134	0.266	<0.062	0.098	0.983	0.351	0.495	0.365	0.212	<0.062
Fe 56 (µg/L)	13.5	76.8	<1.92	7.02	6.63	13.20	30.9	13.9	6.60	13.6	1.92	11.7
Mn 55 (µg/L)	0.399	1.22	<0.107	0.159	<0.107	0.418	1.24	0.728	2.54	0.454	0.142	0.210
V 51 (µg/L)	<0.046	<0.046	<0.046	0.051	<0.046	<0.046	0.098	<0.046	0.064	0.063	<0.046	<0.046
Zn 66 (µg/L)	442	511	147	68.34	38.64	37.0	37.8	44.1	34.7	30.1	22.9	7.28

Table 6-12: Elemental analysis of substrates for high purity zinc

Element	1	2	3	4	5	6	7	8	9	10	11	12
Cu 63 (µg/g)	2.53	5.50	0.626	1.50	-	0.518	4.57	1.86	2.45	2.07	1.21	-
Fe 56 (µg/g)	63.0	407	-	39.8	34.5	70.0	143	73.5	32.7	77.0	11.0	63.0
Mn 55 (µg/g)	1.87	6.48	-	0.902	-	2.22	5.75	3.86	12.6	2.57	0.810	1.13
V 51 (µg/g)	-	-	-	0.290	-	-	0.453	-	0.314	0.356	-	-
Zn 66 (µg/g)	2073	2708	685	387	201	196	176	234	172	170	131	39.1
Sum of elemental concentrations (µg/g)	2141	3217	686	430	236	269	330	313	220	252	144	103
Mass of particulates on substrate (g)	2×10^{-5}	3×10^{-5}	7×10^{-6}	3×10^{-6}	1×10^{-6}	2×10^{-6}	1×10^{-5}	3×10^{-6}	3×10^{-6}	8×10^{-6}	8×10^{-6}	2×10^{-6}
Total elemental concentration x particulate mass = Total elemental mass, converted into ng	42.8	96.9	4.80	1.29	0.236	0.538	4.29	0.938	0.659	2.02	1.15	0.206

Total concentration of all analysed elements on the twelve filters, 8249 µg/g

Total elemental masses added together to give the total mass of all analysed elements on the twelve filters, **156 ng**

Table 6-13: Elemental and fractionation results for substrates for high purity zinc

Figure 6-15: Iron distributions for high purity zinc
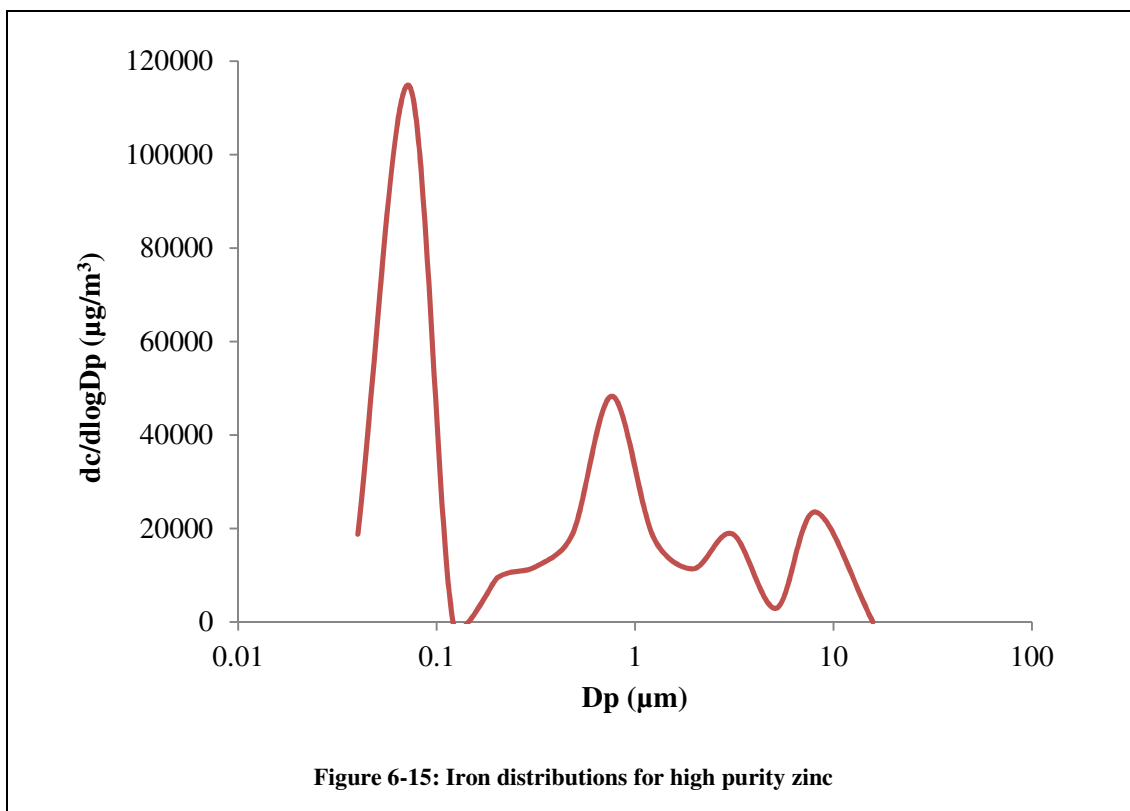
Manganese concentrations varied, with two stages reporting elemental concentrations below the limit of detection, 0.107 µg/L. The smallest concentration was found on stage eleven, 0.810 µg/g, with the largest seen on stage nine, 12.6 µg/g, corresponding to particulates of 1.60 µm in diameter.

The smallest trace elemental concentrations occurred for vanadium. Eight stages gave concentrations below the limit of detection, 0.046 µg/L, with no other stage reporting a concentration above 0.976 µg/g. This indicated that there were very small amounts of vanadium within both the particulates generated through laser ablation and the high purity zinc material itself.

Figure 6-16: Elemental distributions for high purity zinc
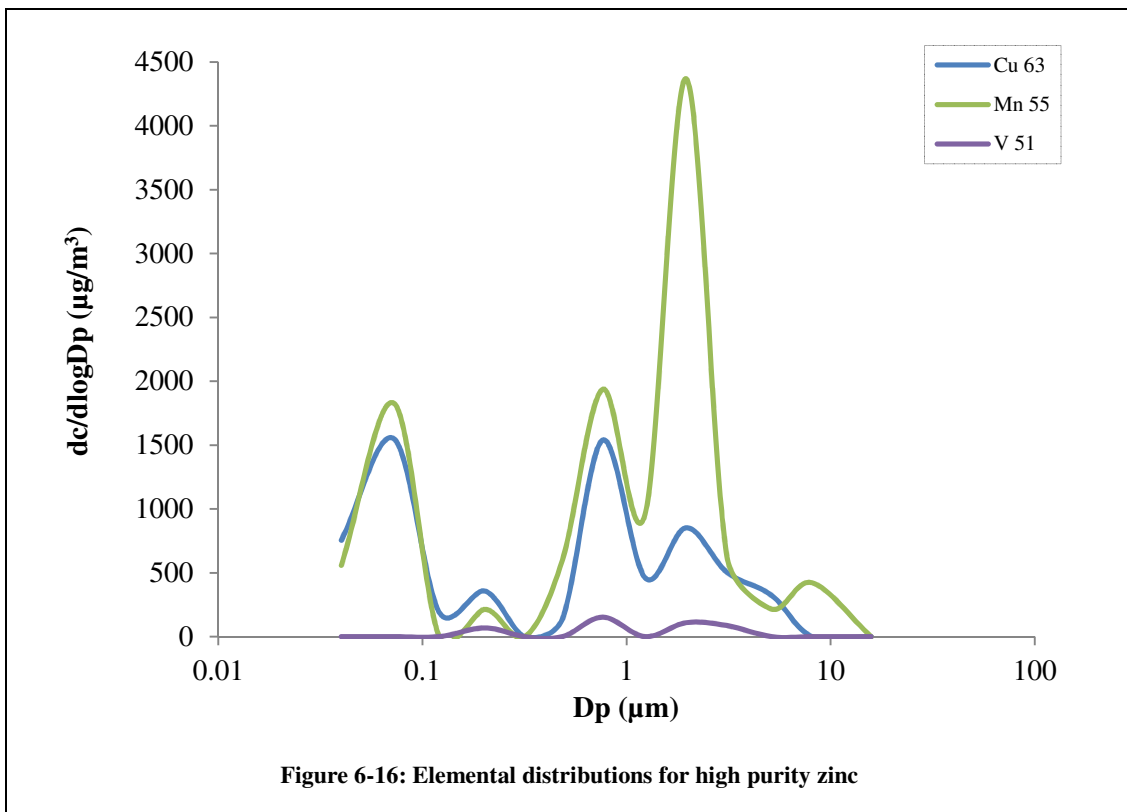
As expected, zinc concentrations were the highest of all elements analysed. The highest concentration of zinc was seen for stage two, 2708 µg/g, with high concentrations also for the first four stages. This indicated that the ablation of the zinc material caused the production of a large number of small particulates, below 0.156 µm in size. The smallest concentration was seen for stage twelve, 39.1 µg/g. As seen in Figure 6-17, the zinc size distributions followed a similar trend to the mass distribution of the substrates, Figure 6-7, especially the peak at 0.07 µm. This indicated that the large mass of particulates on the second stage contained a large proportion of zinc.

**Figure 6-17: Zinc distributions for high purity zinc**
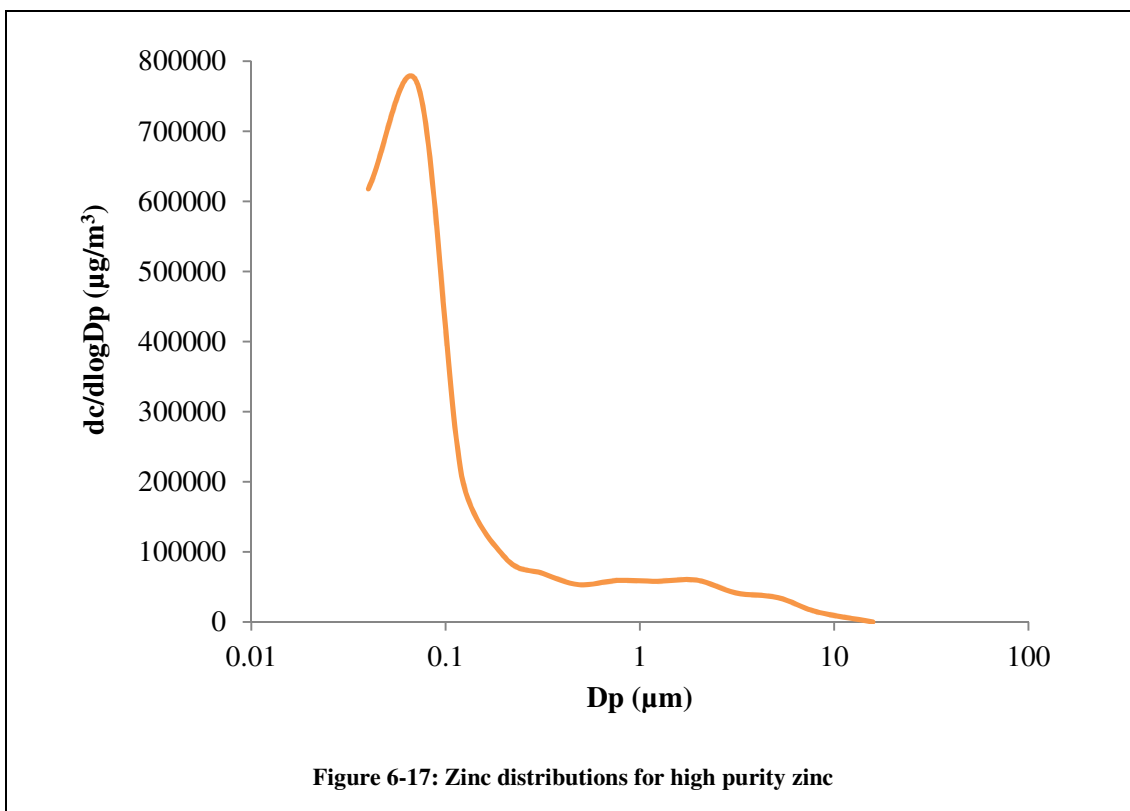
In general the highest elemental concentrations were seen on stage two, with three of the five elements reporting their greatest concentrations on this stage. This indicated that a large number of concentrated particulates were found on this stage which corresponds very well with the mass and number distributions where peaks were seen at 0.07 µm and 0.05 µm respectively. The fact that three elements reported concentrations below the detection limits, with the other two showing lower concentrations, on stage five also corresponded well with the mass distribution where the lowest mass was present on the same stage.

Carbon Steel

Carbon steel contained trace certified concentrations (all below 0.4 percent) of aluminium, antimony, boron, carbon, cobalt, lead, manganese, niobium, phosphorus, sulphur, silicon, vanadium and zirconium. For this analysis only manganese and vanadium were determined. The most concentrated element present upon the carbon steel substrates was iron, Tables 6-14 and 6-15. Iron was especially concentrated on stages one and eleven thus indicating the complex fractionation behaviour of the laser ablation process. The overall gravimetric mass was 133 µg.

This was four orders of magnitude greater than the sum of individual elemental concentrations as determined from the elemental analysis of the substrates, which was 11.8 ng. This was most likely due to the fact that only five elements were analysed and some of those may have remained trapped within the silica matrix, due to the incomplete digestion of the substrates.

Trace concentrations of copper were seen for the carbon steel substrates, with the highest value occurring for stage one, 1.52 µg/g. The smallest detectable concentration was on stage five, 0.411 µg/g. Concentrations for stages three, eight and nine were below the limit of detection, 0.062 µg/L.

Figure 6-18: Copper and vanadium distributions for carbon steel
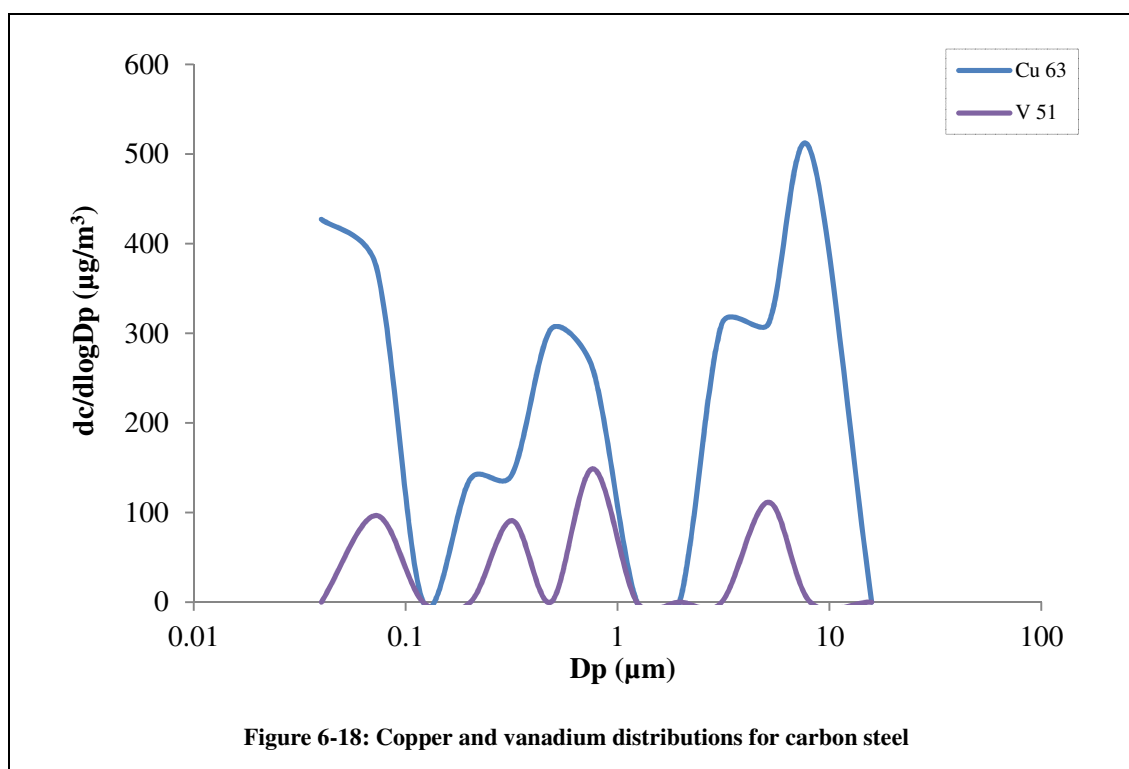
Iron was the most concentrated element, however, concentrations were still quite low in comparison with those obtained for the carbon rod and high purity zinc materials. Iron concentrations ranged from 36.4 µg/g, for stage seven, to 231 µg/g, for stage one, with stage five reporting a concentration below the detection limit, 1.92 µg/L. Peaks in the iron concentration could be seen at stages one, six and eleven, Figure 6-19. The high concentration of particulates, for stages six and eleven, could also be seen in the mass distribution, showing that iron was the major constituent of the generated particulates.

Element	1	2	3	4	5	6	7	8	9	10	11	12
Cu 63 (µg/L)	0.284	0.233	<0.062	0.095	0.074	0.197	0.154	<0.062	<0.062	0.208	0.189	0.233
Fe 56 (µg/L)	42.9	15.6	3.60	7.16	<1.92	23.0	6.97	9.07	10.9	27.1	31.2	11.1
Mn 55 (µg/L)	0.688	0.235	0.149	0.431	<0.107	0.560	1.42	1.77	0.676	0.907	1.40	0.620
V 51 (µg/L)	<0.046	0.060	<0.046	<0.046	0.047	<0.046	0.088	<0.046	<0.046	<0.046	0.068	<0.046
Zn 66 (µg/L)	1.87	<0.966	<0.966	<0.966	<0.966	7.52	<0.966	<0.966	1.12	2.64	2.08	1.10

Table 6-14: Elemental analysis of substrates for carbon steel

Element	1	2	3	4	5	6	7	8	9	10	11	12
Cu 63 (µg/g)	1.52	1.17	-	0.512	0.411	1.12	0.804	-	-	0.990	0.908	1.29
Fe 56 (µg/g)	231	78.5	19.3	38.7	-	131	36.4	48.5	55.2	129	150	61.6
Mn 55 (µg/g)	3.70	1.18	0.797	2.33	-	3.20	0.688	0.594	0.785	1.52	3.62	0.627
V 51 (µg/g)	-	0.302	-	-	0.263	-	0.460	-	-	-	0.326	-
Zn 66 (µg/g)	10.1	-	-	-	-	43.0	-	-	5.67	12.6	9.96	6.11
Sum of elemental concentrations (µg/g)	246	81.2	20.1	41.5	0.674	178	38.3	49.1	61.6	144	164	69.6
Mass of particulates on substrate (g)	1×10^{-5}	1×10^{-5}	1×10^{-5}	1×10^{-5}	8×10^{-6}	1×10^{-5}	1×10^{-5}	1×10^{-5}	5×10^{-6}	7×10^{-6}	1×10^{-5}	1×10^{-5}
Total elemental concentration x particulate mass = Total elemental mass, converted into ng	2.46	0.974	0.381	0.540	0.005	1.96	0.383	0.589	0.308	1.01	2.47	0.766

Total concentration of all analysed elements on the twelve filters, 1095 µg/g

Total elemental masses added together to give the total mass of all analysed elements on the twelve filters, **11.84 ng**

Table 6-15: Elemental and fractionation results for substrates for carbon steel

**Figure 6-19: Iron distributions for carbon steel**
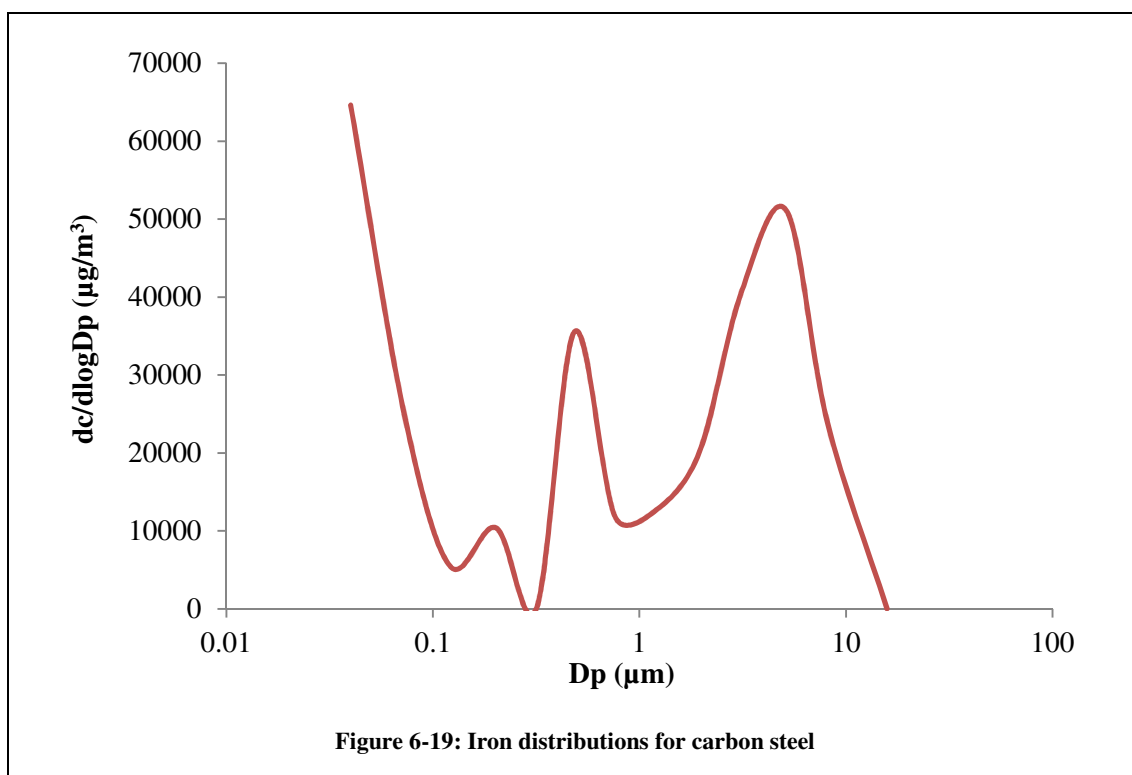
Manganese concentrations were determined for most stages, except stage five, but, in general, trace concentrations were given with no value being greater than 3.70 µg/g. Although present in these trace concentrations manganese, Figure 6-20 gave a similar shaped elemental distribution plot to iron. This indicated that the behaviour of manganese was similar to that of iron, with respect to how, within the steel matrix, it responded to laser ablation.

Vanadium concentrations were the lowest in the carbon steel material. The highest vanadium concentration was reported for stage seven, 0.460 µg/g and the lowest for stage five, 0.263 µg/g. Concentrations for stages one, three, four, six, eight, nine, ten and eleven were below the limit of detection, 0.046 µg/L. This was most likely due to the chemical composition of the carbon steel. The percentage mass of vanadium within the steel was 0.153 percent and therefore trace vanadium concentrations were expected.

The highest concentration of zinc was found on stage six, 43.0 µg/g and the lowest on stage nine, 5.67 µg/g. Peaks in concentration were also seen for stages one and ten, whilst stages two

to five, seven and eight, reported elemental concentrations which were below the limit of detection, 0.966 µg/L.

Figure 6-20: Magnesium and zinc distributions for carbon steel
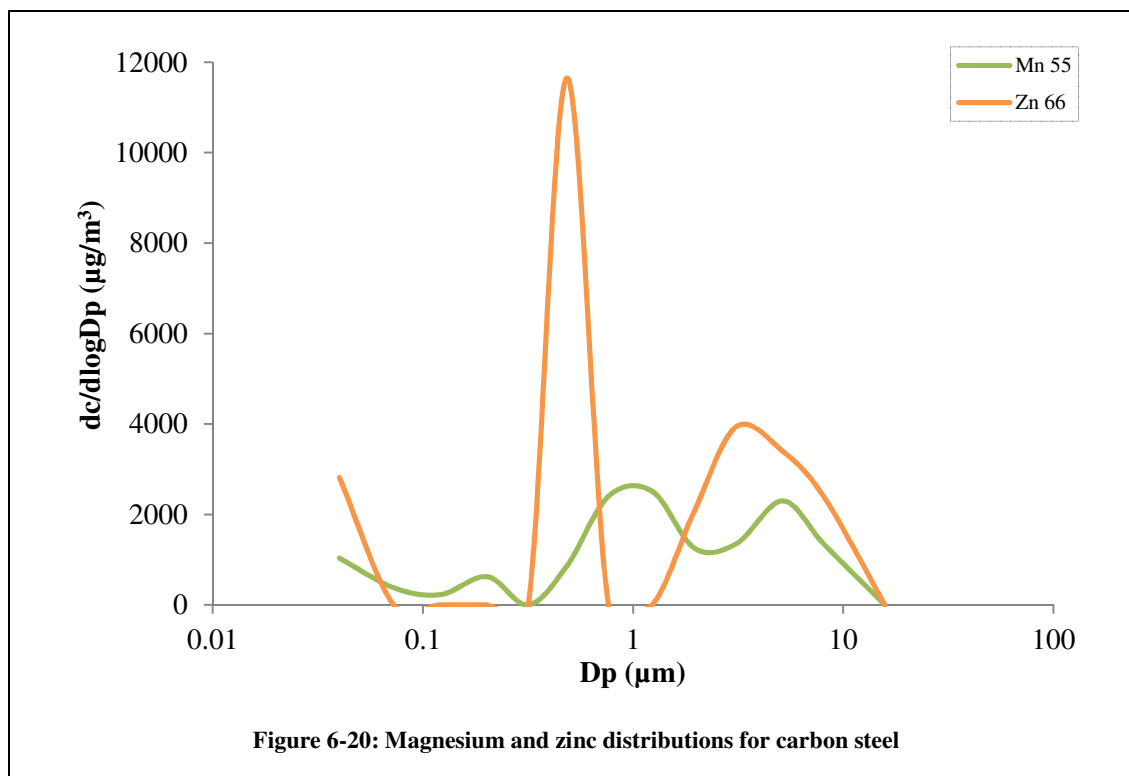
Two of the analysed elements, copper and vanadium, in the carbon steel gave quite low concentrations. The smallest was seen for vanadium on stage five, 0.236 µg/g. Stage five generally gave the lowest elemental concentrations indicating that particulates of 0.262 µm in size were not readily generated. The higher numbered stages, nine to twelve, which collected the larger particulates, mostly gave positive results indicating that the generated and more concentrated particulates were generally larger in size, above 1.60 µm.

Boron Nitride

As expected the boron nitride gave high concentrations of boron and low concentrations of most other elements, data shown in Tables 6-16 and 6-17. The highest concentration of boron was seen on stage two, however the highest concentrations of other elements were seen on other stages which showed that the particulates generated were variable in diameter. In total, boron concentrations accounted for 70 percent of the total elemental mass balance, which was 208 ng. The other 30 percent was accounted for the by trace elements which were analysed. The

gravimetric analysis of the boron nitride substrates gave a total particulate mass of 187 µg, three orders of magnitude greater than the sum of the individual masses of the analysed elements. This was most likely down to the low number of elements which were analysed and the possible incomplete digestion of the substrates.

Boron concentrations, Figure 6-21, followed a similar trend to the mass distribution, indicating a peak in concentration for stage two, 2126 µg/g. This indicated that the generated particulates mainly consisted of boron, as would be expected. Stages eleven and twelve gave concentrations below the limit of detection, 5.53 µg/L, which also corresponded with the mass distribution.

Figure 6-21: Boron distributions for boron nitride
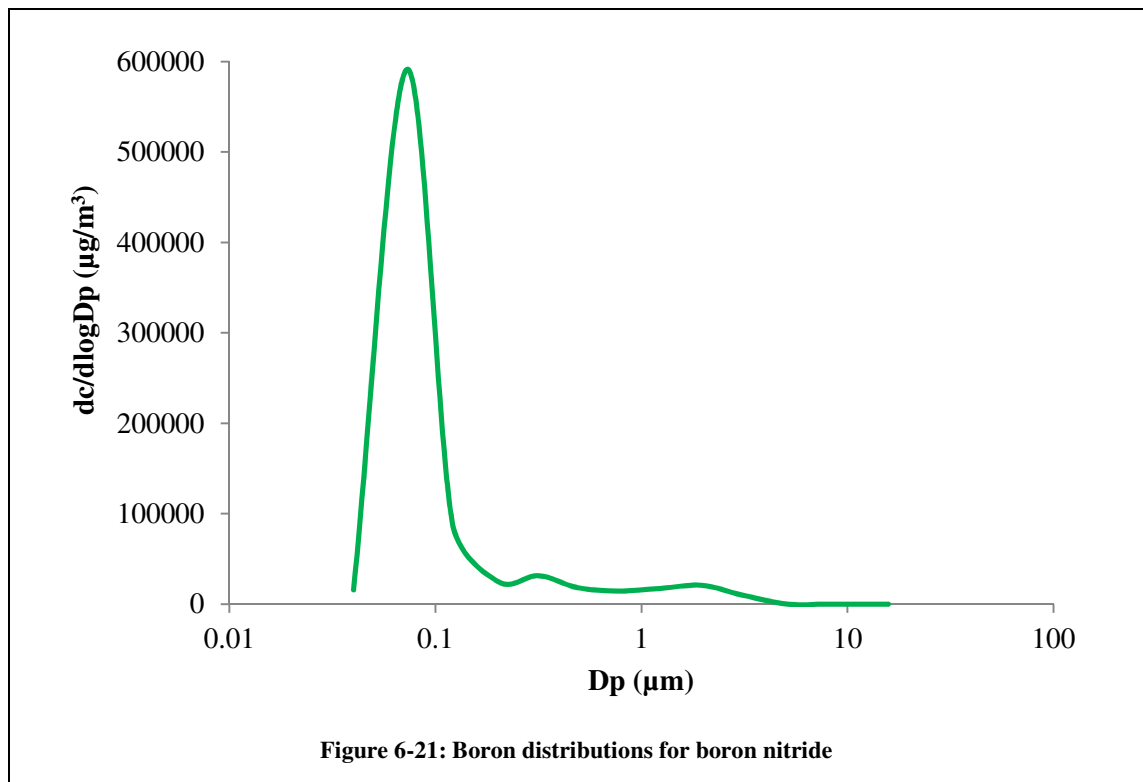
Element	1	2	3	4	5	6	7	8	9	10	11	12
B 208.95 (µg/L)	10.7	376	59.8	17.4	16.7	12.2	8.80	12.5	11.5	6.80	<5.53	<5.53
Cu 63 (µg/L)	0.133	0.131	0.137	0.343	0.530	0.829	0.134	0.227	0.209	0.193	0.200	0.204
Fe 56 (µg/L)	3.46	8.80	27.6	21.6	8.42	28.2	6.06	28.2	10.9	42.3	6.22	16.3
Mn 55 (µg/L)	0.136	0.438	0.261	0.429	0.172	0.332	0.131	0.287	0.409	0.372	0.150	0.253
V 51 (µg/L)	<0.046	<0.046	<0.046	0.064	<0.046	<0.046	<0.046	<0.046	<0.046	<0.046	<0.046	<0.046
Zn 66 (µg/L)	<0.966	<0.966	2.60	<0.966	3.92	1.81	<0.966	<0.966	<0.966	1.30	1.52	1.61

Table 6-16: Elemental analysis of substrates for boron nitride

| Element	1	2	3	4	5	6	7	8	9	10	11	12
B 208.95 (µg/g)	57.5	2126	338	87.2	89.8	69.5	49.7	66.9	65.5	36.9	-	-
Cu 63 (µg/g)	0.714	0.740	0.774	1.72	2.85	4.72	0.759	1.21	1.19	1.05	0.975	0.966
Fe 56 (µg/g)	18.6	49.8	156	108	45.3	161	34.24	151	62.1	229	30.3	77.1
Mn 55 (µg/g)	0.732	2.47	1.48	2.15	0.93	1.89	0.740	1.54	2.33	2.02	0.734	1.20
V 51 (µg/g)	-	-	-	-	-	-	-	-	-	-	-	-
Zn 66 (µg/g)	-	-	14.7	4.53	21.1	10.3	-	-	-	7.07	7.42	7.63
Sum of elemental concentrations (µg/g)	76.8	2177	509	232	195	245	84.7	219	129	274	38.7	85.7
Mass of particulates on substrate (g)	1×10^{-5}	8×10^{-5}	2×10^{-5}	1×10^{-5}	8×10^{-6}	6×10^{-6}	3×10^{-6}	3×10^{-6}	4×10^{-6}	1×10^{-5}	6×10^{-6}	7×10^{-6}
Total elemental concentration x particulate mass = Total elemental mass, converted into ng	1.15	181	14.8	2.79	1.56	1.47	0.254	0.658	0.515	3.02	0.232	0.600

Total concentration of all analysed elements on the twelve filters, 4267 µg/g

Total elemental masses added together to give the total mass of all analysed elements on the twelve filters, **208 ng**

Table 6-17: Elemental and fractionation results for substrates for boron nitride

Copper concentrations ranged from 0.714 µg/g, stage one, to 4.72 µg/g, stage six. No stages reported concentrations which were below the detection limit, 0.062 µg/L.

Iron concentrations were varied for boron nitride, as shown in Figure 6-22. The highest concentration was found on stage ten, 229 µg/g with the lowest on stage one 18.6 µg/g. This was the opposite of boron where the highest concentration was on stage ten and the lowest on stage one. This indicated that these two elements did not react to the laser in similar ways.

Figure 6-22: Iron distributions for boron nitride
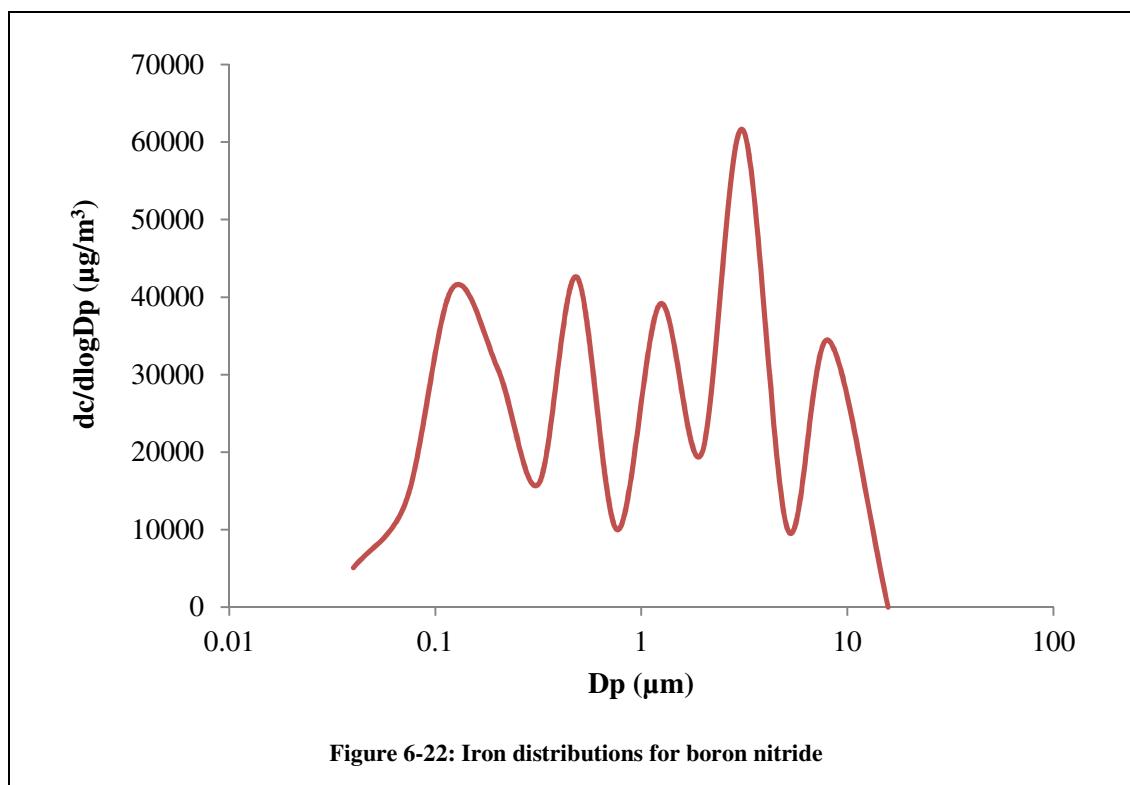
Trace concentrations of manganese were determined on all twelve stages. As with a number of the other elements the lowest concentrations was found on stage one, 0.732 µg/g. The highest concentration was 2.47 µg/g, on stage two, as was seen for boron. This indicated that the particulates only contained trace amounts of manganese, but the two elements reacted similarly to the laser, both producing high concentrations of particulates with a diameter of 0.056 µm.

No stages gave vanadium concentrations which were above the limit of detection, 0.046 µg/L. This indicated that the particulates contained trace levels of vanadium if any at all.

Zinc concentrations were below the limit of detection, 0.966 µg/L, for stages one, two, seven, eight and nine, whilst stage five reported the highest concentration, 21.1 µg/g. The lowest measured concentration was given for stage four, 4.53 µg/g.

Figure 6-23: Elemental distributions for boron nitride
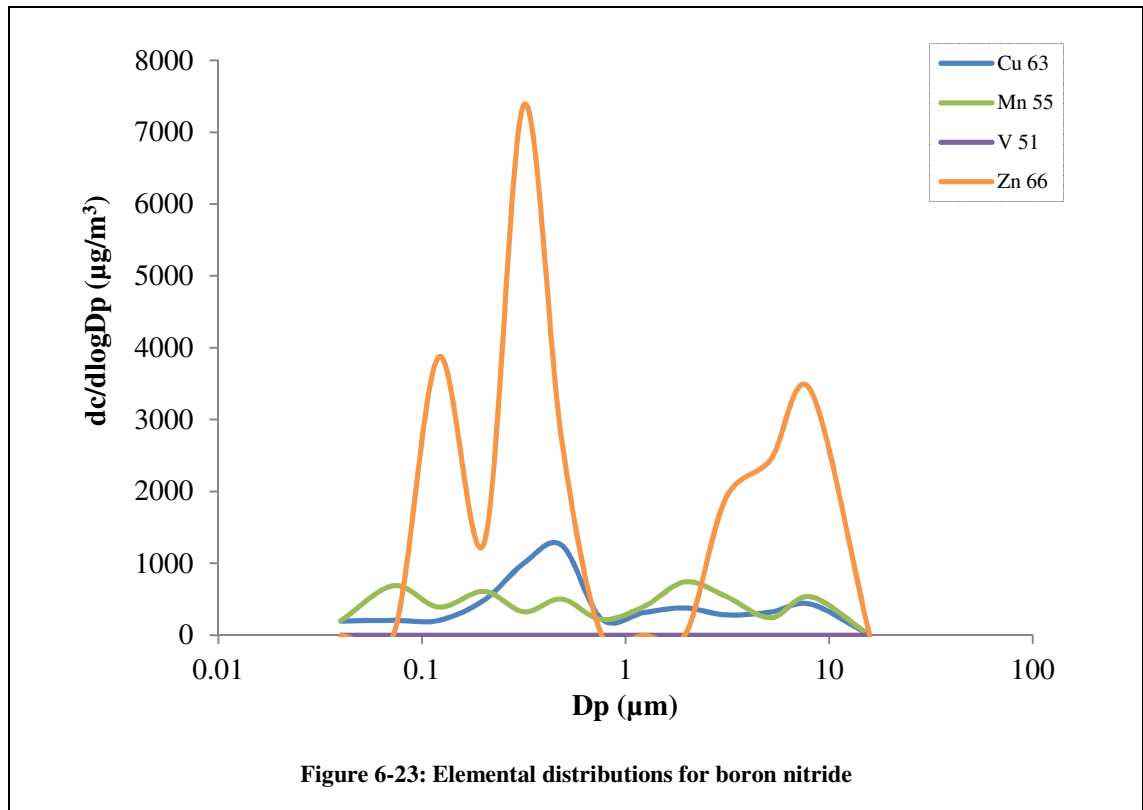
Overall for boron nitride, boron was the only element whose distribution showed similarities with the mass distribution obtained previously. This was expected and indicated that boron was one of the main constituents of the particulates which were analysed. None of the other analysed elements followed a similar trend showing that they were only present in trace quantities.

6.4 Main Findings

The coupling of a LA (1064 nm) unit to an ELPI has provided new and useful information on size fractionation. Particulates were successfully generated through laser ablation and collected onto substrates followed by their digestion and elemental analysis. Four materials were ablated and independently characterised to obtain gravimetric data as well as number, mass and elemental size distributions.

The four materials, carbon rod, high purity zinc, carbon steel and boron nitride, revealed the presence of high numbers of generated particulates at approximately 0.05 μm in diameter. However, the mass distributions gave different results. Large masses of particulates which were 0.07 μm in diameter were seen for both the high purity zinc and the boron nitride materials whilst the carbon rod and carbon steel materials reported high masses of larger particulates, 0.32 μm and 0.12 μm, respectively. This signified that although large numbers of very small particulates were present, for both the carbon rod and carbon steel materials, they did not have a great mass and thus, the larger particulates contributed more to the mass distributions. Both the metallic materials, high purity zinc and carbon steel, underwent melting, whilst the other two materials, carbon rod and boron nitride, underwent thermal shock due to their high melting points.

Alongside the digestion and analysis of the substrates a QC and an SRM were analysed to determine the precision and accuracy of the measurements. In terms of the QC, the results obtained were very good, with all elements reporting values close to the reference value of 20 μg/g. Low RSDs, generally below three percent, were also obtained showing excellent precision. The SRM recoveries were over 90 percent for all elements except vanadium, 88 percent. This indicated that some vanadium had remained trapped within the undigested silica matrix. To allow the complete digestion of the SRM in future work it is necessary to use hydrofluoric acid. The RSDs were all below nine percent, again indicating acceptable precision.

Limits of detection were calculated for each element. They were generally no greater than 1.0 µg/L, except for boron and iron which were 5.53 µg/L and 1.92 µg/L, respectively.

All substrates held particulates which were generated by the laser ablation of a solid material. Most substrates exhibited a peak in elemental concentration between 0.32 µm and 0.76 µm as well as at 3.10 µm. To have an increased elemental concentration on a substrate there must have been an increase in the number of particulates held upon that substrate. This indicated that the ablations must therefore have produced large numbers of particulates with these sizes for all four materials.

For three of the materials, high purity zinc, carbon steel and boron nitride, the main constituent element was characterised, zinc, iron and boron, respectively, and elemental distributions were obtained. The respective elemental distributions for these materials corresponded well with their associated mass distributions indicating that the generated particulates contained high concentrations of these elements. None of the carbon rod elemental distributions corresponded with the mass distribution, as would be expected since the main constituent, carbon, was not analysed. The elemental distributions for the three main constituent elements were not comparable with each other. This indicated that both the materials and the elements themselves interacted differently when undergoing laser ablation, thus, generating particulates which were different in both size and elemental composition. One point of interest is that all of the four materials characterised using the LA (1064 nm)-ELPI method contained relatively high concentrations of iron. Although iron is a common trace constituent it was not expected to be present in large concentrations in all four materials. It was thought that the increased concentrations may have been due to contamination from the ELPI, microwave digestion vessels or the ICP itself. However, the concentrations over the twelve substrates did differ indicating that it was not necessarily a contamination issue. If it had been, similar concentrations of iron would be expected on the same substrates for all four materials. The other elements which were analysed, copper, manganese and vanadium were generally present in all

of the materials in trace quantities, with a number reporting concentrations which were below the limits of detection. In a number of cases the trace elements produced similar elemental distributions for a single material. This indicated that there were similar concentrations of these elements present within that material and that they had undergone similar processes during laser ablation.

In future it would be preferable to analyse the substrates for other elements, such as carbon and nitrogen, especially for the carbon rod and the boron nitride. Carbon analysis can prove to be difficult with ICP-AES so SEM analysis could be completed instead. This would also allow the size of the particulates held upon each substrate to be checked. Unfortunately further analysis was not possible here because replicate analyses were not completed and therefore no spare substrates were available for SEM analysis.

The previous studies mentioned in Section 6.1 mostly concerned ablation of a brass material to generate particulates.[14-16] This research has allowed a range of materials to be ablated to produce laser generated particulates which were characterised both chemically and physically.

An alternative option to solution ICP-MS, for future work to examine, would be LA-ICP. This would reduce the analysis time since pre-digestion would not be required and the substrates could be analysed directly, although there could be issues with calibration standards and reproducibility. Replicate analyses using the same method should also be completed to determine the reproducibility of the results.

Real time measurement of particulate matter

M. Barker[1], C.W. McLeod[1], D. Ciaparra[2], D.R. Anderson[2], A.I. Whitehouse[3]

[1]*Department of Chemistry, University of Sheffield, Sheffield, S3 7HF, UK*
[2]*Tata Steel Europe, Swinden Technology Centre, Rotherham, S60 3AR, UK*
[3]*Applied Photonics, Unit 8 Carleton Business Park, Skipton, BD23 2DE*

Studies have shown that particulate matter present within the atmosphere can cause numerous respiratory problems including chronic bronchitis.[1] In light of these health risks and environmental implications,[2] the characterisation of chemical and physical properties of particulates is important. Current sources of particulate matter in the iron and steel making industry include the generation of dusts from processes as well as the handling and stockpiling of raw materials. A real time measurement capability would allow an improved understanding of particulate formation.

In initial work, an Aspect morphology analyser was coupled to a rotating drum sampler (RDS), Figure 1. Four raw materials were characterised in duplicate. A mixture of differing particulate shapes and sizes were observed for the four samples with duplicates showing good reproducibility. Individual characteristic fingerprints were also extracted from binary mixture profiles. The morphological fingerprints which have been generated in this study allowed an insight into the properties of particulate matter present on an integrated steel works.

A novel instrument configuration that provides both chemical and physical information has been conceived. A laser induced breakdown spectrometer (LIBS) has been coupled to the Aspect morphology analyser to enable the morphology of a laser generated aerosol to be characterised in real time, Figure 2. Using an argon atmosphere signal stability studies were performed as well as method development. From preliminary work, using a carbon steel certified reference material, both morphological fingerprints and elemental spectra were acquired. High concentrations of mostly spherical particulates at 0.5 μm in diameter were detected. No particulates were present with a diameter greater than 3 μm. LIBS spectra confirmed the presence of iron as well as carbon. Morphological profiles and LIBS spectra were reproducible between replicates. Studies of selected samples are planned to determine whether the chemical composition of a sample can affect the laser ablated aerosol morphology.

Figure 1: RDS- Aspect coupling   Figure 2: LIBS-Aspect coupling
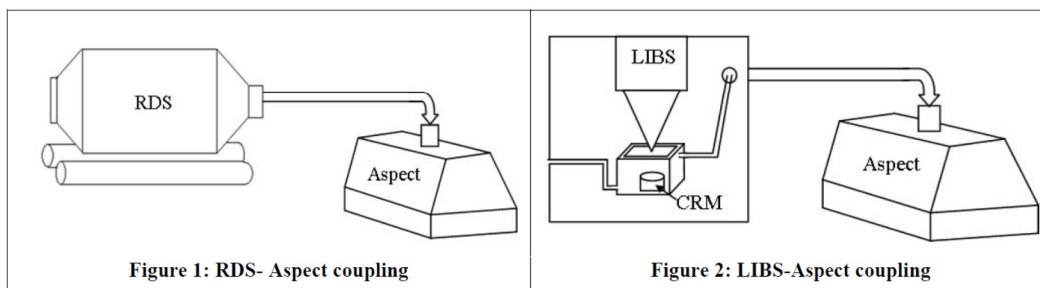
References
1. J. Schwartz, *Environmental Research*, 1993, **62**, 7-13
2. K. Ravindra, A. K. Mittal and R. Van Grieken, *Review on Environmental Health*, 2001, **16**, 169-189

An abstract of work presented as an oral presentation at Tata Steel Academic Symposium, Warwick, 2012.

6.5 References

1.   S. Tanaka, N. Yasushi, N. Sato, T. Fukasawa, S. J. Santosa, K. Yamanaka and T. Ootoshi, *Journal of Analytical Atomic Spectrometry*, 1998, **13**, 135-140.
2.   S. Gligorovski, J. T. van Elteren and I. Grgic, *Science of the Total Environment*, 2008, **407**, 594-602.
3.   C.-J. Chin, C.-F. Wang and S.-L. Jeng, *Journal of Analytical Atomic Spectrometry*, 1999, **14**, 663-668.
4.   W. Chung, V. N. Sharifi, J. Swithenbank, O. Osammor and A. Nolan, *Modern Applied Science*, 2008, **2**, 17-32.
5.   Y.-K. Hsieh, L.-K. Chen, H.-F. Hsieh, C.-H. Huang and C.-F. Wang, *Journal of Analytical Atomic Spectrometry*, 2011, **26**, 1502-1508.
6.   J. Koch, A. von Bohlen, R. Hergenröder and K. Niemax, *Journal of Analytical Atomic Spectrometry*, 2004, **19**, 267-272.
7.   B. Hattendorf, C. Latkoczy and D. Günther, *Analytical Chemistry*, 2003, **75**, 341 A-347 A.
8.   K. R. May, *Journal of Scientific Instruments*, 1945, **22**, 187-195.
9.   *ELPI User Manual*, Dekati Ltd, 2008.
10.   *Dekati PM10 Impactor Brochure*, Dekati Ltd, 2010.
11.   *Gravimetric Impactor Brochure*, Dekati, 2010.
12.   www.dekati.com, Accessed 4th July 2013
13.   P. M. Outridge, W. Doherty and D. C. Gregoire, *Spectrochimica Acta Part B: Atomic Spectroscopy*, 1997, **52**, 2093-2102.
14.   R. Jaworski, E. Hoffmann and H. Stephanowitz, *International Journal of Mass Spectrometry*, 2002, **219**, 373-379.
15.   H.-R. Kuhn and D. Günther, *Analytical Chemistry*, 2003, **75**, 747-753.
16.   C. Y. Liu, X. L. Mao, J. Gonzalez and R. E. Russo, *Journal of Analytical Atomic Spectrometry*, 2005, **20**, 200-203.
17.   R. Glaus, J. Koch and D. Günther, *Analytical Chemistry*, 2012, **84**, 5358-5364.
18.   P. M. Outridge, W. Doherty and D. C. Gregoire, *Spectrochimica Acta Part B: Atomic Spectroscopy*, 1996, **51**, 1451-1462.
19.   K. Jackson, PhD Thesis, University of Sheffield, 2009.
20.   R. Xie, K. A. Jackson, H. M. Seip, C. W. McLeod, G. Wibetoe, M. J. Schofield, D. Anderson and J. E. Hanssen, *Journal of Environmental Monitoring*, 2009, **11**, 336-343.
21.   M. Thompson, S. Chenery and L. Brett, *Journal of Analytical Atomic Spectrometry*, 1990, **5**, 49-55.
22.   R. R. Whitlock and G. M. Frick, *Journal of Materials Research*, 1994, **9**, 2868-2872.
23.   S. E. Jackson and D. Günther, *Journal of Analytical Atomic Spectrometry*, 2003, **18**, 205-212.
24.   S. Chenery, A. Hunt and M. Thompson, *Journal of Analytical Atomic Spectrometry*, 1992, **7**, 647-652.

Chapter Seven

Conclusions and Further Work

7.1 Conclusions

The principle aim of this research was to develop novel methods to chemically and physically characterise particulate matter. To achieve this, new instrumental configurations had to be investigated and devised to allow proof of concept whilst also obtaining primary results which were reliable. Current and existing methods have been used as a basis, however, they had been modified and adapted to allow the production of new methods which can now be taken forward. Four new methods have been developed in total concentrating around two main instruments, the Aspect morphology analyser and the ELPI. These instruments along with ICP techniques have allowed chemical and physical characterisation of a range of materials.

Chapter One concentrated upon the bulk indirect chemical analysis of materials obtained from a steelworks using both ICP-AES and ICP-MS. The four materials, two ores and two dusts, were digested using a microwave and aqua regia to allow the quantification of their elemental compositions. The precision of the data obtained using each technique was compared and the preferred technique noted. In most cases this was ICP-MS, apart from iron, which due to its high concentrations within the four materials was best analysed using ICP-AES. The results allowed an insight into the chemical compositions of the four materials before they were physically and further chemically characterised. The method used for this analysis was based upon one used within the steel industry which had been accredited by UKAS and fulfilled the requirements of ISO 17025.

Novel experimental methods were developed which coupled a rotating drum system to an Aspect morphology analyser and an ELPI successively. These two couplings allowed

morphological profiles as well as number and mass distributions to be obtained. In both cases a control material, titanium dioxide was also characterised to check the coupling had been completed correctly and successfully. Each of the instruments focused on particulates with different sizes and therefore it is not possible to compare the results obtained from each of them. The reproducibility of the individual results which were obtained here was excellent, showing that the physical properties of the particulates were consistent. SEM photographs were obtained of the materials and these were compared to the morphological profiles. The photographs indicated the presence of particulates within the materials with the same morphology as was seen in the obtained profiles. This signified that the Aspect was correctly determining particulate morphologies.

One aim of this section of work was to start to develop individual characteristic profiles of each of the materials so that they could be used in on-site work. These fingerprints, which have been successfully obtained, will become the basis for a database of materials found on and near a steelworks. A preview of this database in action was also described when a source apportionment study at an integrated steelworks was completed. The results obtained on site were compared with the morphological profiles obtained in Chapter Three to allow the sources of the characterised dust to be established.

When using the ELPI, as well as generating number and mass distributions, the substrates were digested and chemically analysed using ICP-MS. A similar method, as was used to characterise the solid materials, was developed and employed. The elemental distributions which were obtained corresponded well with both the number and mass distributions which indicated that the constituent elements had been correctly analysed and identified. This extra study also allowed the generation of more characteristic information, on the four materials, which could be taken forward to be utilised within the material database.

Following the characterisation of these anthropogenic aerosols, the characterisation of six laser generated aerosols was completed, again using the Aspect morphology analyser and the ELPI. This was completed to allow an insight into the physical characteristics of particulates generated through laser ablation of solid materials.

A large amount of research and development was needed into the method and parameters required for the successful ablation and generation of particulates. Each of the laser parameters was examined thoroughly to determine the most ideal parameters required. The ablation atmosphere, as well as the wavelength of the laser used for ablation, was also investigated and comparisons made. It was decided that an argon atmosphere provided more reproducible results than a laboratory air atmosphere due to its stable nature. The two lasers which were examined, each with a different wavelength, were both capable of generating particulates and the morphological profiles obtained from each laser were comparable. The obtained photomicrographs also allowed the craters to be examined in relation to the wavelength of the laser used. The use of both the Aspect morphology analyser and the ELPI allowed a wide range of particulates with different diameters to be characterised, something which could not have been completed if only one of these instruments had been used. The ELPI substrates containing laser generated particulates were again digested and chemically characterised using ICP-MS. As before the elemental distributions, specifically the main components were comparable with the number and mass distributions which indicated that the coupling of the laser to the ELPI was successful.

By researching and understanding some of the laser material interactions as well as knowing the properties of the six materials, it was possible to describe why each of the materials reacted in a specific way to ablation and generated particulates of a specific size and shape. This knowledge can now be taken forwards and used with other materials to hypothesise the physical characteristics of laser generated particulates, just by knowing a few key details, such as a materials melting point and thermal conductivity.

7.2 Further Work

Overall the principle aim of this research has been completed, however, there are a number of areas where improvements may be made to allow either a larger range of data to be acquired or to confirm the data that has already been obtained.

One of the key points is that more replicates should be completed, especially for the generation and characterisation of particulates using lasers. This would allow the reproducibility of the data to be confirmed as well as allowing a number of key issues to be investigated. Another two points which cover the majority of the work discussed here are the characterisation of a wider range of materials and the analysis of a greater number of elements. These points would both allow more information to be obtained which could be carried forward from these initial studies.

Specifically for the digestion of both solids and substrates the use of hydrofluoric acid should be investigated. This would allow it to be determined as to whether the materials had been digested properly and the elements had remained in the silica matrix or not.

In terms of the Aspect morphology analyser a larger range of both binary and tertiary mixes should be characterised to determine if a single, individual morphological profile can be easily picked out from a morphological profile which is generated from two or three materials.

The analysis of the ELPI and LA substrates could also be investigated. Firstly, when using the RDS-ELPI method a reference material should undergo the same steps as the materials, rather than just the digestion stage. Secondly, the use of LA-ICP-MS could be investigated as an analysis technique rather than solution ICP-MS.

For the generation and characterisation of particulates using lasers a number of lasers, with differing wavelengths and energies could be examined to determine how they affect the shape

and size of the particulates generated. The fluence of the lasers should also be examined to determine if it affects the laser material interaction.

Finally to allow this work to be put into use in industry a database should be generated which contains information on the shape and size of particulates as well as their number, mass and elemental distributions. This could be also furthered using artificial neural networks to determine the individual parts of a mixture. The storage of all this information in one place would permit source apportionment to be completed more readily, allowing the sources of particulate matter to be established and the relevant abatement procedures put into place.

Appendices

Appendix One

Physical and elemental studies of particulates using an RDS-ELPI method and ICP-MS
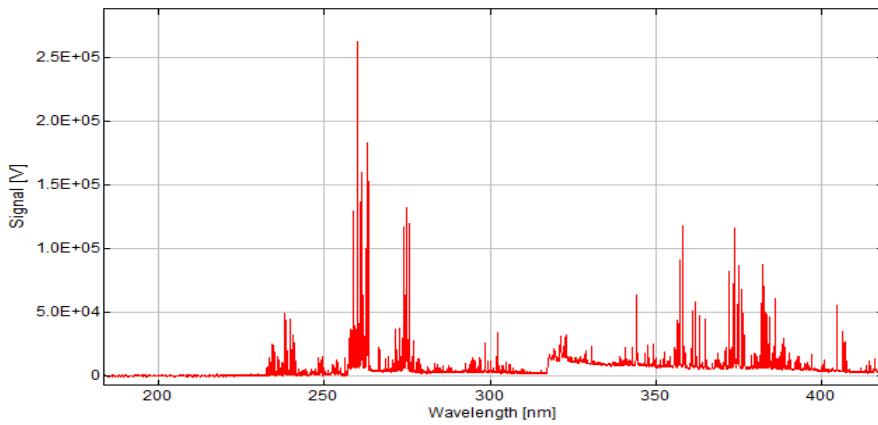
Material	ELPI Stage	Mass in digestion (mg)	Mass in digestion (g)	Mass of particulates on filter (mg)	Mass of particulates on filter (g)
Ore D	1	6.15	0.00615	0.005	0.000005
Ore D	2	6.376	0.006376	0.006	0.000006
Ore D	3	5.364	0.005364	0.001	0.000001
Ore D	4	6.366	0.006366	0.003	0.000003
Ore D	5	5.787	0.005787	0.005	0.000005
Ore D	6	5.259	0.005259	0.017	0.000017
Ore D	7	6.07	0.00607	0.01	0.000010
Ore D	8	6.058	0.006058	0.013	0.000013
Ore D	9	5.616	0.005616	0.008	0.000008
Ore D	10	5.452	0.005452	0.008	0.000008
Ore D	11	5.923	0.005923	0.005	0.000005
Ore D	12	5.867	0.005867	0.004	0.000004
Ore F	1	5.753	0.005753	0.023	0.000023
Ore F	2	5.633	0.005633	0.004	0.000004
Ore F	3	5.436	0.005436	0.012	0.000012
Ore F	4	5.337	0.005337	0.012	0.000012
Ore F	5	5.953	0.005953	0.017	0.000017
Ore F	6	6.079	0.006079	0.02	0.000020
Ore F	7	6.425	0.006425	0.024	0.000024
Ore F	8	6.392	0.006392	0.001	0.000001
Ore F	9	5.723	0.005723	0.033	0.000033
Ore F	10	6.186	0.006186	0.135	0.000135
Ore F	11	5.864	0.005864	0.128	0.000128
Ore F	12	5.415	0.005415	0.15	0.000150

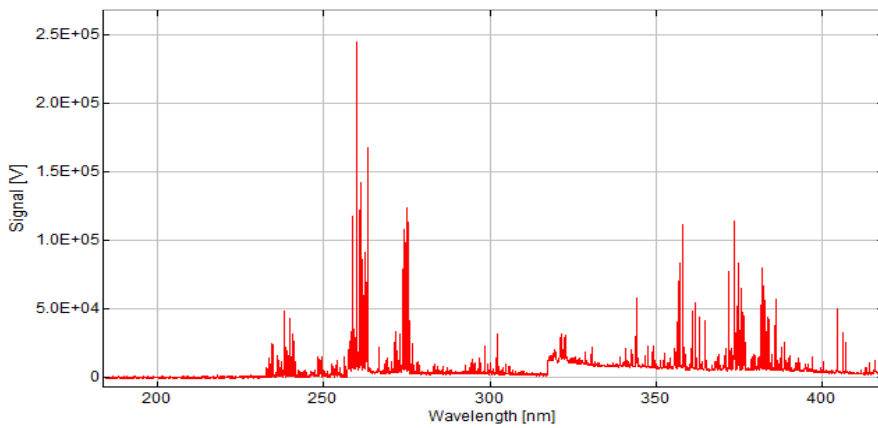| Material	ELPI Stage	Mass in digestion (mg)	Mass in digestion (g)	Mass of particulates on filter (mg)	Mass of particulates on filter (g)
Flue Dust	1	6.004	0.006004	0.002	0.000002
Flue Dust	2	5.4	0.0054	0.011	0.000011
Flue Dust	3	5.661	0.005661	0.026	0.000026
Flue Dust	4	6.031	0.006031	0.022	0.000022
Flue Dust	5	6.122	0.006122	0.037	0.000037
Flue Dust	6	6.379	0.006379	0.033	0.000033
Flue Dust	7	5.316	0.005316	0.043	0.000043
Flue Dust	8	5.614	0.005614	0.05	0.000050
Flue Dust	9	5.456	0.005456	0.104	0.000104
Flue Dust	10	6.106	0.006106	0.164	0.000164
Flue Dust	11	5.847	0.005847	0.235	0.000235
Flue Dust	12	5.805	0.005805	0.177	0.000177
Sinter Dust	1	6.197	0.006197	0.014	0.000014
Sinter Dust	2	5.318	0.005318	0.01	0.000010
Sinter Dust	3	5.204	0.005204	0.018	0.000018
Sinter Dust	4	5.751	0.005751	0.017	0.000017
Sinter Dust	5	6.346	0.006346	0.02	0.000020
Sinter Dust	6	6.022	0.006022	0.013	0.000013
Sinter Dust	7	6.058	0.006058	0.011	0.000011
Sinter Dust	8	5.584	0.005584	0.014	0.000014
Sinter Dust	9	5.44	0.00544	0.036	0.000036
Sinter Dust	10	5.49	0.00549	0.085	0.000085
Sinter Dust	11	6.117	0.006117	0.106	0.000106
Sinter Dust	12	6.429	0.006429	0.092	0.000092

Appendix Two

Morphological studies of laser generated particulates using LA-Aspect methods
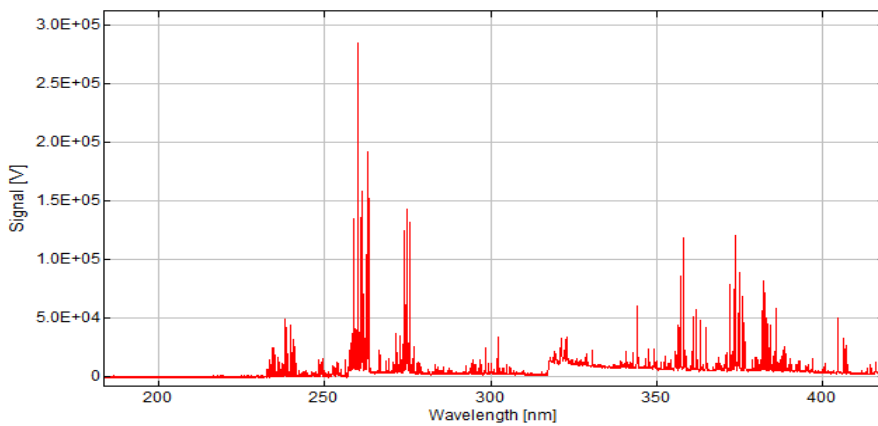
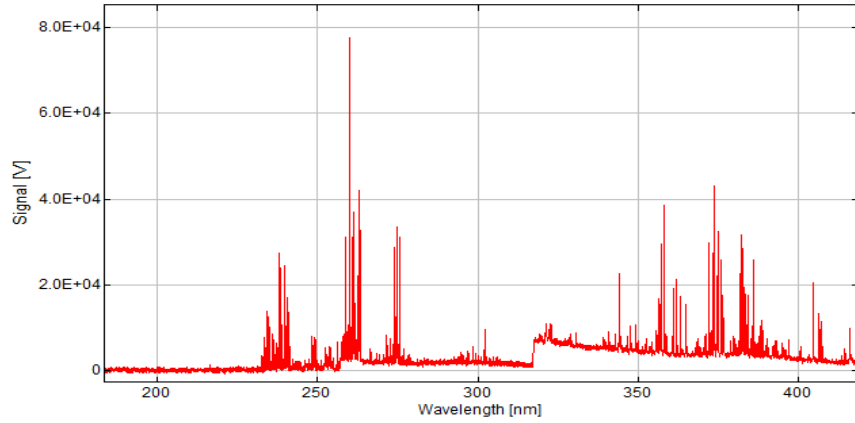**Set 1, First laser fire:** Peak height = 13016

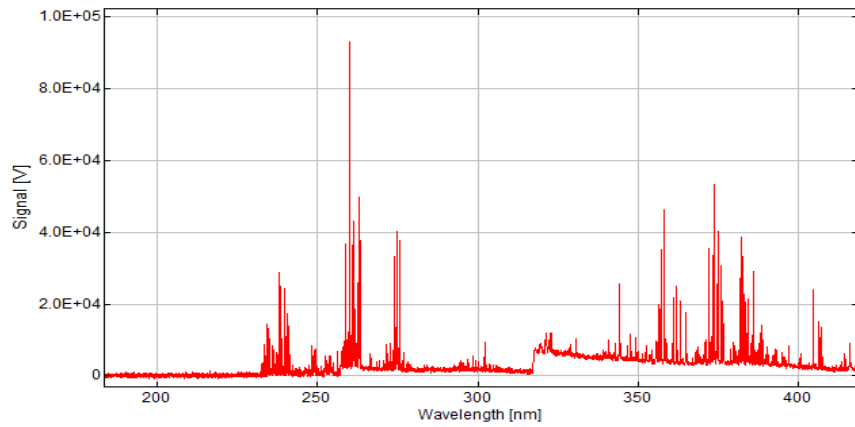**Set 1, Second laser fire:** Peak height of 12648
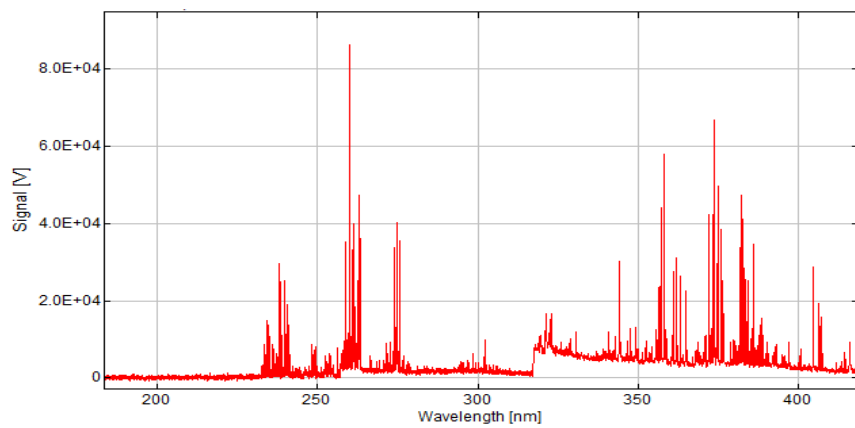

Set 1, Third laser fire: Peak height = 12476

Set 2, First laser fire: Peak height = 9821

Set 2, Second laser fire: Peak height = 8922

Set 2, Third laser fire, Peak height = 9286

Appendix Three

Physical and elemental studies of particulates using an LA-ELPI method and ICP-MS

Material	ELPI Stage	Mass in digestion (mg)	Mass in digestion (g)	Mass of particulates on filter (mg)	Mass of particulates on filter (g)
Carbon rod	1	5.598	0.005598	0.006	0.000006
Carbon rod	2	5.309	0.005309	0.006	0.000006
Carbon rod	3	5.921	0.005921	0.002	0.000002
Carbon rod	4	5.498	0.005498	0.007	0.000007
Carbon rod	5	6.309	0.006309	0.011	0.000011
Carbon rod	6	5.276	0.005276	0.012	0.000012
Carbon rod	7	6.182	0.006182	0.003	0.000003
Carbon rod	8	5.899	0.005899	0.012	0.000012
Carbon rod	9	5.581	0.005581	0.007	0.000007
Carbon rod	10	5.65	0.00565	0.009	0.000009
Carbon rod	11	5.995	0.005995	0.003	0.000003
Carbon rod	12	5.26	0.00526	0.006	0.000006
High purity zinc	1	6.402	0.006402	0.02	0.000020
High purity zinc	2	5.658	0.005658	0.031	0.000031
High purity zinc	3	6.447	0.006447	0.007	0.000007
High purity zinc	4	5.294	0.005294	0.003	0.000003
High purity zinc	5	5.766	0.005766	0.001	0.000001
High purity zinc	6	5.658	0.005658	0.002	0.000002
High purity zinc	7	6.461	0.006461	0.013	0.000013
High purity zinc	8	5.663	0.005663	0.003	0.000003
High purity zinc	9	6.058	0.006058	0.003	0.000003
High purity zinc	10	5.297	0.005297	0.008	0.000008
High purity zinc	11	5.253	0.005253	0.008	0.000008
High purity zinc	12	5.585	0.005585	0.002	0.000002

Material	ELPI Stage	Mass in digestion (mg)	Mass in digestion (g)	Mass of particulates on filter (mg)	Mass of particulates on filter (g)
Carbon steel	1	5.581	0.005581	0.008	0.000008
Carbon steel	2	5.947	0.005947	0.01	0.000010
Carbon steel	3	5.607	0.005607	0.017	0.000017
Carbon steel	4	5.554	0.005554	0.011	0.000011
Carbon steel	5	5.365	0.005365	0.006	0.000006
Carbon steel	6	5.252	0.005252	0.009	0.000009
Carbon steel	7	5.747	0.005747	0.008	0.000008
Carbon steel	8	5.612	0.005612	0.01	0.000010
Carbon steel	9	5.922	0.005922	0.003	0.000003
Carbon steel	10	6.301	0.006301	0.005	0.000005
Carbon steel	11	6.251	0.006251	0.013	0.000013
Carbon steel	12	5.411	0.005411	0.009	0.000009
Boron nitride	1	5.583	0.005583	0.015	0.000015
Boron nitride	2	5.306	0.005306	0.083	0.000083
Boron nitride	3	5.307	0.005307	0.029	0.000029
Boron nitride	4	5.987	0.005987	0.012	0.000012
Boron nitride	5	5.58	0.00558	0.008	0.000008
Boron nitride	6	5.265	0.005265	0.006	0.000006
Boron nitride	7	5.311	0.005311	0.003	0.000003
Boron nitride	8	5.605	0.005605	0.003	0.000003
Boron nitride	9	5.267	0.005267	0.004	0.000004
Boron nitride	10	5.533	0.005533	0.011	0.000011
Boron nitride	11	6.148	0.006148	0.006	0.000006
Boron nitride	12	6.343	0.006343	0.007	0.000007